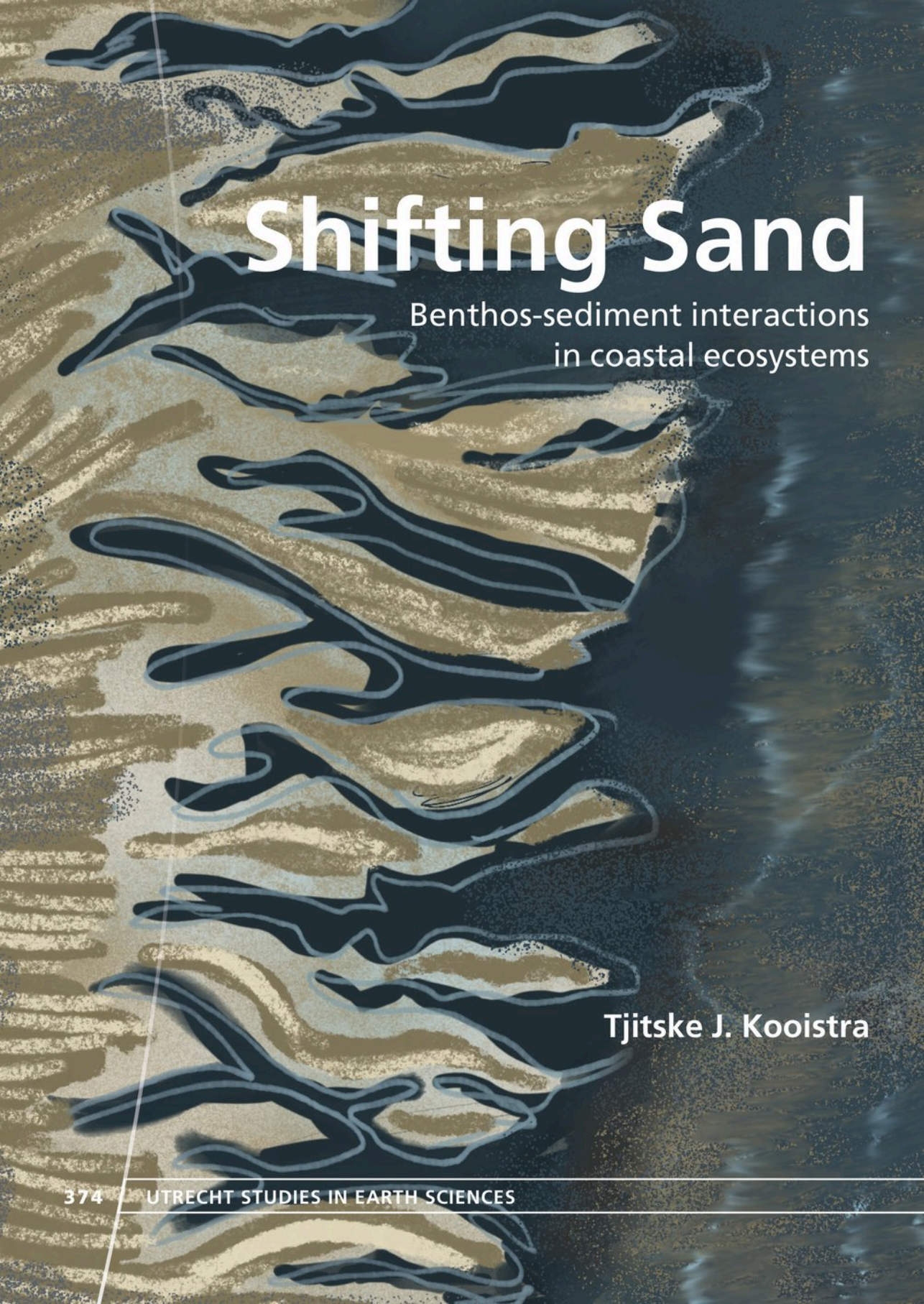

Shifting Sand

Benthos-sediment interactions in coastal ecosystems

Tjitske J. Kooistra

374 UTRECHT STUDIES IN EARTH SCIENCES

Shifting sand

benthos-sediment interactions in coastal ecosystems

Tjitske J. Kooistra

The research presented in this thesis was conducted at the Department of Estuarine and Delta Systems of the NIOZ Royal Netherlands Institute for Sea Research and the Department of Earth Sciences, Utrecht University.

This research was part of the project "Tracking Ameland Inlet Living Lab Sediment (TRAILS)". funded by NWO, grant 17600.

Citation: Kooistra, T.J. (2026). Shifting Sand: benthos-sediment interactions in coastal ecosystems. PhD thesis, Utrecht University, Utrecht, The Netherlands.

ISBN: 978-90-6266-748-2
Utrecht Studies of Earth Sciences (USES) volume number: 374
DOI: https://doi.org/10.33540/3573
Cover design: Emily Liang
Photographs: Bram Fey (page 10), Tjitske Kooistra (pages 28, 62, 98, 130, 172)

Provided by thesis specialist Ridderprint, ridderprint.nl
Printing: Ridderprint
Layout and design: Erwin Timmerman, persoonlijkproefschrift.nl

Shifting sand

Benthos-sediment interactions in coastal ecosystems

Schuivend zand

Benthos-sediment interacties in kustecosystemen

(met een samenvatting in het Nederlands)

Proefschrift

ter verkrijging van de graad van doctor aan de
Universiteit Utrecht
op gezag van de
rector magnificus, prof. dr. ir. W. Hazeleger,
ingevolge het besluit van het College voor Promoties
in het openbaar te verdedigen op

vrijdag 26 juni 2026 des middags te 2.15 uur

door

Tjitske Japke Kooistra

geboren op 12 april 1995
te Sneek

Promotoren:

Prof. dr. K.E.R. Soetaert
Prof. dr. T.J. Bouma

Copromotoren:

Dr. R. Witbaard
Dr. S.G. Pearson

Beoordelingscommissie:

Prof. dr. U. Braeckman
Dr. C. Buschbaum
Prof. dr. M.A. Peck
Prof. dr. ir. K. Philippart
Prof. dr. D.W. Thieltges

Table of Contents

Summary

The world's coasts are under threat of erosion due to sea level rise. To counteract this erosion, sand nourishments are applied. Such nourishments may have ecological implications, both on the site where they are placed, as well as further away. In sedimentary coastal systems, invertebrate animals that live in and on the seafloor, so-called "macrozoobenthos" or "benthos", fulfil essential ecological roles. This dissertation focusses on the different ways in which these benthic animals interact with the sediment they live in, in the context of sand nourishments.

Sediment grain size composition determines the habitat suitability. Even though many benthic species in the Wadden Sea are sediment generalists, several have pronounced median grain size or mud content optima (**Chapter 2**). In the Borndiep basin (Wadden Sea, the Netherlands), sediments were in general coarser and less muddy than optimal for the benthic fauna. In several areas, especially in the intertidal, sediments were near the edge of the tolerance range of the resident fauna. A slight coarsening here could drive a shift in the benthic communities.

Although sediment mud content and food availability are usually correlated, sediment composition appeared to be a stronger driver of performance than food availability for a mud-dwelling species (peppery furrow clam, *Scrobicularia plana*, **Chapter 3**). A sandy sediment resulted in high mortality and a reduced mobility. The species was relatively tolerant to a heatwave, independent of sediment composition and food supply. Therefore, a drastically changing sedimentary habitat is likely to be a risk for this species.

The other way around, benthic animals can influence the transport and composition of the sediment they live in by the structures that they make and their activity. Bivalves produce shells that accumulate in the sediment after the animal dies. These shells can interact with the sediment transport and flow (**Chapter 4**). A higher fraction of shells in the sediment results in a higher threshold for incipient motion of sand grains and a lower bedload transport rate, independent of the shape of the shells. Both elongated and round shells reduce the formation of sand ripples, but elongated shells are sticking out more, therefore round shells decrease roughness most. On the other hand, the elongated shells also covered more of the bed, shielding the sand from erosion. The resulting sand transport modifications was therefore similar for both shell types. In areas with high sed-

iment shell content, significant contributions from shells on sediment transport can be expected.

By their burrowing behaviour, benthic animals can modify the vertical sediment distribution and composition. This bioturbation is particle-size specific (**Chapter 5**): mud and fine particles are preferentially reworked, while sand may better preserve the stratification after deposition by currents and waves. In a young and relatively dynamic intertidal environment, it is challenging to distinguish the effects of constant but small bioturbation displacements from the episodical storm deposition and reworking. Single-grain luminescence is a promising technique for unravelling mixing processes of sand grains. However, further testing and development of the methods are needed before it can be applied to determine reliable bioturbation rates in young and dynamic deposits.

Altogether, the results show that benthic communities and sediment composition and transport are tightly linked. Sediment grain size and mud content determine habitat suitability. The composition and stability of the sediment itself is also influenced by biota. These ecological interactions should be considered in the management of sedimentary coasts.

Samenvatting

Wereldwijd worden kusten bedreigd door erosie, veroorzaakt door zeespiegelstijging. Zandsuppleties worden toegepast om kusterosie tegen te gaan. Deze suppleties kunnen gevolgen hebben voor de ecologie, zowel op de plek waar ze worden aangebracht, als verder van de suppletielocatie. In kustsystemen bestaande uit zand of slib, vervullen ongewervelde bodemdieren, "macrozoobenthos" of "benthos", essentiële ecologische functies. Dit proefschrift richt zich op de wisselwerking tussen de benthos en het sediment waarin zij leven, in verband met zandsuppleties.

De korrelgrootteverdeling van sediment bepaalt de geschiktheid van het leefgebied. Hoewel veel benthische soorten in de Waddenzee sedimentgeneralisten zijn, hebben enkele uitgesproken voorkeur voor een bepaalde korrelgrootte of slibgehalte (**Hoofdstuk 2**). In het Borndiep-kombergingsgebied (Waddenzee, Nederland) was het sediment grover en minder slibrijk dan optimaal voor de bodemfauna. Op verschillende plekken, met name in het intergetijdengebied, lag de sedimentsamenstelling tegen de grove kant van de tolerantiegrenzen van de aanwezige fauna. Een relatief kleine vergroving zou hier al kunnen leiden tot verschuivingen in de soortsamenstelling.

Slibgehalte en voedselbeschikbaarheid hangen doorgaans met elkaar samen. Toch bleek vooral sedimentsamenstelling bepalend voor de overlevingskans van de platte slijkgaper, *Scrobicularia plana* , een schelpdier dat in slijkige gebieden leeft (**Hoofdstuk 3**). Een zandig sediment resulteerde in een groot aantal sterfgevallen en een verminderde mobiliteit. De soort was relatief weerbaar tegen een hittegolf, onafhankelijk van sedimentsamenstelling en voedseltoevoer. Een veranderend sedimenthabitat vormt daarom waarschijnlijk een risico voor deze soort.

Omgekeerd kunnen bodemdieren ook de verplaatsing en samenstelling van het sediment in hun leefomgeving beïnvloeden door hun graafbewegingen en de structuren die ze maken. Schelpen blijven in de zeebodem aanwezig nadat de schelpdieren die ze gemaakt hebben gestorven zijn. Deze schelpen kunnen sedimenttransport en waterstroming beïnvloeden (**Hoofdstuk 4**). Een hoger aandeel schelpen in bodem zorgt dat zandkorrels minder snel in beweging komen en dat er in totaal minder zand getransporteerd wordt. Zowel langwerpige als ronde schelpen verminderen de vorming van zandribbels, maar langwerpige schelpen

steken zelf meer uit; ronde schelpen verlagen daardoor de bodemruwheid het meest. Daartegenover bedekten langwerpige schelpen een groter deel van het bodemoppervlak, waardoor het zand extra wordt afgeschermd. De totale effecten op zandtransport zijn voor beide schepvormen gelijk. Op plekken waar veel schelpen in de zeebodem aanwezig zijn, hebben deze waarschijnlijk een beduidende invloed op sedimenttransport.

Door middel van hun graafgedrag kunnen bodemdieren de verticale verdeling van zand en slib beïnvloeden. Deze "bioturbatie" verschilt per korrelgrootte-klasse (**Hoofdstuk 5**): fijne korrels (slib) worden eerder verplaatst, terwijl zandkorrels minder mobiel zijn en eerder de gelaagdheid na afzetting door golven en stroming kunnen behouden. Met behulp van luminescentie op korrelniveau kunnen deze mengprocessen beter ontrafeld worden. Verdere methodologische ontwikkelingen is echter nodig voordat deze betrouwbaar kan worden toegepast om omwerkingssnelheden te bepalen in jonge en dynamische afzettingen in het intergetijdengebied.

Samengevat laten de resultaten zien dat bodemgemeenschappen en sedimentsamenstelling en -transport nauw met elkaar verweven zijn. Korrelgrootte en slibgehalte bepalen de habitatsgeschiktheid, terwijl de samenstelling en stabiliteit van het sediment zelf ook door het bodemleven wordt beïnvloed. Deze ecologische wisselwerkingen zouden moeten worden meegenomen in het beheer van sedimentaire kustsystemen.

Chapter 1

Introduction

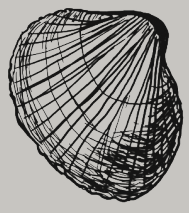

Living at the seaside

Where the land meets the sea, many creatures find a place to live. They dwell here for several reasons: they profit from the abundant nutrition in these areas where a lot of light and nutrients are available, while still living in the relatively stable environment that the marine realm provides. Nevertheless, these coastal zones contain among the most dynamic conditions that you can find in the sea. At exposed locations, sands are constantly subject to strong waves and currents. In intertidal areas, the seafloor that falls dry during low tide is exposed to the fluctuations of the air above, which can be scorching heat in summer or scouring ice in winter. A variety of coastal habitats exist: some shorelines are rocky, some are vegetated by mangroves or salt marshes, and some are characterised by sandy beaches. When a sufficient tidal range is present, and the sedimentary conditions are right, intertidal flats form. These are part of the day covered by water, and part of the day exposed to the air.

Changing coasts

The coastal zone is also the place where most humans interact directly or indirectly with the marine environment. A major and increasing part of the worlds human population inhabits the coastal zone (Neumann et al. 2015), and approximately 775 million people have a high dependence on the resources that coastal marine ecosystems provide (Selig et al. 2019). Human pressures on these ecosystems are high and have led to loss of biodiversity (Lotze et al. 2006), and with this also loss of important ecosystem services (Worm et al. 2006).

The impacts that humans have on coastal ecosystems range from local and regional, to global scale (He and Silliman 2019). Anthropogenic activities, including fisheries, tourism, resource extraction, energy production and infrastructure can locally and regionally impact marine systems. On a global level, climate change influences coastal environments. Firstly, the warming climate is resulting in higher water and air temperatures, as well as an increase in extreme events, such as heatwaves, storms and precipitation extremes (Parmesan et al. 2022). Secondly, global sea level is rising at an increasing rate (3.6 mm $year^{-1}$ in the last decade) and predicted to keep rising to 0.43–0.84 m by the end of the 21st century (Oppenheimer et al. 2019). Especially in low-lying coastal areas, this increases the flood risk and coastal erosion, while also affecting the adjacent marine habitats

by modifying hydrodynamics, and thus morphology (Ranasinghe et al. 2013; Ranasinghe 2016).

Several measures can be taken to protect coastal regions from rising sea levels and the consequently eroding soft-sediment coastlines (Williams et al. 2018). On the one hand, so called "hard" solutions include the construction of dykes, groins or breakwaters. On the other hand, ecosystem-based coastal defence measures harness natural structures and processes for counteracting erosion, as well as restoring coastal ecosystems (Temmerman et al. 2013). Sediment nourishments are a "soft" defence solution and represent a more natural alternative to protect sandy shores compared to hard structures (de Schipper et al., 2021; Hanson et al., 2002). They usually entail the deposition of sediment on or near an eroding location, after which waves, wind, and currents are allowed to redistribute it naturally. Most of these nourishments take place on, or in front of, sandy beaches. Such sand nourishments are applied globally and currently keep coastal erosion at bay, but the need for nourishing has strongly increased and is predicted to keep rising during the coming century (Brand et al., 2025; Haasnoot et al., 2020; Vousdoukas et al., 2020). Not only an increasing nourishment size and frequency, but also new nourishment types are needed (e.g., Box I). For instance, mega-nourishments could offer efficient longer-term coastal protection (Stive et al. 2013).

Sand nourishments can affect coastal ecosystems in multiple ways. First, the seafloor, at the place where the sand gets taken from, is disrupted (Witbaard et al. 2025; Schultz et al. 2025). Then, during nourishment placement, the seafloor or the beach at the nourishment location gets covered by a layer of sand, and the sediment concentration in the water is increased (Peterson and Bishop 2005; Speybroeck et al. 2006). What we know little about, is how nourishments actually affect marine ecosystems on a longer timescale and further away from the nourishment location. Furthermore, we also still have a lot to learn about how marine organisms themselves can influence the distribution, stability and composition of the sediment. These questions were at the basis of this PhD.

The Wadden Sea

Before diving deeper, I will introduce my study system: the Wadden Sea. This shallow coastal sea spans 500 km, from the Netherlands to Denmark (Fig. 1). On the North Sea side lie barrier islands, like a giant's trail, forming a permeable

boundary. Through the inlets between the islands, the tide flows twice a day in and out of the tidal basins. As the tide lowers, large parts of the seafloor fall dry. The vast (4700 km^2) areal extent of these intertidal flats are one of the features which make the Wadden Sea unique worldwide. Its geology, natural dynamics and biodiversity have granted this system a UNESCO world heritage status.

Figure 1. the Wadden Sea as seen from space, looking towards the east (Jeff Williams, ISS). This thesis focuses on the Dutch Wadden Sea, located in the lower half of this photograph. The inset shows the location of the Wadden Sea in Europe (red), with the box indicating the focus area in the photograph.

Morphology and dynamics

The Wadden Sea is a relatively young system, as its formation started approximately 7500 years ago, with the ongoing gradual sea level rise after the end of the last ice age. It is mainly shaped by natural dynamics: the tidal flow and the constantly counteracting processes of sedimentation and erosion which change the course of gullies and the shape of tidal flats and islands. Sediment is continuously on the move and is exchanged between coastal zone, ebb-tidal deltas and basin. How much sediment moves depends on the supply *("how much sediment is available?"*), the transport capacity *("are the currents and waves strong enough to carry the sediment along?"*), and the sediment accommodation space ("*is there a demand for sediment and the opportunity to settle?*"). The sand that is deposited in the Wadden Sea originates from the coastline and the ebb-tidal deltas on the open seaward side in front of the tidal inlets. Currently, the supply is sufficient to keep up with sea level rise. However, with increasingly rising sea level, a rate at which the supply can no longer meet the demand may be reached.

At this critical rate, estimated at 4 mm year^{-1} for larger tidal basins, the tidal flats are predicted to drown (Wang et al. 2018; Lodder et al. 2019).

Box I: Introducing the TRAILS project

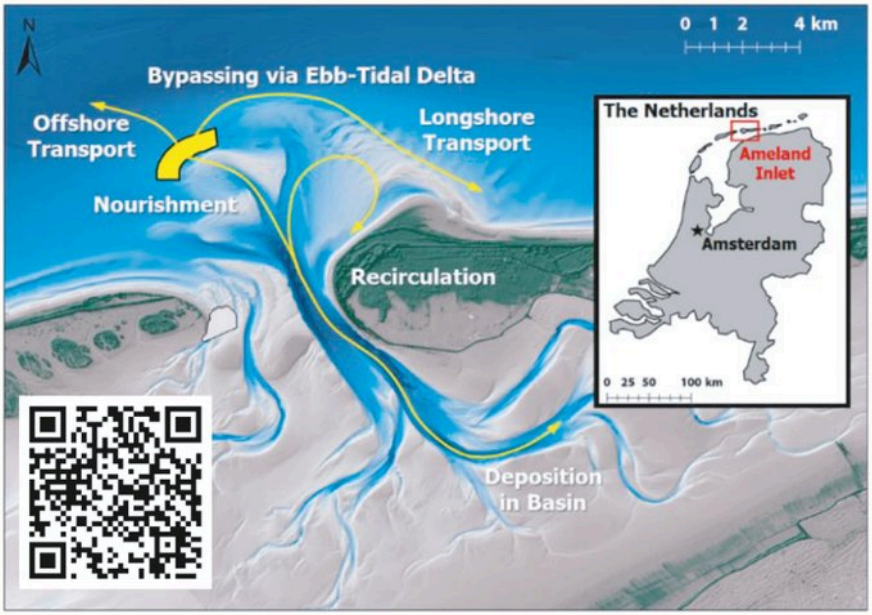

Figure 2. The location of the ebb-tidal delta nourishment and possible sediment pathways. The inset QR-code leads to the 'TRAILS late night show', an outreach video where we summarise our research.

In 2018, a 5 million m^3 sand nourishment was placed on the Ameland ebb-tidal delta (Fig. 2). This nourishment was a pilot, to test whether ebb-tidal deltas can be nourished, and if this influences the system. The rationale behind nourishing ebb-tidal deltas is that they are part of the sediment-sharing system of the North Sea coastline and the Wadden Sea basin. The ebb-tidal deltas form a sediment buffer for the entire system but are currently decreasing in volume (Elias et al. 2012). Adding sediment to the ebb-tidal deltas could provide a means to ensure sufficient sediment supply for counteracting coastal erosion. In the research programmes Coastal Genesis 2.0 and SEAWAD (Lodder et al. 2023), the direct morphological and ecological effects of the nourishment were assessed. These

first investigations concluded that the morpho-dynamics of the ebb-tidal delta had not been drastically altered. Instead, the nourishment had rather gradually adapted to ebb-tidal delta dynamics and was therefore classified as a "system-following nourishment" (Elias 2021). The benthic ecosystem at the nourishment site had largely recovered after three years, as it originally consisted mainly of mobile and short-lived species (Escaravage 2022). Bivalves had however not yet fully recovered. At nearby sites on the ebb-tidal delta, no clear ecological effects were observed, possibly due to an inherently high ecological variability. The long-term and far-field effects, as well as how benthos may have affected the nourishment sand distribution, remained to be investigated.

Some questions remained: where did the nourished sand exactly go? Can this nourishment help us to develop novel tracers and models to predict the trajectories of sand grains? How do such of nourishments, adjacent to a large intertidal flat ecosystem such as the Wadden Sea, interact with ecology on a larger scale? And how can stakeholders be involved in the co-assessment of nourishment strategies? In the project TRAILS (TRacking Ameland Inlet Living lab Sediment), from which my PhD is part, we tried to answer these questions. The TRAILS project consists of five interlinked work packages (WPs). They concerned the co-assessment of future nourishment strategies with stakeholders in a living lab setting (WP A), the development of tracers that make use of luminescence, an inherent signal of sand grains that is reset by light (WP B), the interaction between benthic fauna and nourishment sand (WP C, this PhD), the development of simulations that trace sediment particle pathways (WP D) and the integration of all findings (WP E).

Anthropogenic interventions have also shaped the morphological development of the Wadden Sea (e.g., Box II). In the Dutch Wadden Sea, the largest change in the last century was the closure of the Zuiderzee in 1932, with the construction of the Afsluitdijk, which still affects morphodynamics in the western part of the Wadden Sea (Elias et al., 2012). Furthermore, salt and gas mining result in land subsidence (Fokker et al. 2018) and large volumes of sediment are dredged from the basins to keep fairways accessible (e.g., Rijkswaterstaat, 2022), while the islands are being kept in place by hard coastal defence structures, or sand nourishments, preventing them from migrating and the coastline from retreating

landwards (Elias et al. 2012). These human interactions with natural sediment dynamics have consequences for the sedimentary ecology (Eriksson et al. 2010).

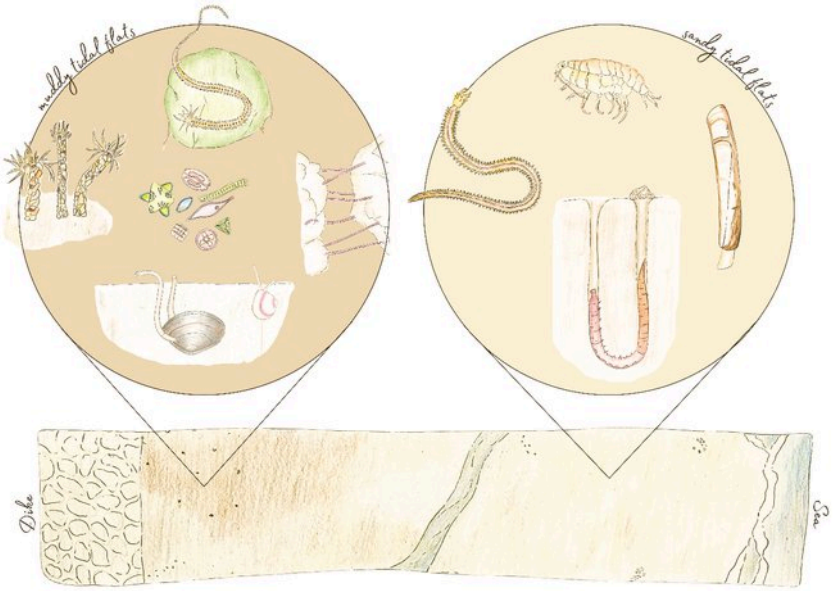

Figure 3. An impression of Wadden Sea benthic habitats and a few species commonly found in muddier (left) and sandier (right) sediments. From left to right: *Lanice conchilega*, *Scrobicularia plana*, benthic diatoms (centre), *Phyllodoce mucosa*, *Macoma balthica*, *Heteromastus filiformis*, *Nephtys cirrosa*, *Urothoe poseidonis*, *Arenicola marina* and *Ensis leei* (illustration: Luka Biemond).

Ecology

Even if at first glance, the Wadden Sea may seem to be just a muddy puddle, it contains unique habitats (Fig. 3). When you climb over the dyke at the mainland coast, you may see salt marshes stretched out in front of you. These are coastal lands that now and then are flooded with water during unusual high tides or storms. The plants that built these lands need to withstand intermittent inundation by salt water. Further from the dike, the high marsh transitions into the low marsh, the pioneer zone where only annual *Salicornia* plants grow, and then into the high mud flats. Close to the coast, and at other sheltered locations, the intertidal flats are very muddy, which means that you might sink in until over your knees. On the surface of the mud, in summer you can see a brown-green layer: benthic diatoms, or seafloor microalgae, which form the basis of the food

web here (Christianen et al. 2017). The smell may be sulfuric, and you may hear bubbling, plopping, and crisping noises. If you keep walking, you may encounter a mussel or an oyster reef. These reefs form a habitat for many other organisms; they trap sediment and can even protect the coast because they dampen the waves (Ysebaert et al. 2018). Further on, the more exposed tidal flats are sandier. The bobbly surface of holes and stringy heaps reveals the presence of large lugworms beneath the surface. Now and then you cross a tidal creek. These creeks are full of shrimp and small fish. A few spoonbills can be seen hunting for them by sweeping their bills through the water. The small creeks turn into larger channels–now we are in the subtidal. The animals living here are not constantly subjected to exposure to the air, but are always inundated by the water, and therefore more species can live here. Closer to the inlet, the gullies get deeper and the currents get stronger, as the water from the entire basin must flow in and out through this entrance every tide. The seafloor consists of coarse sand, and the organisms living here are mobile and adapted to this dynamic environment (e.g., Reiss & Kröncke, 2001). After exiting the Wadden Sea, the ebbing tide loses power and the sediments it carried have a chance to settle. Here, the ebb-tidal delta is formed and the Wadden Sea ecosystem gradually turns in that of the North Sea.

The highly productive Wadden Sea ecosystem is an essential feeding ground for 12 million migratory birds and form a nursery for fish (Reise et al. 2010; Kloepper et al. 2022). The basis of the food web is formed by microalgae that live on the sea floor (mainly benthic diatoms), and algae from freshwater and marine origin. These primary producers sustain an enormous biomass of animals living in and on the seafloor, macrozoobenthic invertebrates, the focus of this thesis.

Benthic fauna

Macrozoobenthos are all invertebrates living in the seafloor that are large enough to be seen with the naked eye (usually >1 mm). The macrozoobenthic diversity in coastal habitats, such as the Wadden Sea, consists of worms, molluscs, crustaceans, and many other phyla. They can be herbivores, feeding on benthic microalgae or phytoplankton; detritivores, feeding on dead organic matter from the sediment; or predators, feeding on other macro- or meiozoobenthos (animals smaller than 1 mm). The biodiversity in coastal sedimentary habitats, especially systems that are young on evolutionary timescales, such as the Wadden Sea, is typically lower compared to deeper marine habitats. Nevertheless, total benthic

biomass here is large and individual species or groups play an important role in the functioning of the ecosystem as a whole (Snelgrove 1998; Levin et al. 2001).

Benthic animals are an essential part of the coastal ecosystem. They play a key role in the nutrient flows, as they couple the benthic (seafloor) with the pelagic (water column) system, they decompose detritus and provide food for a lot of other animals (Herman et al. 1999). Besides their trophic role, they can influence sediment chemistry and the exchange of substances between sediment and water with their burrowing and bio-irrigating activity (Aller 1982). By mixing and oxygenating the sediment, they have an influence on sediment carbon storage (Aller and Cochran 2019; Song et al. 2022). Many benthic species are ecosystem engineers: they self-structure their habitats (Reise 2002; Meadows et al. 2012). Some build reefs that can accumulate sediment, aid in coastal protection and shape the benthic community (Rabaut et al. 2007; Ysebaert et al. 2018). Others engineer their living space by oxygenating and reworking (Gray 1974; Rhoads and Boyer 1982). Soft-sediment habitats are characterised by facilitating interactions–organisms help each other to live here–and cooperative engineering (Passarelli et al. 2014; Rademaker et al. 2025).

The relation between benthic animals and sediment is two-way: on the one hand, the sediment type determines which animals can live in a certain location, on the other hand the fauna themselves can modify sediment composition. As benthic animals are relatively long-lived (up to several years) and usually stay in place, the benthic community is likely to reflect changes in the sedimentary habitat.

Box II: The Ameland inlet

To set the scene for the study area, let me take you to the village in Friesland, The Netherlands, where I grew up (Fig. 4). A millennium before I was born, an estuarine bay was located here: the Middle Sea. From the river Boorne, the water washed out between Oostergo and Westergo—the current Friesland— into the Borndiep basin and entered the North Sea between the islands of Ameland and Terschelling. My family's farm is named after a channel, de Scheender, in the most inner part of the Middle Sea. Around the year 1000, the Middel Sea reached its maximum landward extent, with even a connection to the adjacent Vlie basin through the Marne inlet. To defend their houses and lands against the more frequent

floodings, the Frisians started building dykes. One of the older dykes forms the driveway to the farm today. Nowadays, the sea is nowhere to be seen. Continuous silting up by the clay brought in by the tides, as well as land reclamation, slowly but steadily turned the Middel Sea into land. The Borndiep tidal basin is the seaward remain of the ancient Middle Sea that lives on

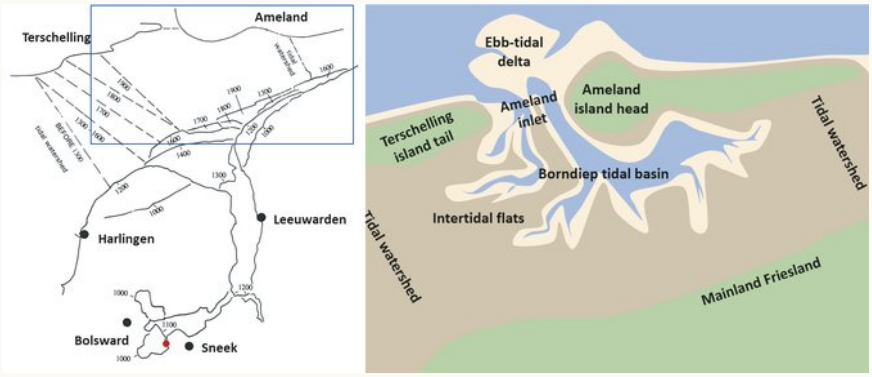

Figure 4. Left: the extent of the Middle Sea during the last millennium (van der Spek 1995). The approximate years of dike construction and tidal watershed position are indicated. The red dot shows my home village. Right: schematic map of the main morphological features of Ameland Inlet.

today and is the focus of this dissertation.

In the 19th century new, large-scale land reclamation plans were made: the Zuiderzee, which lay between Friesland and North Holland, and the Wadden Sea should be dammed and turned into agricultural land. To this end, a dam was built over the Ameland tidal divide in 1872, connecting the island with the mainland. After repeated storm breaching, the plans were abandoned, and the dam was deconstructed a decade later. The Zuiderzee was closed in 1932 by the construction of the Afsluitdijk. In the Borndiep basin, these engineering works also impacted the morphological development (Elias et al. 2012). Nowadays, Ameland inlet is still characterised by human impacts. Since 1986, gas is being extracted near the eastern tip of the island of Ameland. This results in subsidence of the seafloor (Fokker et al. 2018), which is nearly instantly compensated by sedimentation (Krol et al. 2024). The large volume of nourishment sand on the coast of Ameland (20 million m^3 sand since 1980) has enabled the island to remain its position and has likely fed the extra sediment demand caused by subsidence (Wang

et al. 2018). Besides sand added to the coast, sediment is dredged from the basin as well. Nearly continuous dredging to keep fairways accessible, results in a relocation of approximately 2 million m^3 of mud annually (Rijkswaterstaat 2022).

Sediment shapes the benthic community

As macrozoobenthos live in and on the sediment, they are closely linked to sediment composition (Young and Rhoads 1971; Gray 1974). The size of sediment grains (median grain size) and the mud content are often found to determine to a large degree the community composition (e.g., Compton et al., 2013; de Jong et al., 2015; Pratt et al., 2014; Thrush et al., 2003; Van Colen, 2018; Ysebaert & Herman, 2002). Besides grain size composition, other sediment characteristics, such as bulk density (Wiesebron et al. 2021) and food content (Herman et al. 1999), determine habitat suitability. Sediment texture is not only driving the species composition, but also the functional diversity of the benthic community (Gusmao et al. 2022). However, as sediment composition usually correlates with other environmental variables, such as hydrodynamics, it is difficult to distinguish which effects are solely sediment-composition driven (Snelgrove and Butman 1994). Besides, not all species are equally sensitive to grain size composition.

To predict the extent to which a change in sediment composition—for instance due to sediment nourishments—can influence the benthic community, the preferred sediment niche needs to be determined per species. In **Chapter 2**, I determine the sediment preferences of benthic species and communities, using large benthic monitoring datasets from before to after the nourishment. Such large datasets over environmental gradients are needed to reconstruct reliable species-environment relationships.

Since sediment composition co-varies with many other environmental variables, these other variables may also be a stronger driver for some species. A change in sediment is then less likely to result in a change in community, especially if other variables remain the same. At muddy locations, food availability is often higher than at sandy locations, as muddy sediments contain more organic matter and benthic diatoms grow at the sediment surface. Controlled experiments can help to untangle whether this food content, or the actual texture of the sediment is the reason why certain species select a muddy habitat. In the future, additional stressors such as heatwaves may pose another challenge for the intertidal fauna.

In **Chapter 3** I look at the performance and heatwave tolerance of a mud-preferring clam in different sediment-food habitats. These sorts of measurements can give insight into the mechanisms of sediment preference and the resilience of species under potential future changes in their habitats.

Benthic animals influence sediment characteristics

Benthic animals are not just influenced by the sediment type: they can also affect the physical sediment characteristics themselves. The influence of animals on the sediment they live in was already described by Darwin (1881), in his publication "On the formation of vegetable mould, through the action of worms, with observations on their habits", where he writes about the reworking of soils by earthworms. This was soon followed by a study from Davison (1891) on "the work done by lobworms" in intertidal sediments. Since these first classic studies, the feedback that benthic animals can have on their environment, also called "bioengineering", has received substantial scientific attention (reviewed by e.g., Dapples, 1942; Meadows et al., 2012; Murray et al., 2002).

The presence of benthic fauna can result in altered sedimentation and sediment transportability due to their interaction with hydrodynamics. For instance, biogenic structures such as tubes and shells that are sticking out of or lying on the sediment surface can influence sediment transport by modifying bottom boundary flow (e.g., Cheng et al., 2021). At low densities, they can promote erosion by scouring, while at high densities, they can promote sedimentation of mud or protect the seabed from erosion by armouring (Nowell and Jumars 1984). When these structures have a greater longevity than the animals themselves, their engineering effects go beyond the life span of the animals that produce them. In **Chapter 4**, I describe the effects of empty bivalve shells of different shapes on sand transport. I compared a native (rounded) with an invasive (elongated) shell and measured sand transport rates in a flume experiment. Such measurements can help improving sediment transport models.

Besides the structures they produce, benthic fauna can influence the sediment they dwell in through their activity. They crawl on the surface, construct burrows, feed and defaecate in or on top of the sediment. Hereby, they can either stabilise or destabilise the sediment, as they can produce mucus which binds particles together, or by creating a looser and more erodible layer on top of the sediment. They can also move particles vertically and influence the grain size composition by preferentially reworking or resuspending certain sediment fractions.

This reworking of sand and mud fractions is what I present in **Chapter 5**. On an intertidal flat, I performed a field experiment with the aim of distinguishing the reworking of coarse and fine sediment fractions by biota and hydrodynamics.

Content

The body of this thesis contains the chapters addressing benthos-sediment interactions, as outlined in the previous section. Fig. 5 shows an overview of the chapters and their place within this interaction. After the main body, I synthesise the findings in Chapter 6, where I place them in a broader context, discuss their implications and give recommendations for follow-up research.

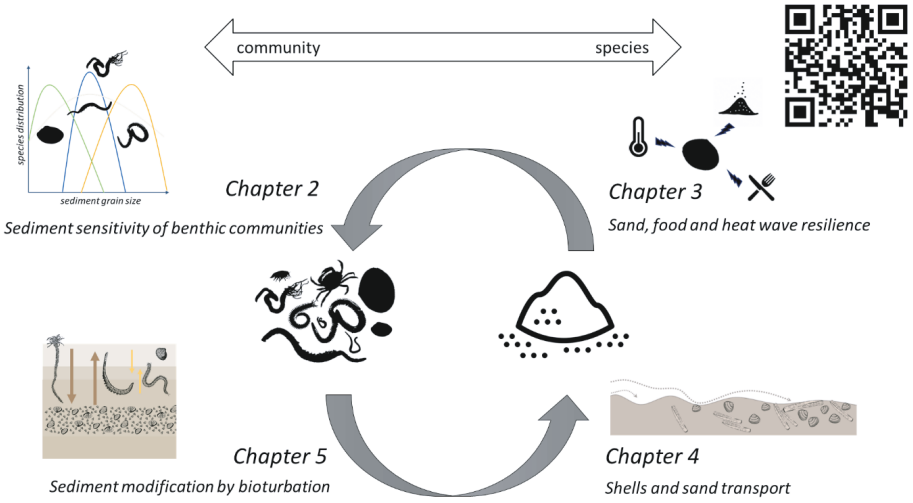

Figure 5. Conceptual diagram placing the chapters of this dissertation in the context of benthos-sediment interactions (top: effects of sediment on benthos, bottom: biotic feedback to sedimentary processes). The QR-code in the top left corner links to a video summarising the content of this dissertation in sand.

Chapter **2**

Sediment sensitivity of benthic communities

Coarsening coasts: quantifying sensitivity of benthic communities to sandification

Published in Estuarine, Coastal and Shelf Science, 2025,
https://doi.org/10.1016/j.ecss.2025.109303

Tjitske J. Kooistra, Rob Witbaard, Tjeerd J. Bouma, Stuart G. Pearson, Allert I. Bijleveld, Tjisse van der Heide, Oscar Franken, Karline Soetaert

Abstract

Sea level rise, increased storminess, and changes in sediment supply due to nourishments are all expected to drive coarsening (i.e., 'sandification') of muddy coastal sediments in the decades to come. Since the composition of soft-bottom benthic communities is associated with the sediment grain-size and mud content, this may result in habitats becoming less suitable for some species, leading to species shifts. **Species-sediment relations** can help to predict how this foreseen sandification may affect benthic fauna. We explore and quantify the sandification-sensitivity of benthic communities, with a tidal basin in the Dutch Wadden Sea as a model system. We identify the species' sediment optima and tolerance ranges using **non-linear quantile regression models**, summarise preference and sensitivity at the community level, and determine the difference between optimal and realised sediment habitat. We find that sediment optima are taxon-specific and that most species in this area are sediment generalists. On community level, there is a difference between the preferred and realised sediment habitat. In many areas, the actual inhabited sediment is **coarser and sandier** than expected based on the preferences of the resident species. Future sandification of the area would further decrease sediment habitat suitability for benthic communities in these places. This detailed knowledge of area-specific sensitivity of benthos can be used to inform coastal management decisions.

Graphical abstract

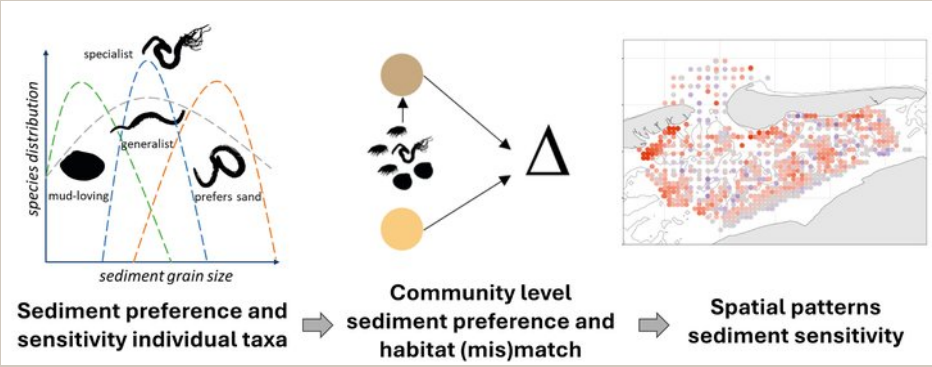

Introduction

Soft-sediment coastlines may be expected to coarsen in the decades to come – a process which can also be referred to as 'sandification'. Firstly shallow coastal areas are increasingly affected by sea level rise and storminess, both resulting in larger waves hitting the coasts and hence coarsening of sediments (Ranasinghe et al. 2013; Ranasinghe 2016). Secondly, humans have altered sediment fluxes on a global scale (Syvitski et al. 2022). By modifying sediment supply, anthropogenic activities can regionally result in coarser sediment. For example, fine sediment input to the sea is strongly reduced by river damming (Syvitski et al. 2005; Dethier et al. 2022) and sand mining (Jordan et al. 2019). Between 1950 and 2010, the land to sea flux of sediment has been reduced by 23% (Syvitski et al. 2022). On the other hand, the supply of coarse sediment has increased by sand nourishments (Huisman et al. 2018; de Schipper et al. 2021). To compensate for rising sea levels and coastal erosion, the need for sand nourishments has strongly increased over the last decades and will keep growing (Vousdoukas et al. 2020; Brand et al. 2022). These structural additions of large volumes of sand may alter the sediment supply to and composition of connected muddy coastal systems (de Schipper et al. 2021). Sandification could have major implications for the ecological functioning of such systems. We use a protected UNESCO World Heritage–The Wadden Sea–as example to assess the role of sandification on ecology.

The Wadden Sea is a shallow coastal sea in Western Europe, bordered by barrier islands. Its habitats range from muddy intertidal flats and sand banks to deep gullies characterized by coarser sediment and high current velocities. Especially the muddy intertidal flats and sand banks give this area a unique ecological value (Reise et al. 2010). Primary productivity by benthic micro-algae (Christianen et al. 2017), combined with advection of organic matter from freshwater sources (Jung et al. 2019), support a high macrozoobenthic biomass (Beukema and Dekker 2020) on which large (migratory) bird populations feed (Zwarts and Wanink 1993). In the Wadden Sea, both the sand budget of the coast and the transport capacity through its tidal inlets determine sediment transport into the basin and towards the tidal flats (Wang et al. 2018). The North Sea coastline of several of the Wadden islands is structurally nourished with large volumes of sand, and also new types of nourishments are being developed and applied (Perk et al. 2019; Lodder et al. 2023). However, long-term and far-field ecological effects of such nourishment programmes on sediment composition and their in-

fluence relative to that of natural sediment transport processes are not well-understood yet (Speybroeck et al. 2006; Staudt et al. 2021). Although no general sandification trends were observed in the Dutch part of the Wadden Sea over the period 2009-2019 (Folmer et al. 2023), the eastern part of the Wadden Sea may already be mud-limited, i.e. the supply of suspended mud is lower than the accommodation space for deposition, and this mud deficit is expected to increase under sea level rise (Dolch and Hass 2008; Colina Alonso et al. 2024). Therefore, the Wadden area is at high risk of sandification.

Soft-bottom benthic species are linked to the sediment they inhabit (Young and Rhoads 1971; Gray 1974) and the composition of benthic communities can largely be explained by sediment median grain size and mud content (Ysebaert and Herman 2002; Compton et al. 2013; de Jong et al. 2015; Van Colen 2018). Also functional traits, such as feeding mode and burrowing capability, show relationships with preferred sediment (Gusmao et al. 2022). Each species has its own preferred optimum for grain size and mud content (Anderson 2008; Kraan et al. 2010; Cozzoli et al. 2013; Armonies 2021). Some are, however, more specialised than others (Robertson et al. 2015). In other words: their niche breadth differs. Following ecological theory, a species' niche optimum is defined by the conditions under which the highest abundance or biomass can be achieved, while niche breadth is defined by the range of conditions that a species can tolerate (Hutchinson 1957; Treurnicht et al. 2020). Whereas generalists have a broad niche and can reach high biomass along a range of environments, habitat specialists are most affected by changing environmental factors (Pandit et al. 2009; Rodil et al. 2018). The proportions of generalist and specialist species in a community can determine the ecosystem functioning and recovery after disturbance (Richmond et al. 2005). Therefore, the niche breadths of individual species can be used to define ecosystem sensitivity and hence robustness to environmental change.

Defining accurate species-sediment relations remains challenging. Firstly, multiple variables affect both sediment composition and benthos distributions. Sediment grain size composition and organic matter content is correlated with, amongst others, hydrodynamics: fine-grained sediments are found in low-stress hydrodynamics conditions and contain higher amounts of organic matter, while coarser sediments are poor in organic matter and are present under higher hydrodynamic stress. This co-variation complicates description of the causation between sediment and community composition (Snelgrove and Butman 1994). Species distributions are, in turn, associated with multiple environmental vari-

ables like hydrodynamic stress (Herman et al. 2001) exposure time of intertidal flats (Kraan et al. 2010) and food availability (Herman et al. 1999), as well as with other biotic interactions such as predation and competition (Bijleveld et al. 2015). The benthic fauna themselves can also influence sediment composition, for instance by their burrowing activity or physical structure (Rhoads and Boyer 1982; Meadows et al. 2012). In practice, acquiring measurements or reliable estimates of all these ecologically relevant variables is challenging.

Several statistical modelling approaches deal with the problem of many confounding, unmeasured variables in ecological research. One of them is quantile regression (Koenker and Bassett 1978; Cade and Noon 2003). With quantile regression, all quantiles of a species' distribution over a parameter of interest are determined, without assuming a parametric distribution of the model error. The upper quantiles of a species' distribution over the parameter of interest reflect the instances where all other, unmeasured, parameters are least constraining, representing the "ecological factor ceiling" (Thomson et al. 1996), which is an indication of the potential species distribution (Vaz et al. 2008). Quantile regression has been proposed as a suitable technique for modelling benthos-sediment relationships in several studies (Anderson 2008; Cozzoli et al. 2013; Chauvel et al. 2024). These studies investigated community composition over a mud gradient, the relative importance of coarse sediments for benthic communities, and differences in species sediment preferences between basins. However, to date, these approaches have not yet been employed to quantify species and community sensitivity to sediment composition. It largely remains to be investigated exactly how sensitive benthic communities are to a change in sediment composition, and how their current distribution relates to their potential sediment habitat.

In this study, we quantify sediment preferences of macrozoobenthos and their potential sensitivity to changes in sediment composition, to explore how benthic communities may respond to sandification resulting from climate change effects and coastal engineering. Our goal is to estimate *where* changes in sediment composition may have the strongest implications for community composition, and *which species* will be most affected. Based on the location of the optimum, and on the width of non-linear quantile regression curves, we classify species as sand or mud-preferring and sediment generalists or specialists. We then combine the optima of the different species, weighted according to their relative abundance in a community, to derive the preferred community optimum. Comparison of the preferred and actual sediment habitat then indicates suitability of the sediment

composition for that community and can be used to identify sensitivity hotspots, where further changes may affect benthic communities most. Pinpointing these sensitivity hotspots for sediment change may inform coastal management decisions on nourishment locations and substrate. We apply this method to a case study of the Ameland inlet and tidal basin in the Dutch Wadden Sea.

Methodology

Case site description: the Borndiep tidal basin, Dutch Wadden Sea

The Borndiep (53°N 5°E) is a tidal basin in the Dutch Wadden Sea, connected to Ameland tidal inlet and bordered by the tidal divides under the islands of Terschelling and Ameland. The basin is approximately 25 km wide between the two tidal divides, and approximately 15 km long from the inlet to the mainland coast. Anthropogenic activities within the area include fishing, sand nourishments and dredging. Shrimp trawlers visit the deeper subtidal parts 3–9 times per year (Rippen et al. 2021). The navigation channel between Ameland and the mainland requires daily dredging to remain accessible for ferries, amounting to a yearly dredged volume of nearly 2 million m^3 (Rijkswaterstaat 2022). In 2018, a 5 million m^3 nourishment was placed at the outer edge of Ameland ebb-tidal delta, located on the North Sea side of Ameland inlet, to stimulate natural sand supply to the northwestern tip and North Sea coast of the island, which suffers from ongoing erosion. This mega-nourishment affected the local benthic communities at the nourishment site, but monitoring of the fauna showed that these communities largely recovered after 3 years (Escaravage 2022). However, it remained unclear if and to what extent the nourishment influenced the fauna deeper into the tidal basin.

Benthos and sediment sampling

To test sediment preference and sensitivity of benthic communities, we use faunistic data collected between 2015 and 2020. These samples were taken from intertidal flats, subtidal gullies, and the ebb-tidal delta, the area just outside the inlet (Fig. 1). The sampled area covers a wide range of sediment types and environmental conditions.

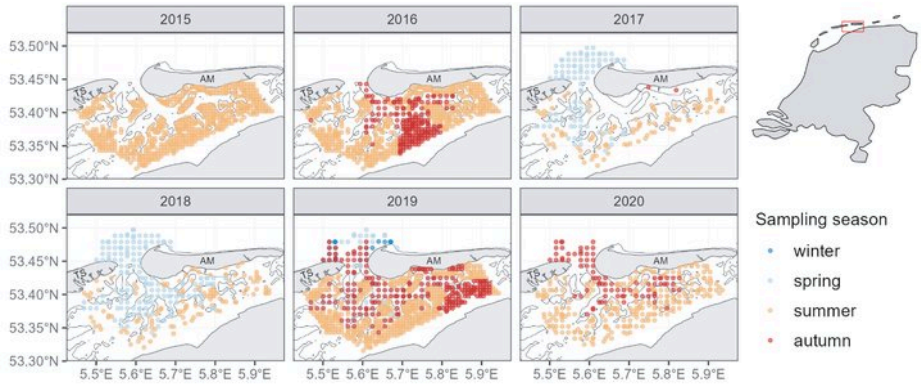

Figure 1. Overview of all samples used in this study. The inset shows the Netherlands, with the sampling area indicated by the red box. The Borndiep tidal basin and Ameland inlet is located between the islands of Ameland (AM) and Terschelling (TS). The ebb-tidal delta, sampled from 2017 onwards, lies on the north side of the inlet. The gully outlines are shown by the black contour line. Data point colour indicates in which (meteorological) season the samples were taken. Note that in 2019, the subtidal areas were sampled twice: in spring and autumn.

Benthos and sediment samples were collected as part of the intertidal and subtidal benthic surveys performed by the Royal Netherlands Institute of Sea Research (NIOZ). Intertidal data was obtained through the synoptic intertidal benthic survey (SIBES; Bijleveld et al. (2024; Bijleveld et al. 2025)). This dataset covers 639 sampling stations in the Ameland Inlet, of which 525 are located on a regular 500x500m grid and 114 are randomly placed (Bijleveld et al. 2012). Stations were sampled by foot with a hand core (0.0177 m^2 surface area) or by RIB combining two long cores (0.0175 m^2 combined surface area). For details on the sampling procedure, we refer to Compton et al. (2013) and Bijleveld et al. (2025). Subtidal samples were collected as part of NIOZ subtidal sampling campaigns and within the projects TRAILS and WaddenMosaic (Franken et al. 2025). Subtidal stations, 145 on a 1000x1000 m grid and 41 randomly placed, were sampled by ship with a boxcore (0.06 m^2 surface area) or by zodiac boat combining 4 long cores (0.035 m^2 combined surface area). For more details on the subtidal sampling, we refer to Franken et al. (2025). In figure 1, an overview of all 2991 samples, mapped per year and season, is given.

Sediment samples were taken from the top 4 cm of the sediment and stored at -20°C. Prior to analysis, the samples were freeze-dried, homogenised with mortar

and pestle, weighed and added to auto-sampler tubes with degassed reverse osmosis water. Grain size composition was determined with a laser diffraction particle size analyser (Coulter LS 13320).

Benthos samples were sieved using a 1 mm mesh size and all material and fauna remaining on the sieve were stored at 4-6% formaldehyde, buffered with borax and stained with Rose Bengal (CAS Number: 4159-77-7). In the laboratory, all macrozoobenthos were sorted out of the sample and identified to the lowest possible taxonomic level. Per taxon, dry weight was determined after oven drying them for 2-3 days at 60°C and ash free dry weight was measured after 5 hours combustion at 560°C. For details on the laboratory procedure, we refer to Compton et al. (2013) and Bijleveld et al. (2025). For our main analysis, we focused on the abundance data, as biomass could not be established for all species because samples sometimes contained only a limited number of individuals with a small body size, which therefore fell below the detection limit of the scale. We validated our findings by repeating the analysis with the available biomass data.

Sediment composition and other environmental variables

To explore whether sediments changed over the studied period, we tested for trends of both median grain size (d_{50}) and mud content. We constructed linear regression models of sediment composition over time (year) for all stations which were sampled at least 3 times and mapped the slope parameters of all significant regressions.

We explored the correlations between d_{50}, mud content and several other environmental variables. Elevation data were obtained from the bathymetric survey done by Rijkswaterstaat in 2015. Mean salinity, salinity variation, current velocity and bed shear stress were obtained from the Dutch Wadden Sea Model (DWSM) in Delft3D-Flexible Mesh (FM) (Van Weerdenburg 2024). Bed level change since 2014 was obtained from a stratigraphic model (Pearson et al. 2020). To explore the significance of d_{50} and mud % as predictors of community composition, we performed a redundancy analysis (RDA). Benthos abundance data was transformed to relative abundance, i.e. the number of individuals per species was divided by the total number of individuals in the sample. Environmental data was standardised by centring and scaling. We checked environmental variables for collinearity using variance inflation factors (VIFs). A higher VIF value means a stronger collinearity with other variables. We sequentially eliminated variables with the highest VIF, until all variables showed VIF below 10 (Montgomery and

Peck 1992). This resulted in the removal of current velocity and mean salinity. We performed stepwise forward and backward selection of variables, with 999 permutations for each test and a *p*-value threshold for inclusion at 0.05 and for exclusion at 0.1. Next, we tested the significance of the resulting RDA and each selected variable (d_{50}, mud %, salinity variability, bottom shear stress, orbital velocity, elevation and bed level change) through permutation tests, with 999 permutations.

Species-sediment relations by quantile regression

Quantile regression enables to study differential responses of benthos over sediment of different ends of a species' distribution. When multiple variables are limiting abundance, the top quantiles reflect the instances in which all variables are supposedly least limiting. Therefore, these quantiles are the best representation of the potential species distribution over the variable of interest (Cade and Noon 2003). We use the τ=0.95 quantile, representing the value under which 95% of the observations is expected to fall. This 95th quantile strikes a balance between displaying the upper end of the taxon's distribution, and minimising the effect of outliers, to which higher quantiles are sensitive (Cade et al. 1999; Anderson 2008).

Here we are interested in the role of grain size and mud percentage. The dataset needs to be sufficiently large to encompass optimal conditions for all measured and unmeasured variables over the gradient of interest. As the extensive sampling schemes cover the whole tidal basin, this guaranteed that we captured all possible abiotic gradients. Samples were taken from inter- to subtidal locations, and from muddy to sandy sediments characterized by high to low-dynamic conditions. However, as the sampling resolution between the intertidal and subtidal areas in the original data sets differed, 78% of the samples were from the intertidal. To correct for spatial autocorrelation and to balance the number of inter- and subtidal stations, the data was spatially resampled with a minimum distance between stations set to 750 m. This resampling, which was repeated 100 times, resulted in subsample datasets with on average 1150 samples, of which approximately 60% were intertidal stations. See figure S1 for an example of a spatial subset.

Fitting the upper quantiles can be problematic when data density is low. Therefore, only taxa occurring in at least 10% of the samples were selected for quantile regression model fitting, which resulted in the selection of 22 taxa. Furthermore, to prevent overestimation of abundance at the extremes of the sediment gradi-

ent, where data was also scarce, we removed the lower and upper percentile of d_{50} observations and the upper percentile of mud content observations. Absences of biota observations were assumed to reflect unsuitable habitat conditions. Therefore, zeros were included in the analysis, although these have a minimal influence on the modelled relationship when using the 95th quantile (Cade et al. 1999).

Since benthos-sediment relationships are generally not linear, we constructed non-linear quantile regression models using B-splines (Koenker et al. 1994; Thompson et al. 2010). With B-spline smoothing, piecewise polynomials of a specified degree are fitted without predetermining curve shape by a function. For selecting the appropriate polynomial spline degrees, we used Akaike's information criterion corrected for small samples (AICc) (Hurvich and Tsai 1990; Burnham and Anderson 2004). As suggested in previous studies (Cade et al. 2005; Anderson 2008; Cozzoli et al. 2013), we fitted models with 2, 3, 4 or 5 spline degrees and selected the model with the lowest AICc. To further smoothen the model fit, we used a lasso algorithm (Tibshirani 1996), with parameter lambda = 1. The R code for constructing the quantile regression models can be found in the appendix (Supplement B).

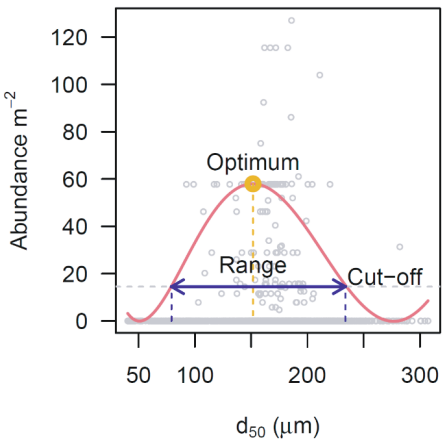

Figure 2. Conceptual illustration of the derivation of the taxon sediment preference. Indicated are sediment optimum (yellow circle) of the 95th spline regression quantile (red curve), and range (blue arrows), determined by the curve width at a cutoff of 25% of the optimal abundance. The observations, including zero's, are plotted in grey.

The spatial resampling followed by quantile regression model fitting was performed 100 times. For individual taxa, the maximum abundance of the 95th quantile distribution demarcated the sediment optimum. We defined the minimum and maximum of the optimum tolerance range by the sediment composition at a curve cutoff of 25% of the abundance optimum (Fig. 2). The optimum and minimum and maximum tolerance per taxon were calculated, averaged over all rounds of resampling.

Community sediment sensitivity

For each sample, we estimated the community weighted mean sediment optimum (CWM_{d50} and CWM_{mud}). This was done as follows (eq. 1), weighing the sediment optima (*opt*) by the relative abundances (*w*) of each taxon *i* in that specific sample:

$$\mathrm{CWM} = \sum_{i=1}^{n} (opt_i \cdot w_i) \qquad \text{(eq. 1)}$$

We then determined the difference between this inferred community sediment optimum and the actual sediment composition for each sample, with respect to the d_{50} and mud content (Δ_{d50} and Δ_{mud}; eq. 2):

$$\Delta_{d50} = d_{50} - \mathrm{CWM_{d50}} \quad \text{and} \quad \Delta_{mud} = mud\,\% - \mathrm{CWM_{mud}} \qquad \text{(eq. 2)}$$

We compared the distributions of these residuals for the intertidal and subtidal area and mapped the mean value per station over the entire study period. For each sample, we also determined which fraction of the taxa occurred outside their preferred sediment range.

All analyses were performed in R version 4.4.1 (R Core Team 2024), with the packages "vegan" (Oksanen et al. 2024) for multivariate analysis, "quantreg" (Koenker 2024) for fitting quantile regression models, and "spatialEco" (Evans and Murphy 2023) for spatial subsampling.

Results

Sediment and environmental variables

Sediment was finest on the intertidal flats near the mainland coast (Fig. 3a and d). The coarsest sediments are found in the deeper subtidal gullies in the basin and at the ebb-tidal delta outside of the inlet. Median grain size (d_{50}) ranged from 19–431 µm with a median of 161 µm, and mud fraction ranged from 0–81 % with a median of 6 %. Sediment composition did not show distinct linear temporal trends over the studied period for the entire basin (fig. 3b and e), nor did we observe spatial patterns in coarsening or fining during our study period (fig. 3c and f).

Mud content and d_{50} were related, and showed correlations with elevation, salinity and hydrodynamics (see fig. S2 for correlations between all parameters). The RDA analysis (R^2_{adj} = 0.14, p = 0.001; table S1) showed that mud content was the main variable driving community composition. The first RDA axis (explaining 7.8 % of the total variation) was mostly related to sediment composition, while the second axis (explaining 4.6 % of the total variation) was mostly related to elevation and bottom shear stress (fig. S3).

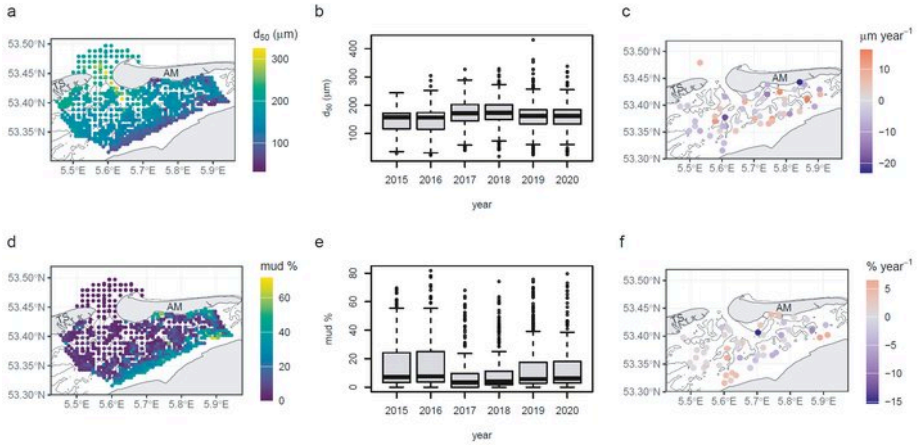

Figure 3. Spatial and temporal distribution of sediment composition: (a) mean d_{50} and (d) mud content per station over all sampled timepoints; boxplot of (b) d_{50} and (e) mud content per year; and trends in (c) d_{50} and (f) mud content, quantified as the slope of (significant) linear regressions of sediment composition over time.

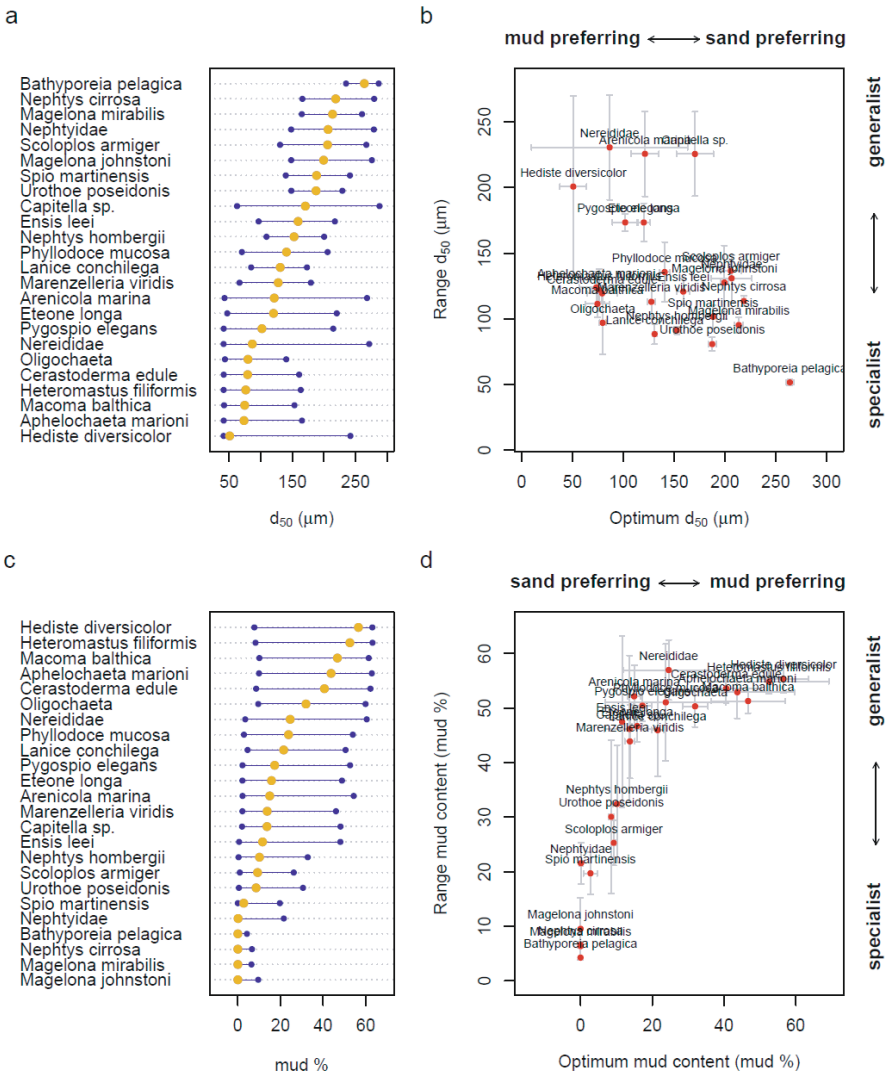

Figure 4. Taxon-specific sediment preferences. (a) d_{50} and (c) mud content optima (orange dot) and range (blue segments) for taxa selected for this study. Position of optimum (b) d_{50} and (d) mud content (%) compared to range breadth, which indicates the level of sediment preference and specialisation. Error bars in b and d show the standard deviations of optimum and range breadth over 100 spatial subsampling permutations and consecutive quantile regression model fitting.

Species sediment relations

For the 22 most abundant taxa, clear abundance maxima of the 95th quantile for both d_{50} and mud content were found (see for example quantile regressions fig. S4, and for a table containing all optima and sediment ranges table S2). Figures 4a (d_{50}) and 4c (mud) show that taxon sediment optima range from coarse to fine sediment. For instance, *Nephtys cirrosa*, *Magelona mirabilis* and *Scoloplos armiger* show sand preference while *Hediste diversicolor*, *Heteromastus filiformis* and *Macoma balthica* show mud preference.

There are large differences in the tolerance ranges of different species. Generalist species with the largest tolerance ranges (wider than 200 µm) are *Hediste diversicolor*, *Arenicola marina* and *Nereididae*. More specialised species like *Urothoe poseidonis*, *Lanice conchilega* and *Nephtys hombergii* have a tolerance ranges smaller than 100 µm (Fig. 4a).

Species with a preference for sand (e.g. *Magelona johnstoni*, *Magelona mirabilis* and *Nephtys cirrosa*) have generally narrower tolerance ranges than species with a preference for mud (e.g. *Hediste diversicolor*, *Heteromastus filiformis* and *Macoma balthica*). This is reflected in a negative relationship between sediment grain size optimum and tolerance range (Fig. 4b), and a positive relationship between optimal mud content and tolerance (Fig. 4d).

Sediment optima calculated based on biomass data show a strong relation with abundance-based optima (Fig. S5). Only for a few taxa, biomass and abundance optima differ. Several species have a higher d_{50} optimum (most pronounced in *Arenicola marina*, *Hediste diversicolor*, *Nephtys cirrosa*, *Magelona mirabilis* and *Magelona johnstoni*) or a lower mud content optimum (*Hediste diversicolor*, *Heteromastus filiformis* and *Macoma balthica*) for biomass compared to abundance. This means that these species reached their highest biomass in coarser sediment, compared to where they reach their highest abundance. *Marenzelleria viridis* is the only species with a pronounced sandier abundance optimum and muddier biomass optimum.

Community sediment preference and sensitivity

The mean community weighted optimum for median grain size (CWM_{d50}) ranges from approximately 50 to 270 µm (Fig. 5b). In the intertidal zone, CWM_{d50} lies most frequently below 150 µm while in the subtidal Wadden Sea and in the ebb-tidal delta, optima above 150 µm occur more frequently. CWM_{mud} displays peaks at

0% mud, mostly representing subtidal stations containing benthos with a sand preference, and between 10 and 20% mud.

The difference between the CWM_{d50} and the actual d_{50} (Δ_{d50}) per sample is skewed to the right, i.e., in many places the sediment is coarser than the optimum of the actual community. This difference is most pronounced in the intertidal zone. In the subtidal Δ_{d50} is centred around 0 (Fig. 5c).

The average Δ_{mud} has a negative skew (Fig. 5f). This suggests that actual mud content lies below the preferred optimum of the communities. Again, this skewness is most pronounced in the intertidal but also present in the subtidal.

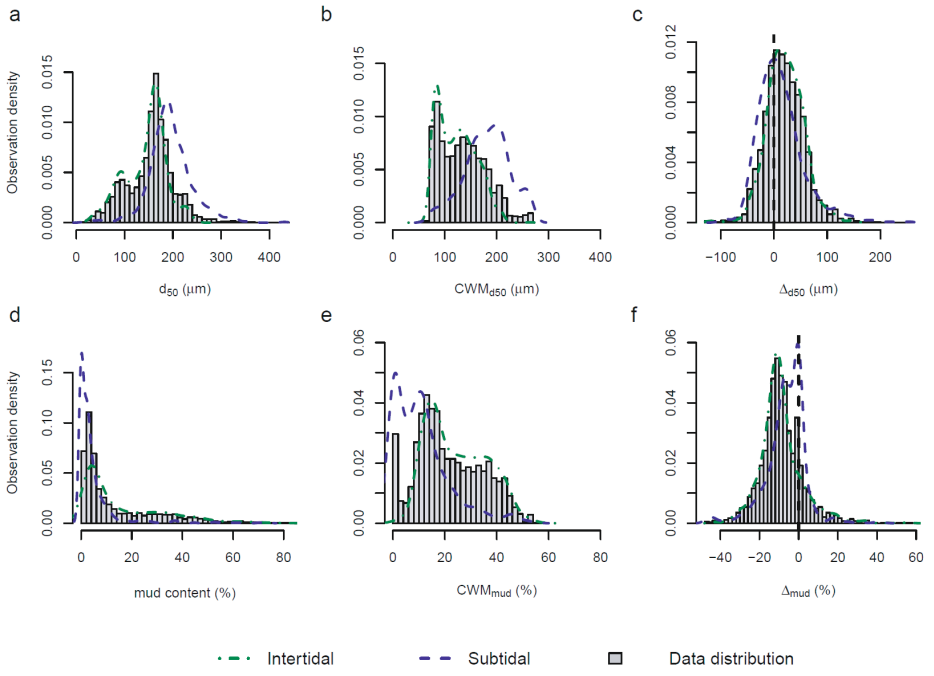

Figure 5. Distribution of sediment composition, community optimum and community-sediment mismatch. The observation density for (a) d_{50} and (d) mud content; (b) community weighted mean (CWM) optimum d_{50} and (e) mud content; and (c; f) difference between sediment composition and CWM optimum per station (Δ_{d50} and Δ_{mud} resp.).

Looking closer at which taxa are responsible for these community-level patterns, we found that the distribution of more than half of the surveyed taxa is skewed towards coarser than optimal sediments (Fig. S6). For a few, mainly sand-prefer-

ring, taxa (*Bathyporeia pelagica, Scoloplos armiger, Nephtys cirrosa*, *Magelona mirabilis* and *Magelona johnstoni*), sediment was often finer than optimal. Taxa for which the sediment preference matched the actual sediment characteristics, i.e., the distribution of Δ_{d50} and Δ_{mud} was centred around 0, are *Capitella sp.* and *Ensis leei* for d_{50}, and *Spio martinensis* and the sand-preferring taxa for mud content.

Temporally, neither Δ_{d50} nor Δ_{mud} showed linear trends over the studied period (Fig. S7).

Spatial patterns

There are coherent spatial patterns in the distribution of both Δ_{d50} and Δ_{mud} (Fig. 6a and b). Stations in the intertidal and subtidal zone as well as stations in the ebb-tidal delta have positive values for Δ_{d50}. This indicates that the actual d_{50} is above the community optimum that is calculated based on the preferences of individual species. Also, stations from the watershed south of Terschelling show a mismatch towards coarser grainsizes. In contrast, along the mainland coast, at the watershed south of Ameland and in several stations near the southern coast of Ameland, d_{50} is below the community optimum (negative Δ_{d50} values), denoting finer than optimal sediments. In line with this, Δ_{mud} is negative for most stations, i.e., mud content is below the level which would be expected based on the average community preference (Fig. 6b).

Locations where the actual sediment composition lies beyond the optimal range for a large fraction of the present community are spatially clustered. At the intertidal areas south of the eastern part of Terschelling as well as the western part of Ameland, the d_{50} is larger than the optimum range of significant fractions (up to approximately 75%) of the present species (Fig. 6d). The stations where d_{50} is finer than preferred are located at the ebb-tidal delta and the ends of the gullies south of Ameland (Fig. 6b). Mud content is lower than the sediment preference range of >25% of the community at large parts of the intertidal area, except in the regions close to the mainland coast and the watershed south of Ameland (Fig. 6e). Only at a few stations, mud content is above the preference range for fauna (Fig. 6f).

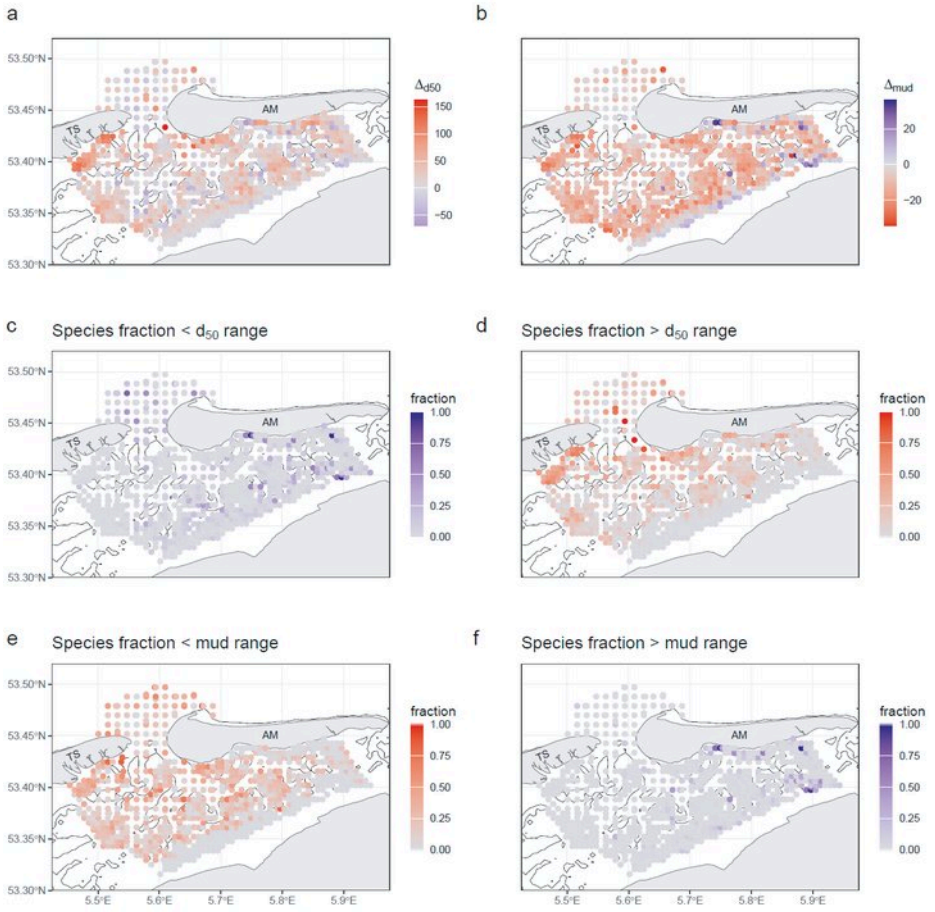

Figure 6. Spatial patterns in sediment sensitivity. The differences (a; b) between sediment composition and CWM optimum per station, Δ_{d50} (µm) and Δ_{mud} (%), indicate whether the sediment is coarser/sandier (red) or finer/muddier (blue) than optimal for the present community. The fraction of the present taxa occurring (c) below or (d) above their d_{50} range, i.e. for which the sediment is almost too fine (blue, c) or too coarse (red, d). The fraction of the present taxa occurred (e) below or (f) above their mud content range, for which the sediment is nearly too sandy (red, e) or too muddy (blue, f). All values shown are averaged over all sampled time points per station.

Discussion

Validity of benthos-sediment relations using quantile regression

Quantile regression is still not widely applied in benthic ecology, one of the reasons being that sufficiently large datasets containing samples over the environmental gradient are required to capture the complete biological response. In the current study, we had access to such a dataset. By using non-linear regression splines of the 95th quantile, we derive benthos-sediment relations which are robust to outliers and covariates and flexible in shape. Compared to previous quantile regression applications in benthic species distribution modelling (Vaz et al. 2008; Anderson 2008; Cozzoli et al. 2013; Cozzoli et al. 2014; Cozzoli et al. 2017; Chauvel et al. 2024), our approach has several additional advantages. Firstly, spatial resampling allowed us to obtain error margins of the predicted model parameters, besides correcting for spatial autocorrelation and balancing the amount of inter- and subtidal data. Furthermore, summarising taxon-derived optima and tolerance on community level enabled us to scale up sensitivity predictions to the entire macrozoobenthic community. Nevertheless, a few limitations of the method should be considered.

Firstly, we assumed that the range of observations in our study contained the optima for all abiotic variables present within our dataset. However, within a single system, this is rarely the case (Thrush et al. 2005). For constructing more reliable benthos-sediment relations, data from different systems with a wider range of environmental conditions is desirable. Secondly, by using the highest quantiles as a reference of maximum species abundance over the sediment gradient, we assume other variables to be constraining. The highest quantiles describe the relation with the sediment less accurately when many facilitating rather than limiting processes are at play (Cade et al. 2005). This may be the case in the intertidal Wadden Sea, where facilitating biotic interactions, such as provided by habitat builders are prevalent (Rademaker et al. 2025). Furthermore, although here we related biota to gradients in sediment composition, some relevant sediment properties, such as cohesiveness, change abruptly rather than gradually (Van Ledden et al. 2004; Colina Alonso et al. 2022). This quality is not linearly reflected in the d_{50} or mud content, therefore we recommend for future studies to look further than these commonly used proxies. Lastly, the methods used in this study describe patterns rather than causation. Not all animals are solely subject to the physical dynamics of the sediment they live in. Some do also actively modify sediment composition, so that benthos-sediment relations

are often two-way interactions. For instance, *A. marina* has been described to coarsen the sediment (Volkenborn et al. 2009; Wendelboe et al. 2013), and *C. edule* to increase fine sediment resuspension (Li et al. 2017) with their destabilising burrowing activity. Through bioturbation, benthic fauna can modify the morphology and sediment composition of their sedimentary habitat on a large scale (Cozzoli et al. 2021; Brückner et al. 2025). However, it remains to be investigated, whether by this bioengineering organisms actually create their preferred sediment habitat (Soissons et al. 2019).

The taxon optima and ranges we defined with the 95th quantile, reflect the potential rather than the realised sediment habitat (Vaz et al. 2008). The actual species' distribution is determined by a myriad of other limiting variables. To gain a mechanistic understanding of why species occur in suboptimal sediments, experimental studies testing interactions with other variables such as food availability, hydrodynamics and interspecific interactions are needed. In suboptimal sediment conditions, species and communities are less resilient to other stressors, such as climate-change related heatwaves and storms (e.g. St-Onge et al. (2007)). To understand the eco-physiological implications for benthic species living outside of their preferred sediment habitat, multiple-stressor experiments are needed.

Most species show sediment preference but few show exclusivity

The order of taxon sediment preference from fine to coarse corresponds to previously described sediment associations of benthic fauna in a comparable geographical area (amongst others, Armonies 2021; Cozzoli et al. 2013; Nehmer & Kröncke 2003; Reiss & Kröncke 2001). Although in most cases, calculated sediment preferences based on biomass corresponded well to preferences based on abundance, we observed differences for a few taxa. These discrepancies might be related to ontogenetic changes in habitat preferences. For instance, for *A. marina*, the differential sediment optima for biomass compared to abundance suggests that fewer but larger individuals are found in coarser sediments. This can be linked to secondary migration of this species from high in the intertidal, where they live as juveniles, to lower in the intertidal for the adult life stage (Beukema and De Vlas 1979). Besides ontogenetic changes in habitat preference, sediment composition may relate to differential growth rates or maximum body size (Witbaard et al. 2001).

While most species considered in this study had wide tolerance ranges, only a few taxa could be considered true sediment generalists. Only 4 taxa (Nereididae,

A. marina, *Capitella sp.* and *H. diversicolor*) had a d_{50} range wider than 200 µm; and only 3 taxa (Nereididae, *H. diversicolor* and *H. filiformis*) had a mud range wider than 55%. Likewise, Armonies (2021) observed few sediment generalists among North Sea benthos. We did not identify true sediment specialists either: d_{50} tolerance ranges were wider than 80 µm for all taxa but one (*B. pelagica*); mud content tolerance ranges were wider than 20% for all but four taxa (*N. cirrosa*, *M. johnstoni*, *M. mirabilis* and *B. pelagica*). Partly, this is a methodological effect: since quantile regression requires a large sample size, species observed in less than 10% of the samples were not considered. Therefore, species, specialized to specific conditions, are probably not retained for the analysis. Our findings thus underline the view that at least the most prevalent benthic species are not restricted to a single type of sediment, even if they show preference for certain sediments over others (Snelgrove and Butman 1994; Armonies 2021).

Furthermore, we observed differential mud tolerance between sand- and mud preferring taxa. Sand-preferring taxa were less tolerant to variations in mud content. These findings correspond with Robertson et al. (2015), who found that taxa with a preference for low mud content were generally more specialised in terms of sediment composition. This could have several explanations. Mud content is generally more variable in muddy areas than in sandy habitats (Colina Alonso et al. 2022). Besides, living in mud requires certain adaptations, such as tolerance to anoxic stress and mechanisms to separate fine sediment particles from food (Snelgrove and Butman 1994; Robertson et al. 2015). This means that organisms inhabiting muddy habitats need these specific adaptations and need to tolerate a variable sediment composition, whereas organisms living predominantly in sand might lack the biological adaptations to tolerate mud.

Other studies have presented benthos-sediment relations in the context of functional traits. In many studies, a shift is documented from small, short lived, deposit feeders in muddy sediments to large, long-lived suspension feeders in sandy sediments (amongst others, Gusmao et al. 2022; Rhoads & Young 1970; van der Wal et al. 2017). Although we did not focus on traits in this study, the species order we found along the sediment gradient does not underline this transition. On the contrary, suspension feeders (e.g., *C. edule*, *M. balthica*, *E. leei* and *L. conchilega*) preferred intermediate to muddy sediment and had relatively wide tolerance ranges for mud (>45% mud). Due to the tidal currents in this dynamic system, areas with coarser sediment are not necessarily less turbid than muddy areas, meaning that they are not always more suitable for suspension feeding.

Besides, some of these suspension feeders (e.g. *M. balthica*) are also facultative surface deposit feeders, utilising the microphytobenthos in muddy areas (Christianen et al. 2017).

Spatially clustered mismatches between community preference and observed sediment

In the subtidal, the actual sediment distribution generally matched the preferences of the resident species. In contrast, in the intertidal, the sediment characteristics are often coarser than the optimal sediment of the community. It appears that the few fine-grained intertidal sites provide optimal conditions, and species reach high densities, so that these sites shape the sediment optima. At the more prevalent sandier sites, the species are still present, but do not reach the optimal density or biomass. It has been shown that non-trophic interactions, such as facilitation, can enhance abundances in muddy sediment. For instance, small worms such as *H. filiformis* can oxygenate muddy sediments, increasing the inhabitable depth of the sediment (Van Colen et al. 2008), and cockles (*C. edule*) can promote microphytobenthos growth, increasing food availability for other species (Eriksson et al. 2017). Alternatively, facilitation may ameliorate conditions in sandy sediments (Bruno et al. 2003). This could widen the tolerance range towards coarse sediments, while not shifting the optimum, if individual densities remain low. Spatially, the mismatch between optimal and realized sediment habitats was most evident at intertidal, coarse-grained stations. Furthermore, we identified clusters of stations where many species occur beyond their optimal sediment envelope. Such locations are usually found at the tidal flats beneath the head and tail of islands bordering the basin on the northern side. The discrepancies were not clearly linked to a few specific species.

A causal link of the above patterns with the 2018 ebb-tidal delta sand nourishment cannot be made, as we observed no change in Δ_{d50}, Δ_{mud} or sediment composition before and after the nourishment. This is in line with modelled sediment pathways, which suggest that it is unlikely that nourishment sand was transported to the locations where we observe sediment mismatches (Pearson et al. 2020; Pearson et al. 2021a). The locations where sediment is almost too fine for many species are situated near the inner ends of the channels and near both the mainland and Ameland ferry harbour. Here, there might be a link with ongoing human activities, such as dredging and dumping of dredged sediments. The ferry harbours and channels are continuously dredged for navigability, after which the dredged areas are filled in with mud (Rijkswaterstaat 2022). Next to

that, disposal of the dredged deposits can lead to an additional supply of mud. However, overall, most sites in our dataset are sandier than the current community prefers. It is crucial to monitor sediment composition at locations where large portions of the community are living beyond their optimal sediment range, as here even a small shift could render the habitat unsuitable for the current benthic species.

Future risks for benthic communities through sandification

As mismatches between sediment optima and habitat were stable over the studied period, communities do not seem to be shifting away from suboptimal sediments within the studied time frame. However, the skewed mismatches (Fig. 5c and f) suggest that, if this basin was to become sandier, less ideal sediment habitat might remain for current macrozoobenthos communities. This risk is largest in the intertidal areas where the difference between optimal and realised habitat is already more pronounced. Besides the foreseen sandification, which we have focussed on here, regional "muddification" of sediments also needs to be considered. For instance, in the Wadden Sea, land subsidence due to gas drilling has resulted in regional fining of the sediment by an average 1 µm decrease of d_{50} and a 3% increase of mud content per year (de la Barra et al. 2023). Given the observed wide tolerance ranges from mud-preferring species, this will likely not result quickly in a community shift. However, such sediment fining should be monitored, especially in areas where species are already living on the edge of their mud tolerance range.

In addition to sand nourishments directly on or in front of a sandy coast, sediment nourishments could be a means to conserve intertidal habitats. Although nourishments are a highly artificial measure, they can supply sediment to prevent loss of ecosystem values when tidal flats drown due to natural and human-induced dynamics (Kabat et al. 2012). However, they should be planned and implemented carefully. Several pilot nourishments aimed at restoring tidal flats have already been performed (van der Werf et al. 2015; van der Werf et al. 2019; Escaravage et al. 2024). Benthic communities at these nourished sites did not recover to reference levels during the monitored time, partly due to the layer thickness and coarse grain size used for the nourishments. Future nourishments using finer grains (e.g., Baptist et al. 2019) might recreate a more suitable habitat for the native benthic community. The findings of our study regarding sediment sensitivity could aid in the design when engineering natural habitats.

On a global scale, coastal sediments are subject to changes in hydrodynamics and depositional regimes due to sea level rise, changes in storm frequency and intensity, and alterations of sediment supply which might result in sandification. How coastal ecosystems will respond to this foreseen sandification depends on the sensitivity of communities to sediment properties such as grain size and mud content. The tools applied in this study aid in quantifying species and community sediment sensitivity, and can help to identify sensitive areas, where a change in sediment composition might further push the community outside of its preferred sediment habitat. Sensitivity maps as presented here could be used in combination with modelled sediment transport and composition, to predict future habitat suitability for benthic communities.

Conclusion

In this research, we revealed sediment preferences of macrozoobenthos, and the potential sensitivity to coarsening, "sandification", of coastal sediments. In our study area, the Borndiep, a tidal basin in the Dutch Wadden Sea, most of the studied macrozoobenthic taxa were sediment generalists, i.e., had a wide sediment preference range. Taxa that preferred coarse sediment, had narrower tolerance ranges than mud-preferring taxa. On community level, we observed a mismatch between actual sediment composition and the preferred sediment characteristics of the resident species. Sediments were in general coarser and contained less mud than expected based on weighted mean preferences, and this difference was more pronounced in intertidal than in subtidal areas. The tools applied in this study can highlight the ecological risks of sediment change and aid in assessing the potential impacts of sandification due to coastal engineering projects and sea level rise on coastal benthic communities.

Acknowledgements

We are very grateful to the current SIBES and Waddenmozaïek core-team for collecting and processing the thousands of samples. In alphabetical order they are Livia Brunner, Hailley Danielson-Owczynsky, Anne Dekinga, Job ten Horn, Anne de Jong, Loran Kleine Schaars, Adrienne Kooij, Anita Koolhaas, Hidde Kressin, Felianne van Leersum, Simone Miguel, Luc de Monte, Dennis Mosk, Dorien Oude Luttikhuis, Reyhaneh Roohi, Marten Tacoma, Evaline van Weerlee en Bas

de Wit. We also thank all former and current employees and the many volunteers and students who have ensured that the SIBES and Waddenmozaïek program have continued in recent years. In particular Bianka Rasch, Jeroen Kooijman and Sander Holthuijsen were essential for the Waddenmozaïek samples. The R.V. Navicula was essential for collecting the samples and in particular we thank the current crew Wim Jan Boon, Klaas Jan Daalder, Bram Fey, Hendrik Jan Lokhorst and Hein de Vries. For the abiotic data, we than Roy van Weerdenburg for data delivery and his assistance with the interpretation. This study was supported by NWO grant 17600: "Tracking Ameland Inlet Living Lab Sediment (TRAILS)". SIBES is currently financed by the Nederlandsche Aardolie Maatschappij NAM, the Directorate General for Public Works and Water Management (Rijkswaterstaat, RWS) and the Royal NIOZ. The subtidal Waddenmozaïek sampling campaign (also known as "Waddentools: habitatheterogeniteit"), was registered under reference number WF2018-187059, and funded by the Waddenfonds, Rijkswaterstaat and the provinces of Noord-Holland, Fryslân and Groningen. Oscar Franken was additionally funded by NWO grant VI.Veni.222.244.

Data availability

Data and R code used in this study are available in Kooistra et al. (2025b) https://doi-org.utrechtuniversity.idm.oclc.org/10.25850/nioz/7b.b.gj.

Supplementary materials

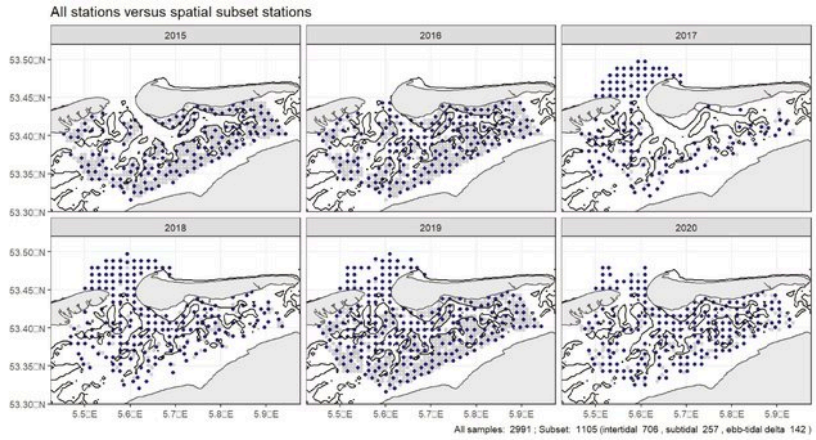

Figure S1. An example of spatial subsampling: all stations are shown in grey, the spatially subsampled stations are shown in dark blue.

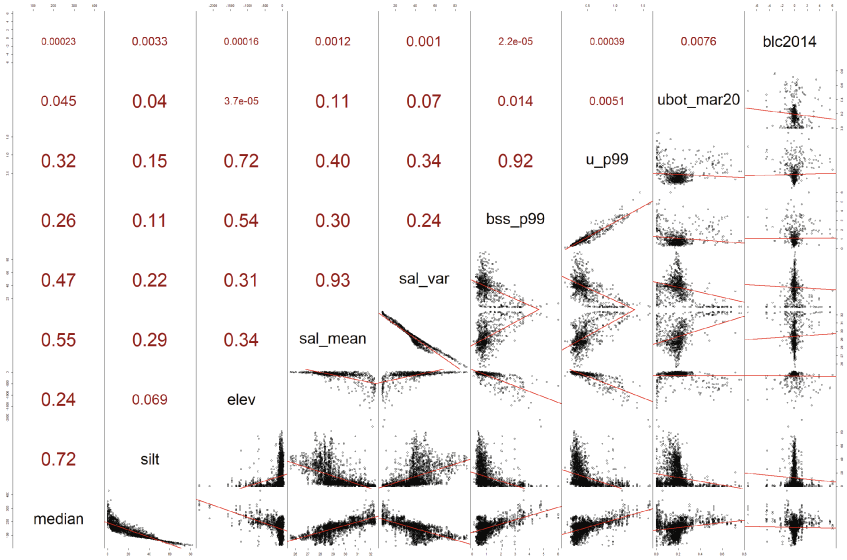

Figure S2. Distribution and correlations between sediment and other environmental parameters in the study area. The upper left panels show the correlation coefficient, the lower right the data and linear regressions. Variables from left to right: d50, mud content, elevation, mean salinity, salinity variance, bottom shear stress, current velocity, orbital velocity, bed level change since 2014).

Table S1. RDA after selection of variables; ANOVA table testing the significance of each variable. Variables from top to bottom: mud content, salinity variance, bottom shear stress, d_{50}, orbital velocity, elevation and bed level change since 2014.

	Df	Variance	F	*Pr* (>F)
mud	1	0.046008	221.1635	0.001
sal_var	1	0.024559	118.0568	0.001
bss_p99	1	0.009549	45.90253	0.001
median	1	0.005353	25.73433	0.001
ubot_mar20	1	0.004239	20.3777	0.001
elev	1	0.003521	16.92727	0.001
blc2014	1	0.000602	2.896252	0.002
Residual	2727	0.567287	NA	NA

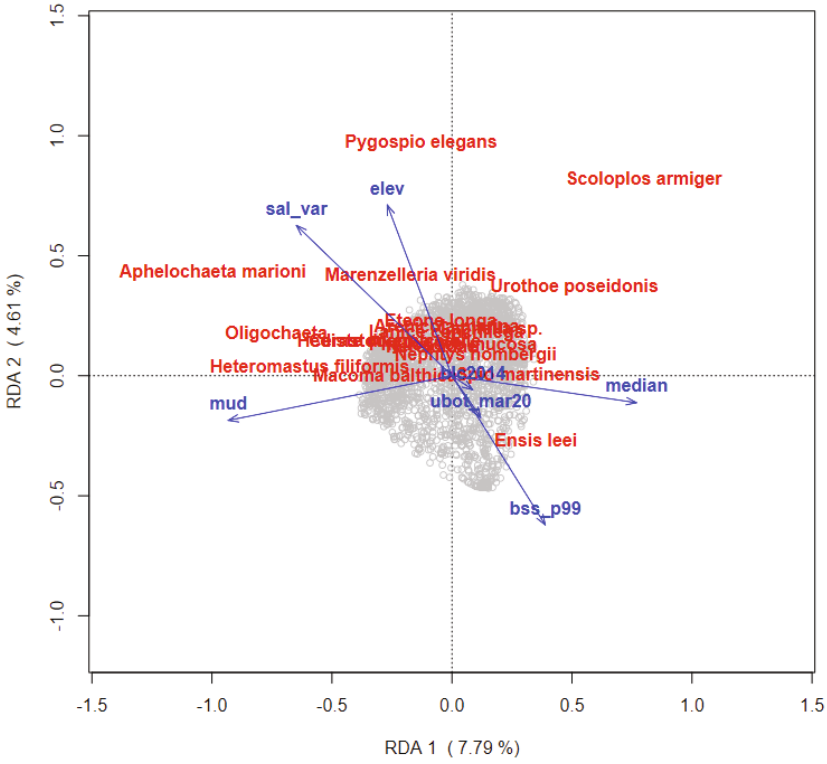

Figure S3. RDA biplot (scaling = 2) with stations (grey), species (red) and environmental factors (blue). R^2adj = 0.14, p=0.001.

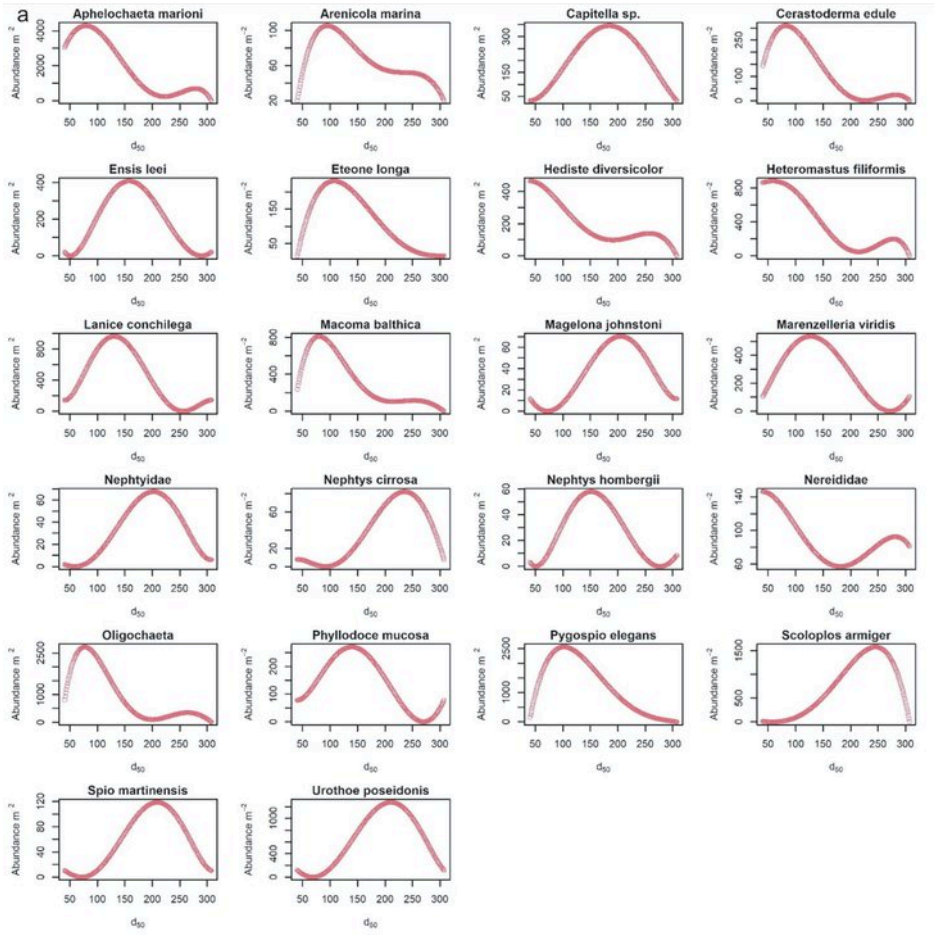

Figure S4a. An example of quantile regression with B-splines of abundance over d_{50} per taxon. The modelled 95th quantile is shown in red.

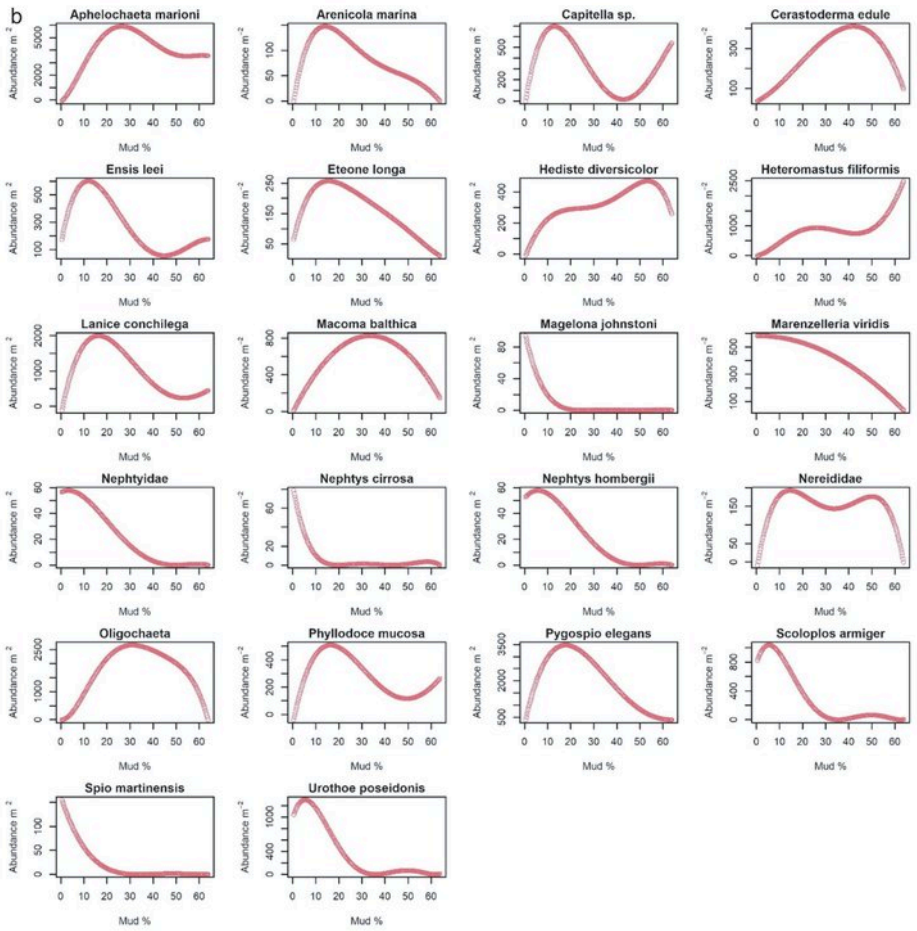

Figure S4b. An example of quantile regression with B-splines of abundance over or mud content per taxon. The modelled 95th quantile is shown in red.

Table S2. Derived d_{50} and mud content optima range minimum, maximum and range breadth for all taxa selected for this study.

Taxon	Opt d_{50} (µm)	Min d_{50} (µm)	Max d_{50} (µm)	Range d_{50} (µm)	Opt mud (%)	Min mud (%)	Max mud (%)	Range mud (%)
Aphelochaeta marioni	73.5	41	165	123.9	43.7	10	63	52.9
Arenicola marina	121.4	43	268	225.6	15.0	2	54	52.2
Bathyporeia pelagica	264.0	235	287	51.6	0.0	0	4	4.3
Capitella sp.	170.6	62	288	225.5	13.7	2	48	46.2
Cerastoderma edule	79.2	41	161	119.4	40.6	9	62	53.6
Ensis leei	159.1	97	217	120.7	11.6	1	48	47.5
Eteone longa	120.2	47	220	173.4	15.8	2	49	46.7
Hediste diversicolor	50.8	41	242	200.7	56.6	8	63	55.4
Heteromastus filiformis	76.3	41	163	122.0	52.6	8	63	54.9
Lanice conchilega	130.9	85	173	88.4	21.5	5	51	46.0
Macoma balthica	74.6	42	153	111.4	46.7	10	61	51.3
Magelona johnstoni	199.5	148	276	127.7	0.0	0	10	9.6
Magelona mirabilis	213.7	165	260	95.3	0.0	0	6	6.4
Marenzelleria viridis	127.7	66	179	113.0	13.8	2	46	43.9
Nephtyidae	206.6	148	279	130.9	0.1	0	22	21.6
Nephtys cirrosa	218.7	166	280	113.6	0.0	0	7	6.6
Nephtys hombergii	152.7	109	200	91.3	10.2	0	33	32.4
Nereididae	86.6	41	272	230.5	24.6	3	60	57.0
Oligochaeta	79.8	43	140	97.0	32.0	10	60	50.3
Phyllodoce mucosa	140.8	70	206	135.6	23.8	3	54	51.1
Pygospio elegans	101.9	41	215	173.4	17.3	2	53	50.5
Scoloplos armiger	205.8	131	267	136.5	9.3	1	26	25.3
Spio martinensis	188.4	140	241	101.6	2.8	0	20	19.7
Urothoe poseidonis	187.5	148	229	80.8	8.6	0	31	30.1

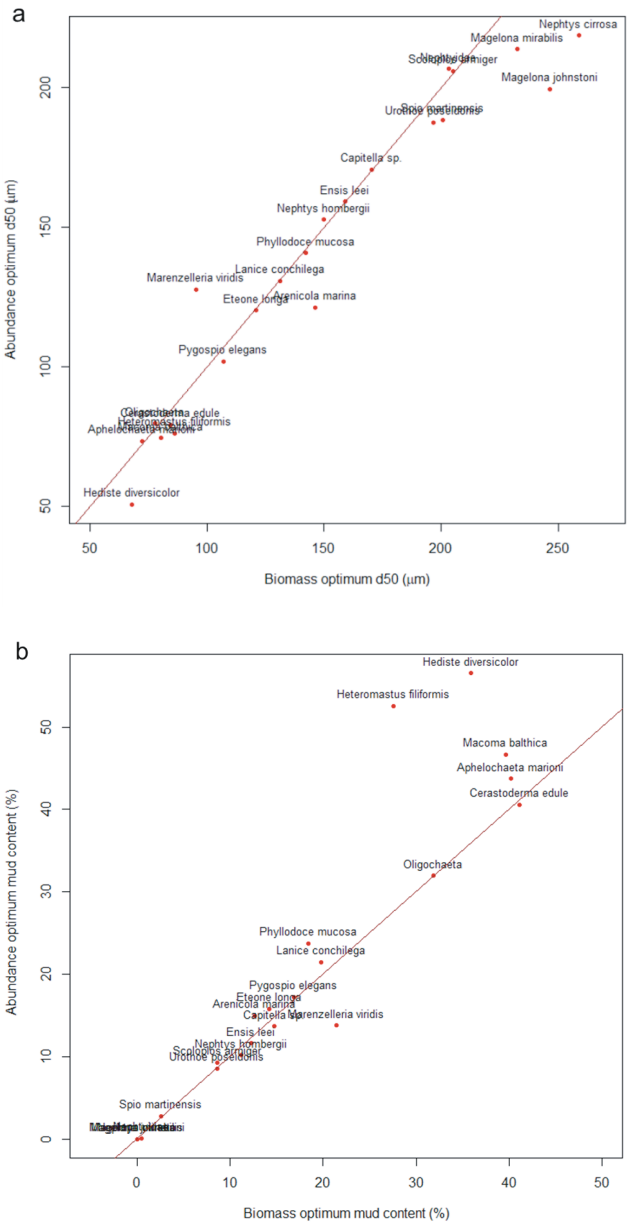

Figure S5. (a) d_{50} and (b) mud content optima based on abundance and biomass data compared. *Bathyporeia pelagica* and Nereididae are missing, because biomass data of these species is available for less than 10% of the samples.

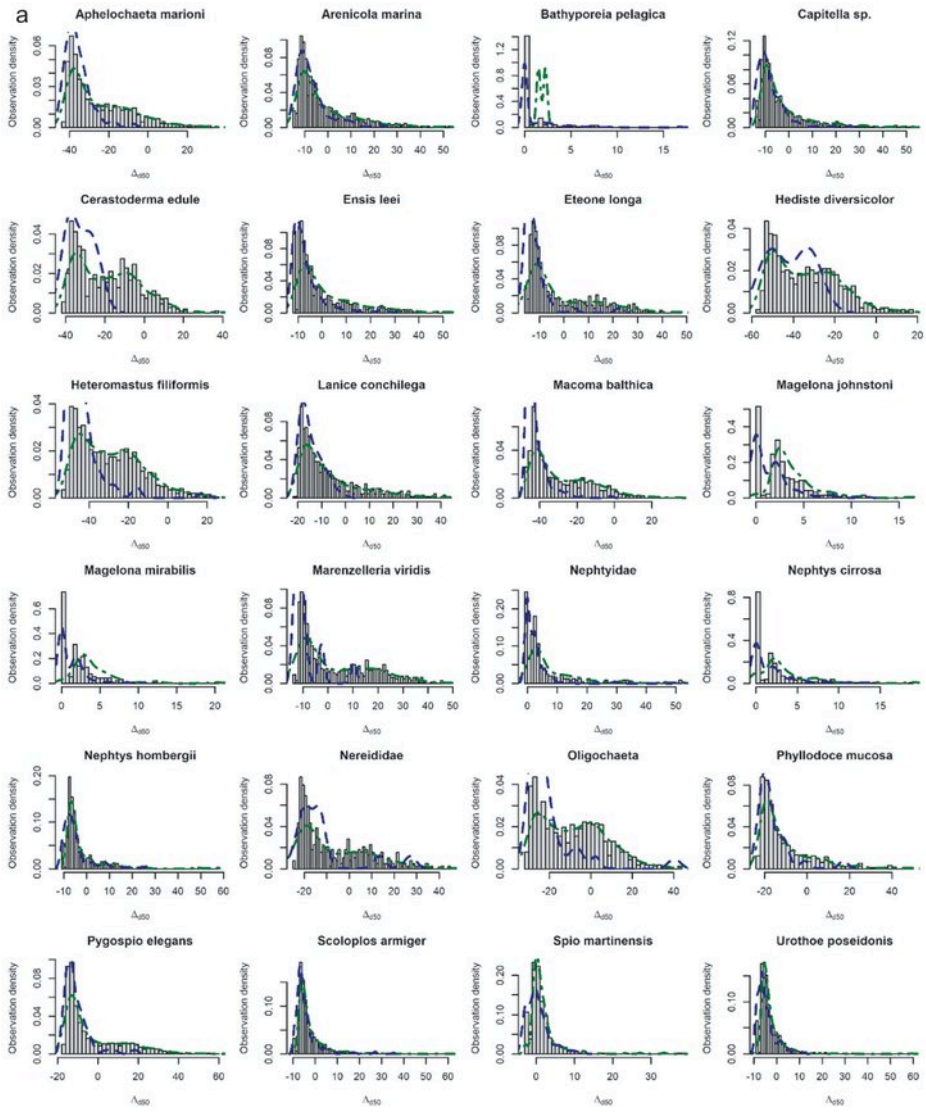

Figure S6. Observation distribution of Δ_{d50} (a) and Δ_{mud} (b) per taxon. The grey bars indicate the distribution of all data, the green striped-dotted line shows the distribution of intertidal observations and the blue striped line of subtidal observations.

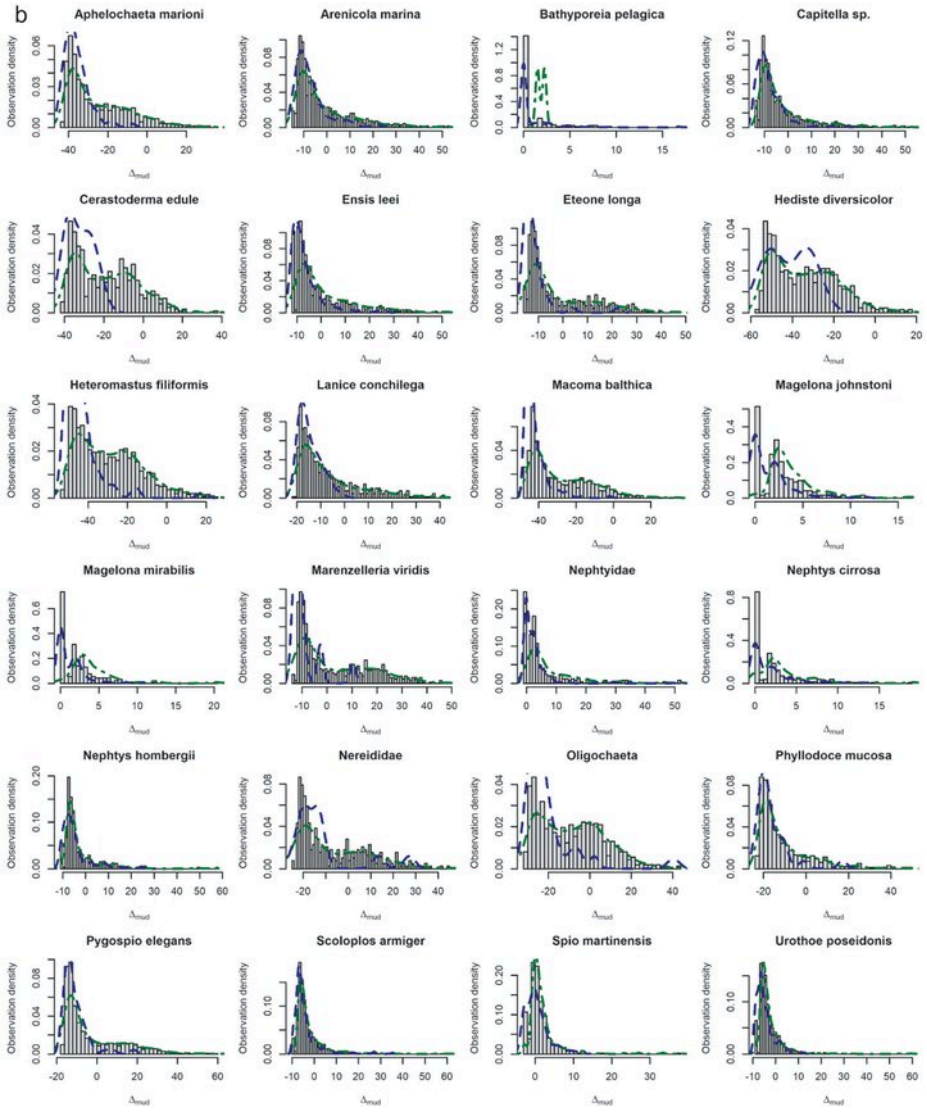

Figure S6. *(Continued)*

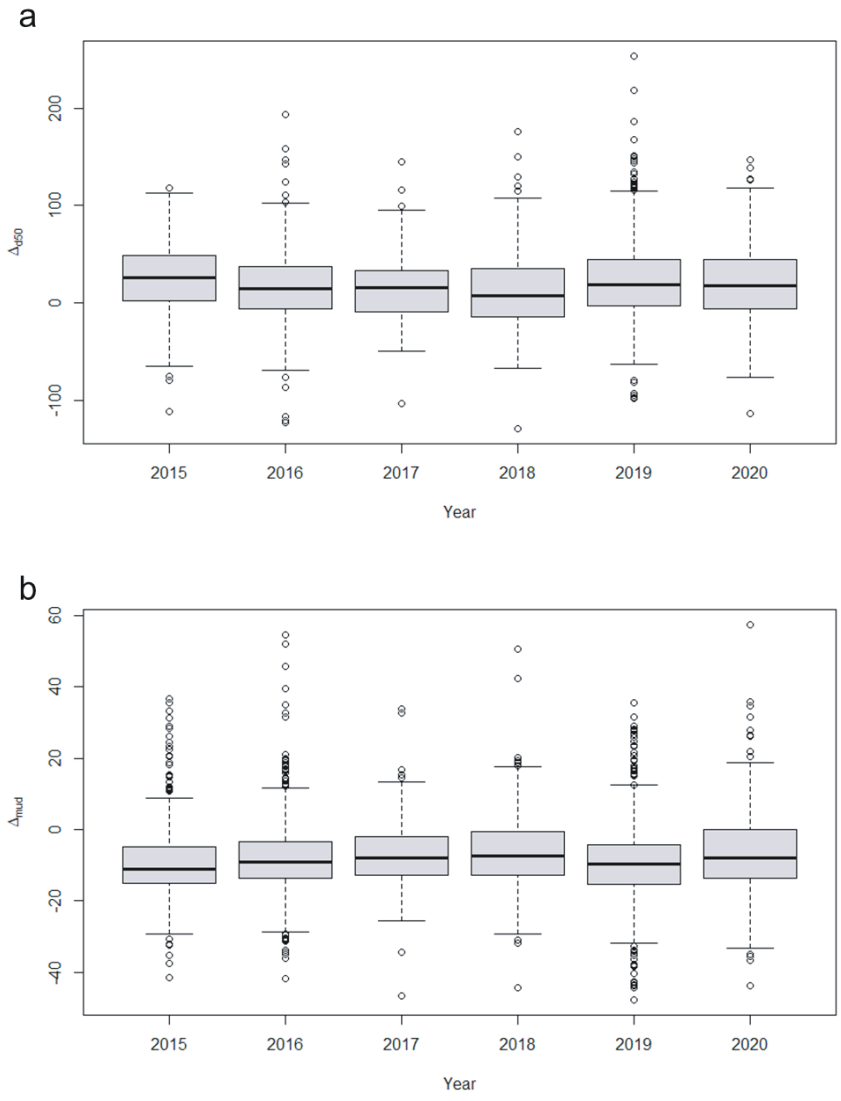

Figure S7. Mean Δ_{d50} (a) and Δ_{mud} (b) of all samples per year.

chapter 3

Sand, food and heatwave resilience

Sediment coarsening and heatwave tolerance of mud-dwelling benthos: a case study on *Scrobicularia plana*

Submitted

Tjitske J. Kooistra, Tjeerd J. Bouma, Stuart G. Pearson, Karline Soetaert, Rob Witbaard

Abstract

With global warming, heatwaves are increasing in frequency, intensity and duration. Additionally, coastal sediments are in many places foreseen to coarsen under sea level rise. To predict the resilience of organisms inhabiting shallow coastal habitats, we need to test their tolerance to these multiple, potentially interacting stressors. The peppery furrow clam, *Scrobicularia plana*, is known as a mud dweller, inhabiting fine-grained intertidal flats. To investigate this species' sensitivity to heatwaves upon habitat change, we performed a mesocosm experiment. Our hypothesis that their muddy sediment preference is driven by food content, and that with sufficient food availability, the clam would perform equally well in sandy habitats was refuted: we observed high mortality in sandy sediment regardless of food availability. While condition index and respiration rate were not impaired, slower reburial rate in sands and lower full valve opening indicated that the mechanical properties of the sandy sediments resulted in a reduced substrate suitability for this species. Only in mud, clams increased full gaping in response to a higher food supply. Although a heatwave did not significantly impact survival, the lower frequency of closed valves pointed towards higher energy expenditure under heat exposure. To conclude, although the species is relatively resilient, a sub-optimal sediment type combined with additive stressors may negatively affect this species under future climatic conditions.

Introduction

Intertidal flats are productive ecosystems which support a high diversity and biomass and provide essential ecosystem services. Due to the proximity of human populations and the changing climate, these ecosystems are subject to environmental change. Firstly, climate change is resulting in an increased temperature and stronger and more frequent atmospheric as well as marine heatwaves (Frölicher et al. 2018, Oliver et al. 2021, IPCC 2023). Secondly, climate-change related sea level rise and meteorological changes are foreseen to cause stronger wave forcing on shallow tidal flats (Zhu et al. 2020). Together with a decrease in fine sediment supply due to the damming of rivers, this may lead to sediment coarsening, or "sandification" of previously muddy intertidal flats (Syvitski et al. 2022, Liu et al. 2022, Colina Alonso et al. 2024).

The inhabitants of the intertidal are not only affected by increasing water temperatures and marine heatwaves. When the tide is low they are also exposed to atmospheric warming and insolation (Johnson 1965, Helmuth et al. 2002). To a certain level, intertidal species are more adapted to larger temperature fluctuations compared to subtidal biota (Stillman et al. 2025). However, with increasing heatwave occurrence in recent years, mass mortalities have been reported (Seuront et al. 2019, Raymond et al. 2022, Hesketh & Harley 2023). One of the species groups sensitive to heatwaves are bivalves, an important component of intertidal soft-bottom ecosystems (Soon & Ransangan 2019, Masanja et al. 2023). The effects of a change in sediment composition may interact with heatwave effects on benthic animals. To cope with heatwaves, animals may need to increase their burial movements (Zhou et al. 2022, 2023). Besides, thermal conductivity and heat capacity differs between sediment types (Liu et al. 2025).

Exposure to multiple stressors and suboptimal habitat conditions may decrease the tolerance to climatic stressors (Hewitt et al. 2016). With decreasing habitat suitability of intertidal sediments, the tolerance to heatwaves may decrease as well. Although many species are sediment generalists, several have a clear sediment texture preference (Kooistra et al. 2025). As sediment composition co-varies with many other environmental factors, such as hydrodynamic regime and organic content, it remains difficult to determine whether the actual grain size, or rather the co-varying factors determine the species' sediment preference. For instance, muddy areas are usually rich in sediment organic content, as the fine, organic particles are able to settle in these calmer areas (Cammen 1982, de Boer 1998),

and benthic diatoms (microphytobenthos) form a sticky layer on the sediment surface that traps fine particles and increases sediment mud content (de Brouwer et al. 2000, Stal 2010). Therefore, food content rather than grain size may drive deposit-feeder occurrence (Whitlatch 1981). On the other hand, mechanical and particle size properties of the sediment may drive sediment preferences. Sediment grain size composition determines the suitability for reburial (Alexander et al. 1993), and bulk density of the sediment determine the burrowing behaviour (Wiesebron et al. 2021). Such behavioural changes may affect performance on the longer term.

The peppery furrow clam, *Scrobicularia plana* (da Costa, 1778), is a mud-dwelling tellinid bivalve. This species lives in intertidal mudflats habitats along the north-east Atlantic coast. It has a wide geographic range and can be found from Norway to Senegal, including the British coast and the Mediterranean (Santos et al. 2011). *S. plana* feeds primarily on microphytobenthos and organic material as a surface deposit-feeder, but it is also capable of suspension feeding on phytoplankton and particulate organic matter from the water column during tidal immersion (Hughes 1970, Riera et al. 1999). The species burrows relatively deep: for large individuals (> 30 mm), burrowing depth is on average 6 cm in summer and 11 cm in winter, and increases with individual size (Zwarts & Wanink 1989, Zwarts et al. 1994). This deeper positioning may protect the species to large temperature fluctuations due to the buffering effect of the sediment (Domínguez et al. 2021), but may also imply a lower thermal tolerance compared to shallower burrowing species (Wilson 1981).

S. plana is predominantly restricted to muddy sediments (Bocher et al. 2007). The species could therefore be expected to be at risk if their sedimentary habitats would coarsen. Food supply has been suggested to drive the functioning and performance of the species across different sedimentary habitats, with lowered performance in sandy areas with low food supply (Worrall et al. 1983). Sedimentary habitat quality has also been observed to mediate the stress resilience of *S. plana*. Populations in coarser, low-food sediments were less resilient to climatic extremes (high rainfall and heatwaves), compared to populations in seagrass meadows with higher mud content and food supply, despite higher recruitment (Verdelhos et al. 2014). These field observations did however not allow for distinguishing the effects of food availability from the effects of sediment type.

In this study, we addressed the following questions: (i) is sediment preference of *S. plana* driven by sediment texture or food availability?, and (ii) does sediment-food habitat affect heatwave tolerance? We hypothesised that food content is the main driver of habitat suitability, followed by sediment composition, and that performance and heatwave tolerance will thus be most impaired in sandy sediment with low food supply. Furthermore, as the distribution of *S. plana* extends to warmer regions, we expect the species to be relatively heat tolerant. Under heat stress, we expect to see behavioural responses (valve gape) first, followed by sublethal metabolic responses (respiration rate, body condition index). Eventually, the results will help to predict the suitability of future coastal habitats for this species.

Methodology

Animal collection, preparation and acclimation

We collected *Scrobicularia plana* individuals from the intertidal flats at Oesterdam, Eastern Scheldt, Zeeland, the Netherlands (52.44°N, 4.22° E) in April 2023. Sediment median grain size (d_{50}) at the collection site was 118 µm and mud content 30 %. We transported collected individuals in buckets with water to the Royal Netherlands Institute for Sea Research (NIOZ) in Yerseke, where we sorted them by size, and kept them in baskets in tanks with flow-through supply of unfiltered Eastern Scheldt seawater at 15 °C in a climate-controlled room. In the days following collection, we selected individuals of 3.5-4.5 cm, labelled them and placed them in boxes with a shallow (~5 cm) layer of sand with flow-through unfiltered seawater supply. Here, they acclimated for 15-20 days prior to the experiment.

Mesocosm set-up

We designed a multifactorial experiment, with two sediment types (sand or mud), two feeding levels (low or high), and heatwave or no heatwave exposure, leading to a total of eight treatment combinations (see supplementary table S1 for an overview of treatment combinations and number of replicates per group and response variable). The experiment was performed in eight tidal tanks, divided over two climate chambers (Fig. 1), set to 18 °C. The tidal tanks consisted of two tanks on top of each other (inner dimensions: 1.10 × 0.95 × 0.6 m). The bottom tank, filled with filtered Eastern Scheldt water, served as the water reservoir. During simulated high tide (09:00 – 15:00 and 21:00 – 03:00), the water (salinity ~33 PSU) from the bottom tank was pumped up to the top experimental tank, creat-

ing a water level of ~25 cm. During low tide (03:00 - 09:00 and 15:00 - 21:00), water drained from the top tank, leaving a water level of approximately 5 cm in the experimental tank. We replaced the reservoir water weekly. High feeding treatments were fed three times per week with 10 mL algal concentrate (Shellfish Diet 1800, Reed Mariculture). Initially, low feeding treatments were not fed at all, however after several mortalities within two weeks, we fed low feeding treatments once a week with 5 mL algal concentrate, starting at day 13. The estimated food availability directly after feeding was then 38 x 10^6 cells L^{-1} or 1.5 mg dry algal biomass L^{-1} in the "high food" treatment and 19 x 10^6 cells L^{-1} or 0.8 mg dry algal biomass L^{-1} in the "low food" treatment.

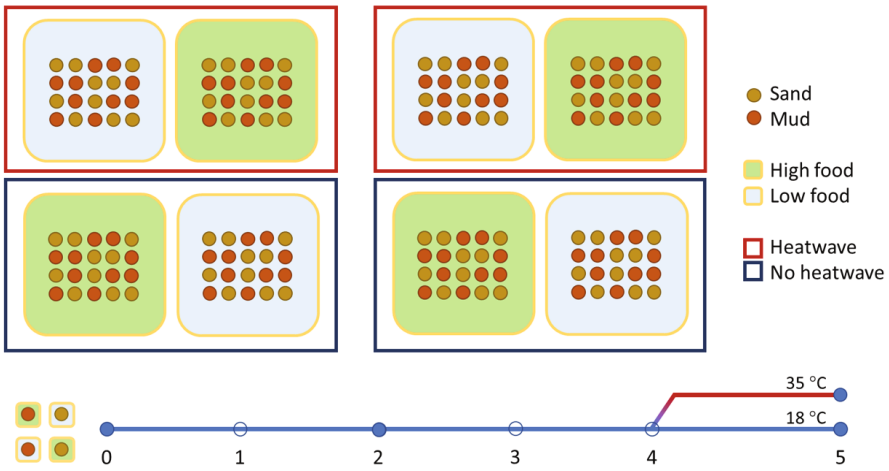

Figure 1. Schematic overview of experimental set-up: eight tanks divided over two climate chambers, each containing pots filled with sand or mud. A schematic timeline for all four sediment-food treatments is shown below, with intermediate measurement points after 2 weeks, the start of heatwave exposure of half of the experimental units after 4 weeks, and a final measurement point after 5 weeks. The indicated temperature in week 5 was the sediment surface temperature during heatwave exposure.

Experimental units and sediment

Within each experimental tank, we placed 18-22 cylindrical pots (Ø 11.5 cm, height 16 cm), which we filled with the experimental sediment mixtures. The position of each pot was randomly assigned.

Table 1. Sediment characteristics of test pots (start) and control pots (end): volumetric mixing rates, d_{50} and mud content, dry weight to wet weight ratio, and mean and cumulative penetration resistance (PR) of the top 10 cm. Mean values and standard deviations are displayed.

	volumetric mixing rates (sand : kaolinite : water)	time	d_{50} (µm)	mud content (%)	water content (%)	bulk density (g mL^{-1})	PR_{mean} (N)	PR_{cum} (N)
"mud"	10 : 10 : 6.7	start	231 ± 1.8	26.0 ± 0.6	29.2 ± 1.2	1.27 ± 0.04	0.53 ± 0.03	989 ± 115
		end	214 ± 9.3	33.2 ± 1.5	28.4 ± 1.1	1.29 ± 0.01		
"sand"	19 : 1 : 2.8	start	259 ± 5.6	3.4 ± 0.8	17.6 ± 1.2	1.53 ± 0.03	234 ± 109	$4.6 \times 10^5 \pm 2 \times 10^5$
		end	258 ± 4.2	4.5 ± 0.8	17.1 ± 0.8	1.56 ± 0.01		

Because food availability was one of our treatments, we used kaolinite clay powder (obtained from Keramikos B.V., The Netherlands) to make an artificial mud without organic matter content. Detailed grain size distribution information of the kaolinite clay powder is displayed in Figure S1. We mixed kaolinite with sand (d_{50} = 256 µm) and water in batches of 20 L, using a hand-held cement mixer (mixing ratios are given in table 1).

We prepared additional control pots, three pots for each of the eight treatment combinations, that did not contain a clam. These were placed in the tanks at the same moment and used as blanks for the metabolic rate incubations. We used 11 of the control pots to determine physical sediment characteristics after the experiment (Table 1, "end"). Besides the experimental pots, we prepared an additional 12 pots to determine physical sediment characteristics at the start of the experiment (Table 1, "start"). In these, we also measured penetration resistance, i.e., the force required to push an arrowhead into the sediment, using a universal testing machine (Instron, Baltimore, MD, United States). For sediment water content and bulk density, we sampled 15 mL of sediment from the top of the core, placed this in a pre-weighed tube to determine the wet weight directly after sampling, and the dry weight after drying for 7 days at 60 °C. Small variations in sediment composition between the pots measured at the start and the experimental control pots may be an effect of time, or of small variations in the sand used for each sediment batch.

Solar heatwave

During week 5 of the experiment, the experimental units were exposed to a 7-day heatwave. This heatwave was created by an infrared terrace heating panel (Frico, EZ212), during the 03:00 – 09:00 low tide. The temperature was regulated by a thermostat with a sensor on the sediment surface, which we calibrated at the start of the heatwave and set to a temperature of 35 °C during the heatwave. The water temperature during the experiment was kept at 18 °C, therefore the heatwave was solely a solar heatwave, during one of the two low tides. In two of the control pots, we placed temperature loggers (HOBO pendant Temperature/ Light Data Logger) between 5 and 15 cm depth to monitor temperature inside the sediment.

Response parameters

Size, mortality, biomass and condition

All tanks were checked daily, or on weekends every other day, for mortalities. If a clam was observed gaping on the sediment surface and it did not respond to mechanical stimuli, it was recorded as dead and frozen for biomass analysis. However, not all individuals resurfaced when they died. Therefore, when we took out the clams at the end of the experiment, we recorded the individuals that had degraded tissue as additional mortalities. From these, the moment of mortality is difficult to estimate.

After two weeks, we collected 10 individuals for all four sediment-food treatments to determine the biomass and condition. At the end of the experiment, biomass was determined for all the remaining clams. The individuals were taken out and frozen until analysis. We measured the length, width and height of all individuals, using callipers. Then, we separated the meat from the shell using a scalpel. Both the meat and the shell were placed in ceramic crucibles, dried for 2–3 days at 60 °C to determine dry weight (DW). After this, the meat was then combusted for 5 h at 560 °C to determine ash-free dry weight (AFDW) as a measure for biomass. We calculated body condition index as the ratio $AFDW_{meat}$:DW_{shell}.

Besides the experimental individuals, we also sampled 15–30 clams from the collection site at the same time points. We used these to compare body condition in the experiment with the field.

Respiration rate

After 2 and 5 weeks, we incubated experimental units to determine respiration rates. The incubation chambers consisted of transparent cylinders (30 cm high, ∅ 14 cm), hermetically sealed with a base plate and lid. The lid contained a magnetic stirrer, a larger opening for pre-incubation aeration, which could be closed with a rubber stopper, and a small, screw-valve opening for sensors. We placed the pots including sediment and clams in the chamber, and filled the remaining volume (4.14 L) with filtered Eastern Scheldt seawater (salinity 32.5 PSU). We also incubated blank units (i.e., pots containing only sediment, no clam) to determine background respiration. The chambers were placed in a thermostatic water bath to ensure constant temperature. The incubations took place in a darkened, climate controlled room, set to 18 °C. Prior to incubation, we allowed the units to acclimate, while an air pump aerated the water to ~100 % saturation. After 1 h,

we removed the aeration, ensured no air bubbles remained, and closed the chamber. During the 4-hour dark incubation phase, O_2 concentration was logged by an oxygen sensor (FiresSting fiberoptic O_2 meter, Pyroscience), calibrated at the start of the experiment, that was inserted in the incubation chamber lid. Oxygen saturation levels did not drop below 70 % during the incubations.

O_2 concentration, measured in % saturation, was converted to µmol L^{-1}, with the O_2 saturation concentration determined based on the temperature and salinity, using the R-package 'marelac' (Soetaert & Petzoldt 2008) following the method of (Weiss 1970). We fitted a linear regression to the O_2 concentration over time, of which we extracted the slope parameter. The mean blank slope per feeding level was subtracted from the slope of each individual unit. Subsequently, we determined the respiration rate scaled to individual biomass (µmol O_2 $hour^{-1}$ g^{-1}):

$$RR = \frac{-(slope - slope_{blank}) * V_{water}}{g\ AFDW} \quad \text{(eq. 1)}$$

With V_{water} as the water volume (L) in the incubation chamber, i.e., the chamber volume excluding the volume of the pot with sediment.

Behaviour: valve gape

To monitor the valve opening and closing behaviour of the clams in real time, we used a valve gape monitor. We used four monitors, each consisting of a waterproof PVC housing with eight pairs of coated electro-coils. Further details of the valve gape monitors are described by Ballesta-Artero et al. (2017). We glued one of each pair of coils to each valve of the clam, using two-component light-curing dental resin cements (3M ESPE RelyX Unicem 2Clicker). One of each pair of coils created an electromagnetic field, which is picked up by the other coil. The magnitude of this electromagnetic field is a measure for the distance between the two valves. To ensure a sufficient number of replicates, we monitored only individuals of the heatwave groups, since we were able to collect their valve gaping data over the entire experimental period. Due to leakage, one monitor failed and data was removed from analysis.

We pre-processed raw electrical field strength data by filtering out the low statistical outliers, following Tukey's fence for lower outliers (Fig. S3). We then converted the electromagnetic signal to approximate distance, following:

$$D \propto \sqrt{\frac{1}{S}} \quad \text{(eq. 2)}$$

Where D represents an approximation of the distance (mm) between the coils, and S the electromagnetic field strength.

Because D is only an approximation, and among individuals the angle and distance between the sensors is likely to differ, we converted distance to relative valve gape:

$$G = \frac{D - \min(D)}{\max(D) - \min(D)} \quad \text{(eq. 3)}$$

In which gape (G), ranging between 0–1, represents the fraction the coils, or valves, are separated relative to their total range. Here, we assume that min(D) represents the value when the valves are fully closed, and max(D) represents fully open valves.

We cropped individual time series based on the time of observed or suspected mortality. Next, we plotted gape (G) averaged per hour and visually inspected the patterns (Figure S4).

Behaviour: reburial

At the start of the experiment, we placed the individuals on top of the sediment and monitored their reburial rate using time-lapse cameras. The cameras were installed above 4 of the tanks and set to take a picture every 20 minutes. We counted the number of individuals per sediment type that was not reburied yet, calculated probability for clams being on the surface ($P_{surface}$) at each 20-min time step per tank and sediment type. We excluded the clams which had a valve-gape sensor, since this might have limited their mobility. This left a total of 26 clams per sediment type for the reburial analysis.

Statistical analysis

All statistical analysis was conducted in R v4.4.1 (R Core Team 2024).

We compared mortality between groups with binomial generalised linear model (GLMs) with sediment type, feeding level, and heatwave exposure as fixed factors. We tested for treatment effects on condition index and respiration rate with a two-way (week 2) and three-way ANOVA (week 5). To account for potential effects of tank, position within tank (which could affect heat level), or effects of the

attached valve gape sensor, we fitted additional mixed-effects models (GLMMs for mortality and LMMs for condition index using packages "lme4" (Bates et al. 2015), "lmerTest" (Kuznetsova et al. 2017)). Since all random factors explained little addional variation, and model fits were not improved by including them, we present the GLM or ANOVA results. We checked model residuals for normality and homogeneity of variances using Shapiro-Wilk and Levene's tests, respectively.

To compare initial reburial in mud and sand, we fitted a binomial logistic GLM of $P_{surface}$ as a function of sediment type and time. Since we only determined reburial at the start of the experiment, when food conditions did not differ between the tanks, sediment type was the only treatment variable here.

We analysed the valve gape data in two stages. To identify the effect of sediment and feeding treatments over a full tidal cycle, we compared valve gape between treatments during the nightly high and low tide in week 4. We selected only the nightly observations to minimise the disturbance from people entering and leaving the (neighbouring) climate rooms. For this analysis, we excluded two individuals that had died before week 4. For the second analysis, where we tested heatwave exposure in addition to sediment and feeding, we compared valve gape during the nightly low tide from two days before the start of the heatwave (week 4) to two days after the start of the heatwave (week 5). Through this temporal selection we maintained the maximum amount of replicates, as more mortalities occurred later during the heatwave period. For this analysis, we removed all individuals that had died within 1 day after the start of the heatwave.

We represented the selected valve gape data from both selected periods in empirical cumulative distribution function (ECDF) plots, from which we inspected the differences in distribution of valve gape between treatments visually. For each individual and within the selected time periods, we then aggregated the observation counts of nearly and fully closed ($G < 0.25$), partly open ($0.25 < G < 0.75$) and fully open ($G > 0.75$) valves for statistical comparison. We selected these threshold after first inspection of the data distribution, as the ranges in which we expected to see differences between the treatments, and because of the biological relevance. To these aggregated counts per individual, we fit a multinomial logistic regression model (MLR) using package "nnet" (Venables and Ripley 2002). Sediment, feeding level and week and their interactions were included, with "mud, high food" or "mud, high food, week 4" as the reference level. Interactive and additive model fits were compared based on Akaike Information

Criterion (AIC). We estimated odds relative to the baseline of closed valves (G < 0.25) and derived 95 % Wald confidence intervals from the standard errors. Due to the large number of gape observations, most effects were statistically supported, thus we focused interpretation on effect sized and predicted probabilities for each gape class.

Results

Mortality

Approximately a third of the *Scrobicularia plana* individuals died during the course of the experiment (Fig. 2). Highest mortality was observed in the treatment "sand + high food + heatwave" group, where 11 individuals died ($P_{mortality}$ = 0.8). Lowest mortality was found in the "mud + low food + no heatwave" group, where only 1 individual died ($P_{mortality}$ = 0.1). Mortality was significantly higher in sand than in mud ($\chi^2(1) = 12.8$, $p < 0.001$). Effects of feeding level, heatwave exposure or their interactions on mortality were not significantly different (all $p > 0.14$).

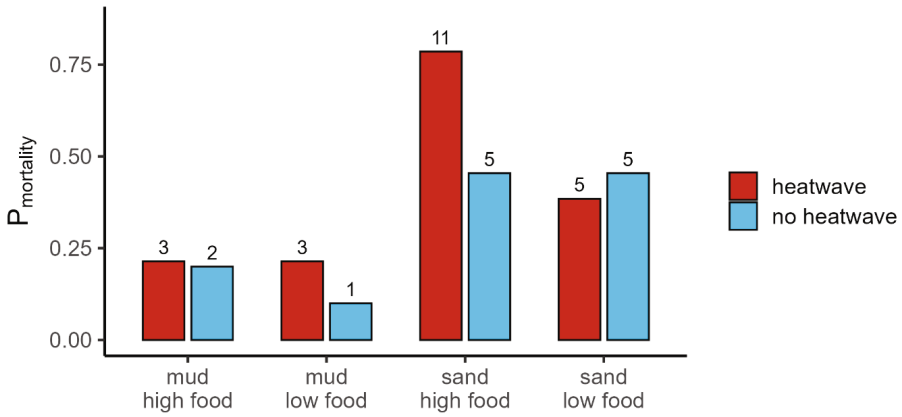

Figure 2. Fraction mortality ($P_{mortality}$) per sediment type, feeding level and heatwave exposure group. The numbers above the bars indicate the total individuals that died per group. Because of mortalities occurring before the start of the heatwave, the total group sizes differed.

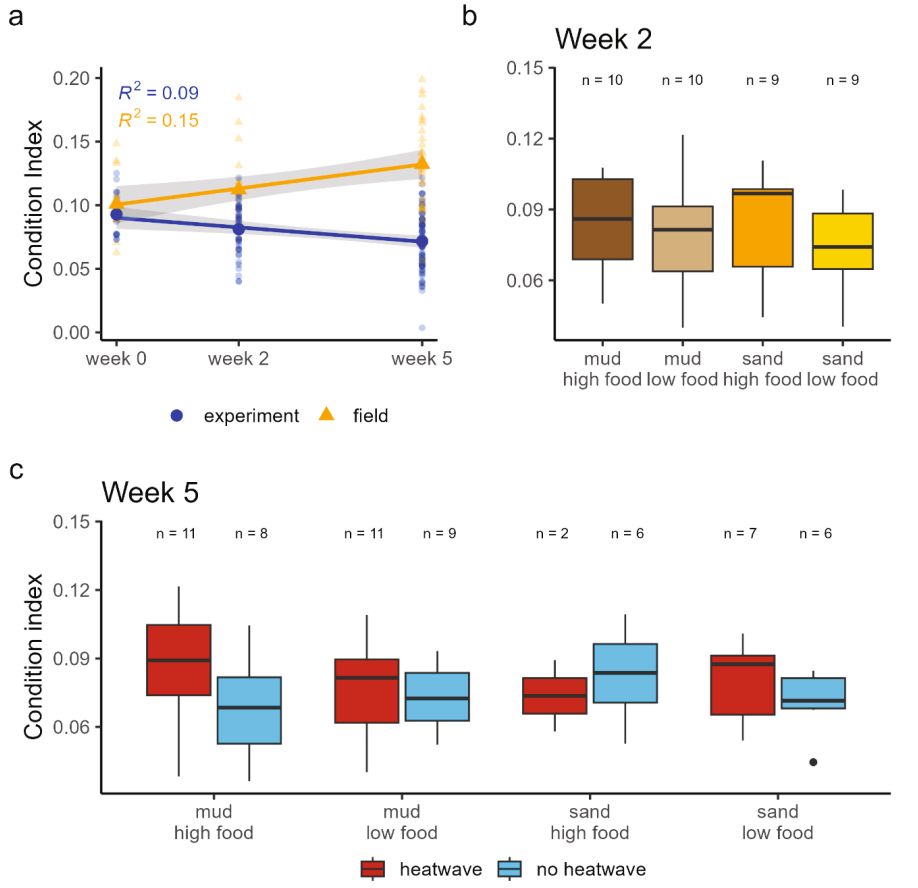

Figure 3. (a) condition over the experimental period in the experiment compared with the field. Linear regressions with shaded 95 % confidence intervals and R^2 values are indicated, and data is shown as transparent points. (b, c) condition index in all sediment and food treatments in week 2 and sediment, food and heatwave treatments in week 5.

Condition index

During the experiment, overall bivalve body condition index declined significantly over time (t = -3.43, p = 0.001), while during the same period, condition of individuals in the field increased (t = 3.28, p = 0.002; Fig. 3a). After removing individuals that had recently died, the experimental treatments did not result in any significant differences in condition within each week. However, comparing treatment groups with field groups per week showed a significant differences ($F_{4,47}$ = 4.03, p = 0.0069). Tukey post-hoc tests showed that only the "low food"

treatments in week 2 had a significantly lower condition compared to the individuals collected in the field in that week (p = 0.025 for "mud + low food" and p = 0.011 for "sand + low food"). In week 5, all experimental groups had a significantly lower condition compared to field individuals in that week ($F(4,47) = 4.03$, $p < 0.005$ for all group), except for "sand, low feeding, heatwave", where only two individuals remained due to high mortality in this treatment. The decrease in condition seems to be feeding-treatment dependent after the first two weeks, but not treatment-dependent after 5 weeks.

Respiration rate

In week 2, we did not observe differences in respiration rate between sediment and feeding treatments. In week 5, respiration rates under heatwave exposure tended to be higher compared to those of clams not exposed to heatwaves, especially in the "high food" treatments. This effect was however not significant ($p > 0.3$), which may have been a result of the small group size due to high mortality in sand. Respiration in week 5 was higher compared to week 2 (mean over all treatment groups 37.3 ± 27.2 µmol O_2 h^{-1} g^{-1} in week 5 versus 29.2 ± 16.7 µmol O_2 h^{-1} g^{-1} in week 2).

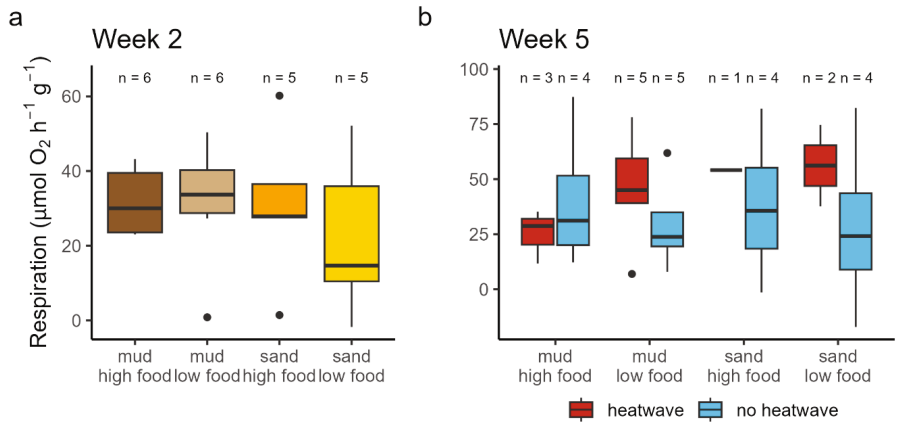

Figure 4. Respiration rate normalised to individual biomass (g AFDW) in all sediment and food treatments in week 2 (a) and in all sediment, food and heatwave treatments in week 5 (b). Note differences in Y-scale axis. The amount of replicates per group is indicated.

Reburial rate

Reburial rate at the start of the experiment was faster in mud compared to sand. A binomial logistic regression revealed a significant effect of sediment type on reburial probability (z = -2.89, p = 0.004). Two individuals did not rebury after 23 h in sand.

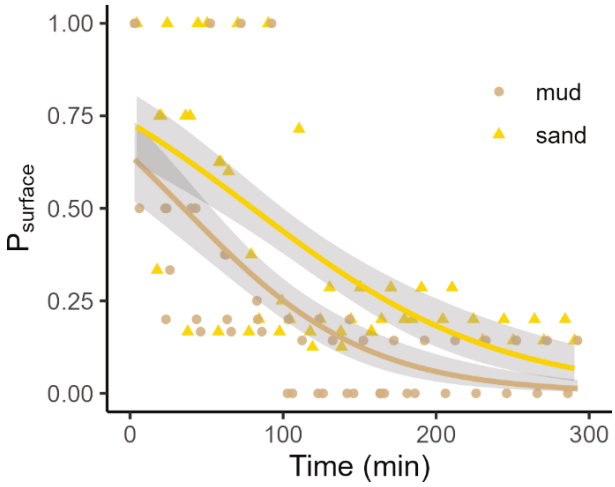

Figure 5. The initial reburial rate shown as the probability that clams remained visible on the sediment surface during the first 5 hours of the experiment, for both sediment types. The fitted binomial logistic regressions are shown with 95 % confidence intervals as grey bands. The scattered data represent the reburial probabilities per tank.

Valve gape

During the full nightly tidal cycles in week 4, the ECDF plots of valve gape suggested effects of feeding level and sediment type on valve gape (Fig. 6a; Fig. 7a). The MLR confirmed this (Table 2): in sand, clams were less likely to be fully open compared to in mud (β = 1.26, SE = 0.013, p < 0.001; OR = 0.29) and at low feeding levels they were less likely to be fully open compared to high feeding levels (β = 0.94, SE = 0.011, p < 0.001; OR = 0.39). Sediment and feeding treatments also had interactive effects: in mud, high feeding resulted in an increase in full gape (a probability of 0.68 versus 0.25 for low feeding; Table S2), while in sand, this was not the case (a probability of 0.24 compared to 0.27 for low feeding). This interaction was confirmed by the improved model fit of the interactive compared to the additive model (ΔAIC = 31147).

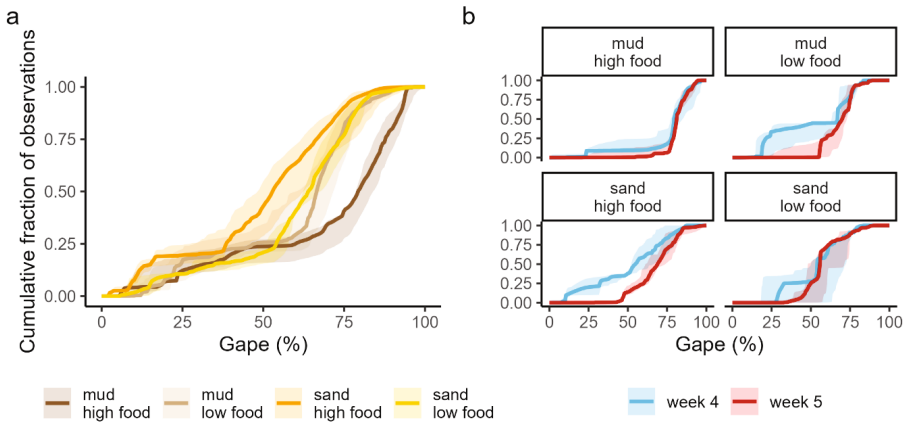

Figure 6. Empirical cumulative frequency distribution function (ECDF) plots for valve gape in week 4 (a) and before (week 4) and during (week 5) heatwave exposure (b). The solid lines represent the median ECDF across individuals in each sediment-feeding treatment, and the shaded bands indicate inter-individual variation (interquartile range).

Comparing the nightly low tide before and during the heatwave (Fig. 6b), sand and low food supply again reduced the observation probability of full gaping, and increasing the frequency of medium gaping (Table 2; Fig. 7b). Furthermore, heatwave exposure decreased the probability for valve closure (Fig. 6b) from 0.09 to 0.02 during the heatwave (Fig. 7b), while medium and full gaping were increased with a factor 2.25 and 4.32, respectively (Table 2). Also here, the model including all interactions provided an improved fit compared to the additive model (ΔAIC = 9816), illustrating that interactions between feeding, sediment and heatwave exposure were significant.

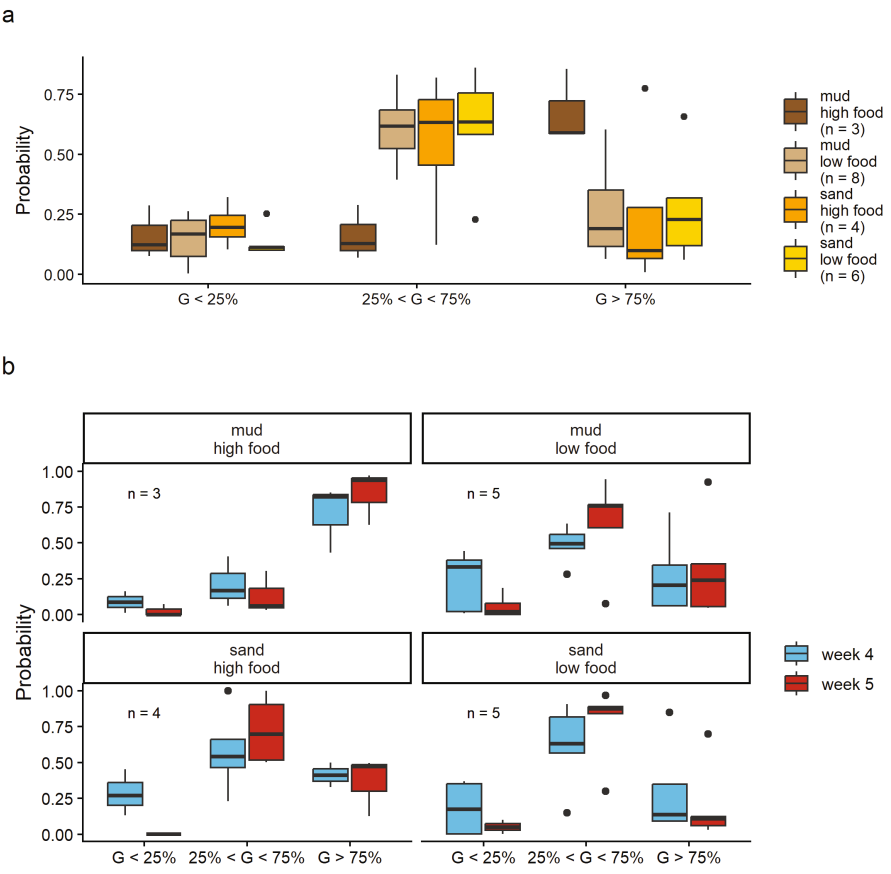

Figure 7. Probability of observation of each gape class—fully closed (G < 25 %), partly open (25 < G < 75 %) and fully open (G > 75 %) valves—for each treatment (a) during a full tidal cycle in week 4, and (b) comparing low tide pre-heatwave (week 4) with low tide during the heatwave (week 5). Boxplots represent inter-individual variability in predicted probabilities.

Table 2. Summary of MLR coefficients for valvegape categories with "mud, high food" or "mud, high food, week 4" as reference level. Odds ratio (OR) estimates are relative to the baseline of closed valves (G < 0.25). pvalues and confidence intervals are derived from the Wald z statistic.

Week 4	**Predictor**	**Logodds (β)**	**SE**	**z**	***p***	**OR**	**CI_{low}**	**CI_{high}**
Partly open (0.25 < G < 0.75)	(Intercept)	0.00	0.01	0.23	0.82	1.00	0.98	1.03
	sediment = sand	0.99	0.01	71.56	**< 0.001**	2.70	2.62	2.77
	feeding = low food	1.40	0.01	106.92	**< 0.001**	4.06	3.96	4.17
	sediment × feeding	-0.70	0.02	-41.17	**< 0.001**	0.50	0.48	0.51
Fully open (G > 0.75)	(Intercept)	1.44	0.01	156.09	**< 0.001**	4.21	4.13	4.28
	sediment = sand	-1.25	0.01	-99.49	**< 0.001**	0.29	0.28	0.29
	feeding = low food	-0.94	0.01	-82.01	**< 0.001**	0.39	0.38	0.40
	sediment × feeding	1.60	0.02	95.97	**< 0.001**	4.96	4.80	5.13
Week 4 and 5	**Predictor**	**Logodds (β)**	**SE**	**z**	***p***	**OR**	**CI_{low}**	**CI_{high}**
Partly open (0.25 < G < 0.75)	(Intercept)	0.88	0.04	24.89	0.00	2.41	2.25	2.58
	feeding = low food	-0.16	0.04	-4.19	**< 0.001**	0.85	0.79	0.92
	sediment = sand	0.12	0.04	2.96	**< 0.001**	1.13	1.04	1.22
	week = week 5	0.81	0.07	11.47	**< 0.001**	2.25	1.96	2.58
	feeding × week	1.09	0.08	13.64	**< 0.001**	2.97	2.54	3.48
	sediment × feeding	0.56	0.05	11.59	**< 0.001**	1.75	1.59	1.92
	sediment × week	4.78	0.26	18.33	**< 0.001**	119	71.4	198
	sediment × feeding × week	-4.42	0.27	-16.47	**< 0.001**	0.01	0.01	0.02

Table 2. Summary of MLR coefficients for valvegape categories with "mud, high food" or "mud, high food, week 4" as reference level. Odds ratio (OR) estimates are relative to the baseline of closed valves (G < 0.25). pvalues and confidence intervals are derived from the Wald z statistic. *(Continued)*

Week 4	Predictor	Logodds (β)	SE	z	*p*	OR	CI_{low}	CI_{high}
Fully open (G > 0.75)	(Intercept)	2.08	0.03	66.10	**< 0.001**	8.01	7.53	8.52
	feeding = low food	-1.93	0.04	-52.47	**< 0.001**	0.14	0.13	0.16
	sediment = sand	-2.11	0.04	-53.85	**< 0.001**	0.12	0.11	0.13
	week = week 5	1.46	0.07	22.45	**< 0.001**	4.32	3.80	4.91
	feeding × week	0.03	0.08	0.45	0.66	1.03	0.89	1.20
	sediment × feeding	2.48	0.05	50.28	**< 0.001**	11.9	10.8	13.1
	sediment × week	4.07	0.26	15.66	**< 0.001**	58.6	35.2	97.5
	sediment × feeding × week	-3.76	0.27	-14.00	**< 0.001**	0.02	0.01	0.04

Discussion

Sediment texture, food availability and heatwave exposure all affected the behaviour of mud-dwelling peppery furrow clam *Scrobicularia plana* (Fig. 8). During the five-week mesocosm experiment, an especially large number of individuals died in sandy sediment. Overall body condition decreased during the course of the experiment, but did not differ significantly between experimental treatments. We were also not able to show a difference in respiration rate between treatments. A decreased reburial rate and decreased time spent with open valves indicated behavioural constraints in the sandy sediment. A higher level of feeding resulted in a higher probability of fully open valves, but only in the muddy sediment. Lastly, heatwave exposure resulted in a lower probability of valve closure. The heatwave did however not significantly affect survival or other performance parameters.

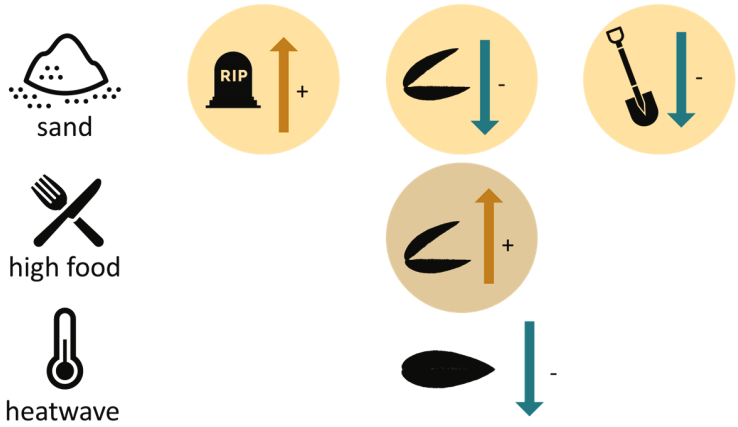

Figure 8. Graphical summary of the main effects of sediment, food and heatwave treatments (top to bottom), on mortality (left), valve gape (centre), and reburial (right). The colour of the circle indicates the sediment type (beige for sand and brown for mud); for the other treatments the effects of high food and of heatwave exposure are shown. Upward arrows indicate an increase, downward arrows a decrease. Condition index and respiration are not displayed here, as we observed no clear effects of experimental treatments on these parameters.

Behavioural responses and lower survival in sand

The high mortality in sand, indicated that the sandy sediment was less suitable for this species. Behavioural responses can partially explain this. Initial reburial was lower in sand than in mud, and two individuals were not able to rebury in sand within a day. This corresponds with previously reported burrowing preferences for this species (Bonnard et al. 2009, Wiesebron et al. 2021). The flat shell shape and foot morphology are traits that reflect rapid and deep burrowing as a predation-avoidance strategy (Stanley 1970, Johnson 2020). Therefore, the clams are likely to spend a considerable amount of energy in attempting to obtain the safest position within the sediment. If mechanical characteristics of the sediment limit their mobility, such extra efforts may pose energetic constraints.

Besides initial reburial, we also saw effects of sediment composition on valve gaping. In sand, valve gape was more often in the intermediate range (25-75 % open), and the sandy sediment seemed to limit full gaping (>75 %). Only clams in the muddy sediment were able to increase their full valve gaping under higher feeding. The lower mechanical plasticity of (compacted) sandy sediments may have inhibited full valve opening.

With grain size distribution, other characteristics of the sediment, such as water content, bulk density and penetration resistance, varied (Table 1). Wiesebron et al. (2021) showed that bulk density is a major factor in burrowing behaviour. In our experiment, bulk density was on the higher end of the range used by Wiesebron et al. (2021), but was relatively similar for both sandy and muddy sediments (Table 1). Penetration resistance was however orders of magnitude higher in the sandy sediment compared to the muddy sediment, consistent with Bokuniewicz et al. (1975). This sediment "hardness" is thus likely to have limited burrowing and valve movement. Contrary to Wiesebron et al. (2021), who tested only cohesive (>35 % mud) sediments, we used a cohesive (~30 % mud) and a non-cohesive (<5 % mud) sediment. As cohesive and non-cohesive sediments each require different burrowing mechanisms (Dorgan 2015), and this species normally occurs in cohesive sediments (Bocher et al. 2007), we expect the low mud content to have limited the species' burrowing behaviour.

Food availability, valve gape and condition decline

Valve gaping activity is linked to important physiological processes such as pumping, feeding and respiration (e.g., Jørgensen et al., 1988; Newell et al., 2001; Riisgård et al., 2003). With higher food availability, valve gaping or feeding rates

in bivalves often increase (Riisgård et al. 2003, 2006, Ballesta-Artero et al. 2017, Tonk et al. 2023). Therefore, the effects of feeding treatments on valve gape activity are not unexpected. At high feeding levels and when in mud, clams were more often fully open (Fig. 7c and e). These individuals may have maximised their pumping and feeding rate to profit from the higher food availability, while clams at low feeding levels may have spent more time probing for food and fed at a lower rate, with valves only partly open (e.g., Hubert et al. 2022).

In order to maintain a sufficient energy intake, bivalves can upregulate their feeding rate when food supply decreases (Pilditch & Grant 1999). *S. plana* individuals from sites with low food availability had higher feeding rates, possibly to compensate their food intake (Worrall et al. 1983). After transplantation they adapted their feeding rate within a few months (Worrall & Widdows 1983). Also *S. plana* populations across habitats can differ in feeding mode: from deposit-feeding in a food-rich seagrass bed to suspension feeding when inhabiting bare sediment (Baeta et al. 2009). The effects of food supply, in particular the increase in partial gaping at low feeding levels, may therefore also reflect the adaptive feeding behaviour of this species.

Lacking food supply in the experiment negatively affected body condition after two weeks, compared to the field. By week five, condition had declined across all treatments, with no differences between feeding levels, suggesting a general negative effect of the experimental setup. This may stem from the "unnatural" sediment: the kaolinite clay was finer than mud found in the natural habitat (Fig. S1), the median grain size (214-259 µm) of both sediment types was coarser than at the collection site (118 µm), and mud content in the sandy sediment (<5 %) was below the mud content in the field (30 %). Scola et al. (2021) also reported a condition decline in this species, attributed to handling or sub-optimal substrate. Additionally, phytoplankton concentrate instead of benthic diatoms as food type may have been less suitable for *S. plana*, although this food type is developed for bivalve culture, and concentrations match those in used in comparable studies (Wiesebron et al. 2021, Zhou et al. 2022).

Heatwave exposure affected behaviour but not mortality

The high mortality was not significantly driven by heatwave exposure. Apparently the intensity and duration of the heatwave were within the tolerance range of *S. plana*. That is not unexpected, as *S. plana* has thermal limits between 25–32 °C for prolonged exposure (Wilson 1981, Verdelhos et al. 2015). For short periods of

time, the species can survive temperatures as high as over 40 °C. (Santos et al. 2011, Verdelhos et al. 2014). Amorim et al. (2020) attributed the absence of heat effects on the survival of *S. plana* to molecular coping mechanisms (e.g., heat shock responses). Such mechanisms may reflect adaptation of bivalves to large temperature fluctuations in an intertidal environment, for they can play a larger role during low tide than during high tide (Zhang et al. 2020).

The ability to burrow deep into the sediment also contributes to heatwave tolerance. Whereas the maximum temperature at the 5 cm depth was 38 °C, at 10 cm depth—the approximate living depth of the clams—we measured a maximum temperature of 33 °C (Fig. S2). With only 6 hours heat exposure per day, it is unlikely that temperature exceeded critical levels for a prolonged time period below 10 cm depth. Temperature decrease over sediment depth was steeper in muddy compared to sandy sediment (Fig. S2). This aligns with expectations, as sandy sediments tend to have a higher bulk thermal conductivity, while muddy sediments with lower pore water flow form a buffer for heat transfer (Douglas et al. 2024, Liu et al. 2025). With the sediment acting as a temperature buffer, deep-burrowing species remain shielded from the highest temperatures at the sediment surface. The organisms' vertical position can therefore also aid in their heatwave tolerance, allowing deeper burrowing species to survive and grow better under heat exposure compared to shallow-burrowing intertidal bivalves (Domínguez et al. 2021).

Clams responded to heatwave exposure by spending a lower proportion of the time fully closed. This might reflect a higher oxygen demand associated with a higher metabolic rate under elevated temperatures and an upregulation of the heat shock response (Tomanek 2010). Meeting this increased oxygen demand would require an increase in pumping, and thus valve opening. In previous studies, *S. plana* increased pumping frequency under warming, showing a thermal optimum for pumping and filtering near 25 °C (Hughes 1969, Van Colen et al. 2020). Similar responses in gaping activity were observed in other bivalves: *Arcuatula senhousia* increased valve gaping upon heatwave exposure (Fouet et al. 2026), *Ruditapes philippinarum* did not increase valve closure during, but only after a heatwave (Xu et al. 2025), and Mytilid mussels and freshwater bivalves showed higher gaping activity during heat exposure (Rodland et al. 2009, Olabarria et al. 2016). Our observations therefore align with behavioural patterns exhibited by various bivalve species.

Contrary to the observations on valve gape, we saw no significant effects of heat exposure on metabolic rate. The underlying reason for the lacking response could be that we measured approximately 1-2 hours after the end of the heat exposure and that the clams had recovered their respiration rates to a normal level by that time. Furthermore, only a few individuals could be measured due to the high mortality rate, and combined with high inter-individual variability, this posed a challenge for detecting significant differences. Lastly, if the clams were closed or inactive during part of the incubation, this might have resulted in lower respiration rates. Nevertheless, the respiration rates we measured were in the same order of magnitude as in previous experiments with this species (e.g., Wiesebron et al., 2021). Condition index was also not affected by heatwave exposure, after removing the individuals that had recently died from the analysis. As for respiration rate, this could be due to the low number of remaining individuals, combined with inter-individual variability. In other studies, respiration rate or condition responses of infaunal bivalves to heat were sometimes also lacking: Pansch et al. (2018) saw no decreases in condition in *Macoma balthica* after exposure to a single heatwave, and Staniek et al. (2025) saw no responses in respiration rate in *C. edule* and *M. balthica* during, but only after heatwave exposure. Body condition was also not affected by other stressors in *S. plana* in several previous studies (Amorim et al. 2020, Islam et al. 2021, Scola et al. 2021). Lacking responses of condition to stressors was often attributed to, again, successful coping strategies or delayed stress effects.

Cumulative stressors and sensitivity of responses

S. plana was tolerant to heat exposure in this controlled experiment. In a field setting a heatwave can however have a cascading effect in which a high temperature results in an environment with multiple stressors. A heatwave co-occurring with hypoxia can result in bivalve mortality (Zhou et al. 2022, Salmond & Wing 2023). The increased temperature can also accelerate organic matter degradation, depleting sediment oxygen levels and rising hydrogen sulphide levels (Al-Raei et al. 2009, Fitch & Crowe 2011). As a deep burrower in usually muddy, organic sediment, *S. plana* has a relatively high tolerance to anoxia and hydrogen sulphide (Oeschger & Pedersen 1994). Nevertheless, the increasing heatwave temperatures and durations may lengthen such hypoxic periods and lower hypoxia tolerance limits (Kodama et al. 2018). Above that, the decreased mobility that we observed in coarser sediment may hamper behavioural coping strategies, for instance the capacity of an animal to escape anoxia or elevated sediment temperature (Zhou et al. 2022, 2023).

Not only the magnitude, but also the duration and frequency of heat exposure can determine responses. In the current experiment we only assessed the effects of a single 7-day heatwave and monitored the response directly after. Therefore we could not report recovery responses or possible acclimation, that have been observed in other bivalves (He et al. 2022b a, Xu et al. 2025). Under multiple, sequential heatwaves, stronger adverse effects can be expected (Pansch et al. 2018, Zhou et al. 2022, 2023). Lastly, larval stages of bivalves might be more sensitive to a combination of stressors such as food availability and heat (Czaja et al. 2023). Therefore, it is important to consider the entire life cycle when making predictions on future habitat suitability.

Integrating both physiological and behavioural responses gives the most complete picture of bivalve responses to climatic stress, as together they can reveal stress mechanisms and coping strategies (Cheng et al. 2025). Nevertheless, bivalve responses and acclimation strategies to multiple stressors may be earlier visible on a molecular level prior to physiological or phenotypical responses (Amorim et al. 2020, He et al. 2022a, Lam-Gordillo et al. 2025). Such measurements may thus give a more sensitive indication of stress.

Conclusions

As evidenced by the reduced survival in sandy sediment, coarsening of coastal sediments is likely to result in a decrease in habitat suitability for *S. plana*, independent of food supply. Reburial and valve gaping behaviour revealed that the negative effects of sand may be related to its mechanical properties. *S. plana* appeared relatively tolerant to heatwave exposure. However, the observed reduction in valve closure reflected higher metabolic needs under heatwave exposure. A reduced mobility due to an unsuitable sediment type can decrease the bivalves' capacity to adapt their behaviour in order to cope with heat exposure. These multiple stressors may thus have implications for organism and, ultimately, ecosystem functioning in the intertidal environment.

Acknowledgements

We wish to thank Femke Heldoorn, Jara Westbeek, Ismaël Heijnis and Aileen Tenconi for their help during the execution of the experiment and initial data

exploration, and Sarah Manni and Milo Wernars for help with the biomass analysis. Furthermore, we want to than Peter van Breugel for grain size analysis and Jeroen van Dalen, Lennart van IJzerloo and Anton Tramper for assistance with the experimental set-up and measurement equipment. Funding for this study was provided by NWO grant no. 17600: "Tracking Ameland Inlet Living Lab Sediment (TRAILS)".

Supplementary materials

Table S1. Number of experimental replicates per treatment group. The column "total" shows the initial number of individuals per group. The following columns describe the number of individuals remaining for measurements of reburial, biomass and respiration rate (RR), after subtracting mortalities. Remaining valve gape replicates are shown after removal of early mortalities and lost data due to equipment failure, initial valve gape replicates are indicated between brackets.

treatment			total	mortality	reburial	biomass		respiration		valve gape
sediment	food	heatwave				w2	w5	w2	w5	
mud	high	yes	14	3	26		11		3	3 (7)
mud	high	no	20	2		10	8	6	4	
mud	low	yes	14	3			11		5	5 (8)
mud	low	no	20	1		10	9	6	5	
sand	high	yes	14	11	26		2		1	4 (8)
sand	high	no	20	5		9	6	5	4	
sand	low	yes	16	8			7		2	4 (8)
sand	low	no	18	3		9	6	5	4	

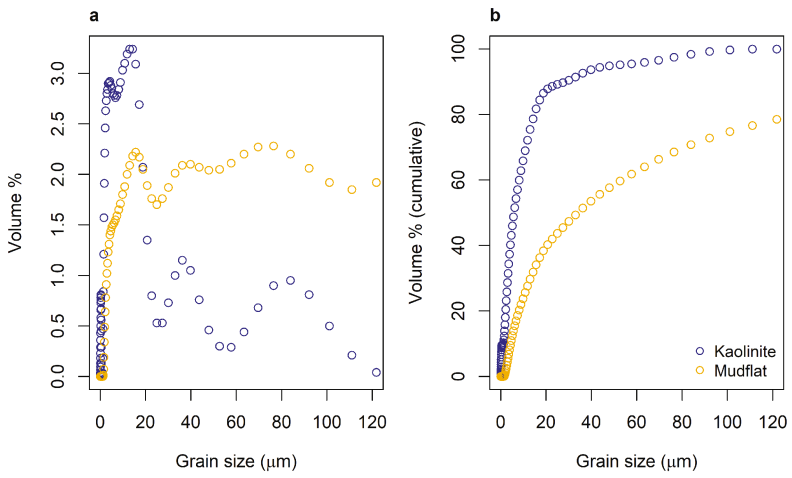

Figure S1. Grain size distribution and cumulative distribution of kaolinite clay particles compared to natural mudflat sediment as measured using a laser diffraction particle size analyser (Coulter LS 13320).

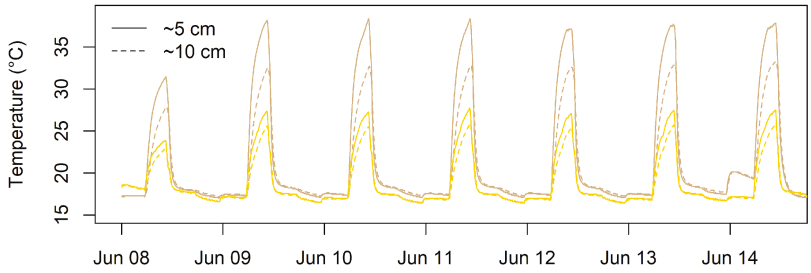

Figure S2. Temperature inside muddy (brown) and sandy (yellow) sediment at different depths. Note the difference in temperature level is likely an effect of pot positioning, as the muddy pot was located centrally under the heating panel, while the sandy pot was located at the edge.

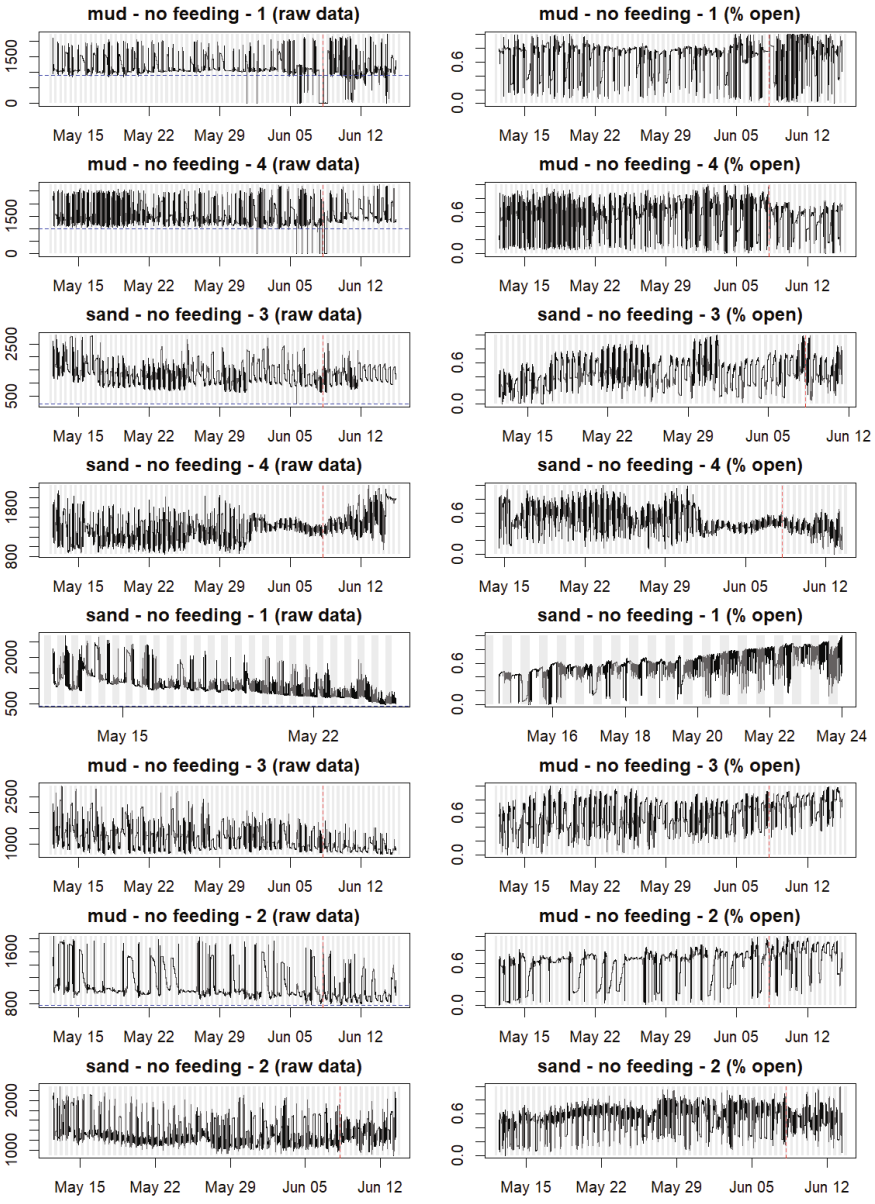

Figure S3a. Raw valve gape measurements (left) and valve gape data filtered and converted to fraction opening (right). The cutoff for low outliers indicated as a horizontal blue dashed line, the start of the heatwave is shown as the vertical red dashed line. Low tide is indicated by grey vertical bands.

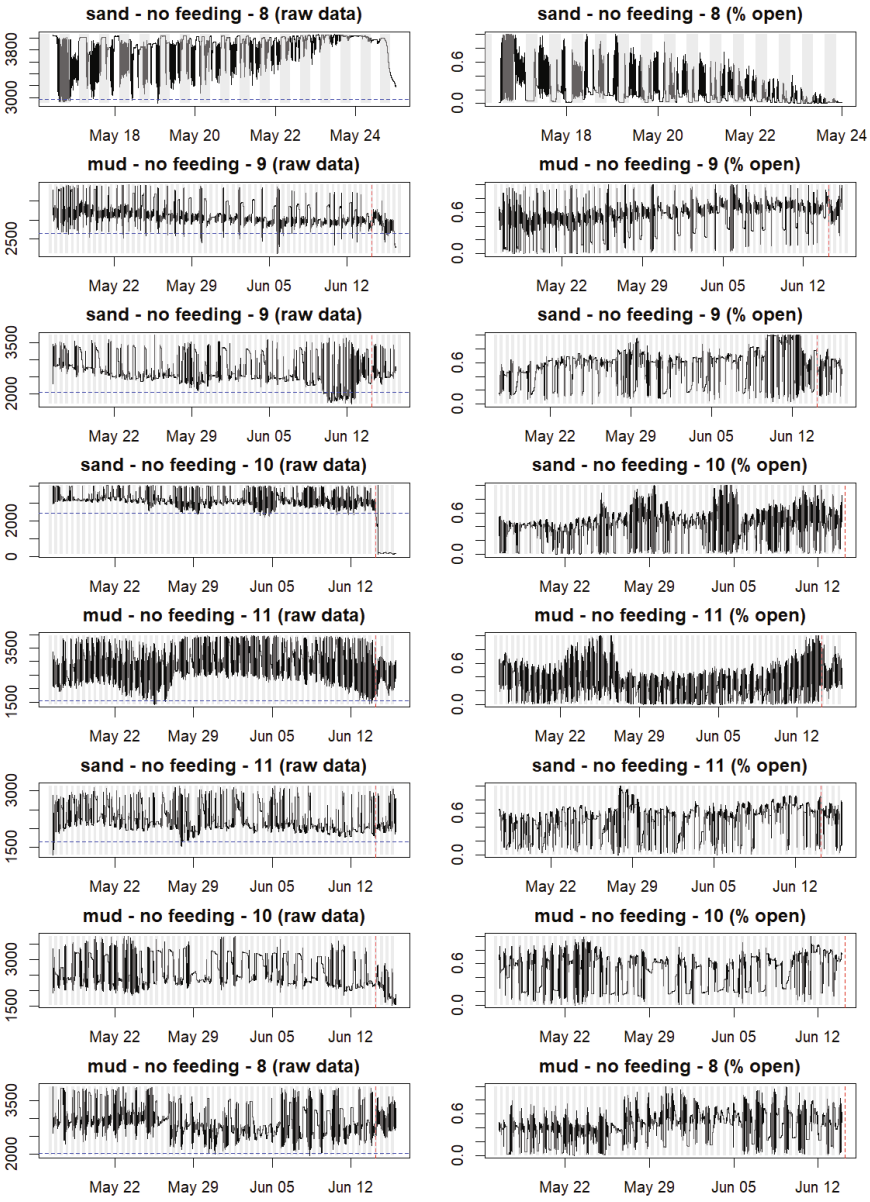

Figure S3b. Raw valve gape measurements (left) and valve gape data filtered and converted to fraction opening (right). The cutoff for low outliers indicated as a horizontal blue dashed line, the start of the heatwave is shown as the vertical red dashed line. Low tide is indicated by grey vertical bands.

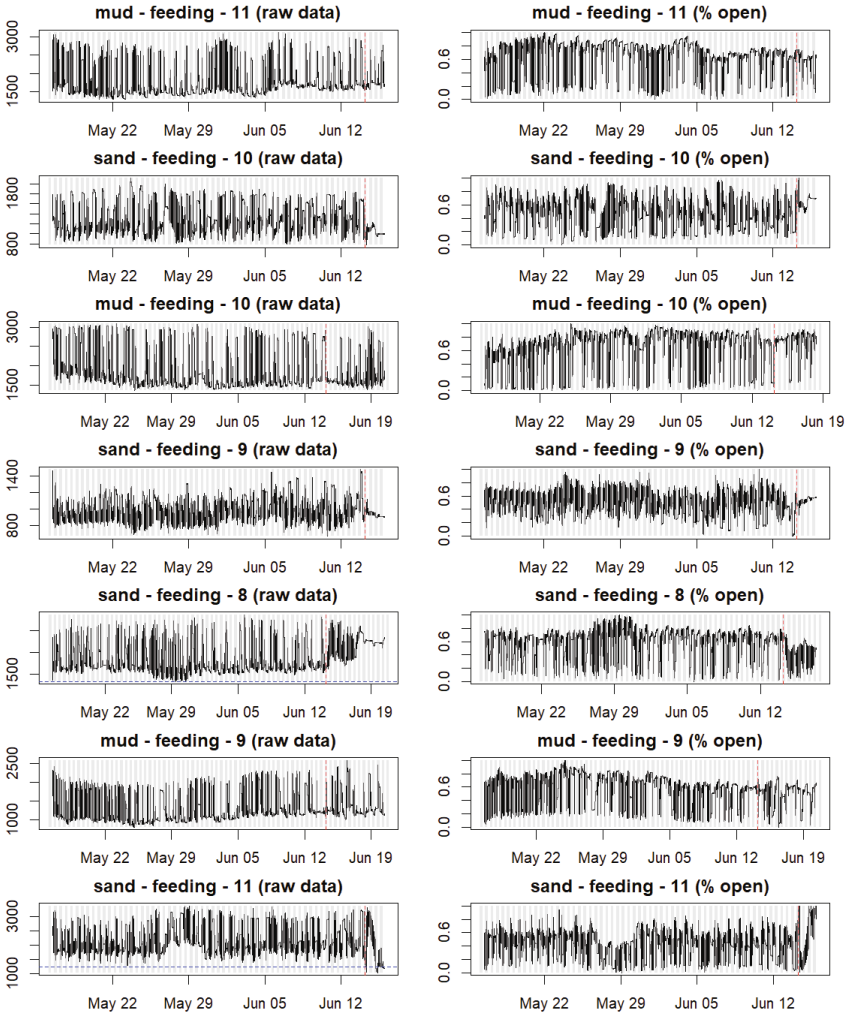

Figure S3c. Raw valve gape measurements (left) and valve gape data filtered and converted to fraction opening (right). The cutoff for low outliers indicated as a horizontal blue dashed line, the start of the heatwave is shown as the vertical red dashed line. Low tide is indicated by grey vertical bands.

Table S2. Multinomial regression predictions for observation probabilities of each valve gape category (closed: G < 25 %; partly open: 25 < G < 75 %; and fully open: G > 75 %) in all treatment combinations: sediment, feeding level and pre- (week 4) or during (week 5) heatwave exposure.

Week 4 tidal cycle	sediment	feeding		gape	probability
	mud	high feeding		closed	0.16
	mud	high feeding		partly open	0.16
	mud	high feeding		open	0.68
	mud	low feeding		closed	0.15
	mud	low feeding		partly open	0.61
	mud	low feeding		open	0.25
	sand	high feeding		closed	0.20
	sand	high feeding		partly open	0.55
	sand	high feeding		open	0.24
	sand	low feeding		closed	0.11
	sand	low feeding		partly open	0.62
	sand	low feeding		open	0.27
Pre- and during heatwave	**sediment**	**feeding**	**week**	**gape**	**probability**
	mud	high feeding	week 4	closed	0.09
	mud	high feeding	week 5	closed	0.02
	mud	high feeding	week 4	partly open	0.21
	mud	high feeding	week 5	partly open	0.13
	mud	high feeding	week 4	open	0.70
	mud	high feeding	week 5	open	0.84
	mud	low feeding	week 4	closed	0.24
	mud	low feeding	week 5	closed	0.05
	mud	low feeding	week 4	partly open	0.49
	mud	low feeding	week 5	partly open	0.69
	mud	low feeding	week 4	open	0.28
	mud	low feeding	week 5	open	0.26
	sand	high feeding	week 4	closed	0.21
	sand	high feeding	week 5	closed	0.00
	sand	high feeding	week 4	partly open	0.58
	sand	high feeding	week 5	partly open	0.75
	sand	high feeding	week 4	open	0.21
	sand	high feeding	week 5	open	0.25
	sand	low feeding	week 4	closed	0.15
	sand	low feeding	week 5	closed	0.02
	sand	low feeding	week 4	partly open	0.60
	sand	low feeding	week 5	partly open	0.77
	sand	low feeding	week 4	open	0.25
	sand	low feeding	week 5	open	0.20

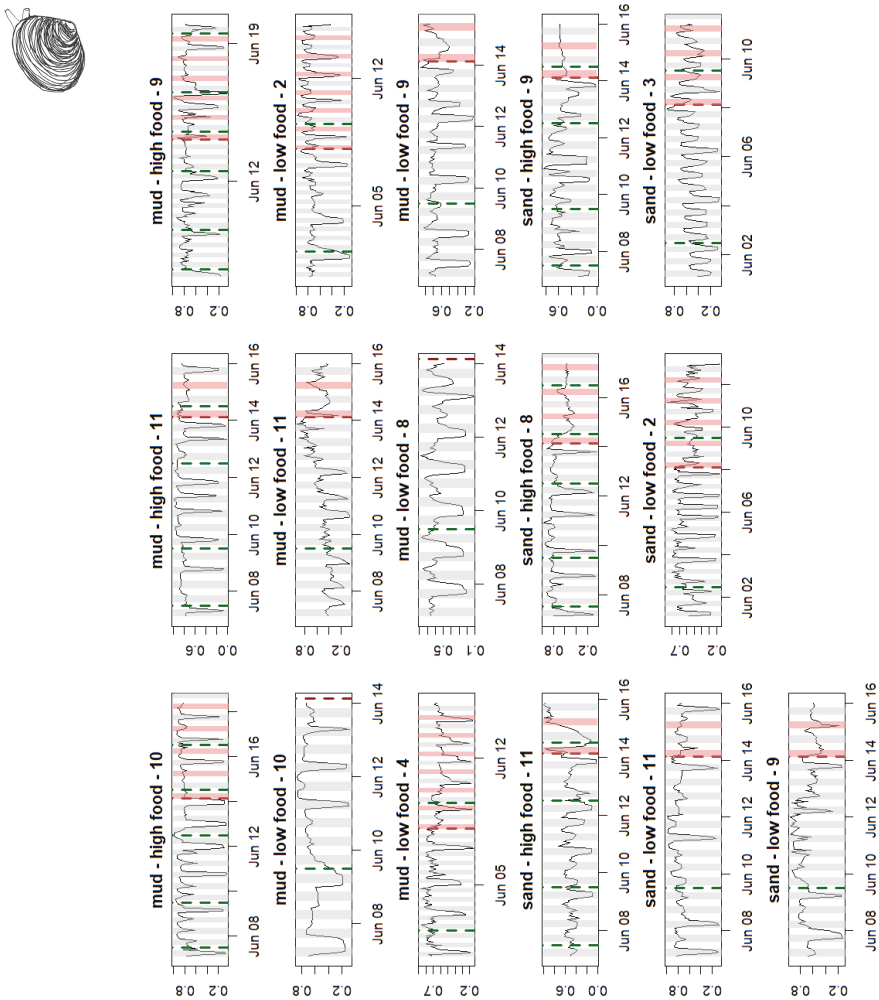

Figure S4. Hourly averaged valve gape time-series per individual, for all individuals selected for analysis in week 4 and 5. Grey areas indicate low tide; green lines indicate feeding; red line indicates start of heatwave; red areas indicate heatwave exposure.

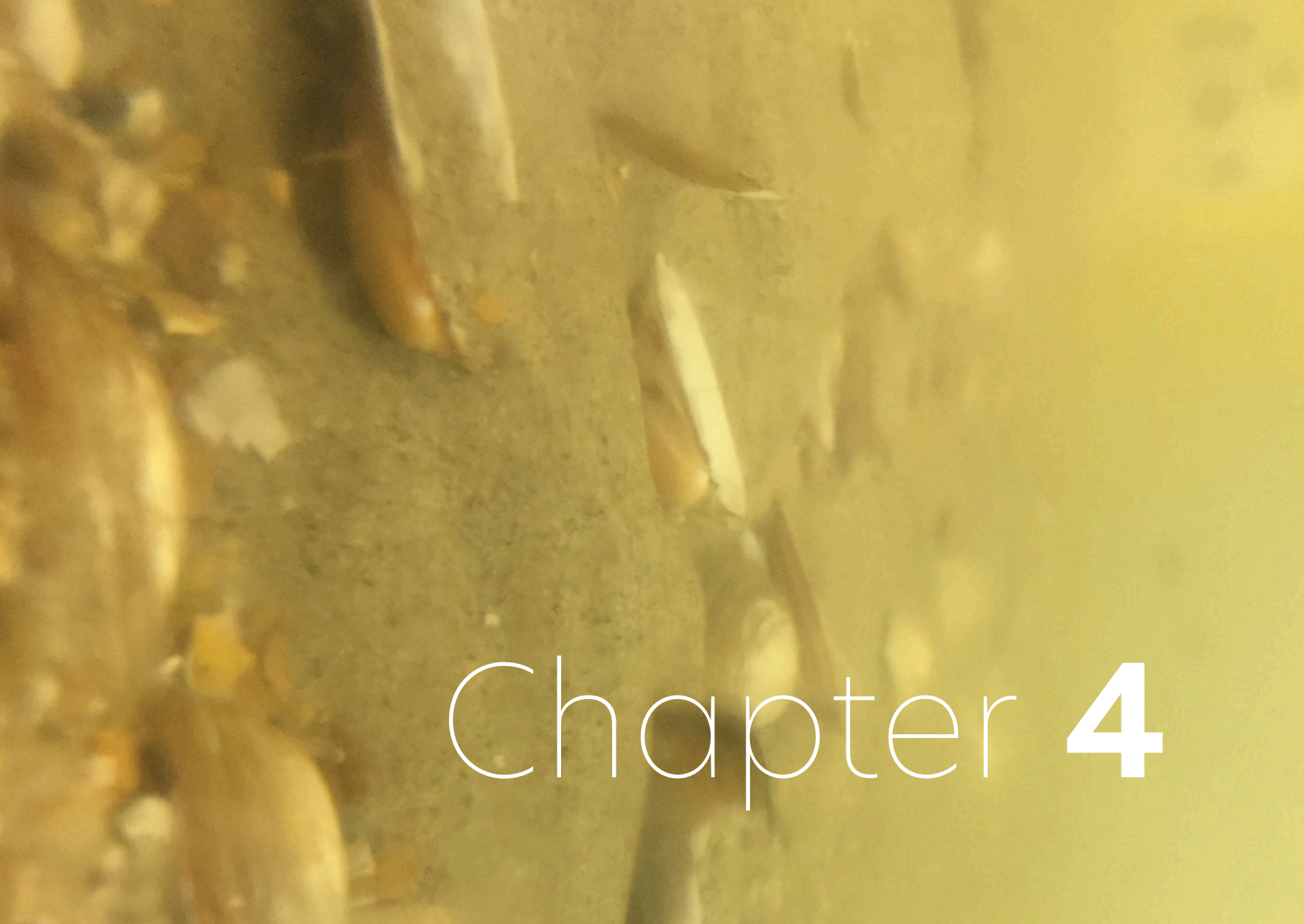

Chapter **4**

Shells and sand transport

How shells of different shapes affect current-driven sand transport

Published in Journal of Geophysical Research: Oceans, 2025, https://doi.org/10.1029/2025JC023346.

Tjitske J. Kooistra, Steven H. Haarbosch, Jorn W. Bosma, Tjeerd J. Bouma, Bram C. van Prooijen, Karline Soetaert, Stuart G. Pearson

Abstract

The seabed rarely consists solely of bare sand: often other materials, such as shells are present. They can influence sand transport by armouring the bed and modifying its roughness. Biogenic shells come in different shapes and sizes, depending on the mollusc species that produce them. To understand how changes in bivalve species composition affect sediment transport, we need a mechanistic understanding of how shell content and shell shape influence the near-bed flow and sand transport. We performed experiments in a racetrack flume, testing the effect of elongated versus rounded shells on unidirectional current-driven sand transport. For both types of shells, a higher depth-averaged flow velocity was needed for initiation of motion and a decrease in bedload transport of sand was found. At a shell content of 20%, the threshold of motion of sand increased up to 75%, and bedload transport was reduced by up to 50%. These effects are explained by a balance between roughness-induced turbulence and bed armouring. Compared to a bare bed, shells decreased bed roughness by reducing ripple formation; rounded shells lowered roughness more than elongated shells, which formed roughness elements themselves, but also covered a larger fraction of the bed. However, there was no clear difference between round versus elongated shells on the overall sand transport; only shell content was key for the overall effect. Our results imply that sediment transport is likely overpredicted when a high number of shells is present in the seabed.

Plain language summary

On sandy sea bottoms, empty shells are often present. They remain in the sand long after the animal that lived in the shell has died. These shells can influence how water currents move sand over the seafloor. Some shells are rounded while others are elongated, and they might influence the transport in different ways. We performed experiments in a flume, a laboratory channel in which a tray with sand and shells was placed, and in which the water current was controlled. We found that both types of shells made it harder for sand to start moving and also reduced how much sand moved in total. Shells made the bed smoother overall, leaving fewer sand ripples. Both shell types had a similar overall effect on sand movement, so the amount of shells in the sand was more important than the shape of the shells. The implications of the study are that we might currently be overestimating how much sand moves when a lot of shells are present in the seabed.

Introduction

Carbonate shells produced by molluscs remain in the sediment long after the animal has died and can persist over geological timescales (Kidwell and Jablonski 1983; Gutiérrez et al. 2003). In highly productive areas, such as intertidal flats, the yearly shell production is typically more than 100 g m-2 (Beukema and Cadée 1999). Because of both high production and durability, shells can occupy a substantial fraction (up to 60%) of the sediment volume and regularly cover considerable parts of the seabed in shallow coastal areas (Kidwell and Jablonski 1983; van der Spek et al. 2022). By adding these persistent structures to the sediment, bivalves can be considered long-term ecosystem engineers (Gutiérrez et al. 2003).

The shell deposits in the top layers of the sediment usually originate from locally occurring species (Al-Dabbas and McManus 1987; van der Spek et al. 2022). Changes in the mollusc community, for instance through biological invasions, can therefore affect the composition of the shell mixture in the surface sediment. An example is the Atlantic razor clam (*Ensis leei*), which was introduced in Western Europe in the 1970s, and has become dominant in terms of biomass and abundance within the first 30 years of its invasion (Tulp et al. 2010; Dekker and Beukema 2012). The elongated bivalve has taken this dominant position from the native cut through shell (*Spisula subtruncata*), characterised by its rounded shells. Ecologically, no significant negative effect of the *E. leei* invasion on *S. subtruncata* populations has been recorded, even though both species occur in the coastal zone (Dekker and Beukema 2012; de Fouw et al. 2024). *E. leei* can reach population densities of hundreds of individuals per square meter (Witbaard et al. 2015), and is already one of the most prevalent shell types in North Sea coastal sediments. Their empty shells typically form large accumulations on beaches (Kerckhof et al. 2007; van der Spek et al. 2022), as well as on the seabed.

Although numerous studies have looked into the settling velocity, incipient motion or transport of shells of different shapes and shell fragments themselves (Mehta et al. 1980; Allen 1984; Al-Dabbas and McManus 1987; Dey 2003; Miedema and Ramsdell 2011; Ramsdell et al. 2011; Kumagai and Nakajima 2012; Diedericks et al. 2018; Fick 2020; Li et al. 2020; Silva et al. 2023; Chen et al. 2024a; Fick et al. 2025), up to date only a few studies investigated the effects of shells on the transportability and composition of the sediment they are embedded in. Shells have been shown to decrease ripple size ripple size, reduce ripple migration rates

(Cheng et al., 2021) and stabilise sediments (Gutiérrez & Iribarne, 1999) under unidirectional flow, and shell fragments decrease bedload transport rates under oscillatory flow (Kumagai and Nakajima 2012). Two main processes could underlie this influence on sediment transport: *i)* alteration of the near-bed flow and turbulence and/or *ii)* armouring of the bed by shielding sediment. Furthermore, in certain configurations, shells in the sediment promote the entrainment of silt in their wake (Pilditch et al. 1997; Witbaard et al. 2017).

Shells can form roughness elements which interact with the flow, comparable to other biogenic roughness elements, such as invertebrate tube structures (Friedrichs et al. 2000; Borsje et al. 2009; Friedrichs et al. 2009; Borsje et al. 2011) and vegetation stems (Bouma et al. 2007; Bouma et al. 2009a; Nepf 2012). For these structures it has been found that they can on the one hand locally increase turbulence and create scouring and thereby promote sediment transport, and on the other hand, at a larger scale, cause skimming flow that protects the seabed (Bouma et al. 2007; Borsje et al. 2009; Bouma et al. 2009a; Borsje et al. 2011). For vegetation, sediment transportability is driven by changes in turbulence level (Hendriks et al. 2008; Hendriks et al. 2010). Here, turbulent kinetic energy (k_t) predicts both the onset of sediment motion and the amount of bedload transport better than bed shear stress (Yang et al. 2016; Yang and Nepf 2018; Zhao and Nepf 2021; Xu et al. 2022). For shells, the interaction with the flow depends on their shape and positioning (Miedema and Ramsdell 2011). Contrary to tubeworms and vegetation, shells are less likely to form vertical structures. Additionally, shells can decrease sand ripple formation and size, which decreases bed roughness and near-bed turbulence (Cheng et al. 2021).

Armouring occurs when the shear stress is above the erosion threshold for the fine fraction but below that of the coarse fraction. This causes a persistent coarse top layer, which shelters the lower layer and reduces further sediment transport (Little and Mayer 1976; Wilcock and DeTemple 2005). Shells have a higher erosion threshold compared to sand and are therefore suitable candidates for armouring (Miedema and Ramsdell 2011; Ramsdell et al. 2011). On beaches, an armouring shell layer can form, reducing wind-driven transport of sand and stabilising the bed (van der Wal 1998; McKenna Neuman et al. 2012). Shells have already been incorporated into aeolian transport equations, which predict transport reasonably well (van Rijn and Strypsteen 2020; Strypsteen et al. 2021). However, in aquatic environments like the seafloor and riverbeds, such transport equations are still lacking due to limited experimental studies quantifying shell-effects on

hydrodynamic-driven sediment transport. In this study, we conducted a flume experiment as a first step towards quantifying how shells of different shapes influence current-driven sand transport.

To date, only very few studies have touched upon the effect of shells or shell fragments on erodibility and transport of sand by hydrodynamic forcing (Gutiérrez and Iribarne 1999; Kumagai and Nakajima 2012; Cheng et al. 2021). The impact of shells has however not yet been quantified in terms of transport rates. This quantification is needed for the implementation of shell-content effects in sediment transport models. Furthermore, the diversity in shell shapes complicates making uniform predictions. If the shape of a shell determines its effect on sediment transport, a change in the morphology of the bivalve community could drive changes in the long-term bioengineering effects of their shells. The research questions we aim to answer are therefore: *i)* how do elongated and round shells affect incipient motion and bedload transport rates of sand, and *ii)* what is the balance between increased transport through roughness and turbulence versus decreased transport through armouring? We hypothesise that shells decrease the transportability of sand through the process of armouring, but that elongated shells create roughness elements which may interact more strongly with the flow. To investigate this, we performed flume experiments on artificial beds of sand mixed with shells from elongated bivalve *Ensis leei* or rounded *Spisula subtruncata*. We explain incipient motion and bedload transport by roughness creation and surface cover. The results from this study can be used as building blocks for improving existing sand transport models. Furthermore, we gain a better understanding of the bioengineering of the diverse types of bivalve shells.

Methodology

Experimental set-up

The experiments were performed in a racetrack flume, located at NIOZ Royal Netherlands Institute for Sea Research in Yerseke (Bouma et al. 2005; Jonsson et al. 2006). The oval flume is 17.5 m long and 3.25 m wide, with a flow channel width of 0.6 m (Fig. 1a). A conveyor belt system on one of the straight sides of the flume creates unidirectional current velocities up to u = 0.6 m s^{-1}. At the end of the opposite straight side, a 2-m long test section with a glass viewing window is located (Fig. 1b). The flume was filled with tap water to a depth of 0.35 m and brought to a salinity of 30 ppm by adding sea salt. We measured salinity prior

to every run using a salinity tester (HI98319, Hanna Instruments). Average water temperature was 12.5 °C.

For measuring current velocity at the test section, we used a Vectrino Acoustic Doppler Velocimeter (ADV, Nortek AS), mounted on a 3D positioning system. The ADV probe was placed approximately halfway along the test bed in the centre of the flume (Fig. 1b), measuring current velocity at 25 Hz, at a level of 0.37*total water depth (*h*) above the bed, to obtain depth-averaged velocity ($\bar{u}$), assuming a logarithmic flow profile (Kleinhans 2005). The experimental set-up also included a Vectrino Profiler (ADVP, Nortek AS), measuring the near-bed velocity profile downstream of the ADV. Due to technical problems, we could not acquire profile data from all the experimental runs. For all available data and runs, see Supplementary information, table S2.

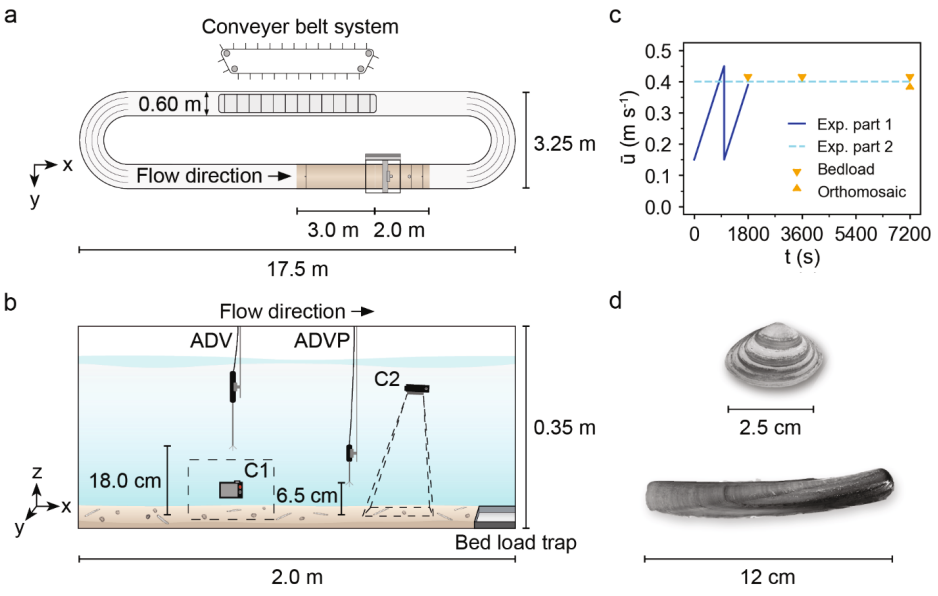

Figure 1. Flume set-up and experimental runs: (a) top view of the racetrack flume with the conveyor belt (top), and supply- and test section (brown, bottom right); (b) side view of the 2-m test section with positioning of instruments (ADV, ADVP), cameras (side view camera C1, and top-view camera C2) and bedload trap; (c) schematic representation of flow velocity settings during experimental runs: part 1 (threshold of motion) with two stages of accelerating flow, part 2 (bedload transport) with constant flow, and time points of sampling bedload and taking orthomosaic pictures in the part 2 experiments; (d) pictures of the two bivalve species shells used: *Spisula subtruncata* (top) and *Ensis leei* (bottom).

We recorded the bed mobility and surface development with two cameras (HERO4 Session, GoPro). The side view camera was mounted outside the window of the test section, at the position of the ADV, and the top view camera was mounted just below the water level, downstream of the ADV. In addition, to monitor the evolution of the bed surface, we captured a set of top-view photos (GoPro HERO4 Silver) of the bed surface over the complete length of the test section at intervals of 5 cm. Ground Control Points (GCPs) were placed on the flume bottom and sides at the start and end of the test section, and on the walls in the middle of the test section. This configuration allowed for the automated stitching of multiple photos into a single orthomosaic (see section 2.4.5).

Bed composition

For the sediment mixture, siliciclastic North Sea sand (d_{50} = 0.348 mm; d_{90} = 0.525 mm) with a density of 2640 kg m^{-3} was used. The grain size composition was measured by laser diffraction (Mastersizer 2000, Malvern Instruments) and the density was tested with a pycnometer. Empty shells of *Ensis leei* and *Spisula subtruncata* (from here on referred to as *Ensis* and *Spisula*, Fig. 1d) were acquired from a shell-processing factory (Meromar Seafoods, Harlingen, Netherlands) and cleaned with enzyme-based detergent. Morphological characteristics of the shells are presented in table S1. We tested sediments with *Ensis*, *Spisula* or a mix of both, in the following bulk volumetric shell contents (P_{shell}): 0% (bare sand), 10% and 20%, for each shell type or a mix of both types. Besides whole shells, we added shell fragments (4 L for every 10 L bulk shell volume) to mimic a natural sand-shell mixture. These shell contents lie within the range found in coastal environments (see section 4.5). The sand and the desired bulk volume of shells were mixed in a standing cement mixer and added to the sediment tray. The dimensions of the trays were 160.5 x 57.5 x 25.5 cm, with a false bottom, leaving the total depth of the sediment at 12 cm. The tray was lifted into the test section, with a lifting crane and the edges were filled with foam strips to prevent the space between the tray edge and the flume walls from becoming a sediment sink. After placing the tray in the flume, several buckets of sediment mixture were added on top of the test bed, so that the surface of the bed was just above the edges of the tray, after compaction. Prior to each experimental run, we re-mixed the sediment and flattened it by raking to ensure that the following run began with a random bed. We covered the flume bottom 3 m upstream of the test section with a thin (~3 cm) layer of the experimental sediment-shell mixture. This was to ensure that the test bed was not supply limited and allow the flow to adjust prior to reaching the test section.

Experimental runs

Two types of experimental runs were performed: i) an accelerating flow experiment to determine the threshold of motion, and ii) a constant flow experiment to determine bedload transport rates. For an overview of all experimental runs and settings, see table S2.

Part 1: threshold of motion

To determine the depth-averaged velocity at the threshold of motion of sand grains, we performed initial experimental runs with slowly accelerating flow (Fig. 1c). The starting current velocity $\bar{u}$ of each run was 0.15 m s^{-1}, increasing by approximately 0.02 m s^{-1} min^{-1} until we observed full bed mobility. Next, $\bar{u}$ was again linearly increased over time, starting from 0.15 m s^{-1}, to test the critical velocity for a water-worked bed, i.e., a bed that has an organised roughness structure created by the streamflow. After the initial analysis, we decided to use the threshold of motion observed during the second acceleration, on a water-worked bed. This gives a more realistic observation, for in nature we rarely find a bed that has been flattened or has not been water-worked. Each experimental run took approximately 30 minutes.

We identified the current velocity at the first motion stage as defined by Breusers & Schukking (1971) and van Rijn (1984): a few rolling grains. For this, we manually determined the onset of incipient motion of sand grains, visual from side and top-view video footage, while using the live observations of initiation of grain movement as a reference point.

Part 2: bedload transport

To quantify the bedload transport, we performed experimental runs with a constant current velocity for 2 hours (Fig. 1c). The tested current velocities ranged from 0.25 to 0.45 m s^{-1}. Since we expected shells to affect turbulence and thus transport, the lowest constant velocity was set near the critical velocity, $\bar{u}_{crit} \approx$ 0.3 m s^{-1}, as determined in part 1.

The transported sediment was collected in a bedload trap (58.5 × 20.0 × 12.0 cm), located at the end of the test section. The current was interrupted to empty the bedload trap after 30, 60 and 120 min — the end of the run. Bedload samples were dried at 60 °C for 8-10 days, then sieved over a 1-mm sieve to separately weigh the coarse (shell) and the fine (sand) fraction, which we summed to acquire the total bedload mass.

Data analysis

The raw data and code to execute the analysis is available in Kooistra et al. (2025a).

Current velocity data processing

We filtered the ADV velocity time-series for correlation values > 70% and a signal-to-noise ratio > 10 dB (Nortek A.S., 2022). After several sensitivity tests, we identified these thresholds to maximise the amount of data kept without affecting the outcomes because of low quality data. Next, we de-spiked the velocity time series applying two filters: (i) a difference filter between two consecutive measurements of 0.5 m s-1, and (ii) a threshold filter (0 < u < 0.7 m s-1; -0.2 < v < 0.2 m s-1; and -0.1 < w < 0.1 m s-1). For the depth-averaged velocity ū in part 1 (threshold of motion), we used the median of the measured depth-averaged velocities from the ADV measurements over the 10 s preceding and the 10 s following the identified motion stage. The selection of a 20-second window was short enough to prevent the filtering out of large turbulent fluctuations, while still being long enough to obtain an accurate velocity measurement. For ū in experiment part 2 (bedload transport) we used the mean of the filtered velocity data over each sampling interval (mean and standard deviations of ū can be found in table S3).

Near-bed velocity and turbulence

We measured near-bed profiles for six experimental runs from the bedload transport experiment (Table S2). For the data processing of the ADVP, we applied similar quality control criteria as with the ADV data: correlation value >70%, a signal-to-noise ratio of >10 dB. Furthermore, we set a minimum amplitude of -40 dB and applied again a difference filter between two consecutive *u*, *v* or *w* measurements of 0.5 m s^{-1}. We selected a 5-minute time window approximately halfway the experimental run, during which the bottom level was constant and corrected the height of the measurement points by the mean value of the detected bottom level.

To check whether the near-bed current velocity followed a logarithmic profile, we fitted a linear regression to *u* (ADVP measurements) over ln(*z*), by a constrained least squares regression fixed at $\bar{u}$ (ADV measurement). Next, we derived shear velocity u_* following the 'law of the wall':

$$\bar{u} = \frac{u_*}{\kappa} \ln \frac{z}{z_0} \quad \text{(eq. 1)}$$

In which u_* is the shear velocity, κ is the Von Karman constant (κ ≈ 0.41) and z_0 is the roughness height. This shear velocity u_* allowed us to compare the skin friction coefficient c_f of shelly versus bare beds:

$$c_f = \left(\frac{u_*}{\bar{u}}\right)^2 \quad \text{(eq. 2)}$$

The standard deviation of the velocity fluctuations relative to the mean gave the turbulence intensity (u', v', w'). From this, we determined turbulent kinetic energy (k_t) near the bed (Soulsby 1983):

$$k_t = \frac{1}{2}\left(u'^2 + v'^2 + w'^2\right) \quad \text{(eq. 3)}$$

The dimensionless turbulent kinetic energy (k_t*) is given by:

$$k_t{}^* = \frac{k_t}{\left(\frac{\rho_S}{\rho_w} - 1\right) g d_{50}} \quad \text{(eq. 4)}$$

in which the sediment density ρ_s = 2640 kg m^{-3}, water density ρ_w = 1027 kg m^{-3} (at 10 °C and a salinity of 30 ppt) and gravitational acceleration g = 9.81 m s^{-2}.

Bed shear stress and friction

The water flow exerts a shear stress on the bed surface. This grain bed shear stress (τ, N m^{-2}) is directly correlated with bed roughness (Van Rijn, 1993):

$$\tau = \rho_w \, g \, \frac{\bar{u}^2}{C^2} \quad \text{(eq. 5)}$$

with the Chézy roughness C, given by the White-Colebrook formula:

$$C = 18 * \log 10 \left(\frac{12R}{k_{s,grain}}\right) \quad \text{(eq. 6)}$$

in which R is the hydraulic radius R = 0.16 m (calculated with the height of the water column and the width of the flume), and grain roughness $k_{s,\,grain}$ = 2×d_{90} = 1.05×10^{-3} m (Kamphuis 2010).

The dimensionless bed shear stress, or Shields number, can be calculated based on the bed shear stress (Van Rijn 1984):

$$\theta = \frac{\tau}{(\rho_s - \rho_w)\, g\, d_{50}} \quad \text{(eq. 7)}$$

Bedload transport

The sediment mass transport rate is computed for each sampling interval by:

$$q_s = \frac{m_{sed}}{W\, \Delta t} \quad \text{(eq. 8)}$$

with q_s as sediment mass transport rate (kg m^{-1} s^{-1}), determined by total dry weight of the transported sediment (m_{sed}) over the width (w) of the flume during each sampled time window (Δt). This can be converted to a non-dimensional bedload transport rate ϕ, or Einstein parameter:

$$\varphi = \frac{q_s}{\rho_s\, w_s\, d_{50}} \quad \text{(eq. 9)}$$

with settling velocity w_s = 0.046 m s^{-1}, following van Rijn (1993) eq. 3.2.22 for non-spherical particles 100 < d_{50} < 1000 µm. This dimensionless sediment transport rate is commonly related to the bed shear stress or Shields number (θ):

$$\varphi = m(\alpha_i\, \theta - \theta_{critical})^{1.5},\ with\ \alpha_i = \frac{\theta_{critical,\ i\%}}{\theta_{critical,\ 0\%}} \quad \text{(eq. 10)}$$

with no transport occurring when $\theta < \theta_{critical}$. This relation was originally formulated by Meyer-Peter and Müller (1948) (MPM), with the critical Shields number defining the onset of sediment motion, $\theta_{critical}$ = 0.047, and a scale factor m = 8. A reanalysis of this formulation by Wong and Parker (2006) (WP) showed slightly different values: $\theta_{critical}$ = 0.0495 and m = 3.97. The original model parameters were based on experiments with featureless bed conditions and uniform sediments, with fully mobile transport conditions (Meyer-Peter and Müller 1948; Wong and Parker 2006). In contrast, our experiments contained bedforms and shells and were conducted using low flow velocities. Therefore, the values of the bedload model coefficients were expected to differ. To account for the effects of the shells on shear stress, we introduce a factor α, which indicates the ratio between the real shear stress (in case of shells) and the shear stress in case for a bare sand bed (no shells). We determine this factor α by determining for which depth-averaged flow velocity sand starts moving for the situation with and without shells in part 1 of the experiment. We emphasize here that the shells change the turbulence and thereby the bed shear stress, and not the initiation of motion of a sand particle. We optimised fitting parameter m using non-linear least square regression (NLS). For this fitting, we selected the data above θ

$_{critical}$ = $\theta_{critical,\ 0\%}$ = 0.0423, as obtained from part 1. As starting parameter, the WP parameter was used (m = 3.97), and $\theta_{critical}$ was set as $\theta_{critical,\ 0\%}$= 0.0423.

Roughness and armouring

For the bed surface structure analysis, we used the top-view orthomosaic images taken after 120 minutes of constant flow (part 2). We used Agisoft Metashape Professional (v. 2.1.3, Agisoft LLC) to create detailed 3D models based on the Structure from Motion (SfM) technique (Westoby et al. 2012). First, a series of images were loaded into the workspace, with low-quality images removed manually. GCP marker data, measured with an approximated accuracy of 5 mm relative to a fixed local 3D coordinate system, was also uploaded; the coordinate system's origin was set at the centre of the test bed at the level of the flume bottom. GCPs were identified automatically, followed by a manual check. Next, we generated a sparse point cloud with automated image alignment, which was refined through calibration using the GCP data and optimising all selectable camera parameters, including additional corrective fits. A dense point cloud was then generated with mild depth filtering. Using this dense point cloud, a Digital Surface Model (DSM) was constructed through planar projection, and an orthomosaic was created based on the DSM. Finally, a bounding box with coordinates [-0.6, -0.2; 0.6, 0.2] was applied to both the DSM and orthomosaic, which were then exported at a spatial resolution of 0.001 m, resulting in images with dimensions of 1200 x 400 pixels each. We determined the areal coverage of shells by manually outlining the shells visible in the orthomosaics using ImageJ. Based on these contours a mask was created and the relative areal cover (%) was calculated (Fig. S2). To avoid capturing side-wall effects on bed roughness, we selected our area of interest as the middle region (0.8 m in x-direction and 0.4 m in y-direction). Roughness was determined as the elevation range of a focal area, i.e. the difference between the minimum and maximum elevation (Wilson et al. 2007), using the package *terra* in R (Hijmans 2020; R Core Team 2024). We selected a focal area of 11x11 pixels to approximate the scale of shells and sand ripples (0.01 m). Total bed roughness ($k_{s,\ bed}$, m) was then calculated as the mean roughness over the entire area of interest.

Results

Threshold of motion

The presence of shells increased the critical depth-averaged velocity and critical Shields at incipient motion in a water-worked bed (Fig. 2). A higher shell content led to a higher $\bar{u}_{critical}$ for initiation of motion of sand grains: from $\bar{u}_{critical}$ = 0.28 m s^{-1} and $\theta_{critical}$ = 0.042 at a bare bed to $\bar{u}_{critical}$ ranging between 0.32-0.36 m s^{-1} and $\theta_{critical}$ between 0.057-0.071 at P_{shell} = 20%. Shell content P_{shell} rather than shell morphology was the driving factor: both elongated as well as round shells resulted in a similar order of magnitude increase in $\bar{u}_{critical}$ and $\theta_{critical}$.

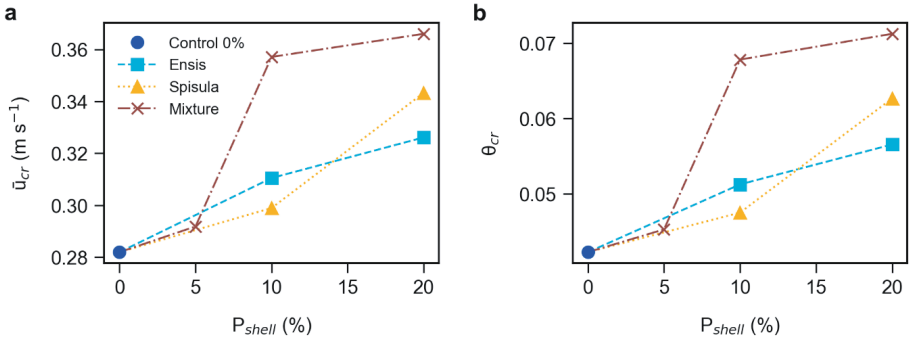

Figure 2. Depth-averaged current velocity at the incipient motion of sand grains for different sand-shell bed compositions.

Near-bed velocity and turbulence

The near-bed current velocity (u; m s^{-1}) approached a logarithmic profile (R^2 ranged between 0.78-0.94; Fig 3a). The presence of shells resulted in lower c_f values compared to bare beds under comparable flow conditions. Near-bed turbulence (k_t*) was higher on bare beds than on beds with shells under comparable depth-averaged flow (Figs. 3b). For some of the shelly beds, k_t* displayed a peak between 0.5 and 1 cm from the bed (z/h=0.01-0.04; Fig. 3b).

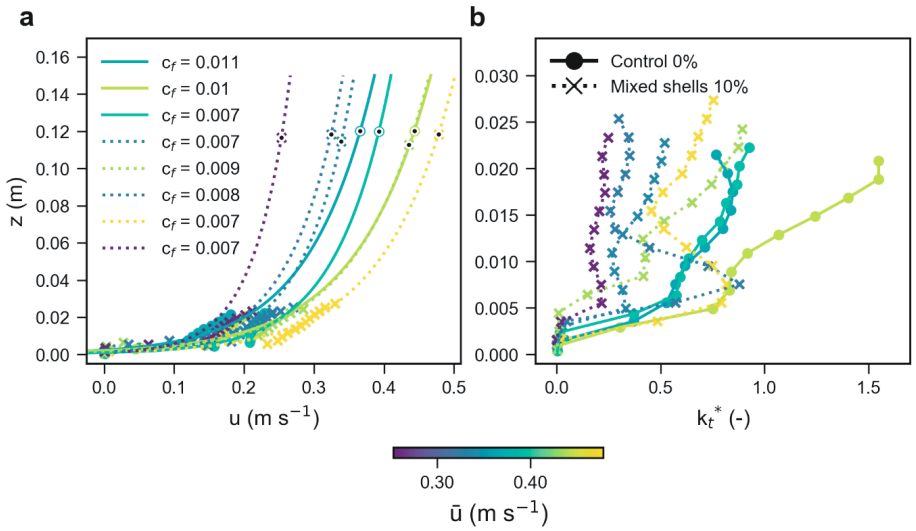

Figure 3. Profiles for the bedload transport experiments (part 2, constant flow), for bare beds (round markers, solid line) and beds containing 10% mixed shells (x-markers, dotted line. Plot colour indicates the mean depth-averaged velocity, with brighter colours indicating higher flow velocity. (a) Near-bed velocity u and logarithmic profiles fitted to all velocity measurements (near-bed u and $\bar{u}$, calculated c_f values are displayed); (b) near-bed turbulence k_t*.

Bedload transport: comparing measurements to literature predictions

Bedload transport was lower when shells were present, while a higher shell content resulted in a greater reduction of bedload transport (Fig. 4a). At P_{shell} = 20% and $\bar{u} = \bar{u}_{max}$, the amount of sand transported was reduced by approximately 50%. At P_{shell} = 10%, the reduction in transport was less pronounced and at $\bar{u} = \bar{u}_{max}$ transport rates approached those of a bare bed. Similar as in part 1, there was no clear difference in the effect of the two different shell types. At the lowest current velocities, near the threshold of motion, bedload transport was close to zero in both bare and shelly beds.

The theoretical WP relations between ϕ and θ overestimated the transported bedload (Fig. 4b). For bare beds as well as sand with shells, optimised scale parameter m was lower than the value given by Wong and Parker (2006). The bare bed resulted in the lowest value (m = 1.08), whereas shells increased m (m = 1.96 for P_{shell} = 10% and m = 1.45 for P_{shell} = 20%). Parameter α, which was set to explain the shell effect on θ as determined in part 1, captured most of the decrease in

transport with increasing shell content ($\alpha_{10\%}$ = 0.76 and $\alpha_{20\%}$ = 0.67). For 10% shells, a steeper curve and hence a higher *m* was then required to capture the high transport rates at $\bar{u}_{max}$. For 20% shells, due to the strongly decreased transport rates at $\bar{u}_{max}$, less steepening was needed and therefore a lower *m* sufficed.

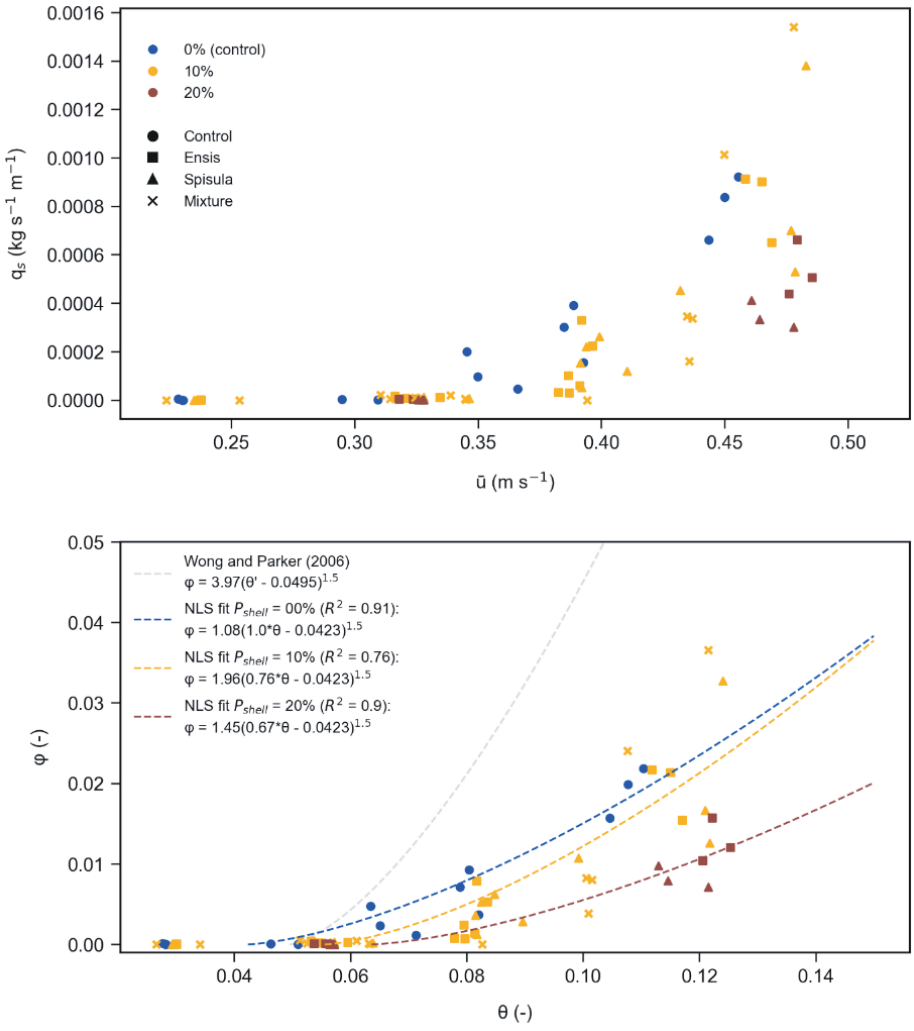

Figure 4. (a) bedload transport flux at different current velocities for all tested bed configurations and (b) dimensionless bedload transport rate (ϕ) over dimensionless grain bed shear stress, or Shields (θ). Plotted lines describe the best-fit bedload models for each shell content (0, 10 and 20%). The predictor with parameters from Wong and Parker (2006) ($\theta_{critical}$ = 0.0495 and *m* = 3.97) is displayed in grey.

Total bed roughness and areal coverage

The sand ripples that increase total roughness of the bed without shells largely disappear when shells are present (Fig. 5). Total bed roughness $k_{s,\,bed}$ decreased with increasing shell content (Fig. 6a). Bare beds and beds with *Ensis* shells resulted in the highest roughness ($k_{s,\,bed}$ = 0.35–0.43 cm), while *Spisula* shells resulted in the lowest roughness ($k_{s,\,bed}$ = 0.27–0.37 cm). (Fig. 6a). *Ensis* shells themselves form large roughness elements, whereas *Spisula* shells form minimal roughness elements. In terms of areal cover, *Ensis* shells covered a larger fraction of the bed compared to *Spisula* shells at P_{shell} = 20% (Fig. 6b).

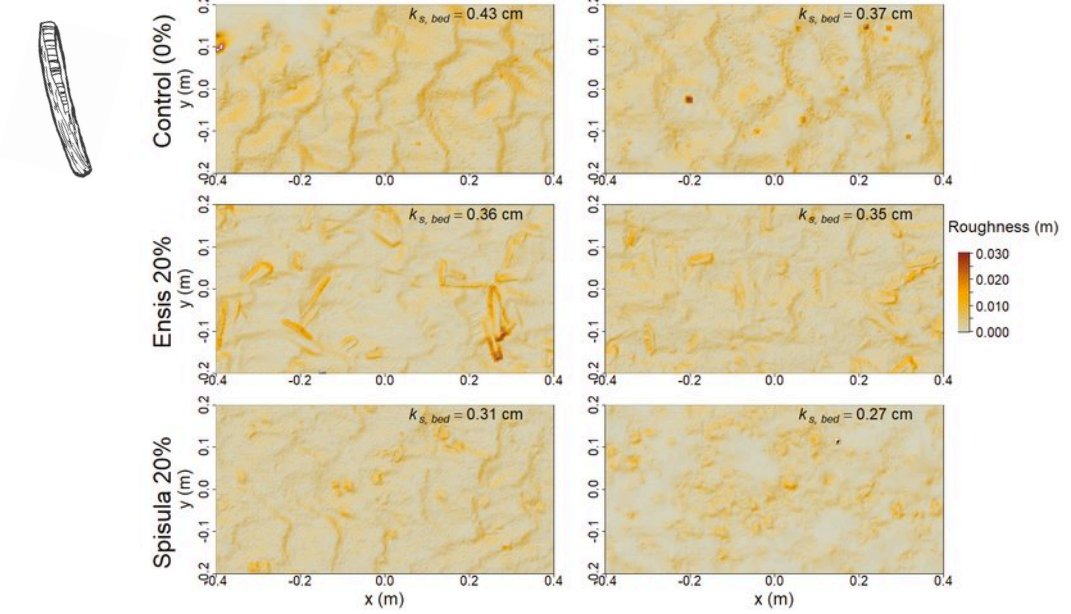

Figure 5. Three example digital surface models (DSMs) after 2 h of constant flow (0.35 or 0.45 m s^{-1}) for beds containing 0% shells, 20% *Ensis* or 20% *Spisula* shells. Note that the colour scale was capped at 0.03 m to increase the visibility of smaller roughness elements.

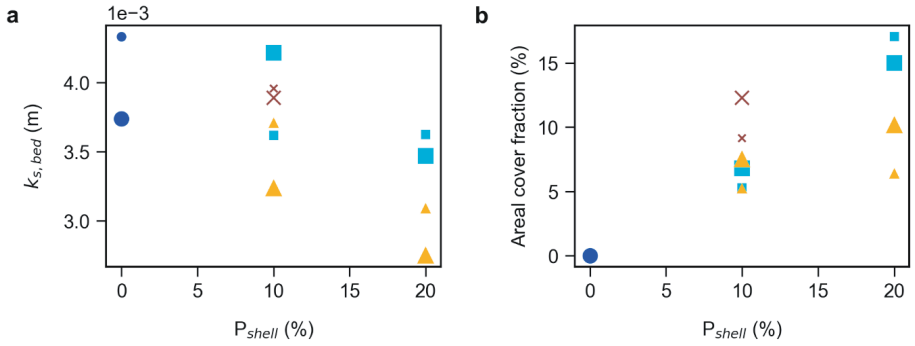

Figure 6. (a) total bed roughness $k_{s,\,bed}$, and (b) areal cover fraction of the comparable constant flow experiments (smaller marker: 0.35 m s^{-1}; larger marker: 0.45 m s^{-1}) for beds containing 0% shells (dot), 10% mixed (x), *Ensis* (square) or *Spisula* (triangle) shells and 20% *Ensis* or *Spisula* shells. Labels for shell types as in Fig. 2.

Discussion

Shells increased the velocity and shear stress at the onset of sediment motion and decreased the bedload transport of sand. While at 10% shell content, transport was only reduced at lower flow velocities, at higher (e.g., 20%) shell content, bedload transport was halved compared to a bare sand bed. This reduction is independent of shell morphology, although shell shape does determine how much the shells interact with bed morphology and hydrodynamics. Both shell types decreased roughness by decreasing ripple formation, but elongated shells formed large roughness elements themselves and thereby lowered total bed roughness to a lesser extent than rounded shells. However, as the elongated shells covered a larger areal fraction of the bed, they sheltered a larger amount of the sediment from near-bed flow compared to rounded shells. These counteracting effects on roughness and bed cover resulted in a similar decrease in sediment transport between shell types (Fig. 7).

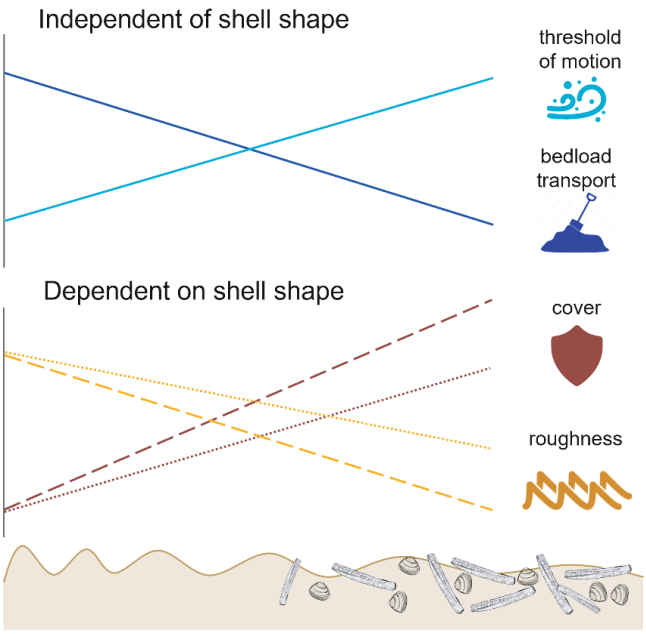

Figure 7. Schematic overview of observed effects of shells on threshold of motion and bedload transport, through bed cover and diminishing roughness. Dashed lines indicate *Ensis*, dotted lines *Spisula*, solid lines indicate effects independent of shell shape.

Shells increased the threshold of motion

Contrary to our findings, Cheng et al. (2021) observed a decrease in $u_{critical}$ and $\theta_{critical}$ up to a shell content of 20%. This could be explained by the fact that we determined incipient motion on a water-reworked rippled bed as would be found in nature, while they looked at an initial, only theoretically existing, flat bed. In our experiment, shells decreased the threshold of motion in some initial beds as well, however, we considered the water-worked bed to be more representative of a natural reference situation. In heterogeneous sand-gravel mixtures, the $\theta_{critical}$ of sand with 20% gravel was in the same order of magnitude as our value of $\theta_{critical}$ at P_{shell} = 20% by McCarron et al. (2019). They attributed this to hiding-exposure effects, a mechanism that plays a role in sand-shell mixtures as well. Furthermore, including factor α in the bedload prediction to represent the effect of shells on $\theta_{critical}$, largely accounted for the decrease in sediment transport at higher shell contents.

What happened close to the bed?

Shells decreased the skin friction coefficient c_f, which is consistent with our findings that shelly beds are less rough than rippled ones. This is also in line with

field measurements above rippled sand beds and shelly beds, as summarised in Soulsby (1983): c_f = 0.0024 for a sand/shell bed, and c_f = 0.0061 for rippled sand. These values lie slightly below the range that we found (0.007–0.01), which might be attributed to the difference in measurement elevation (1 m above the bottom) and field versus experimental context.

Shells decrease near-bed turbulence compared to a bare bed (Fig. 4b). This corresponds to previous observations of lowered near-bed turbulence in the presence of 10% shells (Cheng et al. 2021) or gravel clusters (Curran and Tan 2014). Although our 10% mixed shelly beds, had similar roughness values to the bare bed, shells were distributed in patches, while ripples regularly covered the bare bed (Fig. 5). This could partly explain the differential effect on turbulence, as the shape and spacing of roughness elements play a role in the magnitude of near-bed turbulence (McKenna Neuman et al. 2012). Cheng et al. (2021) saw near-bed turbulence increase for higher shell contents. Therefore, a greater shell content than measured in the current experiment may increase turbulence to a similar level as above the bare bed. Based on our measurements on total bed roughness, we expect the threshold above which shells increase turbulence to depend on shell morphology, and to be lower for round shells compared to elongated shells.

Reduction of bedload transport: magnitude and mechanisms

At the highest shell content (20%), bedload transport was approximately halved compared to a bed without shells. This decrease approaches the 75% decrease in ripple migration rate measured by Cheng et al. (2021), at slightly higher flow (0.5 m s^{-1}). Extrapolating our findings to higher current velocities would likely result in an even larger difference in transported bedload between shelly and bare beds. Furthermore, since transported sand grains do not always maintain contact with the bed but can also move by saltation and in suspension (van Rijn 1984), the ripple migration rate might underestimate bedload transport. The decrease in bedload transport over shelly beds is consistent with field observations of decrease in sand transport when the seafloor consists of a mix of fine sand with shells, compared to bare sand (Pickrill 1986).

Both in the bare and shelly beds, we observed an overestimation of bedload transport by the Wong and Parker (WP) bedload predictor. Several factors could explain this mismatch. Firstly, the WP parameters were defined for a featureless bed. On rippled beds, the WP parameters have been previously observed to be inaccurate (Guevara et al. 2024). Secondly, the original parameters were devel-

oped for fully mobile conditions and have been shown to overestimate transport at low velocities (Ribberink 1998; Kleinhans and van Rijn 2002). In heterogeneous sediments, this could be attributed to the hindrance of small grain movement by larger grains and can be corrected with a hindrance factor (Kleinhans and van Rijn 2002). In our study, different shell shapes and sizes complicated the formulation of a single factor based on particle dimensions. Rather we chose to fit the *m*-parameter (eq. 10) directly, after accounting for the effect of shells on the threshold of motion through a factor α. The decreasing α with shell content captured the decrease in bedload transport by shells compared to bare sand. The fitted *m*-parameter was always lower than the WP value (3.97) but was lowest for bare sand (1.08) and highest for beds with 10% shells (1.96). This increased value for *m* was required to steepen the curve and capture both the lower transport near the threshold of motion as well as the high transport at high flow velocity. These results are consistent with Jumars and Nowell (1984), who note that the impact of benthos on sediment transport rates tends to decrease at higher sediment transport rates. Sediment transport in beds with 20% shells remained below bare-bed transport rates within the tested velocity range, leading to a less steep curve slope and therefore an intermediate fit for *m* (1.45). Overall, these results suggest that P_{shell} = 20% substantially decreases sediment transport, while P_{shell} = 10% might lie below certain thresholds for areal cover or roughness to limit transport at higher flow velocities, analogous to previously identified roughness density thresholds (Nowell and Church 1979; Friedrichs et al. 2009; Bouma et al. 2009a). This threshold could be attributed to a transition from isolated roughness flow to a skimming flow regime.

Shells can modify roughness and shield sand

Shells diminished sand ripples and consequently decreased bed roughness. This confirms the findings from Cheng et al. (2021). Additionally, we saw that the elongated shells reduce roughness to a lesser extent than rounded shells, as elongated shells form roughness elements themselves. This corresponds with a higher drag for particles with a lower shape factor (Li et al. 2020; Chen et al. 2024b), as the shape factor of elongated shells was 0.12, compared with 0.30 for round shells (Table S1). Furthermore, at P_{shell} = 10%, the total roughness of beds, whether with elongated or mixed shells, still fall within the range of bare beds. Contrarily, Cheng et al. (2021) measured minimal roughness based on near-bed turbulence at P_{shell} = 10%, above which bed roughness increased. Although our DSM-based method may contain biases, for instance, due to dependence on the raster resolution (Wilson et al. 2007), we attempted to correct for this by

selecting a suitable scale. Rather than a value derived from local flow conditions, our DSM-based roughness gives a direct measure of the roughness for the entire bed, i.e., at the macroscale level. The lower c_r values for shelly beds also agree with the lower roughness, even though we only have c_r measurements for 10% mixed shells. The decreased roughness could be responsible for the increase in threshold of motion: sediment is less readily entrained due to a decrease in turbulent bursts.

In sediments with armouring, bedload transport is overestimated by the original bedload models (Hunziker and Jaeggi 2002). During our 2-hour experimental runs, the top layer of the sediment did not coarsen (Table S4), possibly due to sufficient upstream sediment supply, nor did the transport rate decrease over time. Shells, however, covered up to 15% of the bed for elongated *Ensis* shells, and 8-10% for the same bulk volume content of rounded *Spisula* shells. In aeolian settings, shells have been shown to limit sand transport already from low shell contents. A 20% shell content reduced the amount of transported sand by up to 80% (van der Wal 1998). This reduction of sediment transport is of the same order of magnitude as our measured bedload transport effects. Bed cover by shells resulted in stabilisation of the sand surface in wind tunnel experiments, resulting in an up to 45% increase of the threshold of motion (McKenna Neuman et al. 2012), which is similar to our observed increase in the threshold of motion. In line with our findings, large shells here also resulted in higher cover fractions than small shells.

As a next step, a shell reduction factor such as the Bagnold equation for aeolian transport (van Rijn and Strypsteen 2020), could be defined for transport equations in aquatic settings. Alternatively, the *m* and a parameters can be adapted directly within an MPM-like bedload predictor, following the results of this study. To increase the accuracy of these parameters, we recommend testing a wider range of shell contents and flow conditions. This would also increase the applicability in a wider range of field conditions.

Outlook and applications

Before upscaling our findings, a few limitations should be considered. Firstly, we tested current velocities up to 0.45 m s^{-1}, in the lower transport stage (as defined by van Rijn (1993)). Tidal currents velocities of 1 m s^{-1} are common in the coastal zone (Elias et al. 2022). Although we observed some mobility, most of our shells remained in place even during the faster flow conditions. With stron-

ger currents, however, they may be swept away. Secondly, we tested unimodal, sandy sediment, while different interactions may be at play when mud is present. The effect of shells in cohesive sediments is therefore to be considered in future experiments.

The shell contents used in this study fall within the range of shell contents measured in the field (Fig. 8) and previously reported (Wells and Kim 1989). Shell distribution is however heterogeneous. To implement shells in sediment transport models, datasets with a higher resolution of sediment shell content are needed. Hydroacoustic mapping could provide such an increased resolution, compared to sediment sampling (Mielck et al., 2014).

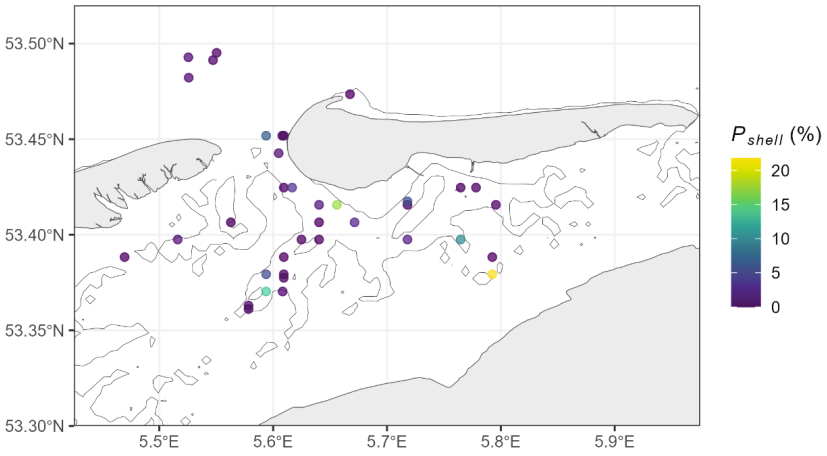

Figure 8: volumetric shell contents measured near the Ameland inlet, Wadden Sea, the Netherlands. Note that shell content here was measured as water-replacement volume and is therefore likely lower than the bulk volume used in the current study. The sampling methodology is described in Text S1.

Elongated and round shells had similar effects on sediment transport, even if their interaction with bedforms and their areal coverage of the bed differs. Therefore, the replacement of a native by an invasive species with a different shell morphology will likely not directly affect the sediment transportability. However, when shell production in an area increases, for instance, because an invasive species has a higher abundance or can colonise habitats that were previously less occupied by similar-sized bivalves, this might have implications for sediment transport processes. *Ensis leei* has been suggested to colonise previously "empty"

habitats because of its resilience to hydrodynamic stress (Dekker and Beukema 2012). Additionally, to date, there is no evidence that this species has replaced native species. Therefore, the large increase in shell production by the colonisation of *Ensis leei* might have influenced sediment transport.

By decreasing sediment transportability, shells may feedback into larger-scale morphological processes, such as sand wave formation and migration. Biogeomorphological effects have previously been implemented in models for sand wave occurrence and morphology (Borsje et al. 2009; Damveld et al. 2020). Additionally, including coarser fractions improved modelled sand wave migration rates (Wang et al. 2019). Given the prevalence of shells in shallow marine basins, incorporating biogeomorphological effects could lead to more accurate predictions of sand wave development. Another problem in morphodynamic modelling is the overestimation of channel incision, which is usually calibrated by modifying bed roughness, increasing sediment grain size or increasing the transverse slope parameter to unrealistic values (Baar et al., 2019; Y. Wang et al., 2016). Shells are prevalent in these deeper gullies and including them might therefore improve predictions of channel incision. Lastly, including shells in sediment nourishments may improve the durability of the nourishment (Strypsteen et al. 2021). The empirical results from our study could serve to predict the effects of shells in the distribution of the nourished sediment. The ecological effects of such applications should however not be neglected (Peterson et al. 2014).

Conclusions

Shells increase the shear stress at threshold of motion and decrease the bedload transport of sand. The magnitude of these effects is similar for different shell shapes, even though the underlying mechanisms—such as the formation of roughness elements and the spatial coverage by shells—vary depending on shell shape. Given the widespread occurrence of shells in marine sediments, these significant effects likely have implications for large-scale sediment transport predictions. By redefining parameters in sediment transport formulation to account for the presence of shells, we made a step towards including their influence in sediment transport models. This knowledge contributes to more realistic forecasting of sediment dynamics.

Appendices

Appendix A: List of symbols

α_i	ratio between $\theta_{critical,\ 0\%}$ and $\theta_{critical,\ i\%}$
C	Chézy roughness [$m^{1/2}\ s^{-1}$]
c_f	skin friction coefficient [-]
d_{50}; d_{90}	median grain size; 90th percentile of cumulative grain size distribution [mm]
g	gravitational acceleration [9.81 m s^{-2}]
θ; $\theta_{critical}$	dimensionless bed shear stress, or Shields number; critical Shields number [-]
k_s; $k_{s,\ bed}$	roughness; total bed roughness [m]
k_t; k_t*	turbulent kinetic energy [$m^2\ s^{-2}$]; dimensionless turbulent kinetic energy [-]
κ	Von Karman constant ($\kappa \approx 0.41$)
m	scale parameter in MPM-like bedload predictor
P_{shell}	shell content [%]
q_s	sediment mass transport rate [kg s^{-1} m^{-1}]
ρ_s; ρ_w	sediment density; water density [kg m^{-3}]
R	hydraulic radius [m]
τ	bed shear stress [N m^{-2}]
$\bar{u}$	depth-averaged velocity in x-direction [m s^{-1}]
u'; v'; w'	turbulence intensity in x, y and z direction [m s^{-1}]
u_*	shear velocity [m s^{-1}]
ϕ	dimensionless bedload transport rate (or Einstein parameter) [-]
w_s	settling velocity [m s^{-1}]
z	height above bed [m]
z_0	roughness length [m]

Acknowledgements

We would like to thank Chiu Cheng, Jaco de Smit and Timothy Price for their involvement in the initial advice and brainstorming during conceptualisation and troubleshooting during the experiment and analysis. Thanks to Lennart van IJzerloo, André den Herder and Arne den Toonder for practical assistance with the flume set-up and Peter van Breugel for analysing sediment samples. We thank

André Seinen from Meromar Seafoods for saving up *Ensis* and *Spisula* shells. Furthermore, we would like to thank Maarten Kleinhans, Gerben Ruessink and Sierd de Vries for their advice and feedback on the methodology and analysis and Rob Witbaard for feedback on the draft manuscript. Funding for this study was provided by NWO grant no. 17600: "Tracking Ameland Inlet Living Lab Sediment (TRAILS)" and NWO grant no. 18035: "Effective Upgrades and REtrofits for Coastal Climate Adaptation" (EURECCA). Additionally, Stuart Pearson received funding from NWO grant no. 21026: "Revealing Hidden Networks of Coastal Sediment Pathways".

Data availability

The ADV and ADVP data, sediment data, and images for determining the initiation of motion, flow characteristics, bed characteristics and bedload transport rates in the study are available at the NIOZ Dataverse via https://doi.org/10.25850/nioz/7b.b.0j with CC0 access(Kooistra et al. 2025a).

Python and R code used for data processing, analyses and creating the figures in this paper is preserved at the NIOZ Dataverse via https://doi.org/10.25850/nioz/7b.b.0j with CC0 access (Kooistra et al. 2025a).

Supplementary materials

Here, the supplementary information is given for **"***How Shells of Different Shapes Affect Current-driven Sand Transport*". The supplements include an overview of the experimental flume runs performed, examples of the masks created for bed cover fraction, sediment composition of the beds before and after each run, and a short description of how the field shell contents were derived.

Text S1. Methodology field sampling shell content

Sediment samples were collected by boxcore in the Ameland tidal inlet, the Netherlands (53°N 5°E). Boxcore samples were collected at several subtidal sites at the ebb-tidal delta, in the main gully and smaller gullies deeper in the tidal basin. The boxcore surface area was 0.06 m2, and the height of the sediment in the box core was measured for each sample, so that the core volume could be determined. Boxcore samples were sieved over a 1 mm sieve and the coarse fraction, which largely consisted of shells, was stored for further processing. In the laboratory, shell volume of each sample which contained >10 mL shells or shell fragments was determined by water measuring water replacement volume in a 500 mL or 2 L beaker. Shell content was then calculated using the core volume.

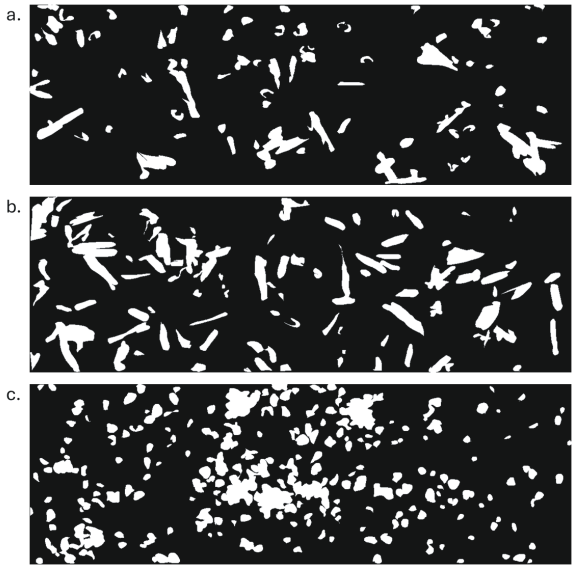

Figure S1. Examples of masks for determining areal shell cover fraction for beds with (a) 10% mixed shells, (b) 20% Ensis shells and (c) 20% Spisula shells.

Table S1. Morphological characteristics of the two shell types used in this study. 100 shells of each species were measured and weighed. Corey's shape factor was determined, with respectively, height, length and width as minimal, maximal and medium dimensions.

Species	N	Length (mm)	Width (mm)	Height (mm)	Thickness (mm)	Weight (g)	Corey Shape Factor $d_{min}/\sqrt{(d_{max} \cdot d_{med})}$
Ensis	100	106.54 (± 8.66)	16.83 (± 1.70)	5.15 (± 0.55)	0.59 (± 0.08)	3.02 (± 0.68)	0.12 (± 0.01)
Spisula	100	28.64 (± 1.97)	20.02 (± 1.40)	7.29 (± 0.73)	1.05 (± 0.17)	1.49 (± 0.45)	0.30 (± 0.03)

Table S2. Overview of all experimental runs used for part 1 (threshold of motion, accelerating flow) and part 2 (bedload transport, constant flow) of this study. Target depth-averaged velocity ū for each run and the available data (top- and side view camera, ADV, ADVP = vectrino profiler) are shown.

Run code	Shell type	P_{shell}	Target ū [m s^{-1}]	Camera Top	Camera Side	ADV	ADVP
P1_0_00_R1	-	0	*accelerating*	1	1	1	1
P1_E_10_R1	*Ensis*	10		1	1	1	0
P1_E_20_R1		20		1	1	1	0
P1_M_05_R1	*Mix*	5		1	1	1	1
P1_M_10_R1		10		1	1	1	1
P1_M_20_R1		20		1	1	1	1
P1_M_50_R1		50		1	1	1	1
P1_S_10_R1	*Spisula*	10		1	1	1	0
P1_S_20_R1		20		1	1	1	0
P2_0_00_R1	-	0	0.35	1	1	1	1
P2_0_00_R2			0.45	1	1	1	1
P2_0_00_R3			0.4	1	0	1	1
P2_0_00_R4			0.3	1	1	1	0
P2_0_00_R5			0.25	1	1	1	0
P2_E_10_R1	*Ensis*	10	0.35	1	1	1	0
P2_E_10_R2			0.45	1	1	1	0
P2_E_10_R3			0.4	1	1	1	0
P2_E_10_R4			0.3	1	1	1	0
P2_E_10_R5			0.25	1	1	1	0
P2_E_20_R1		20	0.35	1	1	1	0
P2_E_20_R2			0.45	1	1	1	0

Table S2. Overview of all experimental runs used for part 1 (threshold of motion, accelerating flow) and part 2 (bedload transport, constant flow) of this study. Target depth-averaged velocity ū for each run and the available data (top- and side view camera, ADV, ADVP = vectrino profiler) are shown. *(Continued)*

Run code	Shell type	P_{shell}	Target ū [m s^{-1}]	Camera Top	Camera Side	ADV	ADVP
P2_M_10_R1	*Mix*	10	0.35	0	0	1	1
P2_M_10_R2			0.45	1	1	1	1
P2_M_10_R3			0.3	1	1	1	1
P2_M_10_R4			0.4	1	1	1	1
P2_M_10_R5			0.25	1	1	1	1
P2_S_10_R1	*Spisula*	10	0.35	1	1	1	0
P2_S_10_R2			0.45	1	1	1	0
P2_S_10_R3			0.4	1	1	1	0
P2_S_10_R4			0.3	1	1	1	0
P2_S_10_R5			0.25	1	1	1	0
P2_S_20_R1		20	0.35	1	1	1	0
P2_S_20_R2			0.45	1	1	1	0

Table S3. Measured mean and standard deviation (σ) of depth-averaged velocity ū for the three sampled time periods in each run in Part 2 of the experiment (constant flow, bedload transport).

Run code	$\bar{u}_{BL1} \pm \sigma$	$\bar{u}_{BL2} \pm \sigma$	$\bar{u}_{BL3} \pm \sigma$
P2_C_0_00_R1	0.37 ± 0.02	0.35 ± 0.03	0.35 ± 0.03
P2_C_0_00_R2	0.44 ± 0.03	0.46 ± 0.03	0.45 ± 0.03
P2_C_0_00_R3	0.39 ± 0.03	0.39 ± 0.03	0.38 ± 0.04
P2_C_0_00_R4	0.29 ± 0.02	0.31 ± 0.02	0.32 ± 0.02
P2_C_0_00_R5	0.23 ± 0.02	0.23 ± 0.02	0.23 ± 0.02
P2_C_E_10_R1	0.39 ± 0.03	0.38 ± 0.03	0.39 ± 0.03
P2_C_E_10_R2	0.47 ± 0.03	0.46 ± 0.04	0.47 ± 0.03
P2_C_E_10_R3	0.39 ± 0.03	0.40 ± 0.03	0.39 ± 0.03
P2_C_E_10_R4	0.32 ± 0.02	0.32 ± 0.02	0.33 ± 0.03
P2_C_E_10_R5	0.24 ± 0.01	0.24 ± 0.01	0.24 ± 0.01
P2_C_E_20_R1	0.32 ± 0.03	0.32 ± 0.03	0.33 ± 0.03
P2_C_E_20_R2	0.48 ± 0.02	0.49 ± 0.02	0.48 ± 0.02
P2_C_M_10_R1	0.34 ± 0.03	0.35 ± 0.02	0.35 ± 0.03
P2_C_M_10_R2	0.44 ± 0.03	0.44 ± 0.03	0.44 ± 0.03
P2_C_M_10_R3	0.33 ± 0.02	0.32 ± 0.03	0.31 ± 0.03
P2_C_M_10_R4	0.48 ± 0.05	0.45 ± 0.03	0.39 ± 0.02
P2_C_M_10_R5	0.26 ± 0.02	0.24 ± 0.03	0.23 ± 0.03
P2_C_S_10_R1	0.39 ± 0.03	0.39 ± 0.03	0.39 ± 0.03
P2_C_S_10_R2	0.48 ± 0.03	0.48 ± 0.03	0.48 ± 0.03
P2_C_S_10_R3	0.41 ± 0.02	0.40 ± 0.04	0.43 ± 0.03
P2_C_S_10_R4	0.35 ± 0.03	0.33 ± 0.06	0.33 ± 0.04
P2_C_S_10_R5	0.24 ± 0.02	0.24 ± 0.02	0.24 ± 0.02
P2_C_S_20_R1	0.33 ± 0.02	0.33 ± 0.02	0.33 ± 0.02
P2_C_S_20_R2	0.48 ± 0.03	0.46 ± 0.03	0.46 ± 0.03

Table S4. bed sediment composition at the start (t0) and end (tend) of each experimental run. Runs from part 2 (constant flow for 2 hours) are displayed. Sediment d50 and d90 are given, as well as the difference between t0 and tend. Negative values (red) indicate coarsening.

Run code	timepoint	d_{50} (µm)	d_{90} (µm)	d_{50} t_0-t_{end}	d_{90} t_0-t_{end}
P2_C_0_00_R1	t0	506.6	338.29	-1.07	-1.41
P2_C_0_00_R1	tend	508.01	339.36		
P2_C_0_00_R3	t0	493.93	329.02	-11.69	-18.06
P2_C_0_00_R3	tend	511.99	340.71		
P2_C_0_00_R4	t0	522.89	347.85	4.48	4.75
P2_C_0_00_R4	tend	518.14	343.37		
P2_C_0_00_R5	t0	503.26	336.62	-15.72	-27.74
P2_C_0_00_R5	tend	531	352.34		
P2_C_E_10_R1	t0	517.74	342.93	-18.84	-56.06
P2_C_E_10_R1	tend	573.8	361.77		
P2_C_E_10_R2	t0	523.04	345.13	10.04	18.37
P2_C_E_10_R2	tend	504.67	335.09		
P2_C_E_10_R3	t0	516.99	341.58	-9.86	-16.18
P2_C_E_10_R3	tend	533.17	351.44		
P2_C_E_10_R4	t0	518.06	344.2	12.54	21.9
P2_C_E_10_R4	tend	496.16	331.66		
P2_C_E_10_R5	t0	546.85	359.41	9.69	18.83
P2_C_E_10_R5	tend	528.02	349.72		
P2_C_E_20_R1	t0	508.97	338.32	-17.43	-35.64
P2_C_E_20_R1	tend	544.61	355.75		
P2_C_E_20_R2	t0	527.41	348.17	17.59	29.84
P2_C_E_20_R2	tend	497.57	330.58		
P2_C_M_10_R5	t0	543.43	361.04	7.9	9.11
P2_C_M_10_R5	tend	534.32	353.14		
P2_C_M_10_R6	t0	519.25	345.45	0.78	2.7
P2_C_M_10_R6	tend	516.55	344.67		
P2_C_S_10_R1	t0	525.39	348.17	12.1	21.47
P2_C_S_10_R1	tend	503.92	336.07		
P2_C_S_10_R2	t0	528.95	348.47	12.85	23.63
P2_C_S_10_R2	tend	505.32	335.62		
P2_C_S_10_R3	t0	503.84	336.66	-5.99	-4.45
P2_C_S_10_R3	tend	508.29	342.65		
P2_C_S_10_R4	t0	530.61	350.28	4.07	10.58
P2_C_S_10_R4	tend	520.03	346.21		
P2_C_S_10_R5	t0	507.57	338.97	-8.04	-18.79
P2_C_S_10_R5	tend	526.36	347.01		

Chapter 5

Sediment modification by bioturbation

Worms and storms: shedding light on bioturbation and physical mixing on an intertidal flat by combining multiple tracers

Published in Biogeosciences, 2026, https://doi.org/10.5194/bg-23-2477-2026

Tjitske J. Kooistra, Anna-Maartje de Boer, Tjeerd J. Bouma, Natascia Pannozzo, Stuart G. Pearson, Ad van der Spek, Henko de Stigter, Rob Witbaard, Jakob Wallinga, Karline Soetaert

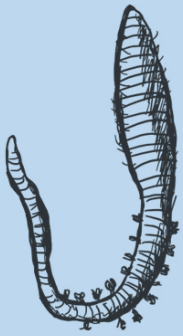

Abstract

Sediment transport and seabed composition can both be influenced by bioturbation and hydrodynamically driven sediment mixing and deposition. In a dynamic intertidal environment, it is challenging to distinguish the relative contribution of both processes. We aim to unravel their relative importance by combining several tracers, each having its own specific timescale and target particle size. We combined (1) ^{210}Pb that quantifies long-term (years-decades) mixing of fine sediment fractions with (2) Chlorophyll-*a* and (3) luminophores that both quantify short-term mixing of fine sediment fractions (days-weeks), and (4) multi-grain quartz and single-grain feldspar luminescence dating, which use the bleaching of sand grains' inherent luminescence signal by light to assess mixing of sand and thereby quantifies long-term mixing. Single grain feldspar luminescence is here for the first time applied in the intertidal environment. We compare results for a sandy and a muddy intertidal flat at the island of Texel (Wadden Sea, the Netherlands), each with their own characteristic benthic community. Recent bioturbation became apparent from Chlorophyll-*a* and luminophore profiles: particles were rapidly reworked to a depth of decimetres. ^{210}Pb also suggested mixing and non-local exchange of particles by bioturbation. The combination of luminescence signals suggested that after deposition, not all sand grains did re-surface repeatedly and for longer time periods through bioturbation. Coarse- and fine-grained tracer profiles show the differential behaviour and reworking of the mud and sand fraction within the sediment matrix: as expected with particle-selective bioturbation, mud is preferentially bioturbated and infiltrates passively, while sand grains have a higher ability to conserve layering. Single-grain feldspar luminescence is a promising technique to demonstrate the long-term reworking of sand grains, however, in young and dynamic environments, a combination of tracers remains necessary to inform on the origin of mixing.

Summary

On intertidal flats, it is hard to distinguish sediment mixing by animals from reworking by waves and currents. We combined tracers to identify reworking of grains of different sizes on the short- and long term. Coarse (sand) grains were less mobile than fine (mud) grains, and partly kept their layering after deposition. The luminescence properties of sand grains can be used for sediment dating and can show sediment mixing, but this method needs to be tested more for young, intertidal sediments.

Summarising figure.

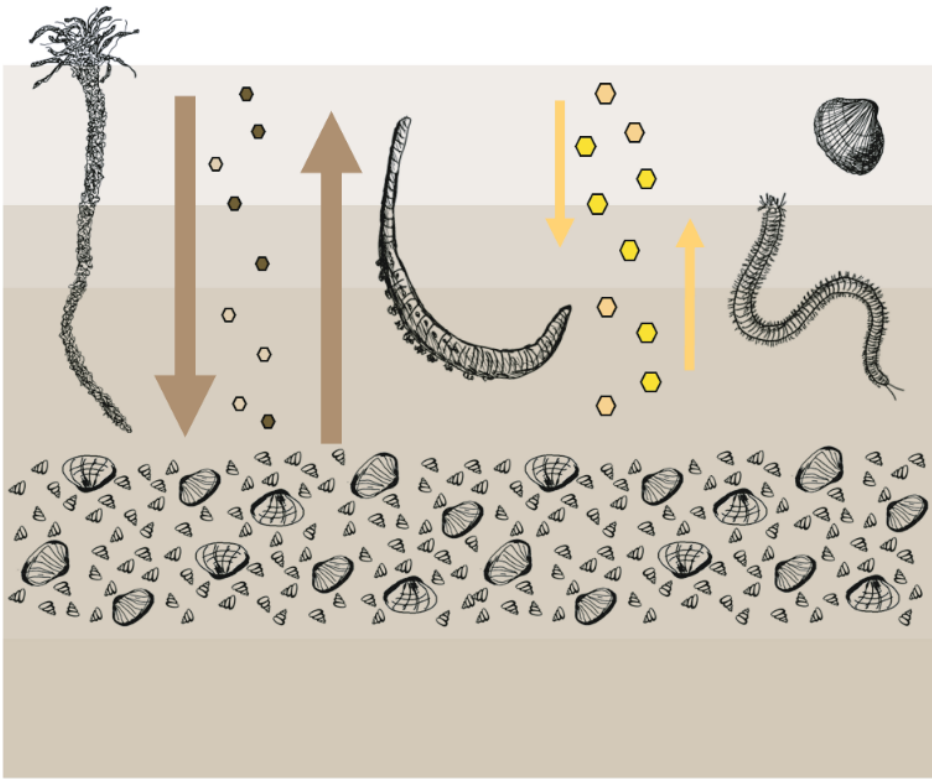

Introduction

In dynamic, soft-sediment seafloors, such as intertidal flats, sediment grain size is influenced by physical and ecological processes. The grain size composition of sediments determines sediment stability and erosion thresholds (Staudt et al., 2019). This, in turn, impacts daily sediment dynamics, and morphology on a larger spatial and temporal scale (Belliard et al., 2019). Sediment composition is also a crucial ecological factor, as it shapes the benthic community (e.g., Compton et al., 2013; Gray, 1974; Kooistra et al., 2025). It is therefore important to understand the drivers of grain-size distribution on intertidal flats. However, obtaining such knowledge is complicated, as the relevant interacting physical and ecological processes can act on different timescales.

Benthic animals e.g. like worms and bivalves can influence their sedimentary habitats by bioturbation (Davison 1891; Kristensen et al. 2012; Meysman et al. 2006; Richter 1952). With their burrowing, feeding and ventilating behaviour, they can influence the composition, stability, and density of the sediment (Jumars & Nowell 1984; Rhoads & Boyer 1982; Widdows & Brinsley 2002). This bioturbation has implications for biochemical cycling and carbon storage by remineralisation and burial of organic matter (Aller, 1982; Snelgrove et al., 2018). The mode of bioturbation differs per species: some randomly displace sediments over short distances (diffusive mixing), while others convey sediment upwards or downwards (advective transport) (François et al., 1997; Queirós et al., 2013). Moreover, bioturbators can be selective for particle size and type (Jumars et al. 1982; Taghon 1982).

Physical sediment deposition and reworking is dependent on periodic hydrodynamics, such as tidal currents, as well as waves and currents induced by meteorological conditions. During calm atmospheric conditions, spring- and neap tide periodicity can create layered bedding (Deloffre et al., 2007; Zhou et al., 2021), and tidal currents and wave forcing can result in a dynamic morphological equilibrium with bed level changes of 5–10 cm day^{-1} in macrotidal systems (Grandjean et al., 2023; Hu et al., 2018). In such systems, reworking by tidal current forcing is dominant at lower intertidal flats, while waves, generated by wind, are a major driver in the high intertidal (Belliard et al., 2019). High-energy events, such as storms, can transport large amounts of sediment over a short time span (de Vet et al., 2018). A storm can result in sediment relocations equivalent to at least months–years of sediment displacements under calm conditions, reworking sed-

iment down to 15 cm depth (Fan et al., 2006; Hu et al., 2018; de Vet et al., 2020). Such intense meteorological events can deposit a coarse sand layer on a tidal flat (Zhou et al., 2022), or increase mud deposition by increasing inundation time and suspended sediment concentration as well as creating accommodation space by erosion (Colosimo et al., 2023; Gao, 2018; Grandjean et al., 2023). Storm events can therefore be recognised in layering of the sediment bedding, where the timing relative to the spring-neap tidal cycle and storm chronology determines the storm layer grain size composition (Wang and Cheng, 2016; Zhou et al., 2022). This stratification can however largely be smoothed out by daily bioturbation, thereby erasing the signals of episodic deposition (Wheatcroft, 1990).

It is challenging to disentangle the biological from the physical control on sediment composition, i.e. to determine the extent to which '(per)turbation' is actually 'bio'. While on short timescales (days–weeks) and in controlled experiments, grains reworked by bioturbation can be clearly isolated from those reworked by hydrodynamics, on longer timescales (years–centuries) and in dynamic natural environments, this is nearly impossible. Furthermore, the relative magnitude of these processes is highly site-specific. To obtain insight in the reworking processes in intertidal environments, acting at different frequencies and energy levels, we need tracers that gather information on short- and long-term reworking of different sediment fractions (Fig. 1). A short-term tracer needs to be exposed to a sufficient number of mixing events relative to its timescale, therefore the spatial and temporal scale of sampling should match mixing intensity (Meysman et al., 2010). Long-term tracers may instead provide a more integrated result than short-term tracers, reflecting both long-term sediment dynamics, as well as recent reworking. Vertical profiles can then inform on the short- and long-term reworking and deposition history. A strongly stratified profile might point to episodic deposition events, while a homogeneous signal over depth might indicate intense mixing by biota or hydrodynamics. Bioturbation might also cause sub-surface supply of young material through advective vertical transport (Meysman et al. 2003; Richter et al. 1996). Thus, combining signals can shed light on the origin of mixing processes acting in dynamic coastal sediments.

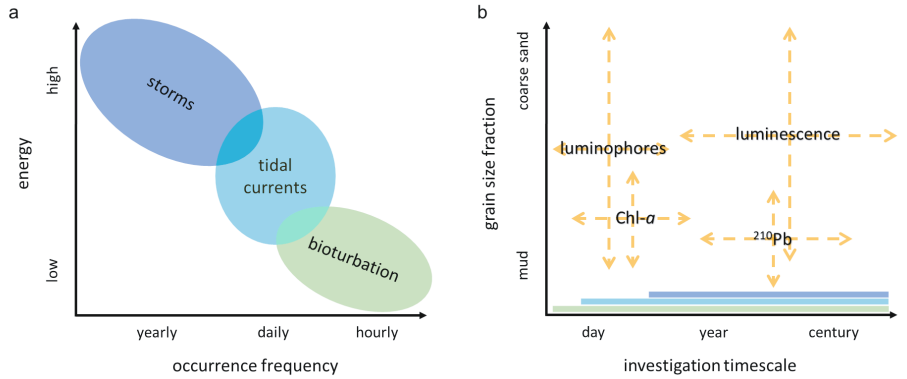

Figure 1. (a) mixing processes with their occurrence frequency and energy; (b) sediment tracers with their relevant investigation timescales and potential target sediment fraction. The mixing processes that are recorded in the tracer distributions, depending on the moment and period of sampling, are indicated as bands along the x-axis.

The relevant timescale and grain size fraction is specific for each tracer type (Table 1). Tracers that are commonly used for studying bioturbation in dynamic marine sediments have been previously reviewed by Maire et al. (2008). Here we highlight several commonly used tracers in the context of timescale and grain size. Tracers that give information on recent bioturbation are Chlorophyll-*a* (Chl-*a*) and luminophores. Due to its wide occurrence, Chl-*a* is often used as a non-conservative short term tracer for bioturbation. Drawbacks are that the decay time varies with environmental conditions (Sun et al., 1993), and herbivorous biota may actively select for Chl-*a* (Taghon, 1982). Luminophores are fluorescent coated particles that are commonly used to describe bioturbation over timescales of days to months to study particle size-specific and species- or community-specific mixing (Gerino et al., 1998; Montserrat et al., 2011; Wintle, 2008). For longer-term sediment bioturbation, radioisotopes, with known half-lives, are commonly used in marine environments. One example is lead-210 (^{210}Pb), which is produced in the atmosphere and water column in the naturally occurring uranium decay chain and is deposited on the seafloor. After burial, ^{210}Pb activity decays until it reaches background levels. ^{210}Pb has been used to determine deposition and mixing of sediments, from the deep sea to estuarine and intertidal environments (Benninger et al., 1979; Richter et al., 1996).

Currently, tracers that allow to study mixing of sand-sized particles over long timescales in intertidal flats are lacking. One inherent characteristic of sand

grains is their luminescence signal (Madsen and Murray 2009). This is a latent light signal that builds up in minerals in response to exposure to ionizing radiation from the natural environment. The luminescence signals are reset upon exposure to light and thereby provide an estimate of the last light exposure of these minerals (i.e. the time grains were last at the surface). The light exposure needed to fully reset luminescence signals varies for minerals and the luminescence signal used. For quartz OSL a few tenths of seconds of direct sunlight is sufficient for resetting (Lindvall et al. 2017) while feldspar post IR IRSL signals reset much slower (de Boer et al. 2026). Moreover, ambient light levels vary in time and space as they are affected wide range of aspects including time of day, latitude and inundation (de Boer et al. 2026).

Table 1. Tracers used in this study with their target grain size fraction, half-life time (Chl-*a* and ^{210}Pb) or bleaching time (luminescence signals). For the tracers with a half-life time, investigation timescales are 5x the tracer half-life (Lecroart et al., 2010; Meysman et al., 2008). Subaerial estimated bleaching times for luminescence signals are shown (Colarossi et al., 2015; Godfrey-Smith et al., 1988; Smedley et al., 2015).

Tracer	Sediment fraction	Half-life	Bleaching time (subaerial)	Investigation timescale
Luminophores	0–500 µm 0–125 µm (this study)	-		1–30 days
Chlorophyll-*a*	organic	3–250 days		15 days – 3 years
^{210}Pb	< 63 µm, organic	22.3 years		111.5 years
Luminescence	6–250 µm (multi-grain) 212–250 µm (single-grain, this study)			10 years – 5 x 10^6 years
Quartz OSL			seconds	up to 1.5 x 10^5 years
Feldspar IRSL			seconds-minutes	up to 5 x 10^5 years
Feldspar pIRIR			minutes-hours	up to 5 x 10^5 years

Multi-grain quartz optically stimulated luminescence (OSL) has been applied for dating intertidal flat sediments (de Boer et al., 2024a; Madsen et al., 2005, 2007, 2011; Mauz et al., 2010; Mauz and Bungenstock, 2007). In the terrestrial environment, luminescence methods are increasingly used to shed light on sediment mixing processes (Heimsath et al., 2002; Kristensen et al., 2015; van der Meij et al., 2025; Reimann et al., 2017; Stockmann et al., 2013; Zhang et al., 2025). Madsen et al. (2011) estimated sedimentation and bioturbation rates on an intertidal sandflat using large-aliquot quartz OSL on the grainsize 90 - 250

µm. However, this tracer only gives the average age of all luminescing grains in a subsample (often referred to as aliquot), which may be biased by a few older grains (Kristensen et al., 2015; Wallinga, 2002; Wallinga et al., 2019). Small-aliquot quartz OSL and single-grain feldspar luminescence advances the applicability of luminescence for studying mixing. Measuring the signal on individual grain level produces more meaningful results regarding mixing, as it also shows the fraction of reworked grains, and therefore the effectiveness or reworking (Reimann et al., 2017; Wallinga et al., 2019). Single grain luminescence has been successfully applied in terrestrial systems to determine effective bioturbation rates (Román-Sánchez et al., 2019) and has potential to quantify mixing by different bioturbation modes (van der Meij et al., 2025). Feldspar infrared stimulated luminescence (IRSL) or post-infra-red IRSL (pIRIR) measured at varying temperatures are commonly used single-grain signals. As these signals are less light sensitive than quartz OSL: they need longer light exposure to be fully reset and can therefore hold additional information on the transport and deposition history (de Boer et al., 2026b, a; Choi et al., 2024; Guyez et al., 2023).

Measuring single-grain luminescence signals with differential bleaching rates can inform about the light exposure duration and whether bleaching occurred under water (de Boer et al., 2026b). They can therefore be used to identify intertidal storm deposits (Pannozzo et al., 2023), or to infer whether bleaching occurred during subaqueous transport or during subaerial exposure on the tidal flat. Bleaching potential is low during storms and strong hydrodynamic conditions, due to high turbidity and low light exposure, while biotic mixing also takes place during calm conditions and intensifies in the summer season, when light and thus bleaching potential is higher. Moreover, biotic mixing also occurs in the moist tidal flat during low tide, when the flat is subaerially exposed (Cadee 1976).

The goal of this case study is twofold: firstly we aim to unravel the relative contributions of bioturbation and physical dynamics to sediment mixing in a (micro) tidal flat environment, using tracers that act on different timescales and on different sediment fractions. Secondly, we test the application of single-grain luminescence to study sand grain reworking in the intertidal environment, and compare tracer profiles with traditional short-term (Chl-*a*, luminophores) and long-term (^{210}Pb) tracers. We aim to answer the questions: (i) how do short- and long-term tracers aid in distinguishing bioturbation from physical mixing? And (ii) can single-grain luminescence be meaningfully applied as a bioturbation tracer in such dynamic environments? We hypothesise that, if biotic mixing dominates, we

will observe tracer-dependent mixing and, depending on the benthic community, diffusive or advective transport. With intense bioturbation, the slow-to-bleach luminescence signals will also be more fully bleached. If physical dynamics, such as wind and tidal reworking, are responsible for the deposition and sediment mixing, we expect a clearer stratification. Slow-to-bleach luminescence signals will be poorly bleached. We compare two adjacent intertidal locations: a sandy and a muddy flat in the Dutch Wadden Sea.

Methodology

Site description

The sampling site is located in the western Dutch Wadden Sea, near the northern tip the island of Texel (Fig. 2). We selected two adjacent intertidal locations: a muddy site (53°9.0740 N, 4°53.670 E; -0.055 m relative to Dutch ordinance datum (NAP)—approximately mean sea level), with visible benthic activity (small cast mounds, burrows), and a sandy site (53°9.0130 N, 4°53.9310; 0.004 m), with presence of large lugworms (large cast mounds and depressions). The sites are microtidal, with a mean tidal range of 1.43 m at the nearest measurement station (Oudeschild). This implies that during high tide the maximum water depth is 0.7 m (0.8 m during spring tides). The sites are located approximately 5 km south-eastwards of the tidal inlet and are relatively sheltered from the prevailing south-westerly winds. Our findings apply therefore to similar microtidal sites.

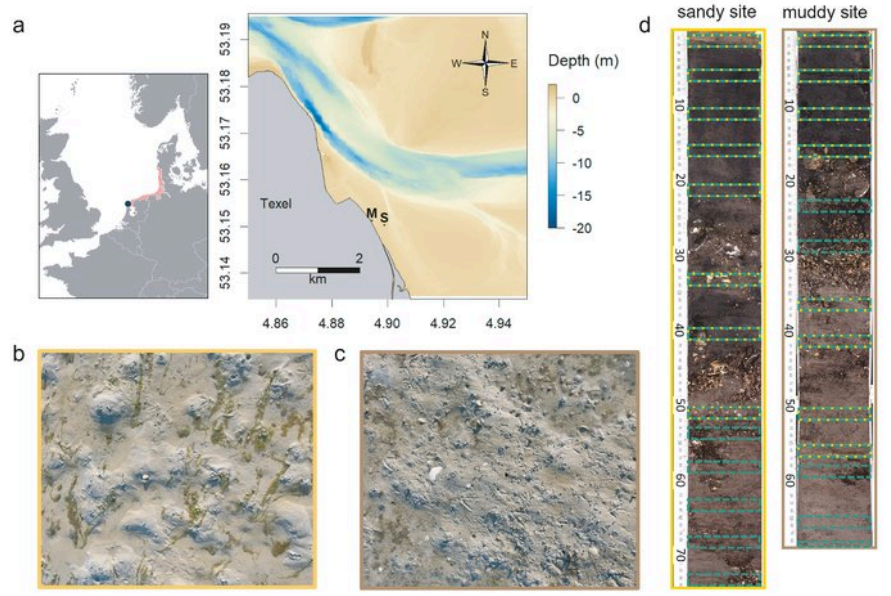

Figure 2. a. Map and bathymetry of the study area, located north-east off the island of Texel Wadden Sea (Netherlands), with muddy (M) and sandy (S) sampling locations indicated. The inset shows the location of the Wadden Sea (red) in western Europe, and the location of the study site (blue dot); picture of sediment surface at the sandy site (b - yellow) and muddy site (c - brown); d. core scan from long cores from both sites, with the sampling intervals for ^{210}Pb (green) and luminescence (yellow) samples indicated.

Benthic community sampling and analysis

To describe the benthic community, we sampled both sites using a hand corer (surface area of 0.0177 m^2), which was pushed into the sediment until encountering the first shell layer (depth approximately 0.25 m). The core sample was sieved over 1 mm mesh size and the remaining coarse fraction including biota was conserved in 4 % formaldehyde, buffered with borax and stained with Rose Bengal (CAS Number: 4159-77-7). In the laboratory, samples were sorted and biota were identified. Next, dry weight (DW) was measured after drying at 60°C for 2-3 days and ash free dry weight (AFDW) was measured after combustion at 560°C for 5 hours, to yield biomass per taxon. Due to the limited area and depth of our samples and the lower density of larger *Arenicola marina* individuals, we did not capture this species in our samples. From the field observations of large *A. marina* casts at the sandy location, we expected this species to dominate bioturbation. Therefore, we also derived *A. marina* density based on cast counts from pictures from both locations (4 pictures per site). To estimate individual

biomass, we actively collected *A. marina* from both sites with a spade (N = 17), which were dried in the same way as the benthic community samples. We derived bioturbation traits and living depth from a trait database (Beauchard et al., 2023) and calculated the total biomass per trait group.

Sampling of long cores

Two replicate sediment cores were collected at each site in August 2023 for grain size analysis, geochemical composition (X-ray fluorescence, XRF), ^{210}Pb and luminescence analysis. The cores were obtained by hammering two PVC tubes (inner diameter 96 mm) side by side vertically into the tidal flat deposits. After extraction from the tidal flat, the cores were sealed and transported to a dark container where under subdued amber-light conditions a core slicer was used to split each core into two halves. One of the cores halves was kept for luminescence and ^{210}Pb sampling, the other was kept for XRF scanning and sediment composition. We subsampled luminescence and ^{210}Pb samples by cutting 25 mm thick slices from the top to the bottom of each core, of which we selected eight per core for luminescence analysis (see Fig. 2 and Table A1 for intervals). The inner portion of each slice was used for luminescence equivalent dose (D_e, Sect. 2.6.1) estimation and ^{210}Pb analysis, while the outer material was reserved for determining the environmental dose rate ($\dot{D}$, Sect. 2.6.2). The sediment was wet-sieved in a dark room environment to separate the grain-size range of 212–250 µm, used for luminescence analysis, from the fraction smaller than 63 µm, used for ^{210}Pb analysis. We measured ^{210}Pb for five additional samples of each core, amounting to a total of 13 ^{210}Pb samples per core.

Sediment composition: grain size and X-ray fluorescence (XRF)

For grain size distribution, half of each long core was subsampled in 25 mm slices. These samples were freeze-dried, sieved over 1000 µm and measured by laser diffraction (Mastersizer 2000, Malvern Instruments). We determined the volumetric content of sediment size fractions from mud to coarse sand, and the median grain size (d_{50}), and 10th and 90th percentile of the grain size distribution (d_{10} and d_{50}).

We measured bulk elemental composition over the entire depth of the long cores at 10 mm resolution by X-ray fluorescence, using an AvaaTech XRF core scanner at the Royal Netherlands Institute for Sea Research (NIOZ) (Richter et al., 2006). Each section was exposed for 10 s with a power supply of 10 kV/0.60 mA, or 30 kV/1.6 mA. This yielded bulk elemental composition as element intensities in total counts or counts per second. We selected the following elements and ratios as

environmental proxies: Si:K (sand indicator), Cl:Fe (saline pore water indicator, thus proxy of porosity); Ca:Fe (shell content indicator; Croudace et al. (2006)), Rb (silt/clay mineral indicator; Guyard et al. (2007); note that the XRF detector window contains rubidium crystals, explaining high counts for this element); and Br (organic content indicator; Ziegler et al. (2008)).

^{210}Pb measurement via alpha spectrometry

The downcore distribution of ^{210}Pb in the mud fraction (<63 µm) of the sediment was determined indirectly through alpha spectrometry measurement of its grandchild isotope polonium-210 (^{210}Po) (de Stigter et al. 2011). To this end, 0.5 g of dried and homogenized mud, wet sieved from the bulk sediment sample, was spiked with 1 ml of a standard solution of ^{209}Po in 2 M HCl, and then leached for 6 h in 10 ml of concentrated HCl, heated in a hotblock to 85 °C. After diluting the fluid with 45 ml of Milli-Q water and adding 5 ml of an aqueous solution of ascorbic acid (40 g L^{-1}), natural ^{210}Po and added ^{209}Po were collected from the fluid by spontaneous electrochemical deposition on silver plates, with the fluid kept at 75 °C in a hotblock for 16 h. For subsequent alpha-spectrometry, Canberra Passivated implanted Planar Silicon detectors were used. ^{210}Pb activity was calculated from the measured ^{210}Po activity, assuming secular equilibrium and correcting for the time elapsed since collection of the samples.

Luminescence measurements

The luminescence samples were prepared at the Netherlands Centre for Luminescence Dating (NCL) under amber light conditions.

Equivalent dose (De) measurements

Quartz and feldspar luminescence samples were prepared following a standardised protocol (Appendix A2.1). The multi-grain quartz aliquots (48 per sample) were measured using an automated Risø TL/OSL DA-15 reader, following a Single-Aliquot Regenerative-dose protocol (SAR) (Table 2). The single-grain feldspar measurements were performed using an automated Risø TL/OSL DA-20 reader with an automated detection and stimulation head (DASH) and an EMCCD camera (Kook et al., 2015). A multiple-elevated-temperature (MET) pIRIR measurement protocol was used (Table 2) (de Boer et al., 2024b; Li and Li, 2011). Three single-grain discs per sample were used, resulting in approximately 250 grains measured per sample. For more details on the measurement procedure, see Appendix A2.1.

Table 2. Luminescence measurement protocols: Single-Aliquot Regenerative-dose protocol (SAR) for multi-grain quartz measurements and multiple-elevated-temperature (MET) pIRIR measurements for single-grain feldspar.

#	Multi-grain quartz protocol	OSL signal	Single-grain feldspar protocol	Feldspar signal
1	Natural/ regenerative dose (Gy) (0, 7.3, 0, 7.3, 7.3)		Natural/ regenerative dose (Gy) (0, 1.4, 2.8, 5.6,11.3,0,1.4)	
2	Preheat at 200 °C (10 s)		Preheat at 200 °C (60 s)	
3	*IRSL at 30 °C (40 s)		IRSL at 50 °C (108 s)	IRSL-50 Li
4	OSL at 125 °C (20 s)	OSL-125 Li	IRSL at 175 °C °C (108 s)	IRSL-175 Li
5	Test dose (4.7 Gy)		Test dose (2.8 Gy)	
6	Preheat at 180 °C (10 s)		IRSL at 50 °C (108 s)	IRSL-50 Li
7	OSL at 125 °C (20 s)	OSL-125 Li	IRSL at 175 °C (108 s)	IRSL-175 Li
8	Bleach with OSL at 190 °C (40 s)		Hot bleach with IR-LEDs at 210 °C (108 s)	

*Only in the last regenerative run to check for feldspar contamination

Dose rate ($\dot{D}$) measurements

Environmental dose rates, the natural amount of natural ionizing radiation absorbed by a sample per unit of time, were determined with gamma-ray spectrometry (Appendix A2.2). Results are combined with information on burial history, water and organic content history, and the measured grain-size fraction to calculate the effective external beta and gamma dose rates (Cunningham et al., 2022). For cosmic dose rate calculation (Prescott et al., 1994), we assumed gradual burial of the samples to the present depth. This is a crude assumption given the episodic nature of deposition and potential reworking of grains after deposition in this environment. However, the effects of this assumption are minor as the cosmic dose constitutes a minor fraction of the total dose rate experienced by the grains (< 25 % even for samples closest to the surface). Per core, the average water content over all samples was used, yielding gravimetric water content of 28.5 % (muddy core) and 25.5 % (sandy core), with a relative uncertainty of 25 % to account for variations over time. The organic content per sample was used to account for attenuation. We included an internal alpha dose of 0.010 ± 0.005 Gy ka^{-1} for quartz (Vandenberghe et al., 2008) and 0.050 ± 0.025 Gy ka^{-1} for feldspar (Kars et al., 2012). An internal K-content of 12.5 % was assumed for the K-feldspar grains. As gamma-rays penetrate 20–30 cm in the deposits, contributions from adjacent layers are accounted for following the approach of Wallinga et al. (2010).

Data analysis

The sample age is calculated by dividing the equivalent dose value by the mean dose rate: age (years) = D_e (Gy) / $\dot{D}$ (Gy year^{-1}) (Rhodes, 2011). To interpret the quartz OSL single-aliquot (multi-grain) and feldspar IRSL and pIRIR single-grain age distributions, we used several approaches. Firstly, a mean was calculated after iterative removal of datapoints that deviate more than two standard deviations from the mean. This iterative approach aims to identify the mean age, while minimising bias due to outliers that may be caused due to poor bleaching or recent input of young (bleached) grains. Secondly, a logged version of the Central Age Model (CAM) (Galbraith et al., 1999) was used to quantify the overdispersion and obtain a mean burial age for samples that are relatively well-bleached. Finally, the logged bootstrapped Minimum Age Model (bMAM) (Cunningham and Wallinga, 2012; Galbraith et al., 1999) with a sigma-b of 0.25 ± 0.05 was used to determine the absorbed dose of the youngest population of grains. Lastly, we determined the interquartile range (IQR) of the age distribution of each signal, as a direct metric of the width of the distribution for each signal (van der Meij et al., 2025). All analyses were performed in R (R Core Team, 2024) with use of the Luminescence package (Kreutzer et al., 2025).

Luminophore tracer experiment

Simultaneous to the long core sampling, we started a luminophore tracer experiment adjacent to both sampling locations. Fluorescent coated luminophores (red/pink tracer, size range: 0–125 µm) were mixed with sieved native sediment from each site (ratio 1:10 for the muddy sediment and 1:17 for the sandy sediment) and applied to the sediment surface as 15x15x0.5 cm frozen tiles. Per site, three experimental plots were created by aligning four of these tiles—thus each covering a total area of 30x30 cm. These were sampled on day 2, 16 and 30 by pushing a PVC tube (diameter 36 mm) at least 20 cm deep into the sediment. The resulting sediment cores (one per plot) were frozen upright. In order to find evidence of recent bioturbation of the fine particles, the frozen cores were sliced in length direction with a tile saw. The cutting surface was scraped clean in lateral direction until the still frozen sediment was reached. If cutting had resulted in visible artefacts in the sediment (cavities or disturbed sediment surface), the damaged core or half core was excluded from analysis, leaving two replicate cores per site per time point. Next, both halves of the core were photographed in a dark room under ultraviolet light, with a ruler for scale reference. The images were processed using ImageJ (Schneider et al., 2012): first, we adjusted the display settings Level ≈ 50 and Window ≈ 100. Red and orange pixels were then identified per 2-cm

depth slice by extracting RGB values of each pixel, and applying thresholds (R > 150, G > 40, G < R -30, B < 100). The total count of pixels meeting these criteria was recorded as the red-orange pixel count. The average number of pixels per depth interval were averaged over both core halves.

Chlorophyll-a sampling and measurements

Chlorophyll-*a* cores were collected next to the luminophore tracer experiment. Cores (inner diameter 36 mm) were collected on August 22nd and October 5th, 2023 (day 1 and day 45 of the luminophore experiment, respectively two and three cores per site). The cores were pushed into the sediment as deep as possible, or at least 15 cm deep. We sliced the cores every 0.5 cm down to 3 cm depth, then every 1 cm down to 15 cm depth. The samples were stored at -80 °C and freeze-dried for 72 hours before analysis. Next, we homogenised and weighed an aliquot of the sediment (approximately 1000–1500 mg for the sandy site samples and 300–500 mg for the muddy site samples). We extracted Chl-*a* by adding 5 ml 90 % acetone in 50 ml centrifuge tubes and running them in a bullet blender (BB50-AUCE, Next Advance) for 15 min, after which 5 ml 90 % acetone was added again and extraction was repeated for another 15 min. The extracts were measured in a spectrophotometer (Specord 210, Analytik Jena) at 630, 647, 664, 665 and 750 nm. From the measured extinction values, we calculated Chl-*a* concentration following Ritchie (2006).

Results

Benthic community

Macrozoobenthic community biomass and abundance (excluding *Arenicola marina*) were higher on the muddy site (approximately 19 g AFDW m^{-2}) than on the sandy site (3.8 g m^{-2}; Appendix A3, Table A2). Both locations contained a large fraction of taxa which could be classified as biodiffusers (Appendix A3, Fig. A1). The sandy site contained a larger fraction of downward conveyors, while more upward conveyors inhabited the muddy site. Density of downward conveying lugworms (*A. marina*) was higher on the muddy site (98 ± 42 individuals m^{-2} versus 44 ± 11 individuals m^{-2} on the sandy site), while worms were larger on the sandy site (0.16 g $individual^{-1}$ versus 0.05 g $individual^{-1}$ on the muddy site). We estimate total *A. marina* biomass therefore to be slightly higher on the sandy site (6.9 g AFDW m^{-2} versus 5.1 g AFDW m^{-2}), and to form a substantial part (approximately 60 %) of the total biomass at the sandy site, compared to 20 % at the muddy site.

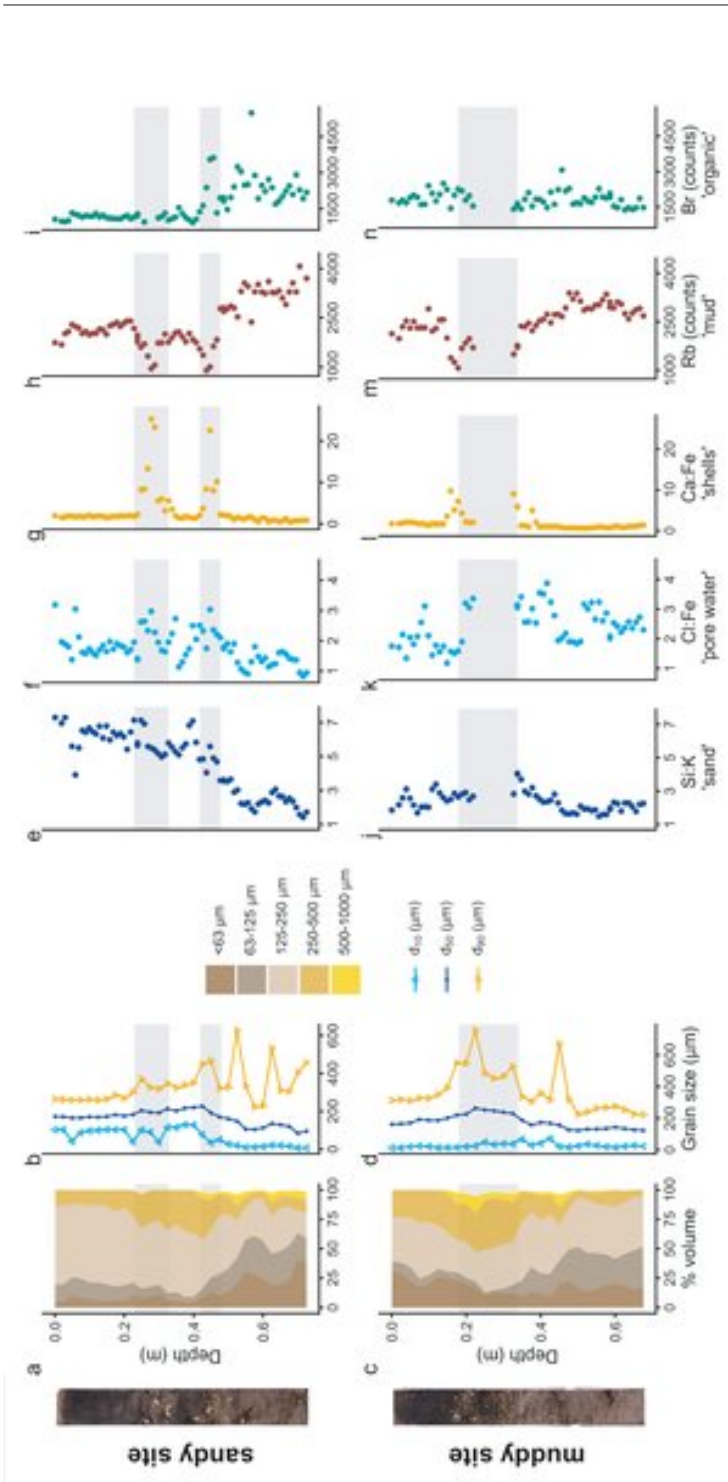

Figure 3. Sediment composition at the sandy site (top) and muddy site (bottom): stacked grain size fractions (a, c); d_{10}, d_{50} and d_{90} (b, d); elemental composition (e-n): Si:K, higher ratios indicate sand; Cl:Fe, higher ratios indicate marine pore water; Ca:Fe, higher ratios indicate shells; Rb counts representative of silt and clay, and Br counts, representative of organic matter. Note that the cumulative grain size fractions (a, c) do not amount to 100 % when coarse >1000 µm material was present. The data gap in the mud cores (j-n) resulted from a scanning failure due to the presence of a brick. Grey bands show the shell layers. The core scans are shown left of the figure.

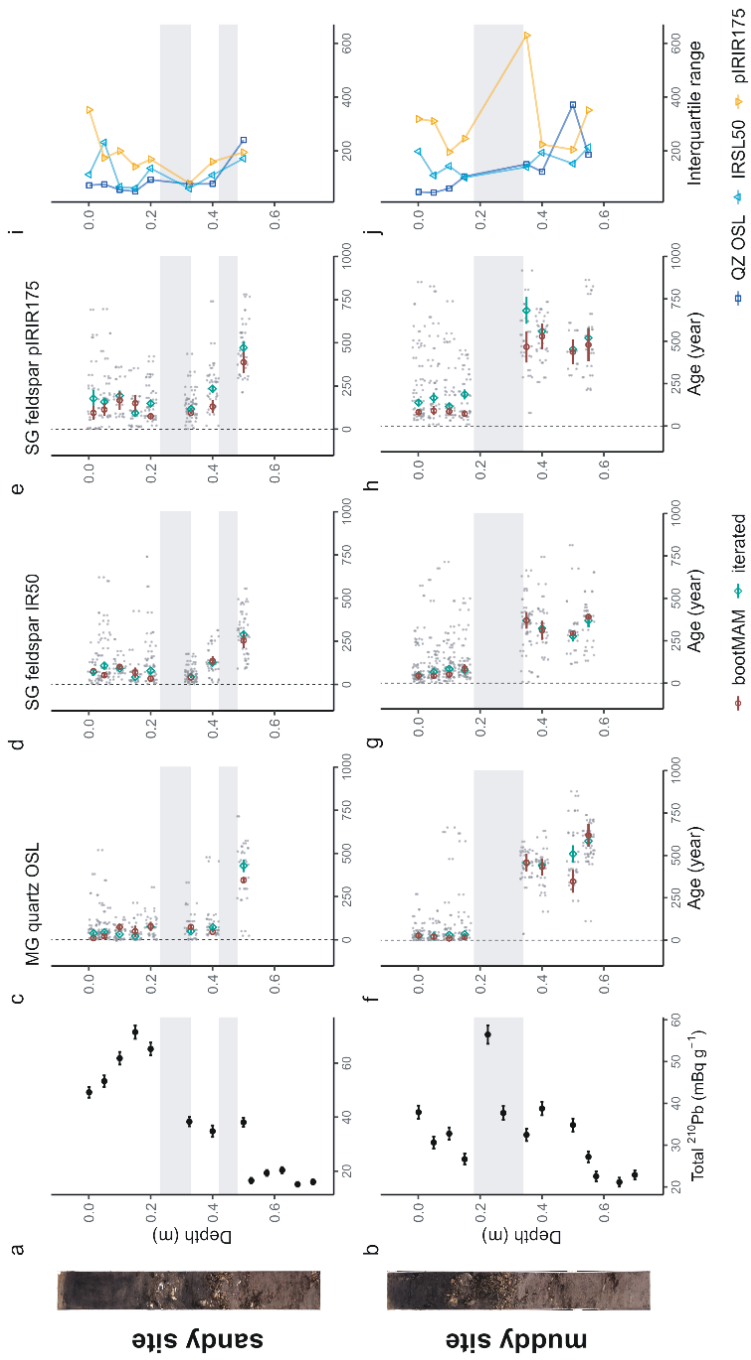

Figure 4. Tracer profiles from ^{210}Pb (a, b) and luminescence signals, with the single-aliquot or single-grain data jittered in grey and green and red markers indicating the modelled iterated or bootMAM age with standard error (c-h); interquartile range of luminescence age distribution (i, j) for the sandy (top) and muddy site (bottom). Grey bands indicate the shell layers. The core scans are shown left of the figure.

Sediment composition and grain size

On the sandy site, the top ~0.3 m of the sediment consists mainly of fine sand, with a mud content under 10 % (Fig. 3a). From here, the coarse sand fraction gradually increases to ~40 % at a depth of 0.45 m. Below 0.45 m, the sediment is less well-sorted, containing both a 20–40 % mud fraction, as well as coarse and very coarse sand and a variable d_{90} (Fig. 3b) We observed shell layers between 0.27–0.29 and 0.44–0.47 m, also reflected in increased Ca:Fe ratios from the XRF measurements. Below the second shell layer, the marine pore water (Cl:Fe) decreases and organic matter content (based on the Br indicator) increases (Fig. 3e-i).

At the muddy site, the top 0.15–0.20 m of the sediment is less well sorted: a large mud fraction (10–25 %), as well as a substantial fine and medium sand fraction are present (Fig. 3c, d). A shell layer was present between 0.18–0.34 m. Between 0.2–0.45 m, some layers contain coarse particles (500–1000 µm), which is also reflected in peaks in d_{90}. The amount of marine pore water (Cl:Fe) slightly increases downcore, whereas sand content (Si:K), mud content (Rb) and organic matter (Br) remain relatively constant (Fig. 3j-n). A brick present in the shell layer gives evidence of anthropogenic influence and suggests a relatively young deposit.

Long-term tracers: ^{210}Pb and luminescence profiles

Above the first shell layer at the sandy site, ^{210}Pb activity was lowest in the surface slice (0–0.025 m depth), and increased to a subsurface peak at 0.15 m (Fig. 4a). Below the first shell layer (<0.29 m), activity decreased, to a nearly constant level below 0.5 m. At the muddy site, ^{210}Pb activity slightly decreases down to 0.15 m, peaked in the first shell layer at 0.225 m (Fig. 4b). Until down to 0.4 m, below the second shell layer, ^{210}Pb activity remained high. Activity then decreased to an apparently constant level of ~22 mBq g^{-1} between 0.5–0.6 m.

In discussing the luminescence ages, we focus on the quartz OSL ages obtained through the iterated age model; given that quartz OSL resets most rapidly upon light exposure this provides the best estimate of the last light exposure of the majority of the grains. Quartz bootMAM ages indicate the last time of introduction of light exposed grains through bioturbation. For feldspar, heterogeneous bleaching is to be expected due to slower resetting of the luminescence signals and therefore we focus on the interquartile range of the age distribution and bootMAM derived ages to infer information on light exposure and thus process information.

The quartz OSL iterated ages suggest last light exposure well within the past 100 years for sediments within the top 0.4 m at the sandy site (Fig. 4c) and 0.15 at the muddy site (Fig. 3i) (Appendix A4, Table A3a). A jump in age is observed between the samples at 0.4 and 0.5 depth at the sandy site, with an age of 430 ± 40 years for the latter according to the iterated model. For the muddy site, older ages (440 ± 30 to 640 ± 40 years) were obtained for the part below the shell layer.

The feldspar IR50 and especially the pIRIR175 signals were not fully bleached in a large fraction of the grains in the top 0.2 m of both cores. At the sandy site, grains with a low pIRIR175 age were only present at 0, 0.15 and 0.325 m; at the muddy site such young grains could be identified at 0.05 and 0.15 m. The ages obtained using the bootMAM approach on the IR50 signal tend to be a few decades older than those obtained through quartz OSL iterated mean, while bootMAM derived pIRIR175 ages are significantly older (typically by a few centuries, Table A3b, c). An exception is formed by the samples from the deeper parts, where IR50 results tend to be younger than quartz OSL, while pIRIR175 agree with quartz OSL. The single-grain age distributions obtained on both feldspar signals are also broader than those obtained through quartz OSL.

Short-term tracers: Chlorophyll-*a* and luminophore profiles

Both short-term tracers show a high spatial variability. Whereas two muddy cores and one sandy core contained sub-surface maxima of Chl-*a* concentration (Fig. 5a, b; at 3, 15 and 6–8 cm depth respectively), in the other cores the Chl-*a* concentration showed a more exponential decrease with depth. At the bottom of the cores in all sites, still some Chl-*a* was present above the analytical detection limit (0.2 µg g^{-1}), which could indicate the supply of Chl-*a* younger less than 3 months ago, or reflect Chl-*a* adsorption to sediment.

Some luminophore particles were already worked down to 18 cm (sandy site) and 20 cm (muddy site) within 2 days (36 hours) after initiation of the experiment (Fig. 5c, d). In these cores, the reworking could be clearly linked to bioturbation, as two bivalves were found in the cores with increased luminophore concentration around their burrows (Appendix A5, Fig. A2; *Scrobicularia plana* at 12–15 cm depth at the sandy site and *Cerastoderma edule* at 0–3 cm depth at the muddy site). Similar high subsurface luminophore concentrations were not observed in the cores collected at later time points, although some luminophores could be found

at greater depths. We saw similar between-core and thus spatial variability as in the Chl-*a* measurement.

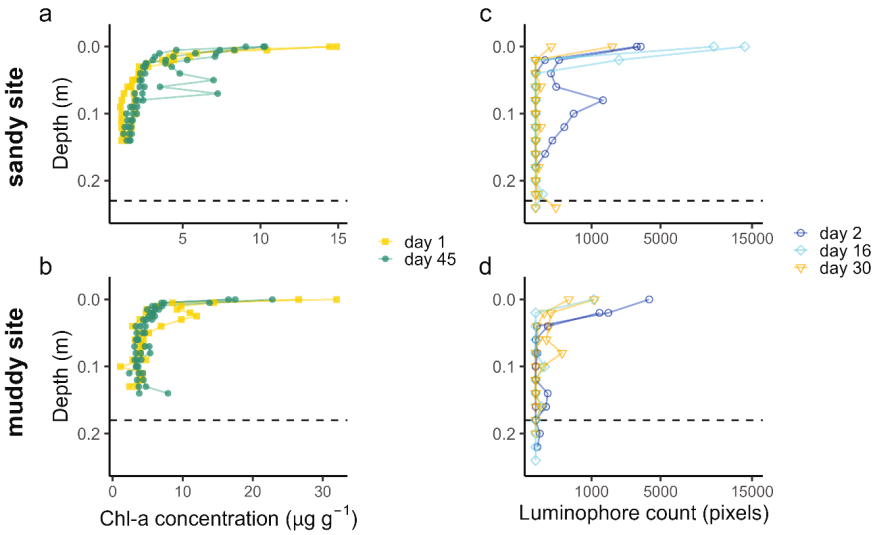

Figure 5. Chlorophyll-*a* (a, b) and luminophore (c, d) profiles from the sandy site (top) and muddy site (bottom), sampled at different time points (day, starting from August 21st, 2023). Note that the x-axis of the luminophore plots was square-root-transformed to increase the visibility of low pixel counts. The dashed line indicates the depth of the top of the shell layer, as determined from the deep cores.

Discussion

The signal-depth profiles were tracer-dependent. We observed subsurface maxima of Chl-*a* and luminophores on both the sandy and the muddy site down to a depth of 0.15–0.25 m. This rapid translocation of young particles to depths of 0.15–0.25 m also showed in the ^{210}Pb profiles and to some extent in the feldspar pIR175 luminescence profiles. The quartz and feldspar IR50 luminescence results rather suggested that at least the top 0.15–0.2 m of the sediment was deposited recently, hampering identification of even younger sand grains mixed in through bioturbation. The slow-to-bleach feldspar signals were not fully reset in the top layer, although some input of young grains to deeper layers could be identified. This suggests episodic deposition of the top layers, or insufficient mixing to expose all grains long enough to unfiltered light. In what follows, we

will provide a combined interpretation of what these results tell about deposition and mixing processes in dynamic intertidal environments.

Worms or storms?

In the sediment composition, we did not observe any clear layering in the top decimetres of sediment at both sites which could be attributed to storm deposition. This may be due to an overly coarse vertical sampling resolution, even though our resolution of 25 mm should have been sufficient to capture storm deposited layers, which can have a thickness of centimetres (Zhou et al. 2022b). At the sandy site the top of the profile was relatively homogeneous. The top decimetres of the sandy core also appeared to be better sorted than the top part of the muddy core (Fig. 3a-d). Generally, hydrodynamic reworking would be expected to result in more uniformly sorted sediment, whereas biota can create localised patches of finer or coarser material (Aller & Cochran 2019; Bentley & Nittrouer 2012) thus resulting in variable sorting of individual sediment samples (Rhoads & Stanley 1965). Furthermore, the presence of shell layers may indicate biotic influence, since bioturbators such as *A. marina* are unable to ingest coarse particles like shells, which then remain at the feeding depth (Reise 2002; van Straaten 1952), while the ingested sand will be deposited on the sediment surface and subsequently mixed into the sediment.

The tracers targeting the fine-grained sediment fraction showed clear signs of bioturbation. During the luminophore experiment, no storms or strong winds occurred, therefore vertical luminophore displacements can solely be attributed to bioturbation. Both the short-term (luminophores and Chl-*a*) and the long-term (^{210}Pb) tracers showed sub-surface peaks, illustrating that advective vertical transport of particles occurred. This is coherent with the observed macrozoobenthic species that are known non-local mixers (see Sect. 4.3). In addition, the gradual vertical gradients of ^{210}Pb, and of Chl-*a* till 0.15–0.2 m point to substantial diffusive bioturbation in the top decimetres of the sediment, or rapid deposition within the previous months.

The luminescence data gives more details on the deposition and reworking of sand grains. The narrow age distributions obtained through quartz OSL indicate that this signal was well-bleached. The bootMAM and iterated age estimates are very similar, both likely reflecting the time of deposition. The narrow distributions in the top layer (0.4 m at the sandy site and 0.15 m at the muddy site) imply that the vast majority of grains were recently (within the past few decades) exposed to

sufficient light to fully reset quartz OSL signals. However, the older ages obtained through feldspar IRSL, even for the relatively fast bleaching IR50 signal, indicate that for a large fraction of grains, full light exposure during and after deposition was limited. Especially old (>500 years) pIRIR175 measurements in the top 0.10 m at both sites indicate that light exposure prior to burial was insufficient to bleach this signal. It is less likely that these grains are worked upwards by bioturbators from deeper deposits, as other grains of this age were only found below the shell layer at 0.35–0.5 m depth. Both feldspar signals from the top decimetres were not as homogeneously bleached as would be expected with intensive reworking. We conclude that the luminescence ages primarily reflect the time of deposition, rather than the time of bioturbation. This conclusions holds for all luminescence signals used. However, quartz OSL ages provide most reliable depositional ages while the feldspar IRSL and pIRIR results overestimate the burial age due to incomplete resetting of these signals upon deposition and burial.

The luminescence signals gave a few hints of bioturbation as well. Firstly, at both sites, young grains with nearly fully bleached pIRIR175 signals are present at larger depths. At the sandy site, such young grains can be found at 0.15 m, coinciding with the subsurface ^{210}Pb peak. At the muddy site, the young grains are only present above the shell layer, at 0.05 and 0.15 m. This could point at the advective transport of young sand grains to this depth, or good bleaching conditions during deposition of these layers. Given the combination of bioturbation evidence from the other tracers, and the lack of sedimentary structures, we deem bioturbation to be the most likely process. Secondly, feldspar signals in the very top layer (0–0.05 m) at both sites were less well bleached and had wider distributions than those at 0.1–0.2 m deep. Possibly, grains that are recently deposited under low bleaching conditions and are buried close to the surface, are not always directly resurfaced by bioturbators. These grains require a longer period of bioturbation to be bleached further. This hypothesis is supported by Bentley et al. (2014), who described a shallow (1–4 cm) stratified top layer, which was not yet bioturbated, above a more intensely bioturbated zone in a muddy intertidal environment. Secondly, the luminescence data provides some evidence for exchange of grains between stratigraphic layers of different depositional age. Some grains in the luminescence age distribution had ages similar to those of the underlying deposit, even if a shell layer is present in between. At the muddy site, a high level of ^{210}Pb was also present in and below the shell layer. From these observations combined, we conclude that transport of fine particles can sometimes extend beyond the shell layer.

Madsen et al. (2011) also reported quartz OSL profiles on an intertidal flat and attributed a change in apparent sedimentation rate to bioturbation. Their site was not very dynamic, and bioturbation was more likely to be the main mixing process present. The combined evidence of small aliquot quartz OSL and single grain feldspar IRSL50 and pIRIR175 suggests that deposition at our site was episodic and that bioturbation was less efficient in bleaching these signals by resurfacing the grains. Furthermore, given that deposition was recent, it is not possible to clearly differentiate bioturbated grains from those grains that were last light-exposed prior to deposition as is done in terrestrial soils (e.g., Reimann et al. (2017)). Hence, we cannot deduce bioturbation rates from our data using approaches as suggested by van der Meij et al. (2025).

Age gaps and sedimentation rates

We could not derive sediment accumulation rates, because our combined signals pointed to a combination of sediment mixing and episodic deposition. Therefore, assuming the age-depth profiles to be the result of gradual sedimentation alone would be incorrect in this dynamic environment. Quartz OSL showed a hiatus in age between the top and the middle part of the core at the muddy site but not at the sandy site, while 210Pb also indicated a hiatus in activity at the muddy site only (Fig. 4a). Such age gaps can be caused by erosion followed by rapid accumulation, mounding by bioturbators (Kristensen et al. 2015; van der Meij et al. 2025), or switching between a depositional and an erosional regime with bioturbation penetrating the older deposits (Madsen et al. 2011). The opposing gaps of the radionuclide and luminescence tracer profiles could be an effect of an age underestimation of 210Pb compared to OSL of older sediments (Madsen et al. 2007). However, the 210Pb activity just below the shell layer in the muddy site is too high to be fully explained by such an inaccuracy. Instead, we expect differential transport of fine and coarse particles through the shell layer to play a role.

Combining the information from luminescence signals, deposit composition and 210Pb, we propose the following possible scenarios for sedimentation history (Fig. 6):

- On the sandy site, rapid sediment deposition took place approximately 400 years ago. The original sediment surface was covered with a new thick layer of sand, and the benthic fauna recolonised the new layer. The quartz signals in this new deposit were then uniformly bleached by bioturbation and physi-

cal resuspension and deposition, although incidentally some grains were still exchanged with the bottom layer. Through bioturbation, also the first shell layer was formed. Recently (<100 years ago) another large, rapid deposition event happened. This shifted the bioturbation depth upwards, forming a new shell layer higher up. Still some fines (210Pb) moved downward through the shell layers, but most accumulated on feeding depth of bioturbators.

- On the muddy site, the top 0.2 m of sediment were gradually deposited, starting approximately 500 years ago. The layer that is now at 0.35 m then fell below the bioturbation depth and was not any longer exposed to light. The sediment has then slowly been accumulating with bioturbation resulting in bleached OSL signals and the formation of a gradually thickening shell layer. Elevated 210Pb activity below the shell layer could be due to passive infiltration of fines through the porous shell layer. The strong break in luminescence age suggests little exchange of sand grains through the shell layer, and thus differential displacement of coarse and fine particles.

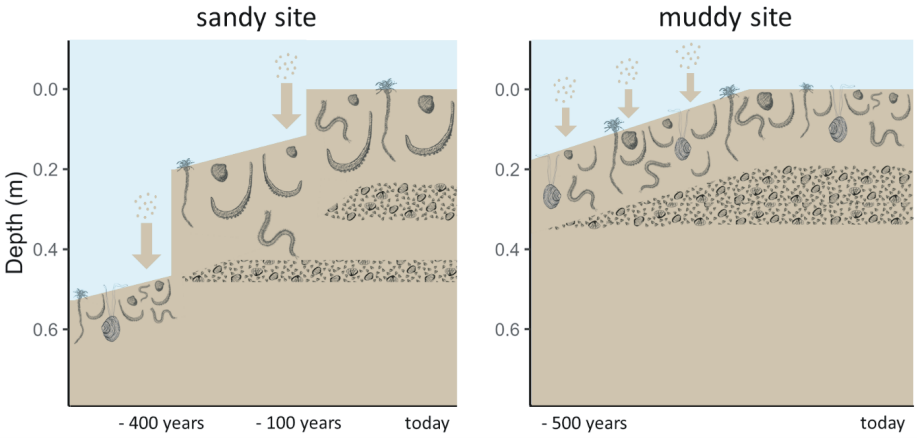

Figure 6. Conceptual diagram of sedimentation history scenarios of the sandy (left) and muddy (right) site. Larger arrows represent more rapid sedimentation. The depth represents the current depth in the cores. Shell layers and benthic community are represented schematically with a lower species abundance and biomass, but larger lugworms (*Arenicola marina*) on the sandy compared to the muddy site.

Differences between sites: hydrodynamics and community type?

The sandy site was relatively more exposed to energetic hydrodynamic conditions than the muddy site. This may have caused the surprisingly low surface ^{210}Pb activity, as waves and tidal currents may resuspend and wash away the recently settled ^{210}Pb-rich material at each tide. The Chl-*a* concentrations were also lower at the sandy site than on the muddy site, but this might be due to differences in degradation rates of Chl-*a* (Sun et al. 1993). The bleaching potential of the luminescence signals could differ between the muddy and sandy tidal flats (Pannozzo et al. 2023). When submerged, higher loads of suspended sediment will decrease subaqueous light penetration during transport and (re)deposition on the muddy site (A. M. de Boer et al., in review). The sandy site is more elevated and therefore slightly more often exposed to subaerial bleaching than the muddy site due to its lower inundation times. These differences in bleaching potential and probability may have resulted in the lesser bleaching and wider distributions (Fig. 4j) of the luminescence signals on the muddy site.

The sandy and muddy site also differed with respect to the density, biomass and composition of the benthic community. The muddy site contained a relatively higher abundance and biomass of taxa that could be classified as biodiffusers and surficial modifiers. This leads to a higher contribution of diffusive mixing and could also partly explain the larger interquartile ranges of the luminescence signals at the muddy site, compared to more effective bleaching through advective vertical bioturbation at the sandy site (van der Meij et al. 2025). Subsurface maxima of fine-grained tracers, pointing to advective transport, were more pronounced in the sandy site. One of the main likely bioturbating agents was conveyor-belt reworking polychaete *A. marina*. While the muddy site contained a higher density of small individuals, this species comprised only a fifth of the biomass here. The sandy site was inhibited by fewer, but larger lugworms, so that this species was dominant in biomass here. Such large individuals live in 0.2–0.4 m deep burrows and often dominate sedimentary processes at sandy intertidal flats. Their presence leads to 4-400 times more likely particle reworking rates and an estimated full overturning of a 0.1–0.6 m layer of sediment per year (Cadee 1976; Riisgård & Banta 1998; Volkenborn et al. 2007a). These lugworms were probably responsible for the subsurface accumulations of ^{210}Pb at feeding depth, as the ^{210}Pb-rich organic material is filtered from the ingested sand (Longbottom 1970).

Other bioturbators might also have contributed to non-local transport of fine tracers at both sites, either by active particle transport or through passive processes such as burrow infiltration. Ragworms (family Nereididae), such as *Hediste diversicolor*, were present at both sites. These worms build a gallery network and can cause diffusive mixing of the surface layer, and advective downward transport, accumulating particles at the lower end of the gallery network due to passive sloping, burrow infilling and during rapid retraction (Foster-Smith 1978; Herringshaw et al. 2010; Ouellette et al. 2004). Another group that we deem responsible for non-local transport of fines are tentaculate polychaetes, which enhance fine particle transport from the water column into the sediment (Frithsen & Doering 1986). *Pygospio elegans*, a tube-building worm present in high densities at both sites, constructs tubes 0.15 m into the sediment, and enhance transport of fine particles down to 3–5 cm depth (Bolam & Fernandes 2003). *Lanice conchilega* feeds on organic particles from the sediment surface or the water column and builds long tubes, down to 0.3–0.4 m into the sediment (Carey 1987). Although this species was only present in the benthos core sample at the muddy site, we observed their tube endings, indicating their presence, on the sediment surface at both locations (Fig. 2b, c).

Scrobicularia plana is described as a surficial modifier in trait databases (Queirós et al. 2013). We however observed that this species also contributes to non-local mixing, as suggested by luminophores that had moved rapidly to the living depth of this bivalve (Fig. A2). Similar discrepancies between 'theoretical' bioturbation traits and field observations were reported by (Morys et al. 2017). Therefore, a single trait-based community index for bioturbation (such as BP_c), could potentially be informative on larger spatial scales when a more extensive dataset is available, but such an index may be less relevant for a local study.

Why are results tracer-dependent?

The differences between tracers are likely the result of particle size-specific physical and biological sorting mechanisms. Fine particles are more easily eroded and transported from the sediment surface by currents and waves. They are therefore less prone to remain on the surface for a prolonged period, whereas coarser sand grains are more stable on the sediment surface. Fines are also more likely to move down into the sediment matrix by passive as well as active processes. In sandy, permeable sediments, fine particles can infiltrate with pore water flux (reviewed by Huettel et al. (2014)). Above that, fine and organic particles are more often selected by bioturbators, after which they may accumulate in deeper

layers of the deposit. This particle selectivity is common among benthic taxa (Self & Jumars 1988).

Although the grain size range we selected for luminescence measurements (212–250 µm) falls outside of the feeding range of many polychaetes (Jumars et al. 2015), *A. marina*, expected to be a dominant bioturbator especially on our sandy site, does feed non-selectively on sediment particles below a size of 1000 µm (Baumfalk 1979). Bioturbation of this species was shown to still result in accumulations of finer (130 µm) as well as coarser (500–1000 µm) particles at its feeding depth (0.1–0.14 m) (Gebhardt & Forster 2018). Bivalves can also exhibit size- and particle-type specific selection, but this usually takes place post-capture (reviewed by Ward & Shumway (2004)). Their burrowing movements rather than their feeding activity may thus vertically displace sand grains. *A. marina* as well as bivalves are therefore expected to have reworked sand grains and affected the luminescence tracer profiles.

It has been demonstrated that benthic fauna select for particle quality as well and prefer organic over inorganic particles (Taghon 1982). Although we saw some advective transport of luminophores (Fig. 5c, d; Fig. A2), we did indeed not observe large sub-surface accumulation over time. One explanation might be that these inorganic particles do not accumulate at the organism's feeding depth in the same way as the organic matter-associated tracers that are retained in the digestive system. This is contrary to Gerino et al. (1998), who observed subsurface peaks of luminophores after 15 days, and additionally modelled Chl-*a* subsurface mixing rates to be in the same order of magnitude as the mixing of non-organic particles in a shallow, muddy environment. In our dynamic intertidal environment, luminophores might have more easily eroded from the sediment surface, resulting in a decrease in surface supply over time, which possibly underlies the lack of later subsurface accumulations (Fig. A3).

A tracer can give meaningful information on mixing processes when the timescale of a tracer (e.g., radionuclide decay rate) matches the timescale of the mixing rate: the longer the tracer timescale, the more particle displacements will have contributed to the signal distribution (Meysman et al. 2003). The luminescence signal is of a different nature than that of radionuclides, as it builds up after burial but resets at each sufficiently long or intense light exposure, rather than gradually declining over a known time. Signals that are more difficult to bleach (e.g. feldspar pIRIR175) require more light exposure to be reset compared to

fast bleaching signals (e.g. quartz OSL). They thus require a higher frequency of reworking events to be fully bleached. If sediments are however too young or intensely mixed, no recently reworked grains can be distinguished, as the sediment will be uniformly bleached. Under the conditions at our intertidal study sites, only the feldspar IR50 and pIRIR175 bleached slowly enough to be not fully reset during deposition or by bioturbation. Therefore, these signals can show subsurface supply of young sand grains (Fig. 4e, h) and incomplete bleaching during deposition (Fig. 4d, e, g, h). In this relatively young and more intensely reworked sediment, where no 'old', never-mixed, sediment fraction appeared to be present, single-grain level measurements cannot be used for determining the bioturbation effectiveness (Reimann et al. 2017). Spatial scale also plays a role, especially for the short-term tracers. The small sampling surface of the Chl-*a* and luminophore cores and the patchy distribution of macrozoobenthos resulted in high variability between cores, and a higher number core replicates may therefore have increased consistency of tracers profiles for these short-term tracers. For the long-term tracers, the number of replicates was lower, however because the distribution of these tracers captures the integrated activity of the macrozoobenthic community over a longer time period, we would expect similar results even if we had used a higher number of replicates.

Which tracer to use when?

Although our findings on sediment reworking are site-specific, the tracers used here are more broadly applicable, provided that the limitations of each tracer are considered. A combination of tracers best represents the intricate reality of physical and biotic sediment mixing processes. This corroborates Gerino et al. (1998), who showed that to accurately model bioturbation modes, measurements of multiple tracers with different characteristics are required. A multi-tracer experiment is however time- and resource intensive, and aligning tracer sampling protocols to improve intercomparison is not always feasible. Therefore, we propose a framework for deciding on the type of tracer to use, depending on the research question at hand (Fig. 7).

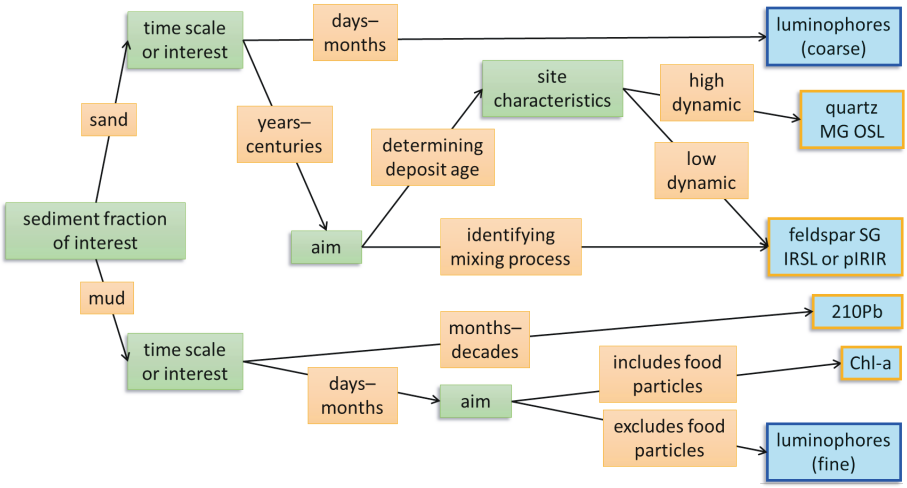

Figure 7. A decision tree for choosing the appropriate tracer type to identifying sediment reworking in intertidal environments. Green boxes indicate the attributes of the research question at hand that should be considered and orange boxes show the possible responses, ultimately leading to the most suitable tracer (light blue boxes). The blue-outlined tracers are particles that actively need to be introduced in a natural system, while the orange-outlined tracers are native in intertidal sediments.

The process timescale, grain size fraction of interest and spatial density need to be considered. Depending on the rate and dominant mode of bioturbation, a short- or long-term tracer may be more appropriate (Lecroart et al. 2010; Meysman et al. 2010). Also, the potential targeting of organic food particles (e.g., Chl-*a*, ^{210}Pb) may be considered. Furthermore, the physical conditions at the field site determine the suitability of a tracer. If the field site is erosive or exposed to higher dynamics, fine luminophores might not be representative over a longer period. With low reworking or light exposure (e.g., long inundation and turbid water), hard-to-bleach luminescence signals are less likely to be bleached by bioturbation.

Outlook and implication

Feldspar single-grain luminescence is a promising tracer for deposition and mixing processes in intertidal environments. Even though luminescence signals at our study sites pointed to high dynamics and rapid deposition, rather than being all fully bleached by bioturbation, they did give more information on long-term deposition and reworking of sand grains than other existing tracers can.

We recommend testing this method in a less dynamic setting, where bioturbation dominates reworking, to improve interpretation of luminescence profiles and further explain the limited feldspar bleaching that we observed. The aim of this research was a qualitative rather than a quantitative description of mixing processes. Given the young age of the sediments and the dynamics of the environment, a quantification of bioturbation as attempted by van der Meij et al. (2025) may be challenging. Nevertheless, single-grain and slow-to-bleach luminescence signals are a promising tool to further test and develop, for ultimately deriving bioturbation rates of sand grains in intertidal settings.

Our results highlight differences between the behaviour and bioturbation of sand and mud within the sediment matrix. This distinction matters for stratigraphy: fines are more mobile within the sediment column, while sand grains have greater potential to preserve layered bedding. Although bioturbation is often assumed to homogenise stratigraphic records (Wheatcroft 1990), our feldspar results suggest that the sand fraction is not intensively reworked by the present bioturbating community. We also observed exchange of particles through the shell layer, suggesting that such layers do not necessarily form a hard boundary for bioturbators. Furthermore, the grain size-specific reworking can inform process-based sediment transport models that quantify the mixing of specific sediment fractions within the bed (e.g., Armanini, 1995). Bioturbation increases the exchange of particles between the active (transportable) and substrate layer of the sediment, with higher exchange probability for small than for large particles.

These findings also bear ecological implications. Fine, organic-rich tracers were rapidly carried below the aerobic zone and accumulated at depth, whereas young sand grains were not. This indicates that bioturbation affects reactive compounds more strongly than coarse particles. Its influence on sand transport may thus be smaller than its role in sediment biogeochemistry and carbon storage. By modifying sediment mud content, bioturbators can modify their own habitat conditions. In sandy sediments, preferential reworking of fines can increase subsurface mud content. Such 'muddification' by cockles was demonstrated in a flume experiment (Soissons et al. 2019) and by *Ensis leei* in a field experiment (Witbaard et al. 2017). On the other hand, resurfaced fines may be mobilised from muddy sediments, decreasing the sediment mud content (Montserrat et al. 2009; Volkenborn et al. 2007b; Wendelboe et al. 2013). These two-way processes affect large-scale intertidal flat morphology and sediment composition (e.g., Brückner et al., 2021; Le Hir et al., 2007). Finally, the integrated contribution of bioturbation

and storms may be comparable when event energy and frequency are considered together. Whereas bioturbation is a continuous process of small particle displacements, storms are infrequent, but high energy events (Fig. 1b). In effect, benthic animals influence daily sediment properties, while storm events 'reset' the system. Because most species have a relatively wide sediment tolerance (Kooistra et al. 2025c), such episodic resetting does not necessarily result in a major community shift, and during calmer periods, bioturbators can once again modify sediments at smaller scales, potentially enhancing their own habitat suitability.

Conclusions

The aim of this study was to distinguish physical from biological mixing over timescales, using tracers that target different grain size fractions. We did not observe clear layering in sediment composition that would point to unbioturbated storm deposits. We showed that sand fractions and mud fractions are mixed differently: fine tracers showed clear signs of bioturbation, while the sand fraction appeared to be less intensely bioturbated than we expected. In conclusion, mud is more mobile within the sediment matrix, due to its higher likelihood to be mixed by bioturbation and physical processes. Sand grains are overall more static and have a higher potential to conserve layering, although single-grain feldspar luminescence signals also showed signs of bioturbation. Over long (decadal) timescales and in dynamic or young environments, it remains impossible to distinguish sediment grains mixed by storms from those reworked by bioturbation with full certainty. Nevertheless, the combination of luminescence signals with different bleaching characteristics can give a more complete picture of the deposition and reworking of sand grains. Multi-grain quartz luminescence was suitable for dating sand grains, while single-grain feldspar luminescence gave information on mixing processes. If applied in consideration of the local environmental conditions, the single-grain signals are a promising technique for tracing bioturbation, but this application needs to be tested further. Until then, a combination of short- and long-term tracers is needed to draw robust conclusions on sediment mixing processes at dynamic intertidal sites.

Acknowledgements

We would like to thank Erna van de Hengel-Voskuilen, Bartel Komin, Birte Leutelt, Bram Parmentier, Eva Lansu, Carlijn Lammers, Paula de la Barra and Sarah Manni for help with field sampling; Erna van de Hengel-Voskuilen and Alice Versendaal

for help with luminescence laboratory analysis and preparation of data; Piet van Gaever and Jeroen Kooijman for XRF and ^{210}Pb analysis and preparation of data; Peter van Breugel for grain size analysis; Jurian Brasser for assistance with Chl-*a* analysis; and Lennart van IJzerloo and Birte Leutelt for help with luminophore analysis. Funding for this study was provided by NWO grant no. 17600: "Tracking Ameland Inlet Living Lab Sediment (TRAILS)". Additionally, Stuart Pearson received funding from NWO grant no. 21026: "Revealing Hidden Networks of Coastal Sediment Pathways".

Data availability

Data and code used for the analysis in this study are openly available through www.doi.org/10.25850/nioz/7b.b.ak (Kooistra et al. 2026).

Supplementary materials

Table S1. Length per core and analysed samples from long cores. The depths from which luminescence samples were analysed are indicated in bold.

	Sandy site	**Muddy site**
Length XRF and grain size core (m)	0.74	0.65
Length luminescence and ^{210}Pb core (m)	0.75	0.72
Number of luminescence samples	8	8
Number of ^{210}Pb samples	13	13
Sample intervals for ^{210}Pb and **luminescence** (cm)	**0-2.5**	**0-2.5**
	5-7.5	**5-7.5**
	10-12.5	**10-12.5**
	15-17.5	**15-17.5**
	20-22.5	22.5-25
	32.5-35	27.5-30
	40-42.5	**35-37.5**
	50-52.5	**40-42.5**
	52.5-55	**50-52.5**
	57.5-60	**55-57.5**
	62.5-65	57.5-60
	67.5-70	65-67.5
	72.5-75	70-72.5

Luminescence analysis

Equivalent dose measurements

The luminescence samples were prepared at the Netherlands Centre for Luminescence Dating (NCL) under amber light conditions. After obtaining the 212–250 µm grain size fraction by wet sieving, carbonates were removed by treating the material with a 10 % HCl solution, followed by the removal of organic matter using a 10 % H_2O_2 solution. Magnetic particles were removed by using a Frantz magnetic separator at a current of 1.4 A on the magnet and under an angle of 10° (Porat 2006). A K-feldspar-rich fraction was extracted through density separation using a separating funnel and LST Fastfloat© with a density of 2.58 g cm^{-3} and washed with demineralized water. A quartz-rich fraction was subsequently isolated from the heavy fraction by performing an additional density separation with

LST of 2.70 g cm^{-3}. The quartz fraction was then rinsed with a 10 % HF solution, followed by treatment with a 40 % HF solution to dissolve feldspar and/or other contaminants and etch the outer skin of quartz grains. Afterward, the material was rinsed with HCl, demineralized water, dried, and sieved.

Each multi-grain quartz sample was measured using an automated Risø TL/OSL DA-15 reader with a calibrated $^{90}Sr/^{90}Y$ beta source. Blue (~470 nm) light emitting diodes (LEDs) were used for optical stimulation. The quartz OSL signals were detected through a 7.5 mm Hoya U-340 filter with a UV detection window. A Single-Aliquot Regenerative-dose protocol (SAR) (Table 2) was used: 1000 datapoints were read out during 20 s of stimulation at 125 °C (0.020 s per datapoint). Channels 1 up to 25 (0.5 s) were taken as initial integration interval; the background interval was set at channel 26 up to 88 (1.24 s). A linear fit was used for dose-response curve fitting, and the curve was forced through the origin. Rejection criteria (recycling ratio, recuperation rate, and test dose error) were set at 15 %. The recuperation rate was taken relative to the first regenerative dose point.

All single-grain feldspar measurements were conducted using an automated Risø TL/OSL DA-20 reader with an automated detection and stimulation head (DASH) and an EMCCD camera (Kook et al. 2015). The system is equipped with a calibrated $^{90}Sr/^{90}Y$ beta source, delivering a dose rate of approximately 0.0707 Gy/s to the feldspar grains on a single-grain disc. To target the 410 nm peak emission of K-feldspar, a blue filter package, BG-3+BG-39 (3.0 + 4.0 mm) was used. A fading test was not conducted. Using a multiple-elevated-temperature (MET) pIRIR measurement protocol was used (de Boer et al. 2024a; Li & Li 2011), a total of 270 datapoints were recorded in 108 seconds (0.400 seconds per datapoint), with 250 datapoints collected during stimulation. For each sample, three single-grain discs were measured, which would correspond to 300 grains if all positions were filled. However, visual inspection revealed that some positions were unoccupied, resulting in an estimated total of approximately 250 grains measured per sample. Channels 11 up to 15 (2 s) were taken as initial integration interval; the background interval was set at channel 226 up to 250 (9.6 s). A linear fit was used for dose-response curve fitting, and the curve was forced through the origin. Rejection criteria (recycling ratio, recuperation rate, and test dose error) were set at 20 %. The recuperation rate was taken relative to the fourth regenerative dose point.

Dose rate measurements

To prepare samples for gamma spectrometry samples were first dried and ashed, documenting weight loss to determine water and organic content. Then the samples were grinded and mixed with wax to create a puck of fixed geometry and retain Radon. Activity concentrations of 40K and several nuclides from the Uranium and Thorium decay chains are measured using a high-resolution gamma ray spectrometer.

Benthic community

Table S2. Benthic community composition at sandy and muddy site and biomass (g ash-free dry weight m^{-1}) per taxon. Note that this table does not include *Arenicola marina*, since this species was not present in the benthic core samples

Sample site	**Latin name**	**Total density (individuals m^{-2})**	**Total biomass (g AFDW m^{-2})**
Sandy site	*Capitella capitata*	226	0.12
	Carcinus maenas	56	0.38
	Cirratulida	169	0.16
	Crangon crangon	56	0.37
	Eteone longa	56	0.09
	Lanice conchilega	56	0.77
	Macoma balthica	56	0.18
	Nereididae	56	0.10
	Oligochaeta	395	0.15
	Pygospio elegans	621	0.15
	Scoloplos armiger	508	1.19
	Urothoe poseidonis	226	0.18
	Sum	**2486**	**3.84**
Muddy site	*Amphipoda*	0*	0.14
	Bivalvia	113	0.13
	Capitella capitata	452	0.20
	Cirratulida	960	0.27
	Corophium volutator	56	0.11
	Eteone longa	1017	0.47
	Gammaridae	169	0.12
	Hediste diversicolor	395	5.97
	Heteromastus filiformis	1186	3.66
	Macoma balthica	226	0.55
	Nereididae	1017	0.26
	Oligochaeta	17514	1.47
	Pygospio elegans	3503	0.37

Table S2. Benthic community composition at sandy and muddy site and biomass (g ash-free dry weight m^{-1}) per taxon. Note that this table does not include *Arenicola marina*, since this species was not present in the benthic core samples *(Continued)*

Sample site	**Latin name**	**Total density (individuals m^{-2})**	**Total biomass (g AFDW m^{-2})**
	Scoloplos armiger	169	0.11
	Scrobicularia plana	282	5.13
	Urothoe	113	0.12
	Sum	**27175**	**19.07**

* as the number of individuals is determined by headcount, when only body parts without head are present, the individuals are identified to the lowest taxonomic level and only analysed for biomass.

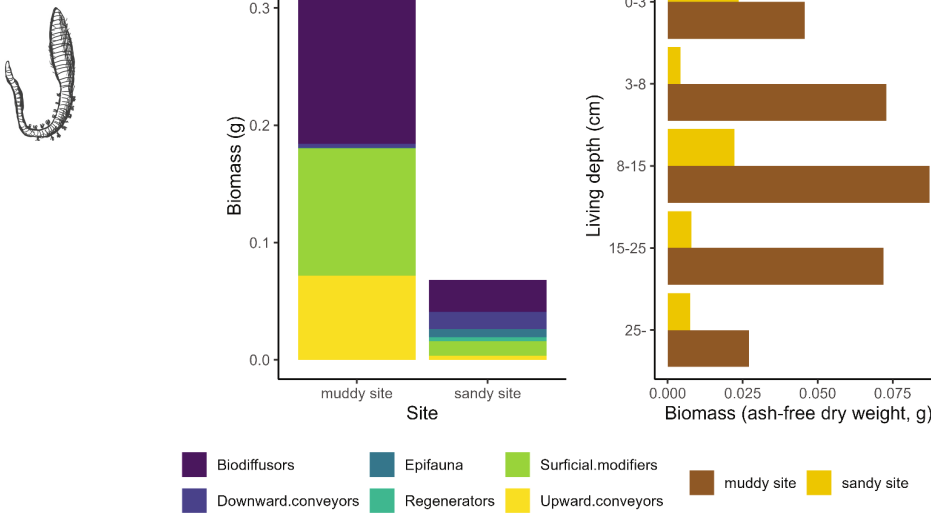

Figure S1. Bioturbation and depth traits from the benthic community, comparing both sites. Relative trait scores are multiplied with total biomass per taxon for bioturbation mode (a) and living depth (b) based on taxon traits. Note that this figure does not include *Arenicola marina*, since this species was not present in the benthic core samples.

Luminescence modelled palaeodose, dose rate and modelled age

Table S3a. Multi-grain quartz luminescence results.

NCL-code	Sample depth [m]	MG-QZ Palaeodose [Gy]			QZ Dose rate [Gy/ka]	MG-QZ Age [a]		
		Iterated	CAM	bootMAM		Iterated	CAM	bootMAM
Sandy core								
NCL-2423121	**0.015**	0.04 ± 0.01	0.05 ± 0.01	0.01 ± 0	1.22 ± 0.06	36.12 ± 6.29	42.97 ± 12.02	9.41 ± 2.84
NCL-2423123	**0.05**	0.05 ± 0.01	0.09 ± 0.02	0.03 ± 0.01	1.3 ± 0.06	41.57 ± 6.2	67.61 ± 16.84	20.37 ± 8.45
NCL-2423125	**0.1**	0.04 ± 0.01	0.09 ± 0.02	0.1 ± 0.03	1.32 ± 0.05	32.17 ± 6.65	70.44 ± 14.23	73.2 ± 19.92
NCL-2423127	**0.15**	0.02 ± 0.01	0.09 ± 0.02	0.06 ± 0.04	1.27 ± 0.06	19.63 ± 4.72	73.08 ± 17.95	49.28 ± 31.72
NCL-2423129	**0.2**	0.1 ± 0.02	0.13 ± 0.03	0.1 ± 0.04	1.34 ± 0.06	74.09 ± 13.92	95.57 ± 19.67	78.13 ± 26.47
NCL-2423134	**0.33**	0.06 ± 0.01	0.09 ± 0.01	0.09 ± 0.02	1.23 ± 0.05	48.78 ± 8.55	69.77 ± 8.08	74.5 ± 16.61
NCL-2423137	**0.4**	0.08 ± 0.01	0.09 ± 0.02	0.05 ± 0	1.08 ± 0.04	72.47 ± 9.36	83.99 ± 14.79	45.12 ± 1.99
NCL-2423141	**0.5**	0.6 ± 0.04	0.63 ± 0.06	0.49 ± 0.01	1.41 ± 0.06	428.32 ± 36.89	449.46 ± 46.26	345 ± 17.2
Muddy core								
NCL-2323092	**0.015**	0.04 ± 0.01	0.07 ± 0.02	0.04 ± 0.02	1.28 ± 0.07	27.52 ± 5.36	55.62 ± 13.72	27.48 ± 14.66
NCL-2323094	**0.05**	0.03 ± 0.01	0.07 ± 0.02	0.03 ± 0.02	1.31 ± 0.06	22.26 ± 4.84	49.61 ± 13.41	21.18 ± 12.59
NCL-2323096	**0.1**	0.04 ± 0.01	0.07 ± 0.02	0.01 ± 0.01	1.33 ± 0.06	31.29 ± 5.93	54.38 ± 17.5	10.78 ± 6.31
NCL-2323098	**0.15**	0.04 ± 0.01	0.1 ± 0.03	0.02 ± 0.01	1.24 ± 0.06	33.77 ± 7.87	79.01 ± 27.92	17.88 ± 11.49
NCL-2323106	**0.35**	0.56 ± 0.02	0.57 ± 0.03	0.57 ± 0.06	1.23 ± 0.06	455.12 ± 29.14	459.57 ± 29.98	458.25 ± 51.93
NCL-2323108	**0.4**	0.63 ± 0.04	0.63 ± 0.03	0.61 ± 0.06	1.42 ± 0.07	442.23 ± 32.97	444.99 ± 29.74	432.32 ± 49.78
NCL-2323112	**0.5**	0.81 ± 0.07	0.87 ± 0.1	0.55 ± 0.1	1.59 ± 0.08	508.46 ± 50.73	546.58 ± 66.86	346.88 ± 66.91
NCL-2323114	**0.55**	0.91 ± 0.03	0.99 ± 0.05	0.96 ± 0.09	1.55 ± 0.08	585.32 ± 34.73	635.13 ± 43.54	619.84 ± 65.96

Table S3b. Single-grain IRSL50 luminescence results.

NCL-code	Sample depth [m]	SG-FS IRSL50 Palaeodose [Gy]			FS Dose rate [Gy/ka]	SG-FS IRSL50 Age [a]		
		Iterated	CAM	bootMAM		Iterated	CAM	bootMAM
Sandy core								
NCL-2423121	**0.015**	0.15 ± 0.03	0.26 ± 0.07	0.16 ± 0	2.1 ± 0.08	72.39 ± 16.7	125.79 ± 32.06	75.91 ± 3.25
NCL-2423123	**0.05**	0.24 ± 0.05	0.33 ± 0.07	0.12 ± 0.03	2.19 ± 0.08	108.86 ± 21.13	152.56 ± 31.25	53.3 ± 15.55
NCL-2423125	**0.1**	0.21 ± 0.02	0.22 ± 0.02	0.22 ± 0.04	2.21 ± 0.08	93.04 ± 10.53	99.18 ± 9.47	101.48 ± 19.08
NCL-2423127	**0.15**	0.09 ± 0.02	0.15 ± 0.04	0.15 ± 0.06	2.16 ± 0.08	42.22 ± 7.44	70.42 ± 20.47	69.21 ± 28.09
NCL-2423129	**0.2**	0.18 ± 0.03	0.25 ± 0.05	0.08 ± 0.02	2.23 ± 0.08	79.33 ± 11.97	113.13 ± 22.53	33.84 ± 11.04
NCL-2423134	**0.33**	0.09 ± 0.01	0.14 ± 0.02	0.09 ± 0	2.12 ± 0.07	43.62 ± 5.24	66.28 ± 9.17	40.54 ± 1.64
NCL-2423137	**0.4**	0.25 ± 0.04	0.27 ± 0.03	0.27 ± 0.05	1.96 ± 0.07	126.54 ± 18.49	136.98 ± 15.18	136.06 ± 26.75
NCL-2423141	**0.5**	0.66 ± 0.05	0.71 ± 0.05	0.58 ± 0.1	2.29 ± 0.08	289 ± 24.74	310.61 ± 26.2	253.87 ± 43.23
Muddy core								
NCL-2323092	**0.015**	0.1 ± 0.01	0.2 ± 0.04	0.1 ± 0.02	2.17 ± 0.09	45.49 ± 5.95	90.73 ± 17.04	44.35 ± 11.5
NCL-2323094	**0.05**	0.14 ± 0.01	0.22 ± 0.03	0.1 ± 0.03	2.2 ± 0.08	64.52 ± 7.21	100.28 ± 16.02	44.37 ± 13.19
NCL-2323096	**0.1**	0.18 ± 0.02	0.27 ± 0.04	0.11 ± 0.04	2.21 ± 0.08	83.56 ± 9.45	123.02 ± 20.72	50.92 ± 16.36
NCL-2323098	**0.15**	0.16 ± 0.02	0.29 ± 0.05	0.18 ± 0.05	2.12 ± 0.08	75 ± 9.04	134.24 ± 22.14	86.15 ± 24.02
NCL-2323106	**0.35**	0.78 ± 0.04	0.83 ± 0.07	0.78 ± 0.1	2.12 ± 0.08	370.04 ± 24.73	392.94 ± 35.06	369.64 ± 48.42
NCL-2323108	**0.4**	0.74 ± 0.08	0.82 ± 0.07	0.72 ± 0.13	2.31 ± 0.09	322.55 ± 38.77	356.69 ± 34.46	311.86 ± 55.75
NCL-2323112	**0.5**	0.69 ± 0.07	0.76 ± 0.07	0.72 ± 0.01	2.48 ± 0.1	276.13 ± 31.42	305.41 ± 31.16	291.75 ± 12.79
NCL-2323114	**0.55**	0.9 ± 0.09	0.97 ± 0.08	0.95 ± 0.02	2.44 ± 0.09	369.58 ± 40.67	396.01 ± 34.86	390.92 ± 17

Table S3c. Single-grain pIR175 luminescence results.

NCL-code	Sample depth [m]	SG-FS pIR175 Palaeodose [Gy]			FS Dose rate [Gy/ka]	SG-FS pIR175 Age [a]		
		Iterated	CAM	bootMAM		Iterated	CAM	bootMAM
Sandy site								
NCL-2423121	**0.015**	0.37 ± 0.1	0.47 ± 0.13	0.2 ± 0.08	2.1 ± 0.08	177.11 ± 47.47	222.61 ± 61.91	94.36 ± 39.41
NCL-2423123	**0.05**	0.35 ± 0.04	0.45 ± 0.07	0.25 ± 0.08	2.19 ± 0.08	157.8 ± 20.99	205.93 ± 33.97	113.2 ± 36.22
NCL-2423125	**0.1**	0.43 ± 0.06	0.45 ± 0.07	0.37 ± 0.12	2.21 ± 0.08	193.18 ± 30.11	206.11 ± 32.86	166.52 ± 53.27
NCL-2423127	**0.15**	0.2 ± 0.04	0.38 ± 0.07	0.32 ± 0.1	2.16 ± 0.08	92.89 ± 16.98	176.25 ± 32.13	149.84 ± 46.48
NCL-2423129	**0.2**	0.33 ± 0.04	0.32 ± 0.05	0.17 ± 0.04	2.23 ± 0.08	149.04 ± 20.02	145.93 ± 21.3	74.94 ± 17.66
NCL-2423134	**0.33**	0.24 ± 0.02	0.3 ± 0.03	0.2 ± 0	2.12 ± 0.07	115.6 ± 8.22	140.59 ± 14.09	93.76 ± 3.79
NCL-2423137	**0.4**	0.46 ± 0.04	0.49 ± 0.07	0.26 ± 0.07	1.96 ± 0.07	234.05 ± 22.61	249.86 ± 35.03	130.99 ± 36.53
NCL-2423141	**0.5**	1.08 ± 0.08	1.01 ± 0.08	0.89 ± 0.14	2.29 ± 0.08	471.45 ± 37.92	442.4 ± 36.81	387.49 ± 60.92
Muddy site								
NCL-2323092	**0.013**	0.3 ± 0.04	0.42 ± 0.07	0.18 ± 0.04	2.17 ± 0.09	137.95 ± 20.62	191.43 ± 32.67	81.82 ± 19.23
NCL-2323094	**0.05**	0.37 ± 0.06	0.52 ± 0.09	0.2 ± 0.06	2.2 ± 0.08	166.52 ± 29.91	235.1 ± 43.91	90.85 ± 25.6
NCL-2323096	**0.1**	0.26 ± 0.03	0.39 ± 0.07	0.19 ± 0.05	2.21 ± 0.08	115.97 ± 14.92	174.32 ± 30.16	86.69 ± 20.85
NCL-2323098	**0.15**	0.4 ± 0.06	0.37 ± 0.07	0.16 ± 0.04	2.12 ± 0.08	186.35 ± 28.56	176.47 ± 33.19	73.08 ± 17.69
NCL-2323106	**0.35**	1.44 ± 0.16	1.49 ± 0.15	0.99 ± 0.19	2.12 ± 0.08	681.17 ± 78.9	705.54 ± 75.29	466.34 ± 91.63
NCL-2323108	**0.4**	1.29 ± 0.06	1.29 ± 0.09	1.22 ± 0.17	2.31 ± 0.09	558 ± 34.9	558.34 ± 46.35	529.36 ± 75.58
NCL-2323112	**0.5**	1.12 ± 0.1	1.08 ± 0.1	1.09 ± 0.18	2.48 ± 0.1	452.58 ± 45.5	436.68 ± 44.81	437.29 ± 72.78
NCL-2323114	**0.55**	1.27 ± 0.14	1.35 ± 0.13	1.17 ± 0.23	2.44 ± 0.09	519.71 ± 59.06	553.49 ± 57.81	478.91 ± 96.25

Luminophore observations

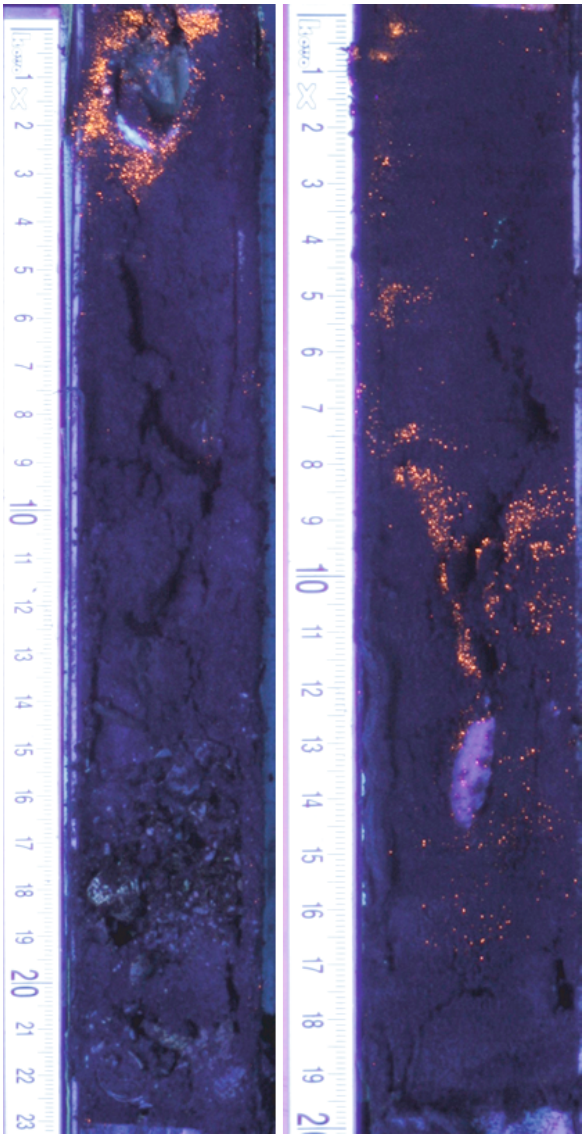

Figure S2. Cores taken 36 hours after luminophore application, indicating observations of downward particle transport reworking by *S. plana* at sandy site (top) and *C. edule* at muddy site (bottom).

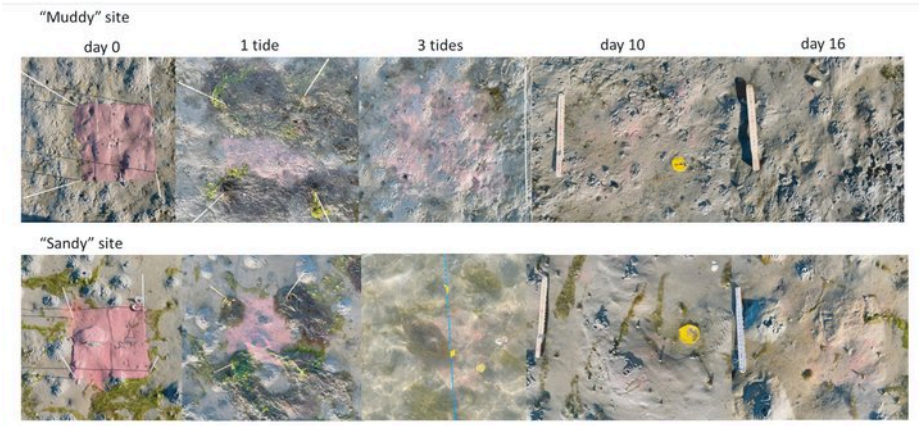

Figure S3. Observations of luminophores on the sediment surface. Note the decrease in luminophores visible on the surface. The sticks placed at the start of the experiment were removed after 1 tide, as they were observed to trap algae.

chapter 6

Synthesis

The overall aim of this dissertation was to unravel the interaction between macrozoobenthos and sediment in the context of large-scale sediment nourishments on ebb-tidal deltas of the Wadden Sea. In this synthesis section, I will give an overview of the main findings (Fig. 1), describe their implications on a larger scale, give recommendations and draw overall conclusions based on my research.

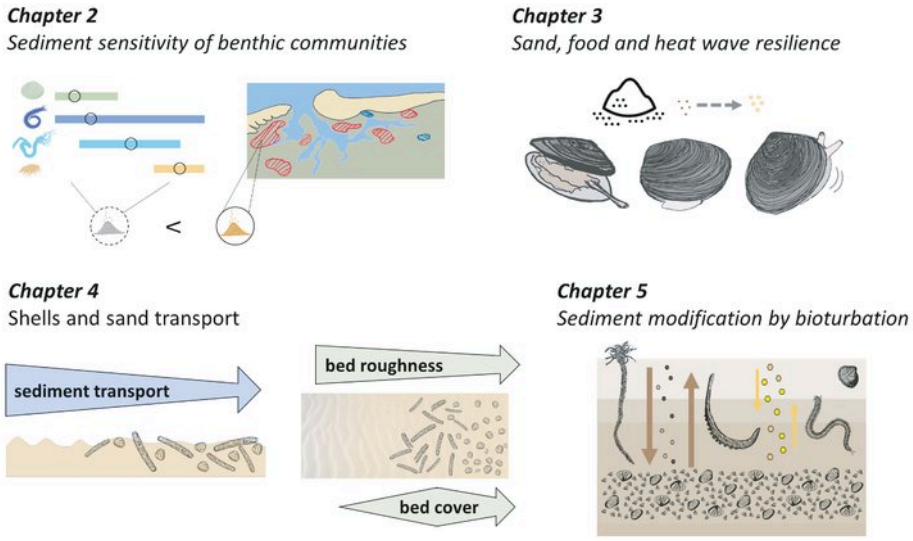

Figure 1. Visual overview of the content and main outcomes this dissertation.

Potential impacts of sand nourishments on macrozoobenthos

The first main question was whether the sand of a 5 million m^3 nourishment on Ameland ebb-tidal delta could have influenced the macrozoobenthic communities in the Borndiep basin and around Ameland inlet. Previously, impacts were found on benthic community composition at the nourishment location (Escaravage 2022). Especially long-lived species such as bivalve species did not recover at the nourishment site within the monitored period. Detecting far-field effects of the nourishments was more challenging. As natural dynamics are high, the benthic communities are also variable (Kröncke & Reiss 2010; Reiss & Kröncke 2005). This is particularly the case at the ebb-tidal delta, the dynamic foreshore, and within the gullies, where most sediment transport could be expected (Holzhauer et al. 2020; Nehmer & Kröncke 2003; Reiss & Kröncke 2001). Furthermore, many

other anthropogenic activities, such as bottom trawling and dredging, also take place in the Wadden Sea and coastal zone. The impacts of these factors cannot easily be separated from those of the nourishment.

Within the TRAILS project, large steps have been made in developing tools to trace sand grains and predict pathways of nourished sediment (de Boer et al., in review, 2024; van Westen et al., 2025). Despite this advancement, we do not yet exactly know where the nourished sand ended up. Furthermore, initially modelled sediment pathways indicated a higher likelihood of sediment being transported to the Ameland coast rather than into the Wadden Sea (Pearson et al. 2020, 2021b). Therefore, changes in benthic communities away from the nourishment site could not directly be linked to nourishment impacts.

Nevertheless, the extensive benthic monitoring data from the area allowed for making predictions of the sensitivity to potential sediment changes (**Chapter 2**). Although general changes in sediment composition linked to the nourishment could not be identified, sediments in the intertidal Borndiep were overall coarser than the optimal for many species living there. The sediment sensitivities of the main resident benthic species suggested that an increase in median grain size or decrease in mud content could further decrease the habitat suitability and drive species beyond their sediment tolerance niche. Some species are more sensitive than others and have a clear sediment preference. For one of these, the mud-dwelling peppery furrow clam (*Scrobicularia plana*), this muddy sediment preference appeared to be independent of the usually co-occurring high food supply: mortality was highest in a sandy sediment independent of the amount of food present (**Chapter 3**). This clam was relatively tolerant to heatwave exposure, and its tolerance was not significantly affected by sediment type. Although we did not observe clear additive effects of heatwaves and sediment on the species, increased intensity and frequency of heatwaves combined with reduced mobility could lower its coping capacity. Such interactions are also likely to play a role in other benthic species, especially those that live closer to the sediment surface, or have a lower thermal tolerance.

Together, these results demonstrate that sediment composition is an important driver of benthic communities. Especially in several intertidal areas, sediment composition is already beyond the preferred range of the current Wadden Sea communities. The risks for community changes associated with “sandification” differ between areas and between taxa.

Feedback of benthic fauna to sediment composition

The second aim of this thesis was to unravel animal feedbacks on sand transport. An extensive literature base already exists on the stabilising and destabilising effects that benthic animals can have on sedimentary processes. Many of the studies focussed on biotic effects on the resuspension of mud and the erodibility of cohesive sediments (Arlinghaus et al. 2022; Brückner et al. 2021; Dairain et al. 2020; de Smit et al. 2021; Kristensen et al. 2013; Le Hir et al. 2007; Volkenborn et al. 2009). Fewer studies have looked into the effects of fauna on non-cohesive sediment transport (Dairain et al. 2020; Harris et al. 2015; Joensuu et al. 2018; Li et al. 2017).

During field sampling in the Ameland inlet, one of the first noticeable differences between the boxcores that were brought up from the subtidal sea floor was the amount of empty shells, variable in shape and size, present on the sediment surface and within the core itself. In a flume experiment (**Chapter 4**), we saw that shells limit sand transport, independent of shell shape. The effect was largest at the higher current velocities that we tested (0.5 m s^{-1}). Besides by their structure, animals can influence the sediment around them through their movement and activity. Such bioturbation of sand is less studied than that of mud, as tracers for sand on longer timescales were lacking. Using a novel type of long-term sand grain tracer (single-grain luminescence) it appeared that sand was reworked less intensely than we expected (**Chapter 5**). Mud was more mobile within the sediment matrix, likely due to passive infiltration combined with the preferentially targeting of mud by bioturbators.

These results taken together show that benthic animals and their remains can contribute significantly to sediment transport and can influence the composition of their sedimentary habitats. The relative magnitude of the biotic feedback on sediment depends on the local hydrodynamic condition.

Relative importance and causality in benthos-sediment interactions

As introduced at the start of this thesis, the strength and direction of benthos-sediment interactions relative to physical dynamics is a long-debated subject. Furthermore, because the feedback between benthic animals and sediment

goes both ways, the causality of effects is not always clear. Although answering these fundamental questions was beyond the scope of this thesis, the main findings of this work are placed in a conceptual context here.

Relative magnitude of biotic feedbacks to sediment transport and composition

In a very dynamic environment, the impact of benthic structures and activities may be insignificant. In less dynamic regimes, the inconspicuous, but nearly continuous sediment displacements by benthic activity pay a fair contribution to the total movement of sediment (e.g., Grant 1983). A conceptual model of biotic effects on sediment mixing was proposed by Cadée (2001), with a minimal biotic contribution at very low or very high energy levels, deemed uninhabitable for biota, and a maximal contribution of bioturbation at intermediate levels of environmental dynamics. Based on this thesis, the hypothetical concept can be extended to the interaction of biota with lateral and vertical sand transport from low- to high-dynamic habitats (Fig. 2). When current velocities increase, biogenic structures, such as shells, have a larger effect. Above their own critical erosion threshold, shells may however not be able to limit sand transport anymore, as they may be washed away themselves. On a tidal flat, the reworking of sand by bioturbators may have been substantial but had not been intense enough to expose all grains to hours of daylight since their deposition—not all luminescence signals in our experiment were fully bleached. Also here, hydrodynamics and deposition history do therefore still play a role in the vertical distribution of sand grains. In less dynamic sites, the relative contribution of bioturbation to vertical sand transport is likely higher. Together, this still results in the highest relative contribution of biota to sediment transport at low and intermediate energy habitats.

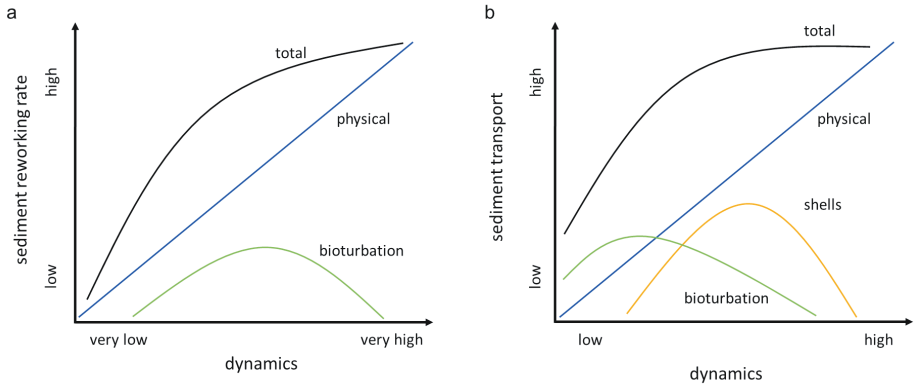

Figure 2. (a) conceptual model of relative physical and biological sediment reworking (separate and combined) against the total range of hydrodynamic energy in coastal sediments (Cadée 2001); (b) a proposed hypothetical conceptual model of relative biotic feedbacks through bioturbation and structure to vertical and lateral sand transport, over a gradient from low to high dynamic habitats.

The causality of sediment preferences

A second main question is: do benthic animals shape the sediments they inhabit, or are they mostly responding to physical sediment dynamics? While benthic animals show preference for certain sediment types and their distribution is determined by sediment characteristics (Chapter 2, 3), they also modify sediment composition. By resuspending mud, reducing the erosion of sand and incorporating fine particles in the sediment matrix, they might engineer their own preferred sediment habitat themselves. Over a large scale (tidal basin), sediment supply and physical dynamics form the boundary conditions that drive the possible gradients in sediment composition. On a smaller scale, benthic species can mediate sediment composition and dynamics in their direct environment (e.g., Soissons et al., 2019; Wendelboe et al., 2013). With high densities of biota and a wide spatial distribution, these effects are substantial again on larger scales (e.g., Brückner et al, 2021). In Chapter 5, we introduced the hypothesis that, by their continuous, small efforts, biota have a similar total effect on sediment mixing as storms do, which are infrequent but have a high energy. Whether the biotic or the physical forces determine the sediment structure does therefore not just depend on the physical characteristics of the studied site, but also on the moment of sampling (calm period or just after a storm?) and the investigated temporal and spatial scale. The results from the chapters of this thesis, and other studies

on benthos-sediment interactions, can form a baseline to estimate effects, but should be considered in their relevant spatio-temporal context.

Looking ahead: future research directions

Within this dissertation, several questions regarding benthos-sediment interactions in the context of sediment nourishments have been addressed. However, it has also brought up numerous new questions and follow-up research opportunities.

Sediment change and effects on benthos: monitoring is key

This research builds upon an extensive database of benthic monitoring data (Bijleveld et al. 2025; Franken et al. 2025). Such large-scale and long-term datasets are essential for addressing fundamental ecological questions, as well as for detecting and interpreting environmental change and anthropogenic impacts. Within the scope of this PhD, I could not directly determine the far-field effects of coastal sand nourishments on benthic communities, partly due to the high natural variability of these systems and the simultaneous influence of multiple other natural and anthropogenic disturbances. However, this does not necessarily imply that sand nourishments have no ecological consequences beyond their immediate application sites. Over longer timescales, the cumulative effects of near-continuous sand nourishment may become evident. To disentangle the effects of nourishments from other drivers and natural variability, as well as to detect potential long-term impacts, continuous monitoring of both environmental parameters and ecological responses remains crucial.

As tracing tools for nourishment sand are advancing, the direct link between a nourishment and its off-site impact can be made with higher certainty. This will provide further opportunities for more robust impact assessments in dynamic systems where multiple disturbances are at play.

The approach used in Chapter 2 for determining sediment sensitivity of benthic fauna in the Ameland inlet and Borndiep basin can be applied in other areas where sufficient data on benthic fauna and sediment composition are available. Although I chose to apply this in one tidal basin where data was available for the inter- as well as the subtidal, openly accessible data (e.g., Bijleveld et al., 2025) can facilitate the determination of sensitivity for a larger area. These can then

be used to identify areas at risk of "sandification", or mud loss at a larger scale. Chapter 2 showed that the most pronounced sediment-species mismatches lie in the intertidal zone. It would therefore be highly relevant to investigate sediment sensitivity in the entire intertidal Wadden Sea. When sufficient data on other factors is available, the same tools can be used to identify sensitivity and risk hotspots of benthic communities to other pressures such as temperature, nutrient inputs or physical disturbance.

In Chapter 2, sensitivity was defined as the tolerance to a range of environmental conditions—in other words, the niche width. Another approach to sensitivity is quantifying the response rate of a population or community to an environmental change. Communities in dynamic habitats are relatively well-adapted to short-term environmental fluctuations, and there were no overall linear trends in sediment change within the studied time frame. As such, the first approach was deemed more relevant in this case. Future investigations into organism and community responses to sediment change could further explore the second approach to sensitivity.

Interactions between multiple stressors

When multiple stressors act simultaneously, their effects can be synergistic, antagonistic, or additive (Piggott et al. 2015). The strength and direction of stressor interaction can vary over levels of ecological organisation (Galic et al. 2018; Simmons et al. 2021). Organisms subjected to suboptimal environmental conditions may for instance have a lower resilience to climatic stressors (Hewitt et al. 2016). When non-native species display a higher tolerance to combinations of stressors (e.g., heat and salinity: Zhou et al., 2025), or species interactions are altered (e.g. Laukaityte et al., 2025), additive effects could drive community shifts. Besides that, interacting environmental factors can mediate their own effects. For instance, as heat penetration and retention differ between sandy and muddy intertidal sediments (Liu et al. 2025), increasing heat is a potentially synergistic or antagonistic stressor combination with sediment change.

To enable better predictions of ecological shifts, the interactions between stressors should be investigated further in laboratory and field settings. Mesocosm experiments can offer mechanistic understanding on the interplay of specific stressors within set levels and their effects on individuals or communities. Findings from *ex-situ* experiments can however not always directly be translated to ecological effects in the field, as the natural timescale and sequence of exposure as well

as the interaction with a multitude of ameliorating and exacerbating factors cannot be replicated in the laboratory. In the mesocosm experiment presented in Chapter 3, sediment type proved to be a stronger driver of the performance of mud-dwelling clam *Scrobicularia plana*, compared to food availability or heatwave exposure. We hypothesised that the reduced mobility of this species in a sandy sediment would ultimately determine heatwave tolerance, if the severity of the heatwave would increase compared to the level we tested. Follow-up experiments are required to test this hypothesis and to verify our findings in a natural intertidal flat setting. The question of how such species-level responses can be translated to effects on community-level can be approached in multi-species mesocosm or field experiments.

Building upon biotic feedbacks to sediment

The large-scale implications of modifications of biota mediated sand transport can be further studied through numerical models. Eventually, biotic feedbacks can be incorporated in sediment transport models as a grain-size dependent exchange of particles between the substrate and the active (transportable) layers (e.g., Armanini, 1995). The sediment transport rate parameters derived in Chapter 4 could be readily implemented in in sediment transport models such as SedTRAILS (van Westen et al. 2025). Together with quantitative sediment shell content data from seafloor surveys, predictions can be made on the effects that shells have on the transport of sand in natural settings. As shells are among the most ubiquitous biotic structures in marine sediments, their effects may be substantial on larger scales.

In Chapter 5, we saw that the vertical distribution of sand grains is influenced by bioturbation, albeit not at the same rate as the reworking of fine particles. Sand is therefore more likely to conserve stratification by storms. However, several questions remained open. To obtain more certainty in distinguishing reworking by storms from bioturbation, controlled (flume) experiments or targeted sampling is needed. Single-grain luminescence samples could for instance be collected directly after a storm, so that signal profiles can directly be related to the hydrodynamic reworking. We were also not yet able to calculate bioturbation rates of sand grains on basis of luminescence in Chapter 5. Nevertheless, with further development and testing of sand particle tracers, such as single-grain luminescence, sand grain reworking rates can potentially be determined in future studies. Combined with spatial distribution datasets of bioturbating species, such

bioturbation rates can then also be implemented in abovementioned numerical sediment transport models.

Besides the feedbacks studied in this thesis, many more bioengineering effects of benthic animals on their sedimentary habitats may play a role. In addition to moving around sediment particles, bioturbating animals also influence sediment roughness by creating tracks, mounds and depressions. These topographical modifications interact with near-bed flow and can influence the transportability of sand (Dairain et al. 2020; Friedrichs et al. 2009). To obtain a more complete view it would be interesting to compare the relative contributions of benthic species to horizontal sand transport versus vertical reworking of sand. Such integrated quantifications of sediment transport by biota are currently still lacking, especially on community level. Further steps can be made to translate bioturbation metrics, such as community bioturbation potential (BPc) to implications on sediment transport (Queirós et al. 2015).

Implications

Resilience of coastal ecosystems

Species living in ever-changing environments are subjected to a range of environmental conditions and therefore relatively tolerant to fluctuations (Gray & Elliott, 2009). They may however also be living close to the edge of their potential niche (Tomanek 2002). Even in dynamic coastal habitats, benthic fauna can be sensitive to sedimentary changes. Especially when multiple stressors are acting in synchrony, benthic communities might shift. Climate change is posing large-scale pressures that act on many different levels of coastal ecosystems (Buschbaum et al. 2024). Sediment change in combination with these large-scale stressors or other local disturbances may decrease ecological resilience.

In this thesis I have shown that many macrozoobenthic species are generalists in terms of sediment preference (Chapter 2) and species can be relatively heat-tolerant (Chapter 3). As these systems are inherently dynamic, e.g., sediment composition is subject to large scale fluctuations (Folmer et al. 2023), small and single disturbances may not directly cause an impact. However, even organisms with high adaptive capacities have limits, especially under multiple stressors. If we cannot recognise warning signs and ensure that the environment stays within these limits, habitats may become unsuitable for some species. It is therefore

important that the ecological state of the system keeps being monitored, and local pressures are reduced as much as possible, especially at sites that are deemed sensitive or may approach a critical stress level (e.g., sediment composition beyond the optimal range, Chapter 2).

Sediment impacts and management

Sediment grain size in the Borndiep tidal basin was coarser than optimal for the resident communities. In a few areas, communities crossed the limits of their optimal sediment envelope. These coarser-than-optimal sediments could not be directly linked to sand nourishments. However, the far-field effects of future nourishments on sediment grain size should be considered. With sea level rise, the required nourishment volumes are predicted to increase. In the Netherlands, this increase could be up to 20 times present-day volumes by 2100 (Haasnoot et al. 2020). Such structural sediment additions are likely to have large ecological implications at their application site and may also increase the sand supply to adjacent muddy coastal systems.

Apart from the potential effects of sand input, a reduction in mud content is another risk identified in Chapter 2. A large fraction of the Borndiep basin had a lower than optimal mud content for the resident communities. The patterns of suboptimal mud were more conspicuous than those for median grain size. Even though mud may be a nuisance when it causes infilling of fairways, it is a finite resource and is already limited in eastern parts of the Wadden Sea (Colina Alonso et al. 2024). Besides the importance of mud availability for intertidal areas to grow with sea level rise, the ecological implications of mud loss should therefore also carefully be considered when managing mud.

Natural values of coastal systems

The intertidal habitats and natural dynamics, as well as the high ecological productivity and biodiversity form the unique natural values of coastal ecosystems (Reise et al. 2010). To protect and conserve these values, management decisions should be taken conscientiously. Of foremost importance is the reduction of greenhouse gas emissions to keep warming and sea level rise at bay. On a regional and local level, a reduction of pressures and active restoration efforts can help conserving and restoring the natural values of these unique ecosystems (Floor et al. 2018; Wiesebron et al. 2024). Currently, conservation efforts are often lacking or inefficient: for instance, protected areas in the Wadden Sea are misaligned with biodiversity hotspots (Meijer et al. 2025). Improving the spatial

cover and distribution of protected areas can potentially enhance biodiversity of coastal ecosystems and contribute to ecological resilience to disturbance. A second way to achieve such goal is by aiding the recovery of foundation species such as bivalve reefs and seagrass meadows, that have the potential to enhance diversity and ecosystem resilience (Dickson et al. 2023, Bouma et al. 2009b; Witte et al. 2025; Ysebaert et al. 2018). Furthermore, such bioengineers can trap sediment on a large scale, further helping tidal flats to keep up with sea level rise (Hoffmann et al. 2025).

Even though the Wadden Sea world heritage is considered one of the "wildest" natural areas in western Europe, it is characterised by centuries of anthropogenic impacts (e.g., Chapter 1, Box II). These have driven ecological shifts during the past century (Eriksson et al. 2010; Lotze 2005). The current state of the Wadden Sea should therefore not be taken as the base line to be maintained, but rather as a starting point for restoration of ecological values to a higher level.

Sea level rise may result in a loss of intertidal area (Lodder et al., 2019; Timmerman et al., 2021). As the intertidal flats drive productivity, hold a vast benthic biomass and support migrating bird populations, such a shift from an intertidal sedimentary system to a shallow subtidal coastal lagoon would have immense implications for ecosystem structure and functioning. Sediment nourishments placed on tidal flats could be an active measure to conserve and restore crucial intertidal habitats (e.g. van der Werf et al., 2015, 2019). Such engineering projects do however also form a disturbance from which the ecosystems do not easily recover (Escaravage et al. 2024). Nourishing with other sediment types, for instance mud, may enhance the ecological suitability (Baptist et al. 2019). Nevertheless, we should ask ourselves the question whether it is preferred to actively manage a system such as the Wadden Sea, that has the dynamic forces of nature and the ever-changing morphology engrained in its identity, or to minimise our own disturbance in such systems and let nature run its course.

Coastal management and sustainable nourishment strategies

If we choose to keep low-lying coastal lands inhabited, flood defence strategies need to be adapted to the global challenges of the coming centuries. We will need sustainable nourishment strategies, which need to not only keep our feet dry but also to work with nature, instead of against it. To make such nourishments more effective and ecologically sound, biotic feedbacks to the distribution and stability of sand should be considered. If we can harness the

bioengineering qualities of biota, we could make nourishments more sustainable, whilst increasing their ecological value. With the aim to make nourishments more stable, borrow areas with higher shell contents could be selected. Furthermore, the potential for recolonisation through stabilising biota could be increased by providing the most suitable sediment type, or by enriching the nourishment top layer with local sediment, containing the local benthos.

Alternatively, we can ask ourselves the question whether nourishments are sustainable solutions. Instead of investing more money and resources to keep sandy coastlines in place at all costs, managed retreat is another option that should be considered (Haasnoot et al. 2021). Damage of natural hazards can be avoided by moving the centres of economic activity and populations away from locations that are at risk of erosion and flooding. This requires enormous reorganisation and relocations but may be the most sensible and sustainable solution on the long run.

General conclusions

In this thesis, I demonstrated interactions between benthos and sediment on many different levels. Benthic animals influence the transport and composition of sediment by bioturbation. By preferentially reworking mud, they can influence the composition of sediments. The structures they produce, such as shells, can stabilise sand. These bioengineering feedbacks can be significant in comparison with physical interactions over time and space. However, the benthic species themselves can also be sensitive to sediment change. Although many species in coastal habitats are sediment generalists, species and communities frequently occur beyond their preferred sediment range. Sediment in a Wadden Sea tidal basin, especially in intertidal areas, were coarser and less muddy than optimal. Experimental investigation into the mechanisms of this sediment preference revealed that sedimentary substrate composition can be a stronger driver than food availability or heat exposure. The outcomes from this dissertation combined, underline that sediment management should be executed with care for the ecological communities.

References

Al-Dabbas MAM, McManus J (1987) Shell fragments as indicators of bed sediment transport in the Tay Estuary. Proceedings of the Royal Society of Edinburgh Section B Biological Sciences 92(3–4):335–344. https://doi.org/10.1017/s0269727000004759

Alexander RR, Stanton RJ, Dodd JR (1993) Influence of sediment grain size on the burrowing of bivalves: correlation with distribution and stratigraphic persistence of selected Neogene clams. Palaios 8(3):289–303. https://doi.org/10.2307/3515151

Allen JRL (1984) Experiments on the settling, overturning and entrainment of bivalve shells and related models. Sedimentology 31(2):227–250. https://doi.org/10.1111/j.1365-3091.1984.tb01961.x

Aller RC (1982) The Effects of Macrobenthos on Chemical Properties of Marine Sediment and Overlying Water. In: McCall PL, Tevesz MJS (eds) Animal-sediment relations: the biogenic alteration of sediments. Springer, Boston, MA, pp 53–102

Aller RC, Cochran JK (2019) The Critical Role of Bioturbation for Particle Dynamics, Priming Potential, and Organic C Remineralization in Marine Sediments: Local and Basin Scales. Front Earth Sci (Lausanne) 7:459885. https://doi.org/10.3389/feart.2019.00157

Al-Raei AM, Bosselmann K, Böttcher ME, Hespenheide B, Tauber F (2009) Seasonal dynamics of microbial sulfate reduction in temperate intertidal surface sediments: controls by temperature and organic matter. Ocean Dyn 59(2):351–370. https://doi.org/10.1007/s10236-009-0186-5

Amorim VE, Gonçalves O, Capela R, Fernández-Boo S, Oliveira M, Dolbeth M, Arenas F, Cardoso PG (2020) Immunological and oxidative stress responses of the bivalve *Scrobicularia plana* to distinct patterns of heatwaves. Fish Shellfish Immunol 106:1067–1077. https://doi.org/10.1016/j.fsi.2020.09.024

Anderson MJ (2008) Animal-sediment relationships re-visited: Characterising species' distributions along an environmental gradient using canonical analysis and quantile regression splines. J Exp Mar Biol Ecol 366(1–2):16–27. https://doi.org/10.1016/j.jembe.2008.07.006

Arlinghaus P, Zhang W, Schrum C (2022) Small-scale benthic faunal activities may lead to large-scale morphological change-A model based assessment. Front Mar Sci 9(1011760). https://doi.org/10.3389/fmars.2022.1011760

Armanini A (1995) Non-uniform sediment transport: dynamics of the active layer. Journal of Hydraulic Research 33(5):611–622. https://doi.org/10.1080/00221689509498560

Armonies W (2021) Who lives where? Macrobenthic species distribution over sediment types and depth classes in the eastern North Sea. Helgol Mar Res 75(1):1–6. https://doi.org/10.1186/S10152-021-00552-1

Baar AW, Boechat Albernaz M, van Dijk WM, Kleinhans MG (2019) Critical dependence of morphodynamic models of fluvial and tidal systems on empirical downslope sediment transport. Nat Commun 10(1):1–12. https://doi.org/10.1038/s41467-019-12753-x

Baeta A, Valiela I, Rossi F, Pinto R, Richard P, Niquil N, Marques JC (2009) Eutrophication and trophic structure in response to the presence of the eelgrass *Zostera noltii*. Mar Biol 156(10):2107–2120. https://doi.org/10.1007/s00227-009-1241-y

Ballesta-Artero I, Witbaard R, Carroll ML, van der Meer J (2017) Environmental factors regulating gaping activity of the bivalve Arctica islandica in Northern Norway. Mar Biol 164(5):1–15. https://doi.org/10.1007/s00227-017-3144-7

Baptist MJ, Gerkema T, van Prooijen BC, van Maren DS, van Regteren M, Schulz K, Colosimo I, Vroom J, van Kessel T, Grasmeijer B, Willemsen P, Elschot K, de Groot A V., Cleveringa J, van Eekelen EMM, Schuurman F, de Lange HJ, van Puijenbroek MEB (2019) Beneficial use of dredged sediment to enhance salt marsh development by applying a 'Mud Motor.' Ecol Eng 127:312–323. https://doi.org/10.1016/j.ecoleng.2018.11.019

Bates D, Mächler M, Bolker BM, Walker SC (2015) Fitting linear mixed-effects models using lme4. J Stat Softw 67(1):1–48. https://doi.org/10.18637/jss.v067.i01

Baumfalk YA (1979) Heterogeneous grain size distribution in tidal flat sediment caused by bioturbation activity of Arenicola marina (polychaeta). Netherlands Journal of Sea Research 13(3–4):428–440. https://doi.org/10.1016/0077-7579(79)90016-4

Beauchard O, Bradshaw C, Bolam S, Tiano J, Garcia C, De Borger E, Laffargue P, Blomqvist M, Tsikopoulou I, Papadopoulou NK, Smith CJ, Claes J, Soetaert K, Sciberras M (2023) Trawling-induced change in benthic effect trait composition - A multiple case study. Front Mar Sci 10:1303909. https://doi.org/10.3389/fmars.2023.1303909

Belliard JP, Silinski A, Meire D, Kolokythas G, Levy Y, Van Braeckel A, Bouma TJ, Temmerman S (2019) High-resolution bed level changes in relation to tidal and wave forcing on a narrow fringing macrotidal flat: Bridging intra-tidal, daily and seasonal sediment dynamics. Mar Geol 412:123–138. https://doi.org/10.1016/j.margeo.2019.03.001

Benninger LK, Aller RC, Cochran JK, Turekian KK (1979) Effects of biological sediment mixing on the 210Pb chronology and trace metal distribution in a Long Island Sound sediment core. Earth Planet Sci Lett 43(2):241–259. https://doi.org/10.1016/0012-821X(79)90208-5

Bentley SJ, Nittrouer CA (2012) Accumulation and intense bioturbation of bioclastic muds along a carbonate-platform margin: Dry Tortugas, Florida. Mar Geol 315–318:44–57. https://doi.org/10.1016/j.margeo.2012.05.002

Bentley SJ, Swales A, Pyenson B, Dawe J (2014) Sedimentation, bioturbation, and sedimentary fabric evolution on a modern mesotidal mudflat: A multi-tracer study of processes, rates, and scales. Estuar Coast Shelf Sci 141:58–68. https://doi.org/10.1016/j.ecss.2014.02.004

Beukema JJ, Cadée GC (1999) An estimate of the sustainable rate of shell extraction from the Dutch Wadden Sea. Journal of Applied Ecology 36(1):49–58. https://doi.org/10.1046/j.1365-2664.1999.00380.x

Beukema JJ, De Vlas J (1979) Population parameters of the lugworm, Arenicola marina, living on tidal flats in the Dutch Wadden Sea. Netherlands Journal of Sea Research 13:331–353

Beukema JJ, Dekker R (2020) Half a century of monitoring macrobenthic animals on tidal flats in the Dutch Wadden Sea. Mar Ecol Prog Ser 656:1–18. https://doi.org/10.3354/meps13555

Bijleveld AI, de la Barra P, Danielson-Owczynsky H, Brunner L, Dekinga A, Holthuijsen S, Ten Horn J, de Jong A, Kleine Schaars L, Kooij A, Koolhaas A, Kressin H, van Leersum F, Miguel S, de Monte LGG, Mosk D, Niamir A, Oude Luttikhuis D, Peck MA, Piersma T, Roohi R, Serre-Fredj L, Tacoma M, van Weerlee E, de Wit B, Bom RA (2025) SIBES: Long-term and large-scale monitoring of intertidal macrozoobenthos and sediment in the Dutch Wadden Sea. Sci Data 12(1):239. https://doi.org/10.1038/s41597-025-04540-9

Bijleveld AI, Tacoma M, Koolhaas A (2024) SIBES dataset

Bijleveld AI, Twietmeyer S, Piechocki J, van Gils JA, Piersma T (2015) Natural selection by pulsed predation: survival of the thickest. Ecology 96(7):1943–1956. https://doi.org/10.1890/14-1845.1

Bijleveld AI, van Gils JA, van der Meer J, Dekinga A, Kraan C, van der Veer HW, Piersma T (2012) Designing a benthic monitoring programme with multiple conflicting objectives. Methods Ecol Evol 3(3):526–536. https://doi.org/10.1111/j.2041-210X.2012.00192.x

Bocher P, Piersma T, Dekinga A, Kraan C, Yates MG, Guyot T, Folmer EO, Radenac G (2007) Site- and species-specific distribution patterns of molluscs at five intertidal soft-sediment areas in northwest Europe during a single winter. Mar Biol 151(2):577–594. https://doi.org/10.1007/s00227-006-0500-4

Bokuniewicz HJ, Gordon RB, Rhoads DC (1975) Mechanical properties of the sediment-water interface. Mar Geol 18(5):263–278. https://doi.org/10.1016/0025-3227(75)90016-X

Bolam SG, Fernandes TF (2003) Dense aggregations of Pygospio elegans (Claparède): Effect on macrofaunal community structure and sediments. J Sea Res 49(3):171–185. https://doi.org/10.1016/S1385-1101(03)00007-8

Bonnard M, Roméo M, Amiard-Triquet C (2009) Effects of copper on the burrowing behavior of estuarine and coastal invertebrates, the polychaete *Nereis diversicolor* and the bivalve *Scrobicularia plana*. Human and Ecological Risk Assessment 15(1):11–26. https://doi.org/10.1080/10807030802614934

Borsje BW, Hulscher SJMH, Herman PMJ, De Vries MB (2009) On the parameterization of biological influences on offshore sand wave dynamics. Ocean Dyn 59(5):659–670. https://doi.org/10.1007/s10236-009-0199-0

Borsje BW, Kruijt M, Werf J Van der, Hulscher S, Herman P (2011) Modeling Biogeomorphological Interactions in Underwater Nourishments. Coastal Engineering Proceedings 1(32):104. https://doi.org/10.9753/icce.v32.sediment.104

Bouma TJ, De Vries MB, Low E, Peralta G, Tánczos IC, Van De Koppel J, Herman PMJ (2005) Trade-offs related to ecosystem engineering: A case study on stiffness of emerging macrophytes. Ecology 86(8):2187–2199. https://doi.org/10.1890/04-1588

Bouma TJ, Friedrichs M, Van Wesenbeeck BK, Temmerman S, Graf G, Herman PMJ (2009a) Density-dependent linkage of scale-dependent feedbacks: a flume study on the intertidal macrophyte *Spartina anglica*. Oikos 118(2):260–268. https://doi.org/10.1111/j.1600-0706.2008.16892.x

Bouma TJ, Olenin S, Reise K, Ysebaert T (2009b) Ecosystem engineering and biodiversity in coastal sediments: Posing hypotheses. Helgol Mar Res 63(1):95–106. https://doi.org/10.1007/s10152-009-0146-y

Bouma TJ, van Duren LA, Temmerman S, Claverie T, Blanco-Garcia A, Ysebaert T, Herman PMJ (2007) Spatial flow and sedimentation patterns within patches of epibenthic structures: Combining field, flume and modelling experiments. Cont Shelf Res 27(8):1020–1045. https://doi.org/10.1016/j.csr.2005.12.019

Brand E, Lodder Q, Quataert E, Slinger J (2025) Sustainable coastline management - the cumulative effects of 30 years of nourishments in the Netherlands. Ocean Coast Manag 270:107895. https://doi.org/10.1016/j.ocecoaman.2025.107895

Brand E, Ramaekers G, Lodder Q (2022) Dutch experience with sand nourishments for dynamic coastline conservation – An operational overview. Ocean Coast Manag 217:106008. https://doi.org/10.1016/j.ocecoaman.2021.106008

Brückner MZM, Coco G, Kleinhans MG (2025) Modelling the adaptation of estuarine morphology to macrobenthic bioturbation and sea level rise. Estuar Coast Shelf Sci 313:109107. https://doi.org/10.1016/j.ecss.2024.109107

Brückner MZM, Schwarz C, Coco G, Baar A, Boechat Albernaz M, Kleinhans MG (2021) Benthic species as mud patrol - modelled effects of bioturbators and biofilms on large-scale estuarine mud and morphology. Earth Surf Process Landf 46(6):1128–1144. https://doi.org/10.1002/esp.5080

Bruno JF, Stachowicz JJ, Bertness MD (2003) Inclusion of facilitation into ecological theory. Trends Ecol Evol 18(3):119–125. https://doi.org/10.1016/S0169-5347(02)00045-9

Burnham KP, Anderson DR (2004) Multimodel inference: Understanding AIC and BIC in model selection. Sociol. Methods Res. 33:261–304

Buschbaum C, Shama LNS, Amorim FLL, Brand S, Broquard CMA, Camillini N, Cornelius A, Dolch T, Dummermuth A, Feldner J, Guignard MS, Habedank J, Hoffmann JJL, Horn S, Konyssova G, Koop-Jakobsen K, Lauerburg R, Mehler K, Odongo V, Petri M, Reents S, Rick JJ, Rubinetti S, Salahi M, Sander L, Sidorenko V, Spence-Jones HC, van Beusekom JEE, Waser AM, Wegner KM, Wiltshire KH (2024) Climate change impacts on a sedimentary coast—a regional synthesis from genes to ecosystems. Marine Biodiversity 54(4):1–33. https://doi.org/10.1007/s12526-024-01453-5

Cade BS, Noon BR (2003) A gentle introduction to quantile regression for ecologists. Front Ecol Environ 1(8):412–420. https://doi.org/10.1890/1540-9295(2003)001[0412:AGITQR]2.0.CO;2

Cade BS, Noon BR, Flather CH (2005) Quantile regression reveals hidden bias and uncertainty in habitat models. Ecology 86(3):786–800. https://doi.org/10.1890/04-0785

Cade BS, Terrell JW, Schroeder RL (1999) Estimating effects of limiting factors with regression quantiles. Ecology 80(1):311–323. https://doi.org/10.1890/0012-9658(1999)080[0311:EEOLFW]2.0.CO;2

Cadee GC (1976) Sediment reworking by Arenicola marina on tidal flats in the Dutch Wadden Sea. Netherlands Journal of Sea Research 10(4):440–460

Cadée GC (2001) Sediment Dynamics by Bioturbating Organisms. Springer, Berlin, Heidelberg, pp 127–148

Cammen LM (1982) Effect of particle size on organic content and microbial abundance within four marine sediments. Mar Ecol Prog Ser 9:273–280

Carey DA (1987) Sedimentological effects and palaeoecological implications of the tube-building polychaete Lanice conchilega Pallas. Sedimentology 34(1):49–66. https://doi.org/10.1111/j.1365-3091.1987.tb00559.x

Chauvel N, Raoux A, Weill P, Dezilleau L, Méar Y, Murat A, Poizot E, Foveau A, Desroy N, Thiébaut É, Dauvin J-C, Pezy J-P (2024) Sediment grain size and benthic community structure in the eastern English Channel: Species-dependent responses and environmental influence. Mar Pollut Bull 200:116042. https://doi.org/10.1016/j.marpolbul.2024.116042

Chen J, Liu J, Jiang C, Wu Z, Yao Z, Bian C (2024a) Incipient Motion of Single Shells under Currents in Flume Experiments. J Mar Sci Eng 12(5):820. https://doi.org/10.3390/jmse12050820

Chen J, Yao Z, He F, Jiang C, Jiang C, Wu Z, Deng B, Long Y, Bian C (2024b) Experimental study on the settling motion of coral grains in still water. J Fluid Mech 990:A15. https://doi.org/10.1017/jfm.2024.469

Cheng CH, Smit JC de, Fivash GS, Hulscher SJMH, Borsje BW, Soetaert K (2021) Sediment shell-content diminishes current-driven sand ripple development and migration. Earth Surface Dynamics (9):1335–1346

Cheng MCF, Ericson JA, Ragg NLC, Dunphy BJ, Zamora LN (2025) Mussels, *Perna canaliculus*, as biosensors for climate change: concurrent monitoring of heart rate, oxygen consumption and gaping behaviour under heat stress. N Z J Mar Freshwater Res. https://doi.org/10.1080/00288330.2025.2461757

Choi J, Van Beek R, Chamberlain EL, Reimann T, Smeenge H, Van Oorschot A, Wallinga J (2024) Luminescence dating approaches to reconstruct the formation of plaggic anthrosols. SOIL 10(2):567–586. https://doi.org/10.5194/soil-10-567-2024

Christianen MJA, Middelburg JJ, Holthuijsen SJ, Jouta J, Compton TJ, van der Heide T, Piersma T, Sinninghe Damsté JS, van der Veer HW, Schouten S, Olff H (2017) Benthic primary producers are key to sustain the Wadden Sea food web: stable carbon isotope analysis at landscape scale. Ecology 98(6):1498–1512. https://doi.org/10.1002/ecy.1837

Colarossi D, Duller GAT, Roberts HM, Tooth S, Lyons R (2015) Comparison of paired quartz OSL and feldspar post-IR IRSL dose distributions in poorly bleached fluvial sediments from South Africa. Quat Geochronol 30:233–238. https://doi.org/10.1016/j.quageo.2015.02.015

Colina Alonso A, van Maren DS, Herman PMJ, van Weerdenburg RJA, Huismans Y, Holthuijsen SJ, Govers LL, Bijleveld AI, Wang ZB (2022) The Existence and Origin of Multiple Equilibria in Sand-Mud Sediment Beds. Geophys Res Lett 49(22). https://doi.org/10.1029/2022GL101141

Colina Alonso A, van Maren DS, Oost AP, Esselink P, Lepper R, Kösters F, Bartholdy J, Bijleveld AI, Wang ZB (2024) A mud budget of the Wadden Sea and its implications for sediment management. Commun Earth Environ 5(1):1–9. https://doi.org/10.1038/s43247-024-01315-9

Colosimo I, van Maren DS, de Vet PLM, Winterwerp JC, van Prooijen BC (2023) Winds of opportunity: The effects of wind on intertidal flat accretion. Geomorphology 439:108840. https://doi.org/10.1016/j.geomorph.2023.108840

Compton TJ, Holthuijsen S, Koolhaas A, Dekinga A, Smith J, Galama Y, Brugge M, Wal D Van Der, Meer J Van Der (2013) Distinctly variable mudscapes: Distribution gradients of intertidal macrofauna across the Dutch Wadden Sea. J Sea Res 82:103–116. https://doi.org/10.1016/j.seares.2013.02.002

Cozzoli F, Bouma TJ, Ysebaert T, Herman PMJ (2013) Application of non-linear quantile regression to macrozoobenthic species distribution modelling: Comparing two contrasting basins. Mar Ecol Prog Ser 475:119–133. https://doi.org/10.3354/meps10112

Cozzoli F, Eelkema M, Bouma TJ, Ysebaert T, Escaravage V, Herman PMJ (2014) A mixed modeling approach to predict the effect of environmental modification on species distributions. PLoS One 9(2):15–17. https://doi.org/10.1371/journal.pone.0089131

Cozzoli F, Shokri M, da Conceição TG, Herman PMJ, Hu Z, Soissons LM, Van Dalen J, Ysebaert T, Bouma TJ (2021) Modelling spatial and temporal patterns in bioturbator effects on sediment resuspension: A biophysical metabolic approach. Science of The Total Environment 792:148215. https://doi.org/10.1016/j.scitotenv.2021.148215

Cozzoli F, Smolders S, Eelkema M, Ysebaert T, Escaravage V, Temmerman S, Meire P, Herman PMJ, Bouma TJ (2017) A modeling approach to assess coastal management effects on benthic habitat quality: A case study on coastal defense and navigability. Estuar Coast Shelf Sci 184:67–82. https://doi.org/10.1016/j.ecss.2016.10.043

Croudace IW, Rindby A, Rothwell RG (2006) ITRAX: Description and evaluation of a new multi-function X-ray core scanner. Geol Soc Spec Publ 267:51–63. https://doi.org/10.1144/GSL.SP.2006.267.01.04

Cunningham AC, Buylaert JP, Murray AS (2022) Attenuation of beta radiation in granular matrices: implications for trapped-charge dating. Geochronology 4(2):517–531. https://doi.org/10.5194/gchron-4-517-2022

Cunningham AC, Wallinga J (2012) Realizing the potential of fluvial archives using robust OSL chronologies. Quat Geochronol 12:98–106. https://doi.org/10.1016/j.quageo.2012.05.007

Curran JC, Tan L (2014) Effect of Bed Sand Content on the Turbulent Flows Associated with Clusters on an Armored Gravel Bed Surface. Journal of Hydraulic Engineering 140(2):137–148. https://doi.org/10.1061/(asce)hy.1943-7900.0000810

Czaja R, Beal B, Pepperman K, Espinosa EP, Munroe D, Cerrato R, Busch E, Allam B (2023) Interactive roles of temperature and food availability in predicting habitat suitability for marine invertebrates. Estuar Coast Shelf Sci 293:108515. https://doi.org/10.1016/j.ecss.2023.108515

Dairain A, Maire O, Meynard G, Richard A, Rodolfo-Damiano T, Orvain F (2020) Sediment stability: can we disentangle the effect of bioturbating species on sediment erodibility from their impact on sediment roughness? Mar Environ Res 162. https://doi.org/10.1016/j.marenvres.2020.105147

Damveld JH, Borsje BW, Roos PC, Hulscher SJMH (2020) Biogeomorphology in the marine landscape: Modelling the feedbacks between patches of the polychaete worm *Lanice conchilega* and tidal sand waves. Earth Surf Process Landf 45(11):2572–2587. https://doi.org/10.1002/esp.4914

Dapples EC (1942) The effect of macro-organisms upon near-shore marine sediments. Journal of Sedimentary Research 12(3):118–126. https://doi.org/10.1306/d426916b-2b26-11d7-8648000102c1865d

Darwin C (1881) The formation of vegetable mould, through the action of worms, with observations on their habits

Davison C (1891) IV.—On the amount of sand brought up by Lobworms to the surface. Geol Mag 8(11):489–493. https://doi.org/10.1017/S0016756800187497

de Boer AM, Kook M, Wallinga J (2024a) Testing the performance of an EMCCD camera in measuring single-grain feldspar (thermo)luminescence in comparison to a laser-based single-grain system. Radiat Meas 175:107168. https://doi.org/10.1016/j.radmeas.2024.107168

de Boer AM, Pannozzo N, Pearson SG, Kooistra TJ, van Prooijen BC, Wallinga J (2026) Resetting of quartz and feldspar luminescence signals under water. Sci Rep. https://doi.org/https://doi.org/10.1038/s41598-026-44245-6

de Boer AM, Seebregts M, Wallinga J, Chamberlain E (2024b) A one-day experiment quantifying subaqueous bleaching of K-feldspar luminescence signals in the Wadden Sea, the Netherlands. Netherlands Journal of Geosciences 103:e22. https://doi.org/10.1017/njg.2024.18

de Boer PL (1998) Intertidal Sediments: Composition and Structure. In: Intertidal Deposits. CRC Press, pp 345–362

de Brouwer JFC, Bjelic S, De Deckere EMGT, Stal LJ (2000) Interplay between biology and sedimentology in a mudflat (Biezelingse Ham, Westerschelde, The Netherlands). Cont Shelf Res 20(10–11):1159–1177. https://doi.org/10.1016/S0278-4343(00)00017-0

de Fouw J, van Horssen PW, Craeymeersch J, Leopold MF, Perdon J, Troost K, Tulp I, van Zwol J, Philippart CJM (2024) Spatio-temporal analysis of potential factors explaining fluctuations in population size of Spisula subtruncata in the Dutch North Sea. Front Mar Sci 11:1476223. https://doi.org/10.3389/fmars.2024.1476223

de Jong MF, Baptist MJ, Lindeboom HJ, Hoekstra P (2015) Relationships between macrozoobenthos and habitat characteristics in an intensively used area of the Dutch coastal zone. ICES Journal of Marine Science 72(8):2409–2422. https://doi.org/10.1093/icesjms/fsv060

de la Barra P, Aarts G, Bijleveld A (2023) The effects of gas extraction under intertidal mudflats on sediment and macrozoobenthic communities. Journal of Applied Ecology. https://doi.org/10.1111/1365-2664.14530

de Schipper MA, Ludka BC, Raubenheimer B, Luijendijk AP, Schlacher TA (2021) Beach nourishment has complex implications for the future of sandy shores. Nat Rev Earth Environ 2(1):70–84. https://doi.org/10.1038/s43017-020-00109-9

de Smit JC, Brückner MZM, Mesdag KI, Kleinhans MG, Bouma TJ (2021) Key Bioturbator Species Within Benthic Communities Determine Sediment Resuspension Thresholds. Front Mar Sci 8(October):1–11. https://doi.org/10.3389/fmars.2021.726238

de Stigter HC, Jesus CC, Boer W, Richter TO, Costa A, van Weering TCE (2011) Recent sediment transport and deposition in the Lisbon-Setúbal and Cascais submarine canyons, Portuguese continental margin. Deep Sea Res 2 Top Stud Oceanogr 58(23–24):2321–2344. https://doi.org/10.1016/j.dsr2.2011.04.001

de Vet PLM, van Prooijen BC, Colosimo I, Steiner N, Ysebaert T, Herman PMJ, Wang ZB (2020) Variations in storm-induced bed level dynamics across intertidal flats. Sci Rep 10(1):1–15. https://doi.org/10.1038/s41598-020-69444-7

de Vet PLM, van Prooijen BC, Schrijvershof RA, van der Werf JJ, Ysebaert T, Schrijver MC, Wang ZB (2018) The Importance of Combined Tidal and Meteorological Forces for the Flow and Sediment Transport on Intertidal Shoals. J Geophys Res Earth Surf 123(10):2464–2480. https://doi.org/10.1029/2018JF004605

Dekker R, Beukema JJ (2012) Long-term dynamics and productivity of a successful invader: The first three decades of the bivalve Ensis directus in the western Wadden Sea. J Sea Res 71:31–40. https://doi.org/10.1016/j.seares.2012.04.004

Deloffre J, Verney R, Lafite R, Lesueur P, Lesourd S, Cundy AB (2007) Sedimentation on intertidal mudflats in the lower part of macrotidal estuaries: Sedimentation rhythms and their preservation. Mar Geol 241(1–4):19–32. https://doi.org/10.1016/j.margeo.2007.02.011

Dethier EN, Renshaw CE, Magilligan FJ (2022) Rapid changes to global river suspended sediment flux by humans. Science (1979) 376(6600):1447–1452. https://doi.org/10.1126/science.abn7980

Dey S (2003) Incipient Motion of Bivalve Shells on Sand Beds. J Eng Mech 129:232–240

Dickson J, Franken O, Watson MS, Monnich B, Holthuijsen S, Eriksson BK, Govers LL, van der Heide T, Bouma TJ (2023) Who lives in a pear tree under the sea? A first look at tree reefs as a complex natural biodegradable structure to enhance biodiversity in marine systems. Front Mar Sci 10:1213790. https://doi.org/10.3389/fmars.2023.1213790

Diedericks GPJ, Troch CNA, Smit GJF (2018) Incipient Motion of Shells and Shell Gravel. Journal of Hydraulic Engineering 144(3):06017030. https://doi.org/10.1061/(asce)hy.1943-7900.0001421

Dolch T, Hass HC (2008) Long-term changes of intertidal and subtidal sediment compositions in a tidal basin in the northern Wadden Sea (SE North Sea). Helgol Mar Res 62(1):3–11. https://doi.org/10.1007/s10152-007-0090-7

Domínguez R, Olabarria C, Woodin SA, Wethey DS, Peteiro LG, Macho G, Vázquez E (2021) Contrasting responsiveness of four ecologically and economically important bivalves to simulated heat waves. Mar Environ Res 164:105229. https://doi.org/10.1016/j.marenvres.2020.105229

Dorgan KM (2015) The biomechanics of burrowing and boring. Journal of Experimental Biology 218(2):176–183. https://doi.org/10.1242/JEB.086983

Douglas EJ, Lam-Gordillo O, Hailes SF, Lohrer AM, Cummings VJ (2024) Characterising intertidal sediment temperature gradients in estuarine systems. Estuar Coast Shelf Sci 309:108968. https://doi.org/10.1016/j.ecss.2024.108968

Elias EPL (2021) Morfologische analyse buitendelta Ameland en de rol van de pilotsuppletie | Deltares. Delft

Elias EPL, Pearson SG, van der Spek AJF, Pluis S (2022) Understanding meso-scale processes at a mixed-energy tidal inlet: Ameland Inlet, the Netherlands – Implications for coastal maintenance. Ocean Coast Manag 222:106125. https://doi.org/10.1016/j.ocecoaman.2022.106125

Elias EPL, Van Der Spek AJF, Wang ZB, De Ronde J (2012) Morphodynamic development and sediment budget of the Dutch Wadden Sea over the last century. Geologie en Mijnbouw/Netherlands Journal of Geosciences 91(3):293–310. https://doi.org/10.1017/S0016774600000457

Eriksson BK, van der Heide T, van de Koppel J, Piersma T, van der Veer HW, Olff H (2010) Major changes in the ecology of the wadden sea: Human impacts, ecosystem engineering and sediment dynamics. Ecosystems 13(5):752–764. https://doi.org/10.1007/s10021-010-9352-3

Eriksson BK, Westra J, van Gerwen I, Weerman E, van der Zee E, van der Heide T, van de Koppel J, Olff H, Piersma T, Donadi S (2017) Facilitation by ecosystem engineers enhances nutrient effects in an intertidal system. Ecosphere 8(12):e02051. https://doi.org/10.1002/ecs2.2051

Escaravage V (2022) Effecten van de zandsuppletie in het Amelander Zeegat op de bodemdieren-gemeenschappen 1 en 3 jaar na aanleg

Escaravage V, van Donk S, de Vet PLM, Vermeer N, de Bakker A, van der Werf J, van Belzen J (2024) Roggenplaatsuppletie (Oosterschelde): morfologische en ecologische ontwikkelingen over de eerste drie jaren (2020T1 - 2021T2 - 2022T3) na aanleg. Yerseke

Evans J, Murphy M (2023) spatialEco

Fan D, Guo Y, Wang P, Shi JZ (2006) Cross-shore variations in morphodynamic processes of an open-coast mudflat in the Changjiang Delta, China: With an emphasis on storm impacts. Cont Shelf Res 26(4):517–538. https://doi.org/10.1016/j.csr.2005.12.011

Fick C (2020) Threshold of motion of bivalve and gastropod shells under oscillatory flow in flume experiments. Sedimentology 67:627–648. https://doi.org/10.1111/sed.12657

Fick C, Favoreto J, Borghi L, Puhl E, Toldo EE, Neves FAPS, Schenk C V., Silva FRS, Vargas VML (2025) Sedimentological and biofabric patterns for hybrid coquina deposits: Insights from wave tank experiments. Sedimentology. https://doi.org/10.1111/sed.70028

Fitch JE, Crowe TP (2011) Combined effects of temperature, inorganic nutrients and organic matter on ecosystem processes in intertidal sediments. J Exp Mar Biol Ecol 400(1–2):257–263. https://doi.org/10.1016/j.jembe.2011.02.005

Floor JR, van Koppen CSA (Kris), van Tatenhove JPM (2018) Science, uncertainty and changing storylines in nature restoration: The case of seagrass restoration in the Dutch Wadden Sea. Ocean Coast Manag 157:227–236. https://doi.org/10.1016/j.ocecoaman.2018.02.016

Fokker PA, Van Leijen FJ, Orlic B, Van Der Marel H, Hanssen RF (2018) Subsidence in the Dutch Wadden Sea. Geologie en Mijnbouw/Netherlands Journal of Geosciences 97(3):129–181. https://doi.org/10.1017/njg.2018.9

Folmer EO, Bijleveld AI, Holthuijsen S, van der Meer J, Piersma T, van der Veer HW (2023) Space-time analyses of sediment composition reveals synchronized dynamics at all intertidal flats in the Dutch Wadden Sea. Estuar Coast Shelf Sci 285:108308. https://doi.org/10.1016/j.ecss.2023.108308

Foster-Smith RL (1978) An analysis of water flow in tube-living animals. J Exp Mar Biol Ecol 34(1):73–95. https://doi.org/10.1016/0022-0981(78)90058-8

Fouet MPA, Baudot L, Romero-Ramirez A, Massé C, Blanchet H, Bernard G, Maire O (2026) Impact of combined atmospheric and marine heatwaves on the filtration activity of the invasive Asian date mussel, *Arcuatula senhousia*. Estuar Coast Shelf Sci 332:109767. https://doi.org/10.1016/j.ecss.2026.109767

François F, Poggiale JC, Durbec JP, Stora G (1997) A new approach for the modelling of sediment reworking induced by a macrobenthic community. Acta Biotheor 45(3–4):295–319. https://doi.org/10.1023/a:1000636109604

Franken O, Holthuijsen SJ, Meijer KJ, Kleine Schaars L, Rasch B, Kooijman J, van Weerlee E, Miguel S, Koolhaas A, Mosk D, Dijkstra A, Greeve Y, van Walraven L, Witte S, Rehlmeyer K, Dickson J, Smeele Q, Bijleveld AI, Olff H, van der Heide T, Govers L (2025) Below Murky Waters: Subtidal Benthic Species and Sediment Distributions in the Dutch Wadden Sea

Friedrichs M, Graf G, Springer B (2000) Skimming flow induced over a simulated polychaete tube lawn at low population densities. Mar Ecol Prog Ser 192:219–228. https://doi.org/10.3354/meps192219

Friedrichs M, Leipe T, Peine F, Graf G (2009) Impact of macrozoobenthic structures on near-bed sediment fluxes. Journal of Marine Systems 75(3–4):336–347. https://doi.org/10.1016/J.JMARSYS.2006.12.006

Frithsen JB, Doering PH (1986) Active enhancement of particle removal from the water column by tentaculate benthic polychaetes. Ophelia 25(3):169–182. https://doi.org/10.1080/00785326.1986.10429748

Frölicher TL, Fischer EM, Gruber N (2018) Marine heatwaves under global warming. Nature 560(7718):360–364. https://doi.org/10.1038/s41586-018-0383-9

Galbraith RF, Roberts RG, Laslett GM, Yoshida H, Olley JM (1999) Optical dating of single and multiple grains of quartz form Jinmium Rock Shelter, Northern Australia: Part I, experimental design and statistical models. Archaeometry 41(2):339–364. https://doi.org/10.1111/j.1475-4754.1999.tb00987.x

Galic N, Sullivan LL, Grimm V, Forbes VE (2018) When things don't add up: quantifying impacts of multiple stressors from individual metabolism to ecosystem processing. Ecol. Lett. 21:568–577

Gao S (2018) Geomorphology and sedimentology of tidal flats. In: Coastal Wetlands: An Integrated Ecosystem Approach. Elsevier, pp 359–381

Gebhardt C, Forster S (2018) Size-selective feeding of Arenicola marina promotes long-term burial of microplastic particles in marine sediments. Environmental Pollution 242:1777–1786. https://doi.org/10.1016/j.envpol.2018.07.090

Gerino M, Aller RC, Lee C, Cochran JK, Aller JY, Green MA, Hirschberg D (1998) Comparison of different tracers and methods used to quantify bioturbation during a spring bloom: 234-thorium, luminophores and chlorophyll a. Estuar Coast Shelf Sci 46(4):531–547. https://doi.org/10.1006/ecss.1997.0298

Godfrey-Smith DI, Huntley DJ, Chen WH (1988) Optical dating studies of quartz and feldspar sediment extracts. Quat Sci Rev 7(3–4):373–380. https://doi.org/10.1016/0277-3791(88)90032-7

Grandjean TJ, de Smit JC, van Belzen J, Fivash GS, van Dalen J, Ysebaert T, Bouma TJ (2023) Morphodynamic signatures derived from daily surface elevation dynamics can explain the morphodynamic development of tidal flats. Water Science and Engineering 16(1):14–25. https://doi.org/10.1016/j.wse.2022.11.003

Gray J, Elliott M (2009) Ecology of marine sediments: from science to management

Gray JS (1974) Animal-sediment relationships. Oceanogr Mar Biol Ann Rev 12:223–261

Guevara O, Guan L, Salinas JS, Zgheib N, Balachandar S (2024) Sediment transport on rippled beds. Physics of Fluids 36(11). https://doi.org/10.1063/5.0236116

Gusmao JB, Thieltges D, Dekker R, Govers L (2022) Comparing taxonomic and functional trait diversity in marine macrozoobenthos along sediment texture gradients. Ecol Indic 145(109718). https://doi.org/10.1016/j.ecolind.2022.109718

Gutiérrez JL, Iribarne O (1999) Role of Holocene beds of the stout razor clam Tagelus plebeius in structuring present benthic communities. Mar Ecol Prog Ser 185:213–228. https://doi.org/10.3354/meps185213

Gutiérrez JL, Jones CG, Strayer DL, Iribarne OO (2003) Mollusks as ecosystem engineers: the role of shell production in aquatic habitats. OIKOS (101):79–90

Guyard H, Chapron E, St-Onge G, Anselmetti FS, Arnaud F, Magand O, Francus P, Mélières MA (2007) High-altitude varve records of abrupt environmental changes and mining activity over the last 4000 years in the Western French Alps (Lake Bramant, Grandes Rousses Massif). Quat Sci Rev 26(19–21):2644–2660. https://doi.org/10.1016/j.quascirev.2007.07.007

Guyez A, Bonnet S, Reimann T, Carretier S, Wallinga J (2023) A Novel Approach to Quantify Sediment Transfer and Storage in Rivers—Testing Feldspar Single-Grain pIRIR Analysis and Numerical Simulations. J Geophys Res Earth Surf 128(2):e2022JF006727. https://doi.org/10.1029/2022JF006727

Haasnoot M, Kwadijk J, Van Alphen J, Le Bars D, Van Den Hurk B, Diermanse F, Van Der Spek A, Oude Essink G, Delsman J, Mens M (2020) Adaptation to uncertain sea-level rise; how uncertainty in Antarctic mass-loss impacts the coastal adaptation strategy of the Netherlands. Environmental Research Letters 15(3):034007. https://doi.org/10.1088/1748-9326/ab666c

Haasnoot M, Lawrence J, Magnan AK (2021) Pathways to coastal retreat. Science (1979) 372(6548):1287–1290. https://doi.org/10.1126/science.abi6594

Harris RJ, Pilditch CA, Hewitt JE, Lohrer AM, Van Colen C, Townsend M, Thrush SF (2015) Biotic interactions influence sediment erodibility on wave-exposed sandflats. Mar Ecol Prog Ser 523:15–30. https://doi.org/10.3354/meps11164

He G, Peng Y, Liu X, Liu Y, Liang J, Xu X, Yang K, Masanja F, Xu Y, Deng Y, Zhao L (2022a) Post-responses of intertidal bivalves to recurrent heatwaves. Mar Pollut Bull 184:114223. https://doi.org/10.1016/j.marpolbul.2022.114223

He G, Zou J, Liu X, Liang F, Liang J, Yang K, Masanja F, Xu Y, Zheng Z, Deng Y, Zhao L (2022b) Assessing the impact of atmospheric heatwaves on intertidal clams. Science of the Total Environment 841:156744. https://doi.org/10.1016/j.scitotenv.2022.156744

He Q, Silliman BR (2019) Climate Change, Human Impacts, and Coastal Ecosystems in the Anthropocene. Current Biology 29:R1021–R1035

Heimsath AM, Chappell J, Spooner NA, Questiaux DG (2002) Creeping soil. Geology 30(2):111–114. https://doi.org/10.1130/0091-7613(2002)030<0111:CS>2.0.CO;2

Helmuth B, Harley CDG, Halpin PM, O'Donnell M, Hofmann GE, Blanchette CA (2002) Climate change and latitudinal patterns of intertidal thermal stress. Science (1979) 298(5595):1015–1017. https://doi.org/10.1126/science.1076814

Hendriks IE, Bouma TJ, Morris EP, Duarte CM (2010) Effects of seagrasses and algae of the Caulerpa family on hydrodynamics and particle-trapping rates. Mar Biol 157(3):473–481. https://doi.org/10.1007/s00227-009-1333-8

Hendriks IE, Sintes T, Bouma T, Duarte C (2008) Experimental assessment and modeling evaluation of the effects of the seagrass Posidonia oceanica on flow and particle trapping. Mar Ecol Prog Ser 356:163–173. https://doi.org/10.3354/meps07316

Herman PMJ, Middelburg JJ, Heip CHR (2001) Benthic community structure and sediment processes on an intertidal flat: Results from the ECOFLAT project. Cont Shelf Res 21(18–19):2055–2071. https://doi.org/10.1016/S0278-4343(01)00042-5

Herman PMJ, Middelburg JJ, van de Koppel J, Heip CHR (1999) Ecology of Estuarine Macrobenthos. Academic Press Inc.

Herringshaw LG, Sherwood OA, McIlroy D (2010) Ecosystem engineering by bioturbating polychaetes in event bed microcosms. Palaios 25(1):46–58. https://doi.org/10.2110/palo.2009.p09-055r

Hesketh A V., Harley CDG (2023) Extreme heatwave drives topography-dependent patterns of mortality in a bed-forming intertidal barnacle, with implications for associated community structure. Glob Chang Biol 29(1):165–178. https://doi.org/10.1111/gcb.16390

Hewitt JE, Ellis JI, Thrush SF (2016) Multiple stressors, nonlinear effects and the implications of climate change impacts on marine coastal ecosystems. Glob Chang Biol 22(8):2665–2675. https://doi.org/10.1111/gcb.13176

Hijmans RJ (2020) terra: Spatial Data Analysis. CRAN: Contributed Packages

Hoffmann TK, Pfennings K, Hitzegrad J, Paul M, Wehrmann A, Goseberg N, Schlurmann T (2025) Sediment accumulation by coastal biogenic structures sustains intertidal flats facing sea level rise in the German Wadden sea. Sci Rep 15(1):1–15. https://doi.org/10.1038/s41598-025-03326-8

Holzhauer H, Borsje BW, van Dalfsen JA, Wijnberg KM, Hulscher SJMH, Herman PMJ (2020) Benthic species distribution linked to morphological features of a barred coast. J Mar Sci Eng 8(1). https://doi.org/10.3390/JMSE8010016

Hu Z, van der Wal D, Cai H, van Belzen J, Bouma TJ (2018) Dynamic equilibrium behaviour observed on two contrasting tidal flats from daily monitoring of bed-level changes. Geomorphology 311:114–126. https://doi.org/10.1016/j.geomorph.2018.03.025

Hubert J, Moens R, Witbaard R, Slabbekoorn H (2022) Acoustic disturbance in blue mussels: sound-induced valve closure varies with pulse train speed but does not affect phytoplankton clearance rate. ICES Journal of Marine Science 79(9):2540–2551. https://doi.org/10.1093/icesjms/fsac193

Huettel M, Berg P, Kostka JE (2014) Benthic exchange and biogeochemical cycling in permeable sediments. Ann Rev Mar Sci 6:23–51. https://doi.org/10.1146/annurev-marine-051413-012706

Hughes RN (1970) An energy budget for a tidal-flat population of the bivalve *Scrobicularia plana* (Da Costa). Source: Journal of Animal Ecology 39(2):357–381

Hughes RN (1969) A study of feeding in *Scrobicularia plana*. Journal of the Marine Biological Association of the United Kingdom 49(3):805–823. https://doi.org/10.1017/S0025315400037309

Huisman BJA, Ruessink BG, de Schipper MA, Luijendijk AP, Stive MJF (2018) Modelling of bed sediment composition changes at the lower shoreface of the Sand Motor. Coastal Engineering 132:33–49. https://doi.org/10.1016/j.coastaleng.2017.11.007

Hunziker RP, Jaeggi MNR (2002) Grain Sorting Processes. Journal of Hydraulic Engineering 128(12):1060–1068. https://doi.org/10.1061/(asce)0733-9429(2002)128:12(1060)

Hurvich CM, Tsai C-L (1990) The Impact of Model Selection on Inference in Linear Regression. Am Stat 44(3):214. https://doi.org/10.2307/2685338

Hutchinson GE (1957) Concluding Remarks. Cold Spring Harb Symp Quant Biol 22(0):415–427. https://doi.org/10.1101/sqb.1957.022.01.039

IPCC (2023) Climate Change 2023. Synthesis Report. Contribution of Working Groups I, II and III to the Sixth Assessment Report of the Intergovernmental Panel on Climate Change. Geneva, Switzerland

Islam N, Garcia da Fonseca T, Vilke J, Gonçalves JM, Pedro P, Keiter S, Cunha SC, Fernandes JO, Bebianno MJ (2021) Perfluorooctane sulfonic acid (PFOS) adsorbed to polyethylene microplastics: Accumulation and ecotoxicological effects in the clam *Scrobicularia plana*. Mar Environ Res 164:105249. https://doi.org/10.1016/j.marenvres.2020.105249

Joensuu M, Pilditch CA, Harris R, Hietanen S, Pettersson H, Norkko A (2018) Sediment properties, biota, and local habitat structure explain variation in the erodibility of coastal sediments. Limnol Oceanogr 63(1):173–186. https://doi.org/10.1002/lno.10622

Johnson EH (2020) Experimental tests of bivalve shell shape reveal potential tradeoffs between mechanical and behavioral defenses. Sci Rep 10(1):1–12. https://doi.org/10.1038/s41598-020-76358-x

Johnson RG (1965) Temperature variation in the infaunal environment of a sand flat. Limnol Oceanogr 10(1):114–120. https://doi.org/10.4319/lo.1965.10.1.0114

Jonsson PR, Van Duren LA, Amielh M, Asmus R, Aspden RJ, Daunys D, Friedrichs M, Friend PL, Olivier F, Pope N, Precht E, Sauriau PG, Schaaff E (2006) Making water flow: A comparison of the hydrodynamic characteristics of 12 different benthic biological flumes. Aquat Ecol 40(4):409–438. https://doi.org/10.1007/s10452-006-9049-z

Jordan C, Tiede J, Lojek O, Visscher J, Apel H, Nguyen HQ, Quang CNX, Schlurmann T (2019) Sand mining in the Mekong Delta revisited - current scales of local sediment deficits. Sci Rep 9(1):1–14. https://doi.org/10.1038/s41598-019-53804-z

Jørgensen C, Larsen P, Møhlenberg F, Riisgård H (1988) The mussel pump: properties and modeling. Mar Ecol Prog Ser 45:205–216. https://doi.org/10.3354/meps045205

Jumars PA, Dorgan KM, Lindsay SM (2015) Diet of worms emended: An update of polychaete feeding guilds. Ann Rev Mar Sci 7:497–520. https://doi.org/10.1146/annurev-marine-010814-020007

Jumars PA, Nowell ARM (1984) Effects of benthos on sediment transport: difficulties with functional grouping. Cont Shelf Res 3(2):115–130. https://doi.org/10.1016/0278-4343(84)90002-5

Jumars PA, Self RF l., Nowell ARM (1982) Mechanics of particle selection by tentaculate deposit-feeders. J Exp Mar Biol Ecol 64(1):47–70. https://doi.org/10.1016/0022-0981(82)90067-3

Jung AS, van der Veer HW, van der Meer MTJ, Philippart CJM (2019) Seasonal variation in the diet of estuarine bivalves. PLoS One 14(6):e0217003. https://doi.org/10.1371/journal.pone.0217003

Kabat P, Bazelmans J, van Dijk J, Herman PMJ, van Oijen T, Pejrup M, Reise K, Speelman H, Wolff WJ (2012) The Wadden Sea Region: Towards a science for sustainable development. Ocean Coast Manag 68:4–17. https://doi.org/10.1016/j.ocecoaman.2012.05.022

Kamphuis JW (2010) Determination of Sand Roughness for Fixed Beds. Journal of Hydraulic Research 12(2):193–203. https://doi.org/10.1080/00221687409499737

Kars RH, Busschers FS, Wallinga J (2012) Validating post IR-IRSL dating on K-feldspars through comparison with quartz OSL ages. Quat Geochronol 12:74–86. https://doi.org/10.1016/j.quageo.2012.05.001

Kerckhof F, Haelters J, Gollasch S (2007) Alien species in the marine and brackish ecosystem: the situation in Belgian waters. Aquat Invasions 2(3):243–257

Kidwell SM, Jablonski D (1983) Taphonomic Feedback Ecological Consequences of Shell Accumulation. In: Biotic interactions in Recent and fossil benthic communities. Springer, Boston, MA, pp 195–248

Kleinhans MG (2005) Flow discharge and sediment transport models for estimating a minimum timescale of hydrological activity and channel and delta formation on Mars. J Geophys Res Planets 110(E12):1–23. https://doi.org/10.1029/2005JE002521

Kleinhans MG, van Rijn LC (2002) Stochastic Prediction of Sediment Transport in Sand-Gravel Bed Rivers. Journal of Hydraulic Engineering 128(4):412–425. https://doi.org/10.1061/(asce)0733-9429(2002)128:4(412)

Kloepper S, Bostelmann A, Bregnballe T, Busch JA, Buschbaum C, Deen K, Domnick A, Gutow L, Jensen K, Jepsen N, Luna S, Meise K, Teilmann J, Wezel A van (2022) Wadden Sea Quality Status Reports 2022

Kodama K, Waku M, Sone R, Miyawaki D, Ishida T, Akatsuka T, Horiguchi T (2018) Ontogenetic and temperature-dependent changes in tolerance to hypoxia and hydrogen sulfide during the early life stages of the Manila clam *Ruditapes philippinarum*. Mar Environ Res 137:177–187. https://doi.org/10.1016/j.marenvres.2017.12.019

Koenker R (2024) quantreg: Quantile regression. cir.nii.ac.jp

Koenker R, Bassett G (1978) Regression Quantiles. Econometrica 46(1):33. https://doi.org/10.2307/1913643

Koenker R, Ng P, Portnoy S (1994) Quantile Smoothing Splines. Biometrika 81(4):673. https://doi.org/10.2307/2337070

Kooistra TJ, de Boer A-M, Bouma TJ, Pannozzo N, Pearson SG, van der Spek A, de Stigter H, Wallinga J, Witbaard R, Soetaert K (2026) Worms and storms: shedding light on bioturbation and physical mixing on an intertidal flat by combining multiple tracers [data and code]

Kooistra TJ, Haarbosch SH, Bosma JW, Bouma TJ, van Prooijen BC, Soetaert K, Pearson SG (2025a) How Shells of Different Shapes Affect Current-driven Sand Transport [data and code]

Kooistra TJ, Witbaard R, Bijleveld AI, van der Heide T, Franken O, Soetaert K (2025b) Coarsening coasts: quantifying sensitivity of benthic communities to sandification - data and code

Kooistra TJ, Witbaard R, Bouma TJ, Pearson SG, Bijleveld AI, van der Heide T, Franken O, Soetaert K (2025c) Coarsening coasts: quantifying sensitivity of benthic communities to sandification. Estuar Coast Shelf Sci 320:109303. https://doi.org/10.1016/j.ecss.2025.109303

Kook M, Lapp T, Murray AS, Thomsen KJ, Jain M (2015) A luminescence imaging system for the routine measurement of single-grain OSL dose distributions. Radiat Meas 81:171–177. https://doi.org/10.1016/j.radmeas.2015.02.010

Kraan C, Aarts G, Van Jaap Meer DER, Piersma T (2010) The role of environmental variables in structuring landscape-scale species distributions in seafloor habitats. Ecology 91(6):1583–1590. https://doi.org/10.1890/09-2040.1

Kreutzer S, Burow C, Dietze M, Fuchs MC, Schmidt C, Fischer M, Friedrich J, Mercier N, Smedley R, Christophe C, Zink A, Durcan JA, King GE, Philippe A, Guérin G, Riedesel S, Autzen M, Guibert P, Mittelstraß D, Gray HJ, Galharret JM, Fuchs M (2025) Luminescence 1.X: Comprehensive Luminescence Dating Data Analysis. https://doi.org/10.5281/ZENODO.596252

Kristensen E, Neto JM, Lundkvist M, Frederiksen L, Pardal MÂ, Valdemarsen T, Flindt MR (2013) Influence of benthic macroinvertebrates on the erodability of estuarine cohesive sediments: Density- and biomass-specific responses. Estuar Coast Shelf Sci 134:80–87. https://doi.org/10.1016/j.ecss.2013.09.020

Kristensen E, Penha-Lopes G, Delefosse M, Valdemarsen T, Quintana CO, Banta GT (2012) What is bioturbation? the need for a precise definition for fauna in aquatic sciences. Mar Ecol Prog Ser 446:285–302. https://doi.org/10.3354/meps09506

Kristensen JA, Thomsen KJ, Murray AS, Buylaert JP, Jain M, Breuning-Madsen H (2015) Quantification of termite bioturbation in a savannah ecosystem: Application of OSL dating. Quat Geochronol 30:334–341. https://doi.org/10.1016/j.quageo.2015.02.026

Krol J, Lodewijks J, Saathof L (2024) Sedimentatie metingen op het wad van Ameland, Paesens, Piet Scheveplaat, Engelsmanplaat en Schiermonnikoog. Nes

Kröncke I, Reiss H (2010) Influence of macrofauna long-term natural variability on benthic indices used in ecological quality assessment. Mar Pollut Bull 60(1):58–68. https://doi.org/10.1016/J.MARPOLBUL.2009.09.001

Kumagai T, Nakajima S (2012) Experimental Study on Bed Load Transport of Shell Fragment-Mixed Sand under Waves. The International Journal of Ocean and Climate Systems 3(2):85–96. https://doi.org/10.1260/1759-3131.3.2.85

Kuznetsova A, Brockhoff PB, Christensen RHB (2017) lmerTest Package: tests in linear mixed effects models. J Stat Softw 82(13):1–26. https://doi.org/10.18637/JSS.V082.I13

Laukaityte S, Bishop MJ, Govers LL, Eriksson BDHK (2025) Warming alters non-trophic interactions in soft bottom habitats. Oecologia 207(2):1–12. https://doi.org/10.1007/s00442-025-05662-y

Le Hir P, Monbet Y, Orvain F (2007) Sediment erodability in sediment transport modelling: Can we account for biota effects? Cont Shelf Res 27(8):1116–1142. https://doi.org/10.1016/j.csr.2005.11.016

Lecroart P, Maire O, Schmidt S, Grémare A, Anschutz P, Meysman FJR (2010) Bioturbation, short-lived radioisotopes, and the tracer-dependence of biodiffusion coefficients. Geochim Cosmochim Acta 74(21):6049–6063. https://doi.org/10.1016/j.gca.2010.06.010

Levin LA, Boesch DF, Covich A, Dahm C, Erséus C, Ewel KC, Kneib RT, Moldenke A, Palmer MA, Snelgrove P, Strayer D, Weslawski JM (2001) The Function of Marine Critical Transition Zones and the Importance of Sediment Biodiversity. Ecosystems 4:430–451

Li B, Cozzoli F, Soissons LM, Bouma TJ, Chen L (2017) Effects of bioturbation on the erodibility of cohesive versus non-cohesive sediments along a current-velocity gradient: A case study on cockles. J Exp Mar Biol Ecol 496(August):84–90. https://doi.org/10.1016/j.jembe.2017.08.002

Li B, Li SH (2011) Luminescence dating of K-feldspar from sediments: A protocol without anomalous fading correction. Quat Geochronol 6(5):468–479. https://doi.org/10.1016/j.quageo.2011.05.001

Li Y, Yu Q, Gao S, Flemming BW (2020) Settling velocity and drag coefficient of platy shell fragments. Sedimentology 67(4):2095–2110. https://doi.org/10.1111/sed.12696

Lindvall A, Stjern R, Alexanderson H (2017) Bleaching of quartz OSL signals under natural and laboratory light conditions. Ancient TL 35(2):12–20. https://doi.org/10.26034/la.atl.2017.514

Little WC, Mayer PG (1976) Stability of channel beds by armouring. Journal of the Hydraulics Division 102(11):1647–1661. https://doi.org/10.1061/jyceaj.0004651

Liu L, Wang H, Yang Z, Fan Y, Wu X, Hu L, Bi N (2022) Coarsening of sediments from the Huanghe (Yellow River) delta-coast and its environmental implications. Geomorphology 401:108105. https://doi.org/10.1016/j.geomorph.2021.108105

Liu Q, Polerecky L, Rios-Yunes D, Soetaert K (2025) Simulating the thermal response of tidal sediments by integrating numerical modeling and field measurements. J Geophys Res Oceans 130(10):e2025JC023263. https://doi.org/10.1029/2025JC023263

Lodder QJ, Slinger JH, Wang ZB, van der Spek AJF, Hijma MP, Taal M, van Gelder-Maas C, de Looff H, Litjens J, Schipper CA, Löffler M, Nolte AJ, van Oeveren C, van der Werf JJ, Grasmeijer BT, Elias EPL, Holzhauer H, Tonnon PK (2023) The Coastal Genesis 2 research programme: Outputs, Outcomes and Impact. Ocean Coast Manag 237:106499. https://doi.org/10.1016/j.ocecoaman.2023.106499

Lodder QJ, Wang ZB, Elias EPL, van der Spek AJF, de Looff H, Townend IH (2019) Future Response of the Wadden Sea Tidal Basins to Relative Sea-Level rise—An Aggregated Modelling Approach. Water 2019, Vol 11, Page 2198 11(10):2198. https://doi.org/10.3390/W11102198

Longbottom MR (1970) The distribution of Arenicola marina (L.) with particular reference to the effects of particle size and organic matter of the sediments. J Exp Mar Biol Ecol 5(2):138–157. https://doi.org/10.1016/0022-0981(70)90013-4

Lotze HK (2005) Radical changes in the Wadden Sea fauna and flora over the last 2,000 years. Helgol Mar Res 59(1):71–83. https://doi.org/10.1007/s10152-004-0208-0

Lotze HK, Lenihan HS, Bourque BJ, Bradbury RH, Cooke RG, Kay MC, Kidwell SM, Kirby MX, Peterson CH, Jackson JBC (2006) Depletion, Degradation, and Recovery Potential of Estuaries and Coastal Seas. Science (1979) 312(5781):1806–1809. https://doi.org/10.1126/science.1128035

Madsen AT, Murray AS (2009) Optically stimulated luminescence dating of young sediments: A review. Geomorphology 109(1–2):3–16. https://doi.org/10.1016/j.geomorph.2008.08.020

Madsen AT, Murray AS, Andersen TJ, Pejrup M (2007) Temporal changes of accretion rates on an estuarine salt marsh during the late Holocene - Reflection of local sea level changes? The Wadden Sea, Denmark. Mar Geol 242(4):221–233. https://doi.org/10.1016/j.margeo.2007.03.001

Madsen AT, Murray AS, Andersen TJ, Pejrup M, Breuning-Madsen H (2005) Optically stimulated luminescence dating of young estuarine sediments: A comparison with 210Pb and 137Cs dating. Mar Geol 214(1–3):251–268. https://doi.org/10.1016/j.margeo.2004.10.034

Madsen AT, Murray AS, Jain M, Andersen TJ, Pejrup M (2011) A new method for measuring bioturbation rates in sandy tidal flat sediments based on luminescence dating. Estuar Coast Shelf Sci 92(3):464–471. https://doi.org/10.1016/j.ecss.2011.02.004

Maire O, Lecroart P, Meysman FJR, Rosenberg R, Duchêne JC, Grémare A (2008) Quantification of sediment reworking rates in bioturbation research: A review. Aquat Biol 2(3):219–238. https://doi.org/10.3354/ab00053

Masanja F, Yang K, Xu Y, He G, Liu X, Xu X, Xiaoyan J, Xin L, Mkuye R, Deng Y, Zhao L (2023) Impacts of marine heat extremes on bivalves. Front Mar Sci 10:1159261. https://doi.org/10.3389/fmars.2023.1159261

Mauz B, Baeteman C, Bungenstock F, Plater AJ (2010) Optical dating of tidal sediments: Potentials and limits inferred from the North Sea coast. Quat Geochronol 5(6):667–678. https://doi.org/10.1016/j.quageo.2010.05.004

Mauz B, Bungenstock F (2007) How to reconstruct trends of late Holocene relative sea level: A new approach using tidal flat clastic sediments and optical dating. Mar Geol 237(3–4):225–237. https://doi.org/10.1016/j.margeo.2006.12.001

McCarron CJ, Van Landeghem KJJ, Baas JH, Amoudry LO, Malarkey J (2019) The hiding-exposure effect revisited: A method to calculate the mobility of bimodal sediment mixtures. Mar Geol 410:22–31. https://doi.org/10.1016/j.margeo.2018.12.001

McKenna Neuman C, Li B, Nash D (2012) Micro-topographic analysis of shell pavements formed by aeolian transport in a wind tunnel simulation. J Geophys Res Earth Surf 117(F4). https://doi.org/10.1029/2012JF002381

Meadows PS, Meadows A, Murray JMH (2012) Biological modifiers of marine benthic seascapes: Their role as ecosystem engineers. Geomorphology 157–158:31–48. https://doi.org/10.1016/j.geomorph.2011.07.007

Mehta AJ, Lee J, Christensen BA (1980) Fall velocity of shells as coastal sediment. Journal of the Hydraulics Division 106(11):1727–1744

Meijer KJ, Franken O, Witte S, Holthuijsen SJ, van der Heide T, Govers LL, Olff H (2025) Hotspots in peril: Misalignment of conservation efforts and ecological values in a shallow coastal sea. People and Nature 7(1):160–179. https://doi.org/10.1002/pan3.10757

Meyer-Peter E, Müller R (1948) Formulas for Bed-Load transport. In: Proceedings of the 2nd meeting of the International Association of Hydraulic Research. Stockholm, Sweden, pp 39–64

Meysman FJR, Boudreau B, Middelburg J (2010) When and why does bioturbation lead to diffusive mixing? J Mar Res 68(6):881–920

Meysman FJR, Boudreau B, Middelburg J (2003) Relations between local, nonlocal, discrete and continuous models of bioturbation. J Mar Res 61(3):391–410

Meysman FJR, Malyuga VS, Boudreau BP, Middelburg JJ (2008) A generalized stochastic approach to particle dispersal in soils and sediments. Geochim Cosmochim Acta 72(14):3460–3478. https://doi.org/10.1016/j.gca.2008.04.023

Meysman FJR, Middelburg JJ, Heip CHR (2006) Bioturbation: a fresh look at Darwin's last idea. Trends Ecol Evol 21(12):688–695. https://doi.org/10.1016/j.tree.2006.08.002

Miedema SA, Ramsdell RC (2011) Hydraulic transport of sand/shell mixtures in relation with the critical velocity. Terra et Aqua

Mielck F, Hass HC, Betzler C (2014) High-Resolution Hydroacoustic Seafloor Classification of Sandy Environments in the German Wadden Sea. J Coast Res 298(6):1107–1117. https://doi.org/10.2112/jcoastres-d-12-00165.1

Montgomery D, Peck E (1992) Introduction to linear regression analysis. Wiley, New York

Montserrat F, Suykerbuyk W, Al-Busaidi R, Bouma TJ, van der Wal D, Herman PMJ (2011) Effects of mud sedimentation on lugworm ecosystem engineering. J Sea Res 65(1):170–181. https://doi.org/10.1016/j.seares.2010.09.003

Montserrat F, Van Colen C, Provoost P, Milla M, Ponti M, Van den Meersche K, Ysebaert T, Herman PMJ (2009) Sediment segregation by biodiffusing bivalves. Estuar Coast Shelf Sci 83(4):379–391. https://doi.org/10.1016/j.ecss.2009.04.010

Morys C, Powilleit M, Forster S (2017) Bioturbation in relation to the depth distribution of macrozoobenthos in the southwestern Baltic Sea. Mar Ecol Prog Ser 579:19–36. https://doi.org/10.3354/meps12236

Murray JMH, Meadows A, Meadows PS (2002) Biogeomorphological implications of microscale interactions between sediment geotechnics and marine benthos: A review. Geomorphology 47(1):15–30. https://doi.org/10.1016/S0169-555X(02)00138-1

Nehmer P, Kröncke I (2003) Macrofaunal communities in the Wichter Ee, a channel system in the East Frisian Wadden Sea. Senckenbergiana Maritima 32(1–2):1–10. https://doi.org/10.1007/BF03043081

Nepf HM (2012) Hydrodynamics of vegetated channels. Journal of Hydraulic Research 50(3):262–279. https://doi.org/10.1080/00221686.2012.696559

Neumann B, Vafeidis AT, Zimmermann J, Nicholls RJ (2015) Future Coastal Population Growth and Exposure to Sea-Level Rise and Coastal Flooding - A Global Assessment. PLoS One 10(3):e0118571. https://doi.org/10.1371/journal.pone.0118571

Newell CR, Wildish DJ, MacDonald BA (2001) The effects of velocity and seston concentration on the exhalant siphon area, valve gape and filtration rate of the mussel *Mytilus edulis*. J Exp Mar Biol Ecol 262(1):91–111. https://doi.org/10.1016/S0022-0981(01)00285-4

Nowell ARM, Church M (1979) Turbulent flow in a depth-limited boundary layer. J Geophys Res Oceans 84(C8):4816–4824. https://doi.org/10.1029/JC084iC08p04816

Nowell ARM, Jumars PA (1984) Flow environments of aquatic benthos. Annual review of ecology and systematics Vol 15 :303–328. https://doi.org/10.1146/annurev.es.15.110184.001511

Oeschger R, Pedersen TF (1994) Influence of anoxia and hydrogen sulphide on the energy metabolism of *Scrobicularia plana* (da Costa) (Bivalvia). J Exp Mar Biol Ecol 184(2):255–268. https://doi.org/10.1016/0022-0981(94)90008-6

Oksanen J, Simpson GL, Blanchet FG, Kindt R, Legendre P, Minchin PR, O'Hara RB, Solymos P, Stevens MHH, Szoecs E, Wagner H, Barbour M, Bedward M, Bolker B, Borcard D, Carvalho G, Chirico M, De Caceres M, Durand S, Evangelista HBA, FitzJohn R, Friendly M, Furneaux B, Hannigan G, Hill MO, Lahti L, McGlinn D, Ouellette M-H, Ribeiro Cunha E, Smith T, Stier A, Ter Braak CJF, Weedon J (2024) vegan: Community Ecology Package. CRAN: Contributed Packages

Olabarria C, Gestoso I, Lima FP, Vázquez E, Comeau LA, Gomes F, Seabra R, Babarro JMF (2016) Response of two Mytilids to a heatwave: the complex interplay of physiology, behaviour and ecological interactions. PLoS One 11(10):e0164330. https://doi.org/10.1371/journal.pone.0164330

Oliver ECJ, Benthuysen JA, Darmaraki S, Donat MG, Hobday AJ, Holbrook NJ, Schlegel RW, Sen Gupta A (2021) Marine Heatwaves. Ann Rev Mar Sci 13(Volume 13, 2021):313–342. https://doi.org/10.1146/annurev-marine-032720-095144

Oppenheimer M, Glavovic B, Hinkel J, van de Wal R, Magnan AK, Abd-Elgawad A, Cai R, Cifuentes-Jara M, Deconto RM, Ghosh T, Hay J, Isla F, Marzeion B, Meyssignac B, Sebesvari Z (2019) Sea Level Rise and Implications for Low Lying Islands, Coasts and Communities

Ouellette D, Desrosiers G, Gagne J, Gilbert F, Poggiale J, Blier P, Stora G (2004) Effects of temperature on in vitro sediment reworking processes by a gallery biodiffusor, the polychaete Neanthes virens. Mar Ecol Prog Ser 266:185–193. https://doi.org/10.3354/meps266185

Pandit SN, Kolasa J, Cottenie K (2009) Contrasts between habitat generalists and specialists: An empirical extension to the basic metacommunity framework. Ecology 90(8):2253–2262. https://doi.org/10.1890/08-0851.1

Pannozzo N, Smedley RK, Plater AJ, Carnacina I, Leonardi N (2023) Novel luminescence diagnosis of storm deposition across intertidal environments. Science of the Total Environment 867:161461. https://doi.org/10.1016/j.scitotenv.2023.161461

Pansch C, Scotti M, Barboza FR, Al-Janabi B, Brakel J, Briski E, Bucholz B, Franz M, Ito M, Paiva F, Saha M, Sawall Y, Weinberger F, Wahl M (2018) Heat waves and their significance for a temperate benthic community: A near-natural experimental approach. Glob Chang Biol 24(9):4357–4367. https://doi.org/10.1111/gcb.14282

Parmesan C, Morecroft MD, Trisurat Y, Mezzi D, Langsdorf S, Löschke S, Möller V, Okem A, Officer S, Rama B, Belling D, Dieck W, Götze S, Kersher T, Mangele P, Maus B, Mühle A, Nabiyeva K, Nicolai M, Niebuhr A, Petzold J, Prentzler E, Savolainen J, Scheuffele H, Weisfeld S, Weyer N (2022) Climate Change 2022:Impacts, Adaptation and Vulnerability Working Group II Contribution to the Sixth Assessment Report of the Intergovernmental Panel on Climate Change

Passarelli C, Olivier F, Paterson DM, Meziane T, Hubas C (2014) Organisms as cooperative ecosystem engineers in intertidal flats. J. Sea Res. 92:92–101

Pearson SG, Elias EPL, Van Ormondt M, Roelvink FE, Lambregts PM, Wang Z, Van Prooijen BC (2021a) Lagrangian sediment transport modelling as a tool for investigating coastal connectivity. In: Proc., Coastal Dynamics Conf.

Pearson SG, van Prooijen BC, Elias EPL, Vitousek S, Wang ZB (2020) Sediment Connectivity: A Framework for Analyzing Coastal Sediment Transport Pathways. J Geophys Res Earth Surf 125(10):e2020JF005595. https://doi.org/10.1029/2020JF005595

Pearson SG, van Prooijen BC, Poleykett J, Wright M, Black K, Wang ZB (2021b) Tracking fluorescent and ferrimagnetic sediment tracers on an energetic ebb-tidal delta to monitor grain size-selective dispersal. Ocean Coast Manag 212:105835. https://doi.org/10.1016/j.ocecoaman.2021.105835

Perk L, van Rijn LC, Koudstaal K, Fordeyn J (2019) A Rational Method for the Design of Sand Dike/Dune Systems at Sheltered Sites; Wadden Sea Coast of Texel, The Netherlands. J Mar Sci Eng 7(9):324. https://doi.org/10.3390/jmse7090324

Peterson CH, Bishop MJ (2005) Assessing the environmental impacts of beach nourishment. Bioscience 55(10):887–896. https://doi.org/10.1641/0006-3568(2005)055[0887:ATEIOB]2.0.CO;2

Peterson CH, Bishop MJ, Anna LMD, Johnson GA (2014) Multi-year persistence of beach habitat degradation from nourishment using coarse shelly sediments. Science of the Total Environment, The 487:481–492. https://doi.org/10.1016/j.scitotenv.2014.04.046

Pickrill RA (1986) Sediment pathways and transport rates through a tide-dominated entrance, Rangaunu Harbour, New Zealand. Sedimentology 33(6):887–898. https://doi.org/10.1111/j.1365-3091.1986.tb00989.x

Piggott JJ, Townsend CR, Matthaei CD (2015) Reconceptualizing synergism and antagonism among multiple stressors. Ecol Evol 5(7):1538–1547. https://doi.org/10.1002/ece3.1465

Pilditch CA, Emerson CW, Grant J (1997) Effect of scallop shells and sediment grain size on phytoplankton flux to the bed. Cont Shelf Res 17(15):1869–1885. https://doi.org/10.1016/S0278-4343(97)00050-2

Pilditch CA, Grant J (1999) Effect of variations in flow velocity and phytoplankton concentration on sea scallop (*Placopecten magellanicus*) grazing rates. J Exp Mar Biol Ecol 240(1):111–136. https://doi.org/10.1016/S0022-0981(99)00052-0

Porat (2006) Use of magnetic separation for purifying quartz for luminescence dating. Ancient TL 24(2):33–36

Pratt DR, Lohrer AM, Pilditch CA, Thrush SF (2014) Changes in Ecosystem Function Across Sedimentary Gradients in Estuaries. Ecosystems 17(1):182–194. https://doi.org/10.1007/s10021-013-9716-6

Prescott JR, Fox PJ, Robertson GB, Hutton JT (1994) Three-dimensional spectral studies of the bleaching of the thermoluminescence of feldspars. Radiat Meas 23(2–3):367–375. https://doi.org/10.1016/1350-4487(94)90066-3

Queirós AM, Birchenough SNR, Bremner J, Godbold JA, Parker RE, Romero-Ramirez A, Reiss H, Solan M, Somerfield PJ, Van Colen C, Van Hoey G, Widdicombe S (2013) A bioturbation classification of European marine infaunal invertebrates. Ecol Evol 3(11):3958–3985. https://doi.org/10.1002/ECE3.769

Queirós AM, Stephens N, Cook R, Ravaglioli C, Nunes J, Dashfield S, Harris C, Tilstone GH, Fishwick J, Braeckman U, Somerfield PJ, Widdicombe S (2015) Can benthic community structure be used to predict the process of bioturbation in real ecosystems? Prog Oceanogr 137:559–569. https://doi.org/10.1016/j.pocean.2015.04.027

R Core Team (2024) R: A Language and Environment for Statistical Computing

Rabaut M, Guilini K, Hoey G Van, Vincx M, Degraer S (2007) A bio-engineered soft-bottom environment : The impact of Lanice conchilega on the benthic species-specific densities and community structure. 75. https://doi.org/10.1016/j.ecss.2007.05.041

Rademaker M, de la Barra P, van Leeuwen A, Bijleveld AI (2025) Benthic invertebrates in the Wadden Sea form a stable community characterized by facilitating relationships. Ecosphere 16(4):e70212. https://doi.org/10.1002/ecs2.70212

Ramsdell RC, Miedema SA, Talmon AM (2011) Hydraulic transport of sand/shell mixtures. In: Proceedings of the International Conference on Offshore Mechanics and Arctic Engineering - OMAE. American Society of Mechanical Engineers Digital Collection, pp 533–547

Ranasinghe R (2016) Assessing climate change impacts on open sandy coasts: A review. Earth Sci Rev 160:320–332. https://doi.org/https://doi.org/10.1016/j.earscirev.2016.07.011

Ranasinghe R, Duong TM, Uhlenbrook S, Roelvink D, Stive M (2013) Climate-change impact assessment for inlet-interrupted coastlines. Nat Clim Chang 3(1):83–87. https://doi.org/10.1038/nclimate1664

Raymond WW, Barber JS, Dethier MN, Hayford HA, Harley CDG, King TL, Paul B, Speck CA, Tobin ED, Raymond AET, McDonald PS (2022) Assessment of the impacts of an unprecedented heatwave on intertidal shellfish of the Salish Sea. Ecology 103(10):e3798. https://doi.org/10.1002/ecy.3798

Reimann T, Román-Sánchez A, Vanwalleghem T, Wallinga J (2017) Getting a grip on soil reworking – Single-grain feldspar luminescence as a novel tool to quantify soil reworking rates. Quat Geochronol 42:1–14. https://doi.org/10.1016/j.quageo.2017.07.002

Reise K (2002) Sediment mediated species interactions in coastal waters. J Sea Res 48(2):127–141. https://doi.org/10.1016/S1385-1101(02)00150-8

Reise K, Baptist M, Burbridge P, Dankers N, Fischer L, Flemming B, Oost AP, Smit C (2010) The Wadden Sea-a universally outstanding tidal wetland. Wilhelmshaven, Germany

Reiss H, Kröncke I (2001) Spatial and temporal distribution of macrofauna in the Otzumer Balje (East Frisian Wadden Sea, Germany). Senckenbergiana Maritima 31(2):283–298. https://doi.org/10.1007/BF03043037

Reiss H, Kröncke I (2005) Seasonal variability of benthic indices: An approach to test the applicability of different indices for ecosystem quality assessment. Mar Pollut Bull 50(12):1490–1499. https://doi.org/10.1016/J.MARPOLBUL.2005.06.017

Rhoads DC, Boyer LF (1982) The Effects of Marine Benthos on Physical Properties of Sediments. Springer, Boston, MA, pp 3–52

Rhoads DC, Stanley DJ (1965) Biogenic Graded Bedding. SEPM Journal of Sedimentary Research Vol. 35(4):956–963. https://doi.org/10.1306/74d713bb-2b21-11d7-8648000102c1865d

Rhoads DC, Young DK (1970) The influence of deposit-feeding organisms on sediment stability and community trophic structure. J Mar Res 78(3):169–195. https://doi.org/10.1357/002224020834162167

Rhodes EJ (2011) Optically stimulated luminescence dating of sediments over the past 200,000 years. Annu Rev Earth Planet Sci 39(Volume 39, 2011):461–488. https://doi.org/10.1146/annurev-earth-040610-133425

Ribberink JS (1998) Bed-load transport for steady flows and unsteady oscillatory flows. Coastal Engineering 34(1–2):59–82. https://doi.org/10.1016/S0378-3839(98)00013-1

Richmond CE, Breitburg DL, Rose KA (2005) The role of environmental generalist species in ecosystem function. Ecol Modell 188(2–4):279–295. https://doi.org/10.1016/j.ecolmodel.2005.03.002

Richter R (1952) Fluidal-Textur in Sediment-Gesteinen und über Sedifluktion überhaupt. Notizbl Hess Landesamtes Bodenforsch Wiesb 6:67–81

Richter TO, Van Der Gaast S, Koster B, Vaars A, Gieles R, De Stigter HC, De Haas H, Van Weering TCE (1996) Modeling 210Pb-derived mixing activity in ocean margin sediments: Diffusive versus nonlocal mixing. J Mar Res 54(6):1207–1227. https://doi.org/10.1357/0022240963213808

Richter TO, Van Der Gaast S, Koster B, Vaars A, Gieles R, De Stigter HC, De Haas H, Van Weering TCE (2006) The Avaatech XRF Core Scanner: Technical description and applications to NE Atlantic sediments. Geol Soc Spec Publ 267:39–50. https://doi.org/10.1144/GSL.SP.2006.267.01.03

Riera P, Stal L, Nieuwenhuize J, Richard P, Blanchard G, Gentil F (1999) Determination of food sources for benthic invertebrates in a salt marsh (Aiguillon Bay, France) by carbon and nitrogen stable isotopes:importance of locally produced sources. Mar Ecol Prog Ser 187:301–307. https://doi.org/10.3354/meps187301

Riisgård HU, Banta GT (1998) Irrigation and deposit feeding by the lugworm Arenicola marina, characteristics and secondary effects on the environment. A review of current knowledge. Vie et Milieu / Life & Environment 48(4):243–257

Riisgård HU, Kittner C, Seerup DF (2003) Regulation of opening state and filtration rate in filter-feeding bivalves (*Cardium edule*, *Mytilus edulis*, *Mya arenaria*) in response to low algal concentration. J Exp Mar Biol Ecol 284(1–2):105–127. https://doi.org/10.1016/S0022-0981(02)00496-3

Riisgård HU, Lassen J, Kittner C (2006) Valve-gape response times in mussels (*Mytilus edulis*) - Effects of laboratory preceding-feeding conditions and in situ tidally induced variation in phytoplankton biomass. J Shellfish Res 25(3):901–911. https://doi.org/10.2983/0730-8000(2006)25[901:VRTIMM]2.0.CO;2

Rijkswaterstaat (2022) Vervolgonderzoek Bereikbaarheid Ameland.

Rippen A, Van Der Zee E, Fieten N, Latour J, Wymenga E (2021) Review effecten natuurlijke bodemdynamiek en menselijke bodemberoering in de sublitorale Waddenzee.

Ritchie RJ (2006) Consistent sets of spectrophotometric chlorophyll equations for acetone, methanol and ethanol solvents. Photosynth Res 89(1):27–41. https://doi.org/10.1007/s11120-006-9065-9

Robertson BP, Gardner JPA, Savage C (2015) Macrobenthic-mud relations strengthen the foundation for benthic index development: A case study from shallow, temperate New Zealand estuaries. Ecol Indic 58:161–174. https://doi.org/10.1016/j.ecolind.2015.05.039

Rodil IF, Lucena-Moya P, Lastra M (2018) The Importance of Environmental and Spatial Factors in the Metacommunity Dynamics of Exposed Sandy Beach Benthic Invertebrates. Estuaries and Coasts 41(1):206–217. https://doi.org/10.1007/s12237-017-0263-9

Rodland DL, Schöne BR, Baier S, Zhang Z, Dreyer W, Page NA (2009) Changes in gape frequency, siphon activity and thermal response in the freshwater bivalves *Anodonta cygnea* and *Margaritifera falcata*. Journal of Molluscan Studies 75(1):51–57. https://doi.org/10.1093/mollus/eyn038

Román-Sánchez A, Reimann T, Wallinga J, Vanwalleghem T (2019) Bioturbation and erosion rates along the soil-hillslope conveyor belt, part 1: Insights from single-grain feldspar luminescence. Earth Surf Process Landf 44(10):2051–2065. https://doi.org/10.1002/esp.4628

Santos S, Luttikhuizen PC, Campos J, Heip CHR, van der Veer HW (2011) Spatial distribution patterns of the peppery furrow shell *Scrobicularia plana* (da Costa, 1778) along the European coast: A review. J Sea Res 66(3):238–247. https://doi.org/10.1016/J.SEARES.2011.07.001

Schneider CA, Rasband WS, Eliceiri KW (2012) NIH Image to ImageJ: 25 years of image analysis. Nat Methods 9(7):671–675. https://doi.org/10.1038/nmeth.2089

Schultz JT, Aarts G, Baptist MJ, Poos JJ (2025) Unravelling the impact of sand extraction pits on macrobenthos distribution in the Southern North Sea. Mar Ecol Prog Ser 772:43–60. https://doi.org/10.3354/meps14965

Scola S, Blasco J, Campana O (2021) "Nanosize effect" in the metal-handling strategy of the bivalve *Scrobicularia plana* exposed to CuO nanoparticles and copper ions in whole-sediment toxicity tests. Science of the Total Environment 760:143886. https://doi.org/10.1016/j.scitotenv.2020.143886

Self R, Jumars P (1988) Cross-phyletic patterns of particle selection by deposit feeders. J Mar Res 46(1):119–143

Selig ER, Hole DG, Allison EH, Arkema KK, McKinnon MC, Chu J, de Sherbinin A, Fisher B, Glew L, Holland MB, Ingram JC, Rao NS, Russell RB, Srebotnjak T, Teh LCL, Troëng S, Turner WR, Zvoleff A (2019) Mapping global human dependence on marine ecosystems. Conserv. Lett. 12:e12617

Seuront L, Nicastro KR, Zardi GI, Goberville E (2019) Decreased thermal tolerance under recurrent heat stress conditions explains summer mass mortality of the blue mussel *Mytilus edulis*. Sci Rep 9(1):1–14. https://doi.org/10.1038/s41598-019-53580-w

Silva FRS da, Borges AL de O, Toldo Jr. EE, Fick C, Puhl E, Oliveira VCB, Cruz FEG da (2023) Threshold of motion and orientation of bivalve shells under current flow. Brazilian Journal of Geology 53(1):e20220080. https://doi.org/10.1590/2317-4889202320220080

Simmons BI, Blyth PSA, Blanchard JL, Clegg T, Delmas E, Garnier A, Griffiths CA, Jacob U, Pennekamp F, Petchey OL, Poisot T, Webb TJ, Beckerman AP (2021) Refocusing multiple stressor research around the targets and scales of ecological impacts. Nat. Ecol. Evol. 5:1478–1489

Smedley RK, Duller GAT, Roberts HM (2015) Bleaching of the post-IR IRSL signal from individual grains of K-feldspar: Implications for single-grain dating. Radiat Meas 79:33–42. https://doi.org/10.1016/j.radmeas.2015.06.003

Snelgrove PVR (1998) The biodiversity of macrofaunal organisms in marine sediments. Biodivers Conserv 7(9):1123–1132. https://doi.org/10.1023/A:1008867313340

Snelgrove PVR, Butman CA (1994) Animal-sediment relationships revisited: cause versus effect. In: Oceanography and marine biology: an annual review. Vol. 32. pp 111–178

Snelgrove PVR, Soetaert K, Solan M, Thrush S, Wei CL, Danovaro R, Fulweiler RW, Kitazato H, Ingole B, Norkko A, Parkes RJ, Volkenborn N (2018) Global Carbon Cycling on a Heterogeneous Seafloor. Trends Ecol Evol 33(2):96–105. https://doi.org/10.1016/j.tree.2017.11.004

Soetaert K, Petzoldt T (2008) marelac: tools for aquatic sciences. CRAN: Contributed Packages

Soissons LM, Gomes da Conceiçâo T, Bastiaan J, van Dalen J, Ysebaert T, Herman PMJ, Cozzoli F, Bouma TJ (2019) Sandification vs. muddification of tidal flats by benthic organisms: A flume study. Estuar Coast Shelf Sci 228. https://doi.org/10.1016/j.ecss.2019.106355

Song S, Santos IR, Yu H, Wang F, Burnett WC, Bianchi TS, Dong J, Lian E, Zhao B, Mayer L, Yao Q, Yu Z, Xu B (2022) A global assessment of the mixed layer in coastal sediments and implications for carbon storage. Nat Commun 13(1):1–10. https://doi.org/10.1038/s41467-022-32650-0

Soon TK, Ransangan J (2019) Extrinsic factors and marine bivalve mass mortalities: an overview. J Shellfish Res 38(2):223. https://doi.org/10.2983/035.038.0202

Soulsby RL (1983) The bottom boundary layer of shelf seas. In: Elsevier Oceanography Series. Elsevier, pp 189–266

Speybroeck J, Bonte D, Courtens W, Gheskiere T, Grootaert P, Maelfait J-P, Mathys M, Provoost SAM, Sabbe K, Stienen EWM, Lancker VVAN, Vincx M, Degraer S (2006) Beach nourishment: an ecologically sound coastal defence alternative? A review. Aquatic Conserv: Mar Freshw Ecosyst 16:419–435. https://doi.org/10.1002/aqc.733

Stal LJ (2010) Microphytobenthos as a biogeomorphological force in intertidal sediment stabilization. Ecol Eng 36(2):236–245. https://doi.org/10.1016/j.ecoleng.2008.12.032

Staniek MA, Pansch C, Shama LNS, Mehler K, Steinmann A, Middelburg JJ, Meysick L (2025) Heatwave intensity drives eco-physiological responses in infaunal bivalves: A mesocosm experiment. Limnol Oceanogr. https://doi.org/10.1002/lno.70012

Stanley S (1970) Relation of shell form to life habits of the Bivalvia (Mollusca). The Geological Society of America, Boulder

Staudt F, Gijsman R, Ganal C, Mielck F, Wolbring J, Hass HC, Goseberg N, Schüttrumpf H, Schlurmann T, Schimmels S (2021) The sustainability of beach nourishments : a review of nourishment and environmental monitoring practice. J Coast Conserv 25(34)

Staudt F, Mullarney JC, Pilditch CA, Huhn K (2019) Effects of grain-size distribution and shape on sediment bed stability, near-bed flow and bed microstructure. Earth Surf Process Landf 44(5):1100–1116. https://doi.org/10.1002/esp.4559

Stillman JH, Amri AB, Holdreith JM, Hooper A, Leon R V., Pruett LR, Bukaty BM (2025) Ecophysiological responses to heat waves in the marine intertidal zone. Journal of Experimental Biology 228

Stive MJF, De Schipper MA, Luijendijk AP, Aarninkhof SGJ, Van Gelder-Maas C, Van Thiel De Vries JSM, De Vries S, Henriquez M, Marx S, Ranasinghe R (2013) A new alternative to saving our beaches from sea-level rise: The sand engine. J Coast Res 29(5):1001–1008. https://doi.org/10.2112/JCOASTRES-D-13-00070.1

Stockmann U, Minasny B, Pietsch TJ, McBratney AB (2013) Quantifying processes of pedogenesis using optically stimulated luminescence. Eur J Soil Sci 64(1):145–160. https://doi.org/10.1111/ejss.12012

St-Onge P, Miron G, Moreau G (2007) Burrowing behaviour of the softshell clam (Mya arenaria) following erosion and transport. J Exp Mar Biol Ecol 340(1):103–111. https://doi.org/10.1016/j.jembe.2006.08.011

Strypsteen G, van Rijn LC, Hoogland MD, Rauwoens P, Fordeyn J, Hijma MP, Lodder QJ (2021) Reducing aeolian sand transport and beach erosion by using armour layer of coarse materials. Coastal Engineering 166:103871. https://doi.org/10.1016/j.coastaleng.2021.103871

Sun M-Y, Lee C, Aller RC (1993) Laboratory studies of oxic and anoxic degradation of chlorophyll-a in Long Island Sound sediments. Geochim Cosmochim Acta 57(1):147–157. https://doi.org/10.1016/0016-7037(93)90475-C

Syvitski J, Ángel JR, Saito Y, Overeem I, Vörösmarty CJ, Wang H, Olago D (2022) Earth's sediment cycle during the Anthropocene. Nat Rev Earth Environ 3(3):179–196. https://doi.org/https://doi.org/10.1038/s43017-021-00253-w

Syvitski J, Vörösmarty CJ, Kettner AJ, Green P (2005) Impact of humans on the flux of terrestrial sediment to the global coastal ocean. Science (1979) 308(5720):376–380. https://doi.org/10.1126/science.1109454

Taghon GL (1982) Optimal foraging by deposit-feeding invertebrates: Roles of particle size and organic coating. Oecologia 52(3):295–304. https://doi.org/10.1007/BF00367951

Temmerman S, Meire P, Bouma TJ, Herman PMJ, Ysebaert T, De Vriend HJ (2013) Ecosystem-based coastal defence in the face of global change. Nature 2013 504:7478 504(7478):79–83. https://doi.org/10.1038/NATURE12859

Thompson P, Cai Y, Moyeed R, Reeve D, Stander J (2010) Bayesian nonparametric quantile regression using splines. Comput Stat Data Anal 54(4):1138–1150. https://doi.org/10.1016/j.csda.2009.09.004

Thomson JD, Weiblen G, Thomson BA, Alfaro S, Legendre P (1996) Untangling multiple factors in spatial distributions: Lilies, gophers, and rocks. Ecology 77(6):1698–1715. https://doi.org/10.2307/2265776

Thrush S, Hewitt J, Norkko A, Nicholls P, Funnell G, Ellis J (2003) Habitat change in estuaries: predicting broad-scale responses of intertidal macrofauna to sediment mud content. Mar Ecol Prog Ser 263:101–112. https://doi.org/10.3354/meps263101

Thrush SF, Hewitt JE, Herman PMJ, Ysebaert T (2005) Multi-scale analysis of species–environment relationships. Mar Ecol Prog Ser 302:13–26. https://doi.org/10.3354/MEPS302013

Tibshirani R (1996) Regression Shrinkage and Selection Via the Lasso. Journal of the Royal Statistical Society: Series B (Methodological) 58(1):267–288. https://doi.org/10.1111/j.2517-6161.1996.tb02080.x

Tomanek L (2010) Variation in the heat shock response and its implication for predicting the effect of global climate change on species' biogeographical distribution ranges and metabolic costs. Journal of Experimental Biology 213(6):971–979. https://doi.org/10.1242/jeb.038034

Tomanek L (2002) Physiological Ecology of Rocky Intertidal Organisms: A Synergy of Concepts. Integr Comp Biol 42(4):771–775. https://doi.org/10.1093/icb/42.4.771

Tonk L, Witbaard R, van Dalen P, Cheng CH, Kamermans P (2023) Applicability of the gape monitor to study flat oyster (*Ostrea edulis*) feeding behaviour. Aquat Living Resour 36:6. https://doi.org/10.1051/alr/2022021

Treurnicht M, Pagel J, Tonnabel J, Esler KJ, Slingsby JA, Schurr FM (2020) Functional traits explain the Hutchinsonian niches of plant species. Global Ecology and Biogeography 29(3):534–545. https://doi.org/10.1111/geb.13048

Tulp I, Craeymeersch J, Leopold M, van Damme C, Fey F, Verdaat H (2010) The role of the invasive bivalve Ensis directus as food source for fish and birds in the Dutch coastal zone. Estuar Coast Shelf Sci 90(3):116–128. https://doi.org/10.1016/j.ecss.2010.07.008

Van Colen C (2018) The Upper Living Levels: Invertebrate Macrofauna. In: Mudflat Ecology. Springer International Publishing, pp 149–168

Van Colen C, Montserrat F, Vincx M, Herman P, Ysebaert T, Degraer S (2008) Macrobenthic recovery from hypoxia in an estuarine tidal mudflat. Mar Ecol Prog Ser 372:31–42. https://doi.org/10.3354/meps07640

Van Colen C, Ong EZ, Briffa M, Wethey DS, Abatih E, Moens T, Woodin SA (2020) Clam feeding plasticity reduces herbivore vulnerability to ocean warming and acidification. Nat Clim Chang 10(2):162–166. https://doi.org/10.1038/s41558-019-0679-2

van der Meij WM, Riedesel S, Reimann T (2025) Mixed Signals: interpreting mixing patterns of different soil bioturbation processes through luminescence and numerical modelling. SOIL 11(1):51–66. https://doi.org/10.5194/soil-11-51-2025

van der Spek A, Forzoni A, Vermaas T (2022) Holocene deposits at the lower shoreface and inner shelf of the Dutch coast. Ocean Coast Manag 224:106203. https://doi.org/10.1016/j.ocecoaman.2022.106203

van der Spek AJF (1995) Reconstruction of Tidal Inlet and Channel Dimensions in the Frisian Middelzee, a Former Tidal Basin in the Dutch Wadden Sea. In: Tidal Signatures in Modern and Ancient Sediments. Wiley, pp 237–258

van der Wal D (1998) The Impact of the Grain-Size Distribution of Nourishment Sand on Aeolian Sand Transport. J Coast Res 14(2):620–631

van der Wal D, Lambert GI, Ysebaert T, Plancke YMG, Herman PMJ (2017) Hydrodynamic conditioning of diversity and functional traits in subtidal estuarine macrozoobenthic communities. Estuar Coast Shelf Sci 197:80–92. https://doi.org/10.1016/j.ecss.2017.08.012

van der Werf JJ, de Vet PLM, Boersema MP, Bouma TJ, Nolte AJ, Schrijvershof RA, Soissons LM, Stronkhorst J, van Zanten E, Ysebaert T (2019) An integral approach to design the Roggenplaat intertidal shoal nourishment. Ocean Coast Manag 172(February):30–40. https://doi.org/10.1016/j.ocecoaman.2019.01.023

van der Werf JJ, Reinders J, van Rooijen A, Holzhauer H, Ysebaert T (2015) Evaluation of a tidal flat sediment nourishment as estuarine management measure. Ocean Coast Manag 114:77–87. https://doi.org/10.1016/j.ocecoaman.2015.06.006

Van Ledden M, Van Kesteren WGM, Winterwerp JC (2004) A conceptual framework for the erosion behaviour of sand-mud mixtures. Cont Shelf Res 24(1):1–11. https://doi.org/10.1016/j.csr.2003.09.002

van Rijn LC (1984) Sediment Transport, Part I: Bed Load Transport. Journal of Hydraulic Engineering 110(10):1431–1456. https://doi.org/10.1061/(asce)0733-9429(1984)110:10(1431)

van Rijn LC (1993) Principles of sediment transport in rivers, estuaries and coastal seas. Aqua Publications, Amsterdam

van Rijn LC, Strypsteen G (2020) A fully predictive model for aeolian sand transport. Coastal Engineering 156:103600. https://doi.org/10.1016/j.coastaleng.2019.103600

van Straaten LMJU (1952) Biogene textures and the formation of shell beds in the Dutch Wadden Sea I. Proc Koninkl Ned Akad Wetenschap 55

Van Weerdenburg R (2024) DWSM-Mud: a sixth-generation 3D model of the Dutch Wadden Sea for hydrodynamics and mud dynamics DWSM-Mud: a sixth-generation 3D model of the Dutch Wadden Sea for hydrodynamics and mud dynamics 2023 release

van Westen B, de Schipper MA, Pearson SG, Luijendijk AP (2025) Lagrangian modelling reveals sediment pathways at evolving coasts. Sci Rep 15(1):1–16. https://doi.org/10.1038/s41598-025-92910-z

Vandenberghe D, De Corte F, Buylaert JP, Kučera J, Van den Haute P (2008) On the internal radioactivity in quartz. Radiat Meas 43(2–6):771–775. https://doi.org/10.1016/j.radmeas.2008.01.016

Vaz S, Martin CS, Eastwood Paul D., Ernande B, Carpentier A, Meaden GJ, Coppin F (2008) Modelling species distributions using regression quantiles. Journal of Applied Ecology 45(1). https://doi.org/doi:10.HH/j.1365-2664.2007.01392.x

Venables WN, Ripley BD (2002) Modern Applied Statistics with S. Springer New York, New York, NY

Verdelhos T, Cardoso PG, Dolbeth M, Pardal MA (2014) Recovery trends of *Scrobicularia plana* populations after restoration measures, affected by extreme climate events. Mar Environ Res 98:39–48. https://doi.org/10.1016/j.marenvres.2014.03.004

Verdelhos T, Marques JC, Anastácio P (2015) Behavioral and mortality responses of the bivalves *Scrobicularia plana* and *Cerastoderma edule* to temperature, as indicator of climate change's potential impacts. Ecol Indic 58:95–103. https://doi.org/10.1016/j.ecolind.2015.05.042

Volkenborn N, Hedtkamp SIC, van Beusekom JEE, Reise K (2007a) Effects of bioturbation and bioirrigation by lugworms (Arenicola marina) on physical and chemical sediment properties and implications for intertidal habitat succession. Estuar Coast Shelf Sci 74(1–2):331–343. https://doi.org/10.1016/j.ecss.2007.05.001

Volkenborn N, Polerecky L, Hedtkamp SIC, van Beusekom JEE, de Beer D (2007b) Bioturbation and bioirrigation extend the open exchange regions in permeable sediments. Limnol Oceanogr 52(5):1898–1909. https://doi.org/10.4319/lo.2007.52.5.1898

Volkenborn N, Robertson DM, Reise K (2009) Sediment destabilizing and stabilizing bio-engineers on tidal flats: Cascading effects of experimental exclusion. Helgol Mar Res 63(1):27–35. https://doi.org/10.1007/s10152-008-0140-9

Vousdoukas MI, Ranasinghe R, Mentaschi L, Plomaritis TA, Athanasiou P, Luijendijk A, Feyen L (2020) Sandy coastlines under threat of erosion. Nat Clim Chang 10(3):260–263. https://doi.org/10.1038/s41558-020-0697-0

Wallinga J (2002) On the detection of OSL age overestimation using single-aliquot techniques. Geochronometria: Journal on Methods & Applications of Absolute Chronology 21:17–26

Wallinga J, Hobo N, Cunningham AC, Versendaal AJ, Makaske B, Middelkoop H (2010) Sedimentation rates on embanked floodplains determined through quartz optical dating. Quat Geochronol 5(2–3):170–175. https://doi.org/10.1016/j.quageo.2009.01.002

Wallinga J, Sevink J, Van Mourik JM, Reimann T (2019) Luminescence dating of soil archives. Reading the soil archives: unraveling the geoecological code of palaeosols and sediment cores. In: van Mourik J, van der Meer J (eds). Elsevier, Amsterdam, pp 115–162

Wang P, Cheng J (2016) Storm Impacts on the Morphology and Sedimentology of Open-Coast Tidal Flats. In: Coastal Storms: Processes and Impacts. Wiley Blackwell, pp 81–98

Wang Y, Yu Q, Jiao J, Tonnon PK, Wang ZB, Gao S (2016) Coupling bedform roughness and sediment grain-size sorting in modelling of tidal inlet incision. Mar Geol 381:128–141. https://doi.org/10.1016/j.margeo.2016.09.004

Wang Z, Liang B, Wu G, Borsje BW (2019) Modeling the formation and migration of sand waves: The role of tidal forcing, sediment size and bed slope effects. Cont Shelf Res 190:103986. https://doi.org/10.1016/j.csr.2019.103986

Wang ZB, Elias EPL, Van Der Spek AJF, Lodder QJ (2018) Sediment budget and morphological development of the Dutch Wadden Sea: Impact of accelerated sea-level rise and subsidence until 2100. Netherlands Journal of Geosciences 97(3):183–214. https://doi.org/10.1017/njg.2018.8

Ward JE, Shumway SE (2004) Separating the grain from the chaff: Particle selection in suspension- and deposit-feeding bivalves. J Exp Mar Biol Ecol 300(1–2):83–130. https://doi.org/10.1016/j.jembe.2004.03.002

Weiss RF (1970) The solubility of nitrogen, oxygen and argon in water and seawater. Deep-Sea Research and Oceanographic Abstracts 17(4):721–735. https://doi.org/10.1016/0011-7471(70)90037-9

Wells JT, Kim SY (1989) Sedimentation in the Albemarle-Pamlico lagoonal system: synthesis and hypotheses. Mar Geol 88(3–4):263–284. https://doi.org/10.1016/0025-3227(89)90101-1

Wendelboe K, Egelund JT, Flindt MR, Valdemarsen T (2013) Impact of lugworms (Arenicola marina) on mobilization and transport of fine particles and organic matter in marine sediments. J Sea Res 76:31–38. https://doi.org/10.1016/j.seares.2012.10.013

Westoby MJ, Brasington J, Glasser NF, Hambrey MJ, Reynolds JM (2012) "Structure-from-Motion" photogrammetry: A low-cost, effective tool for geoscience applications. Geomorphology 179:300–314. https://doi.org/10.1016/j.geomorph.2012.08.021

Wheatcroft RA (1990) Preservation potential of sedimentary event layers. Geology 18(9):843–845. https://doi.org/10.1130/0091-7613(1990)018<0843:PPOSEL>2.3.CO;2

Whitlatch RB (1981) Animal-sediment relationships in intertidal marine benthic habitats: Some determinants of deposit-feeding species diversity. J Exp Mar Biol Ecol 53(1):31–45. https://doi.org/10.1016/0022-0981(81)90082-4

Widdows J, Brinsley M (2002) Impact of biotic and abiotic processes on sediment dynamics and the consequences to the structure and functioning of the intertidal zone. J Sea Res 48(2):143–156. https://doi.org/10.1016/S1385-1101(02)00148-X

Wiesebron LE, Cheng CH, de Vet PLM, Walles B, van Donk S, van Dalen J, van de Lageweg W, Ysebaert T, Bouma TJ (2024) How restoration engineering measures can enhance the ecological value of intertidal flats. Restor Ecol :e14247. https://doi.org/10.1111/rec.14247

Wiesebron LE, Steiner N, Morys C, Ysebaert T, Bouma TJ (2021) Sediment bulk density effects on benthic macrofauna burrowing and bioturbation behavior. Front Mar Sci 8(July):1–16. https://doi.org/10.3389/fmars.2021.707785

Wilcock PR, DeTemple BT (2005) Persistence of armor layers in gravel-bed streams. Geophys Res Lett 32(8):1–4. https://doi.org/10.1029/2004GL021772

Williams AT, Rangel-Buitrago N, Pranzini E, Anfuso G (2018) The management of coastal erosion. Ocean Coast Manag 156:4–20. https://doi.org/10.1016/j.ocecoaman.2017.03.022

Wilson JG (1981) Temperature tolerance of circatidal bivalves in relations to their distribution. J Therm Biol 6(4):279–286

Wilson MFJ, O'Connell B, Brown C, Guinan JC, Grehan AJ (2007) Multiscale terrain analysis of multibeam bathymetry data for habitat mapping on the continental slope. Marine Geodesy 30(1–2):3–35. https://doi.org/10.1080/01490410701295962

Witbaard R, Bergman MJN, van Weerlee E, Duineveld GCA (2017) An estimation of the effects of Ensis directus on the transport and burial of silt in the near-shore Dutch coastal zone of the North Sea. J Sea Res 127:95–104. https://doi.org/10.1016/j.seares.2016.12.001

Witbaard R, Duineveld GCA, Bergman M (2001) The effect of tidal resuspension on benthic food quality in the southern North Sea. Senckenbergiana Maritima 31(2):225–234. https://doi.org/10.1007/BF03043031

Witbaard R, Duineveld GCA, Bergman MJN, Witte HIJ, Groot L, Rozemeijer MJC (2015) The growth and dynamics of Ensis directus in the near-shore Dutch coastal zone of the North Sea. J Sea Res 95:95–105. https://doi.org/10.1016/j.seares.2014.09.008

Witbaard R, Moons S, Schaars LK, Craeymeersch J (2025) Sedimentary and faunistic effects of medium-deep sand mining along the Dutch Coast. Estuar Coast Shelf Sci 321:109337. https://doi.org/10.1016/j.ecss.2025.109337

Witte ES, Franken O, Temmink RJM, Dickson J, de Wit B, Roohi R, Martinez-Garcia P, Heusinkveld J, Holthuijsen SJ, Meijer KJ, Olff H, Govers LL, van der Heide T (2025) Structural complexity of hard substrates shapes shallow marine benthic communities. Oikos 2025(8):e11080. https://doi.org/10.1002/oik.11080

Wong M, Parker G (2006) Reanalysis and Correction of Bed-Load Relation of Meyer-Peter and Müller Using Their Own Database. Journal of Hydraulic Engineering 132(11):1159–1168. https://doi.org/10.1061/(asce)0733-9429(2006)132:11(1159)

Worm B, Barbier EB, Beaumont N, Duffy JE, Folke C, Halpern BS, Jackson JBC, Lotze HK, Micheli F, Palumbi SR, Sala E, Selkoe KA, Stachowicz JJ, Watson R (2006) Impacts of Biodiversity Loss on Ocean Ecosystem Services. Science (1979) 314(5800):787–790. https://doi.org/10.1126/science.1132294

Worrall CM, Widdows J (1983) Physiological changes following transplantation of the bivalve *Scrobicularia plana* between three populations. Mar Ecol Prog Ser 12:281–287

Worrall CM, Widdows J, Lowe DM (1983) Physiological ecology of three populations of the bivalve *Scrobicularia plana*. Mar Ecol Prog Ser 12:267–279. https://doi.org/10.3354/meps012267

Xu Y, Li D, Nepf H (2022) Sediment Pickup Rate in Bare and Vegetated Channels. Geophys Res Lett 49(21):e2022GL101279. https://doi.org/10.1029/2022GL101279

Xu Y, Luo X, He Y, Zang X, Lin W, Liu Y, Zhao L (2025) Valve gaping behavior of bivalves under compound marine heatwaves and acidification extremes. Mar Environ Res 212:107557. https://doi.org/10.1016/j.marenvres.2025.107557

Yang JQ, Chung H, Nepf HM (2016) The onset of sediment transport in vegetated channels predicted by turbulent kinetic energy. Geophys Res Lett 43(21):11,261-11,268. https://doi.org/10.1002/2016GL071092

Yang JQ, Nepf HM (2018) A Turbulence-Based Bed-Load Transport Model for Bare and Vegetated Channels. Geophys Res Lett 45(19):10,428-10,436. https://doi.org/10.1029/2018GL079319

Young DK, Rhoads DC (1971) Animal-sediment relations in Cape Cod Bay, Massachusetts I. A transect study. Mar Biol 11(3):242–254. https://doi.org/10.1007/BF00401272

Ysebaert T, Herman PMJ (2002) Spatial and temporal variation in benthic macrofauna and relationships with environmental variables in an estuarine, intertidal soft-sediment environment. Mar Ecol Prog Ser 244(Levin 1992):105–124. https://doi.org/10.3354/meps244105

Ysebaert T, Walles B, Haner J, Hancock B (2018) Habitat modification and coastal protection by ecosystem-engineering reef-building bivalves. In: Goods and Services of Marine Bivalves. Springer International Publishing, pp 253–273

Zhang A, Long H, Yang F, Zhang J, Peng J, Zhang G (2025) Luminescence dating illuminates soil evolution. Earth Sci Rev 265:105103. https://doi.org/10.1016/j.earscirev.2025.105103

Zhang W, Storey KB, Dong Y (2020) Adaptations to the mudflat: Insights from physiological and transcriptional responses to thermal stress in a burrowing bivalve *Sinonovacula constricta*. Science of the Total Environment 710:136280. https://doi.org/10.1016/j.scitotenv.2019.136280

Zhao T, Nepf HM (2021) Turbulence Dictates Bedload Transport in Vegetated Channels Without Dependence on Stem Diameter and Arrangement. Geophys Res Lett 48(21). https://doi.org/10.1029/2021GL095316

Zhou Z, Bouma TJ, Fivash GS, Ysebaert T, van IJzerloo L, van Dalen J, van Dam B, Walles B (2022a) Thermal stress affects bioturbators' burrowing behavior: A mesocosm experiment on common cockles (*Cerastoderma edule*). Science of The Total Environment 824:153621. https://doi.org/10.1016/J.SCITOTENV.2022.153621

Zhou Z, Fivash GS, Cozzoli F, Walles B, Troost K, Ysebaert T, Bouma TJ (2025) Compound extreme events reshuffle the stacked odds in the gamble between native and introduced bivalves. Glob Ecol Conserv :e03918. https://doi.org/10.1016/j.gecco.2025.e03918

Zhou Z, Liu Q, Fan D, Coco G, Gong Z, Möller I, Xu F, Townend I, Zhang C (2021) Simulating the role of tides and sediment characteristics on tidal flat sorting and bedding dynamics. Earth Surf Process Landf 46(11):2163–2176. https://doi.org/10.1002/esp.5166

Zhou Z, Steiner N, Fivash GS, Cozzoli F, Blok DB, van IJzerloo L, van Dalen J, Ysebaert T, Walles B, Bouma TJ (2023) Temporal dynamics of heatwaves are key drivers of sediment mixing by bioturbators. Limnol Oceanogr 68(5):1105–1116. https://doi.org/10.1002/lno.12332

Zhou Z, Wu Y, Fan D, Wu G, Luo F, Yao P, Gong Z, Coco G (2022b) Sediment sorting and bedding dynamics of tidal flat wetlands: Modeling the signature of storms. J Hydrol (Amst) 610:127913. https://doi.org/10.1016/j.jhydrol.2022.127913

Zhu Z, van Belzen J, Zhu Q, van de Koppel J, Bouma TJ (2020) Vegetation recovery on neighboring tidal flats forms an Achilles' heel of saltmarsh resilience to sea level rise. Limnol Oceanogr 65(1):51–62. https://doi.org/10.1002/lno.11249

Ziegler M, Jilbert T, de Lange GJ, Lourens LJ, Reichart G (2008) Bromine counts from XRF scanning as an estimate of the marine organic carbon content of sediment cores. Geochemistry, Geophysics, Geosystems 9(5). https://doi.org/10.1029/2007GC001932

Zwarts L, Blomert AM, Spaak P, de Vries B (1994) Feeding radius, burying depth and siphon size of *Macoma balthica* and *Scrobicularia plana*. J Exp Mar Biol Ecol 183(2):193–212. https://doi.org/10.1016/0022-0981(94)90087-6

Zwarts L, Wanink JH (1993) How the food supply harvestable by waders in the Wadden Sea depends on the variation in energy density, body weight, biomass, burying depth and behaviour of tidal-flat invertebrates. Netherlands Journal of Sea Research 31(4):441–476. https://doi.org/10.1016/0077-7579(93)90059-2

Zwarts L, Wanink JH (1989) Siphon size and burying depth in deposit-and suspension-feeding benthic bivalves. Mar Biol 100(2):227–240. https://doi.org/10.1007/BF00391963

Author affiliations

Allert Bijleveld
Department of Coastal Systems, NIOZ Royal Netherlands Institute for Sea Research, 't Horntje, the Netherlands

Anna-Maartje de Boer
Soil Geography and Landscape group & Netherlands Centre for Luminescence dating, Wageningen University and Research, Wageningen, the Netherlands

Jorn W. Bosma
Faculty of Geoscience, Department of Physical Geography, Utrecht University, Utrecht, the Netherlands

Tjeerd J. Bouma
Department of Estuarine and Delta Systems, NIOZ Royal Netherlands Institute for Sea Research,
Yerseke, the Netherlands
Faculty of Geoscience, Department of Physical Geography, Utrecht University, Utrecht, the Netherlands

Oscar Franken
Groningen Institute for Evolutionary Life-Sciences, University of Groningen, Groningen, the Netherlands
Department of Coastal Systems, NIOZ Royal Netherlands Institute for Sea Research, 't Horntje, the Netherlands

Steven H. Haarbosch
Faculty of Civil Engineering and Geosciences, Delft University of Technology, Delft, the Netherlands

Tjisse van der Heide
Department of Coastal Systems, NIOZ Royal Netherlands Institute for Sea Research, 't Horntje, the Netherlands
Groningen Institute for Evolutionary Life-Sciences, University of Groningen, Groningen, the Netherlands

Natascia Pannozzo
Faculty of Civil Engineering and Geosciences, Delft University of Technology, Delft, the Netherlands

Stuart G. Pearson
Faculty of Civil Engineering and Geosciences, Delft University of Technology, Delft, the Netherlands

Bram C. van Prooijen
Faculty of Civil Engineering and Geosciences, Delft University of Technology, Delft, the Netherlands

Karline Soetaert
Department of Estuarine and Delta Systems, NIOZ Royal Netherlands Institute for Sea Research, Yerseke, the Netherlands
Faculty of Geoscience, Department of Earth Sciences, Utrecht University, Utrecht, the Netherlands

Ad van der Spek
Deltares, Delft, The Netherlands

Henko de Stigter
Department of Ocean Systems, NIOZ Royal Netherlands Institute for Sea Research, 't Horntje, the Netherlands

Jakob Wallinga
Soil Geography and Landscape group & Netherlands Centre for Luminescence dating, Wageningen University and Research, Wageningen, the Netherlands

Rob Witbaard
Department of Estuarine and Delta Systems, NIOZ Royal Netherlands Institute for Sea Research, Yerseke, the Netherlands.

Acknowledgements

This thesis would not have become what it is without the help and encouragement of a lot of amazing people. Here I would like to thank many of you, though there were numerous others that have made a big or small difference.

Ten eerste wil ik mijn begeleiders bedankten. Het was inspirerend met jullie te werken en ik heb me erg gesteund gevoeld. Jullie hebben me verschillende manieren van denken geleerd, en veel ruimte gegeven om mijn eigen keuzes te maken. **Rob**, ik heb geboft met jou als eerste begeleider. Wanneer ik voor een korte vraag naar je toe kwam, liep ik meestal pas een uur later je kantoor weer uit, omdat je de tijd nam om het tot op de bodem met me uit te zoeken. **Karline**, dank je wel voor je nuchtere blik, dat je er op cruciale momenten voor me was en dat je de moeite nam om grondig mijn stukken door te kijken, waarbij je zelfs de kleinste foutjes eruit kon vissen. **Tjeerd**, ik waardeer het erg dat je me af en toe spontaan belde om te vragen hoe het ging en, al volgde ik het niet altijd direct op, ik zal veel van je wijze raad meenemen. **Stuart**, your endless encouragement motivated me and you gave me space to ask random questions. Your non-ecologist view was also invaluable for out-of-the-box questions, and has helped me set down the more interdisciplinary thesis that I was hoping to write.

To the other TRAILS colleagues, especially **Jakob**, **Bram**, **Ad**, **Quirijn**, **David**, **Natascia** and **Anna-Maartje**, it was a great pleasure to work with you. **Jakob**, dank dat je het TRAILS-project in goede banen hebt geleid. Heel leuk dat je op de eerste officiële TRAILS-cruise spontaan een weekje mee kwam varen en benthosmonsters voor me uit wilde spoelen. **Natascia**, even if you joined only halfway, I'm happy I got to know you! Thank you for teaching me more about sedimentology and geology. **Anna-Maartje**, mijn TRAILS-partner in crime en natuurlijk mijn paranimf, wat hebben we een lol gehad! Van boord van de Navicula, op conferenties, de NCK-zomerschool, tot op ons schrijfweekend op Ameland. Naast dat het erg leuk was om samen te werken, heb ik ook veel van je geleerd—niet alleen over lichtgevende zandkorrels, maar ook over initiatief nemen en grenzen bewaken, waarin je een inspiratiebron voor me bent.

Voor de gootexperimenten in hoofdstuk 4 moest ik een eindje uit mijn comfortzone stappen. Gelukkig stond ik er niet alleen voor, maar kon ik dit avontuur samen met **Jorn** en **Steven** aan gaan. Bedankt dat ik jullie mij keer op keer wilden uitleg-

gen wat bodemschuifspanning was, maar bovenal bedankt voor de gezelligheid tijdens de experimenten en ver nadat ze voorbij waren.

To all interns who helped me at parts of this journey, **Masha**, **Elena**, **Emile**, **Femke**, **Jara**, **Ismaël**, **Aileen**, **Sarah** and **Milo**, thank you for your all your contributions to this thesis, for teaching me lessons on supervision, for your questions, and for providing good company in the field and the lab.

The fact that my time was divided between Texel and Yerseke turned out quite well for me. I am grateful to have spent time on both locations. While I started my PhD from the distance during the COVID-lockdown of 2021, the OEI-MOOT and Couplers-group gave me a sense of belonging. The warm welcome I received whenever I visited Yerseke, gave me more reasons to visit regularly. Thanks **Aditi**, **Anneke**, **Archontoula**, **Chiu**, **Dunia**, **Eleonora**, **Greg**, **Hannah**, **Jeroen**, **Jaco**, **Jeemijn**, **Job**, **Lauren**, **Marte**, **Pieter**, **Ricky**, **Tori**, **Stanley**, **Stef**, **Suzanne**, **Vera**, and many others for the science chats, diving, walks to the beach and bouldering excursions, and making me feel at home in de Kêête. Thank you **Olivier** for spending time on exploring trait-analyses, even if it did not end up in my chapters in the end. Dank je wel, **Peter**, voor het analyseren van eindeloos veel sedimentmonsters. **Daniël**, **Lennart**, **Jeroen** en **Anton** bedankt voor jullie praktische hulp en het meedenken als ik een probleem of een wens had. **Brenda**, dank je wel voor het sparren en het gezelschap tijdens de EMBS in Bodø. Ik ben blij dat ik de samenwerking met jou kan voortzetten!

Although I officially belonged at EDS, I was lucky enough to be adopted in COS. **Sander**, dank je wel dat je me op sleeptouw nam de eerste dag en me hebt geïntroduceerd tot boxcoren in de Waddenzee. **Loran**, **Bianka, Jeroen** en andere assistenten in het benthoslab, bedankt voor jullie tijd en geduld om me uit te leggen hoe ik *Nephtys cirrosa* en *Nephtys hombergii* van elkaar kon onderscheiden. **Eric**, bedankt voor je hulp en gezelschap rond en tijdens de vaartochten, waar je met de lichtmeter veel voor TRAILS betekent hebt. **Tjisse**, **Allert** en **Oscar**, bedankt voor de inspirerende discussies en jullie feedback die vooral mijn analyses in hoofdstuk 2 verbeterd heeft. **Katharina**, thank you for your input and ideas in how to approach my experiments for chapter 3. **Paula**, thanks a lot for all your ideas on benthos data analysis, and for being the first person to turn when I needed advice, on whichever topic, or wanted to exchange ideas with someone.











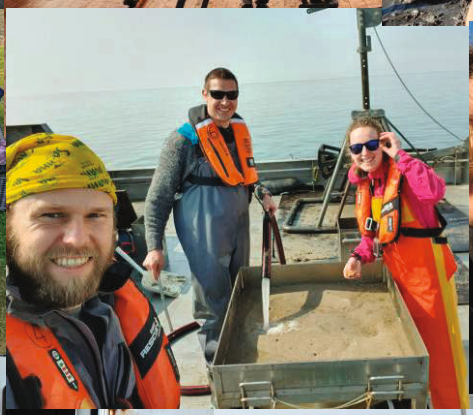



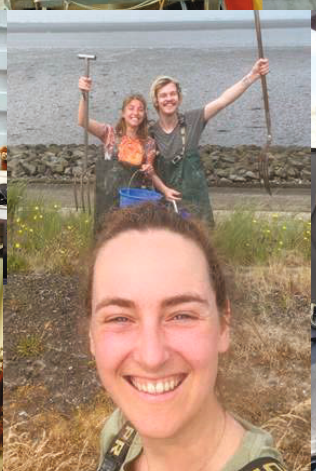

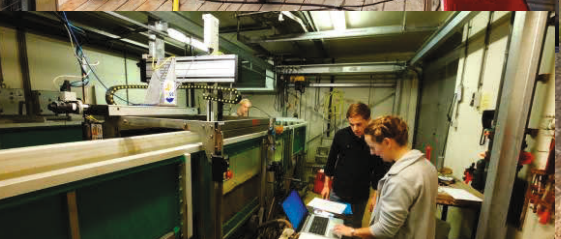








BNR







De beste delen van mijn PhD waren, misschien niet verrassend, de vaartochten. Niet alleen omdat ik ervan genoot dagen achtereen op zee te zijn, maar ook omdat de sfeer (en natuurlijk het eten) aan boord altijd voortreffelijk was. Dat is met name te danken aan de bemanning van R.V. Navicula, **Bram**, **Hein**, **Hendrik**, **Biem**, **Klaas-Jan**, bedankt voor al jullie hulp op zee. **Willem-Anton**, bedankt voor de eerste vaartocht op de TX-96 en dat je me de ins en outs van het kokkelen hebt laten zien.

One of the questions one often receives upon mentioning you live on Texel is "how is life on the island?". Luckily I can answer that I have (had) a lot of amazing colleagues and friends around. **Annalisa**, **Aukje**, **Bram**, **Carlijn**, **Caterina**, **Charlotte**, **Clea**, **Cyril**, **Eva**, **Evy**, **Gabbi**, **Isabel**, **Jesse**, **Jena**, **Jeroen**, **Johannes**, **Jon**, **Jorge**, **Marie**, **Maryann**, **Paula**, **Robert**, **Qing**, **Rosa**, **Sterre**, **Solveig**, **Tini**, **Vesna** and many others. Thanks for making me enjoy going to work, for the refreshing lunch walks, bootcamp (thanks **Wilma**!) and for welcoming me in your houses; thanks to the climbing crew for undertaking the expedition to Alkmaar, and my fellow aspiring surfers for braving the messy North Sea waves together. Thanks **Lea**, **Clea**, **Gabbi** and **Charlotte**, for making me spend more of my free time with my hands in the mud, trying to grow vegetables and fight slugs and weeds. Een van de beste keuzes op Texel was om samen te gaan wonen met **Lea** en **Bram**. Dankzij jullie heb ik me maar weinig alleen gevoeld, stond er vaak lekker eten voor me klaar als ik thuiskwam en ben ik misschien iets beter geworden in Ligretto (maar waarschijnlijk niet).

To all mudflat guides from the **WEX**, thanks for the amazing weekends and guiding weeks, where many of my best memories are made. It's a joy to be part of such an enthusiastic group of volunteers, who love to (literally) dive into the mud and are always hungry for new lugworm facts. Dat Nederland niet zo groot is heeft ervoor gezorgd dat ook mijn andere vrienden niet te ver waren tijdens mijn PhD. **Ingrid** en **Hanna**, de **Biosofen**, **Rijnrunner** ik heb veel plezier met jullie en het geeft mij altijd perspectief om tijd met jullie door te brengen en andere richtingen waarin het leven kan gaan te zien. Thanks to my former housemates, especially **Fara**, **Jane**, **Ella** and **Jorin**, for always welcoming me back in Wageningen, especially during the first years of my PhD. **Violeta**, **Marjolein**, **Marretje** and **Emily**, thanks for keeping sharing bits and pieces of your life with me.

Mem en heit, de basis dy't jimme foar my lein hawwe, hat my hjir brocht. Ik bin tankber dat ik jimme yn dizze tiid sa tichtby hie. Heit, tankewol datsto my dyn

kalmte jûn hast. Altyd as ik in drokke perioade hie troch eksperiminten of fjildwurk, tocht ik oan hoe betiid do op moast stean om de kij te melken, en dan falt myn wurkdei wol wer ta. Mem, do hast my oanmoedigd om te dwaan wat my lokkich makket, wêr't dat my ek hinne brocht, en bist der altyd foar my. Hinke, sorry dat ik dyn idee om nei Texel te ferhúzjen stellen haw, mar ik bin bliid datsto hjir graach komst dat wy ienien sa'n soad sjen kinne. Sipke, ik bin grutk op dy datsto steeds mear dyn plak en wei fynst. Ik bin tankber dat jimme yn myn libben binne.

Adrià, your support, encouragement, listening ear, advice, jokes and, above all, loving, have helped me through every part of this PhD. You give me space to live my life, but are always there when I need you. I feel rich knowing that you are by my side, no matter whether it's close or a bit further away. Life is good with you, and, wonderfully, keeps getting better. T'estimo molt!

About the author

Tjitske Kooistra was born on April 12th, 1995, in Sneek, the Netherlands. Aged 7, wondering which career choices she should make to be able to work with animals and nature, her mother suggested her to become a biologist. Although only much later she would begin to understand what this job entailed, she enthusiastically embarked on the journey. Up to today, there has been no reason to change course. During her Bachelor's Biology at Wageningen University, where she did a thesis on tropical corals and an exchange semester in Tromsø, Norway, her interest for the marine realm grew. Determined to continue in this direction, she started a Master's Biology in Wageningen, specialising in marine biology. This led her again to Norway (IMR, Bergen) for a thesis on deep-sea sponges, to Turkey (Kaș) for a second thesis on Mediterranean sponges, and to Germany (GEOMAR, Kiel) for an internship on seaweed. After working as a teaching assistant at the Aquatic Ecology group in Wageningen, she started her PhD at NIOZ on benthos-sediment interactions. She is not done yet with the Wadden Sea, as she continues as a post-doc at NIOZ, researching heatwave effects on Wadden Sea benthos.

List of publications

Peer-reviewed journal articles

Kooistra TJ, de Boer A-M, Bouma TJ, Pannozzo N, Pearson SG, van der Spek A, de Stigter H, Wallinga J, Witbaard R, Soetaert K (2026) Worms and storms: shedding light on bioturbation and physical mixing on an intertidal flat by combining multiple tracers. Biogeosciences 23(7):2477–2501. https://doi.org/10.5194/bg-23-2477-2026

de Boer AM, Pannozzo N, Pearson SG, **Kooistra TJ**, van Prooijen BC, Wallinga J (2026) Resetting of quartz and feldspar luminescence signals under water. Sci Rep. https://doi.org/10.1038/s41598-026-44245-6

Kooistra TJ, Haarbosch SH, Bosma JW, Bouma TJ, van Prooijen BC, Soetaert K, Pearson SG (2025) How Shells of Different Shapes Affect Current-driven Sand Transport. J Geophys Res Oceans, 130(11) https://doi.org/10.1029/2025JC023346.

Kooistra TJ, Witbaard R, Bouma TJ, Pearson SG, Bijleveld AI, van der Heide T, Franken O, Soetaert K (2025c) Coarsening coasts: quantifying sensitivity of benthic communities to sandification. Estuar Coast Shelf Sci 320:109303. https://doi.org/10.1016/j.ecss.2025.109303

Gökalp M, **Kooistra TJ**, Rocha MS, Silva TH, Osinga R, Murk AJ, Wijgerde T (2020) The effect of depth on the morphology, bacterial clearance, and respiration of the Mediterranean sponge Chondrosia reniformis (Nardo, 1847). Marine Drugs, 18(7), 358 https://doi.org/10.3390/md18070358.

Preprints

Wurz E, Ulvatn T, **Kooistra TJ**, Strauss F, Rapp HT, Goeij JMD, Osinga R (2024) The deep-sea ecosystem engineer Geodia barretti (Porifera, Demospongiae) maintains basic physiological functions under simulated future ocean pH and temperature conditions. *bioRxiv*, 2024-01 https://doi.org/10.1101/2024.01.11.575017.

Conference abstracts, presentations and posters

Kooistra TJ, Bouma, TJ, Pearson, SG, Soetaert K, Witbaard R (2025) Tolerance of a mud-loving clam to sediment change and heat. 16th International Scientific Wadden Sea Symposium.

Kooistra TJ, Bouma, TJ, Pearson, SG, Soetaert K, Witbaard R (2025) Heat wave resilience of a mud-loving clam in different sedimentary habitats. 58th European Marine Biology Symposium.

Kooistra TJ, de Boer AM, de Stigter H, Witbaard R, Wallinga J, Soetaert K (2025) Shedding light on bioturbation: a story of multiple tracers. Dutch Earth and environmental sciences conference (NOW-NAC 2025). *Awarded with "best poster" (2nd place).*

Kooistra TJ, Witbaard R, Bouma, TJ, Pearson, SG, Bijleveld AI, van der Heide T, Soetaert K (2024) SANDsitivity of Wadden Sea benthos – species and community tolerance to changing coastal sediments. 57th European Marine Biology Symposium.

Kooistra TJ, Haarbosch SH, Bosma JW, Pearson SG, van Prooijen BC, Soetaert K, Witbaard R, Bouma TJ (2024) How do shells of different shapes influence current-driven sand transport? Netherlands Centre for Coastal research (NCK days 2024).

Kooistra TJ, Witbaard R, Bouma, TJ, Pearson, SG, Bijleveld AI, van der Heide T, Soetaert K (2024) SANDsitivity of seafloor fauna - Quantifying sediment sensitivity of Wadden Sea benthic communities. Netherlands Annual Ecology Meeting (NAEM 2024).

Kooistra TJ, Witbaard R, Bouma, TJ, Pearson, SG, Soetaert K (2023) How SANDsitive are seafloor animals in the Wadden Sea? Coastal Ecology Workshop (CEW 2023).

Kooistra TJ, Witbaard R, Soetaert K, Bouma, TJ, Pearson, SG (2023) How SANDsitive are seafloor animals in the Wadden Sea? Quantifying sandification sensitivity of Wadden Sea benthic communities. Netherlands Centre for Coastal research (NCK days 2023). *Awarded with "best poster".*

Kooistra TJ, Witbaard R, Soetaert K, Bouma, TJ, Pearson, SG (2022) Sensitivity of benthic communities in a tidal inlet to novel sand nourishments. Estuarine and Coastal Sciences Association (ECSA 59).

Kooistra TJ, Witbaard R, Soetaert K, Bouma, TJ, Pearson, SG (2022) Benthos-sand interactions in the context of an ebb-tidal delta nourishment. Netherlands Centre for Coastal research (NCK) days 2022. *Awarded with "best poster".*

Selection of other output

Podcast and radio episode at BNR Nieuwsradio (August 2023): Onze planeet | Het effect van baggeren en opspuiten op het leven in de bodem. https://www.bnr.nl/podcast/wetenschap-vandaag/10519948/onze-planeet-het-effect-van-baggeren-en-opspuiten-op-het-leven-in-de-bodem

Blog NIOZ@Sea: TRAILS Spring 2022. https://www.nioz.nl/en/blog/trails-spring-2022

Utrecht University
Faculty of Geosciences
Department of Earth Sciences

ISSN 2211-4335